STRESS DISTRIBUTION IN SOME SHELLS OF NEGATIVE GAUSSIAN CURVATURE WITH PARTICULAR REFERENCE TO EDGE EFFECTS

by

B. de V. BATCHELOR, B.Sc., D.I.C., A.M.I.C.E.

A Thesis submitted for the Degree
of Doctor of Philosophy in the Faculty
of Engineering of the University of London.

Imperial College of Science and Technology
London.

October 1963

ABSTRACT

Theoretical and experimental work on thin shallow hyperbolic paraboloid shells are reviewed and discussed. In dealing with the hyperbolic paraboloid shell supported along straight line generators, and for which no known direct solution exists, the homogeneous form of the differential equation involved is studied assuming the existence of the typical edge effect phenomenon in which disturbances from an edge may be considered independently of those emanating from other edges. In particular, it is shown that the approximations introduced by Loof are really equivalent to the Schorer Type approximation.

An account is given of tests carried out, within the elastic range and to failure, on a reinforced cement mortar hyperbolic paraboloid shell supported on straight line generators. The behaviour of the shell was studied when the latter was subjected to certain types of edge loading, to uniform loading over half of the shell, and to uniform loading over the entire shell. In the tests involving the latter type of loading, the stiffnesses of the tie and edge beam were varied.

Comparisons are made between theoretical and experimental results. The existing approximate methods of analysis failed to

predict the behaviour of the shell tested.

The shell behaviour is compared with that of a flat plate with different types of boundary conditions. With rigid edge beams, the deflections in the central region of the shell were reasonably predicted by regarding the shell as a flat plate with clamped edges. Attempts are made to separate the edge beam and tie bar influences. It is shown that the stiffer edge beam favourably affects the stress distribution and deflections throughout the shell , although there is not much to be gained by the use of a very rigid edge beam. The results reveal that torsional stiffness of the edge beam is of little importance but this may have been attributable to the manner in which the detachable edge beams were fixed at the edges.

ACKNOWLEDGEMENTS

The author has been privileged in conducting the research under the general guidance of Professor A.L.L. Baker, D.Sc., M.I.C.E., M.I.Struct.E.

Detailed guidance was given by Dr. J. Munro and the author is indebted to him for his interest and encouragement. Grateful appreciation is also due to Messrs. J.C.de C. Henderson, A.D. Edwards and Dr. C. Yu for their assistance and encouragement at different stages.

The experimental work, which was conducted in the Concrete Structures Laboratory, would have been impossible without the generous assistance of the laboratory staff of the Civil Engineering Department and their help is gratefully acknowledged. Mr. R.W. Loveday has given many helpful suggestions and advice regarding the use of equipment.

Fellow research students have helped in the testing of the model and the author would like to express his thanks in this connection, particularly to Mr. P.J. Moss, whose regular assistance alleviated considerably the problem of enlisting help during testing and who also helped in checking of the typescript.

The research was carried out during the tenure of a Commonwealth Scholarship (U.K. award) and the author is indebted to the donors and to the British Council for the many facilities extended to him. The author also acknowledges his grateful appreciation to the Government of Jamaica for the generous leave facilities granted to enable him to take up the award.

CONTENTS

Abstract 2

Acknowledgements 4

Notation 11

Chapter 1

1.1 : Introduction 14

1.2 : Description of Hyperbolic Paraboloid Shells 14

1.3 : General Approach to Shell Problems 15

1.4 : Scope of Research 19

Chapter 2

2.1 : Review of Theoretical Work 20

2.2 : The Membrane (momentless) Theory 20

2.3 : The Bending Theory 25

2.4 : Approximate Methods 28

2.4a : Hyperbolic Paraboloids supported along parabolic generators. 28

2.4b : Hyperbolic Paraboloid Shells supported along straight line generators. 28

2.5 : Review of Experimental Work 33

2.6 : Discussion of Past Research 38

Chapter 3

3.1 : General 41

3.2 : Differential Equations 42

3.3 : Particular Solutions 47

3.3a : Translational Hyperbolic Paraboloids 47

3.3b : Hyperbolic Paraboloids bounded by straight line generators. 49

3.4 : The Membrane Theory of Ruled Surface Shells 57

3.5 : Approximate solutions for Ruled Surface Shells 62

3.5a : Method by Bleich and Salvadori 62

3.5b : Method by Loof. 78

3.6 : Flat Plate Solutions 105

3.6a : Plate with simply supported edges 105

3.6b : Plate with clamped edges 109

3.6c : Plate simply supported on elastic edges 114

Chapter 4

4.1 : Objects and Design of Experiments 123

4.2 : Description of Shell 125

4.2a : Shell dimensions and materials 125

4.3 : Loading Frame 126

4.4 : Corner Details 127

4.5 : Edge Beam Details 131

4.6 : Tie Bar Details 132

4.6a : Flexible Tie 132

4.6b : Rigid Tie 134

4.7 : Loading Technique 136

4.7a : Uniform Loading and Half Loading 136

4.7b : Edge Loading 139

4.7c : Calibration of Jacks and Pressure Gauges 141

4.8 : Strain Measurement 141

4.9 : Measurement of Deflections 149

Chapter 5

5.1 : Range of Tests 158

5.2 : Tests with Flexible Tie 158

5.2 (1) : Test No.1 - Vertical Shear applied at Edge of Shell 158

5.2 (2) : Test No.2 - Shear and Moment at Edge No.2 159

5.2 (3) : Test No.3 - Uniform Loading over Half of Shell 159

5.2 (4) : Tests Nos.4,5,6 - Uniform Loading with varying Edge Beam Stiffness 159

5.3 : Tests Nos.7,8,9 - Uniform Loading with rigid tie and varying edge beam stiffness 161

5.4 : Test No.10 - Test to Failure 163

5.5 : Testing of Specimens 165

5.5a : Test Slabs 165

5.5b : Test Cubes 170

5.5c : Indirect Tensile Test 170

5.5d : Test on Lee McCall bar 170

Chapter 6

6.1 : Presentation of Results 174

6.2 : Results 176

Chapter 7

7.1 : Discussion of Test Results and Observations. 246

7.1.1 : Edge Loading 246

7.1.2 : Half Loading 247

7.1.3 : Uniform Loading 247

7.1.3a : Actions 247

7.1.3b : Displacements 251

7.1.3c : Corner Movements 252

7.1.3d : Separation of Edge Beam and Tie Bar Influences. 253

7.1.3e : Tie Bar Force 256

7.1.4 : Test to Failure 257

7.2 : General Remarks 258

7.2.1 : Linearity and Symmetry in Tests 258

7.2.2 : Loading System 259

7.2.3 : Strain Gauges 260

7.3 : Comparison of Theoretical and Experimental Results 261

7.3.1 : Extensional Theory 261

7.3.2 : Particular Solution 261

7.3.3 : Approximate Solutions 262

7.3.4 : Plate Solutions 263

Chapter 8

8.1 : Conclusions 266

8.2 : Suggestions for Further Research 268

Appendix

Appendix I : Numerical Calculations based on Loof's Method 270

Appendix II : Further checks on Approximate Methods 292

Bibliography 297

NOTATION

a, b – sides of shell (or plate) rectangular in plan.

d – extension of tie bar

e – exponential function

h – shell rise

i – $\sqrt{-1}$

k, K – constant

l, l_α, l_β – span of shell

m, n – number of terms in series

n_α, $n_{\alpha\beta}$, n_β – extensional actions

m_α, $m_{\alpha\beta}$, m_β, q_α, q_β – flexural actions

q, Q – normal edge shear per unit length of shell or plate

r – vertical edge shear per unit length of shell

t – thickness

u, u_α, u_β, u_γ – displacements

u, w – displacements (plate theory)

x, y, z – suitable orthogonal cartesian coordinates

Λ – constant; also magnification factor when dealing with disturbances.

C – foundation modulus

D – $\frac{Et^3}{12}$ for shell or plate

E, E_b - Young's modulus of shell and beam, respectively

F_1, F_2, F_3, F_4 - functions

$G_\alpha, G_\beta, G_\gamma$ - applied pressures

I, I_b - moments of inertia

$K_\alpha, K_{\alpha\beta}, K_\beta$ - curvatures

M - moments

N - direct forces

$R_\alpha = 1/K_\alpha$

$R_{\alpha\beta} = 1/K_{\alpha\beta}$

$R_\beta = 1/K_\beta$

S_b - area of edge beam

α, β - orthogonal curvilinear coordinates on middle surface of shell.

γ - direction mutually perpendicular to α, β set.

$\varepsilon_\alpha, \varepsilon_{\alpha\beta}, \varepsilon_\beta$ - extensional strains

λ - parameter. (reciprocal of characteristic length in theory of beam on elastic foundation.)

μ - parameter

φ - any stress function; also phase angle

$$\nabla_R^2 = \left[\frac{\partial^2 z}{\partial y^2} \cdot \frac{\partial^2}{\partial \alpha^2} - 2\frac{\partial^2 z}{\partial x \partial y} \frac{\partial^2}{\partial \alpha \partial \beta} + \frac{\partial^2 z}{\partial x^2} \frac{\partial^2}{\partial \beta^2} \right]$$

$$\nabla_R^4 = \nabla_R^2 \nabla_R^2$$

$$\nabla_r^2 = \left[\frac{\partial^2 z}{\partial y^2} \frac{\partial^2}{\partial \alpha^2} + \frac{\partial^2 z}{\partial x^2} \frac{\partial^2}{\partial \beta^2} \right]$$

$$\nabla_r^4 = \nabla_r^2 \nabla_r^2$$

$$\nabla_1^4 = \frac{\partial 4}{\partial \alpha^4} + 2\frac{\partial 4}{\partial \alpha^2 \partial \beta^2} + \frac{\partial^4}{\partial \beta^4}$$

$$\nabla_1^8 = \nabla_1^4 \nabla_1^4$$

CHAPTER 1

1.1 INTRODUCTION

The advantages of the use of shell roofs to cover large areas have long been recognized. Formerly, such structures were restricted mainly to domes and cylindrical shells; but, recently, much attention has been paid to other shells of double curvature and in particular, to hyperbolic paraboloid shells. The popularity of this type of shell is due to the exciting architectural possibilities it has to offer, as well to the ease of construction resulting from the fact that the surface can be generated by a system of straight lines.

It is unfortunate that the development of the analysis relating to shell problems has not kept pace with the structural development of shells. Even in cases for which solutions have been found the labour involved in the computations is considerable. However, with the development of the electronic computer this drawback has been removed, and the problem now consists mainly in achieving realistic solutions of a particular problem.

1.2 DESCRIPTION OF HYPERBOLIC PARABOLOID SHELLS

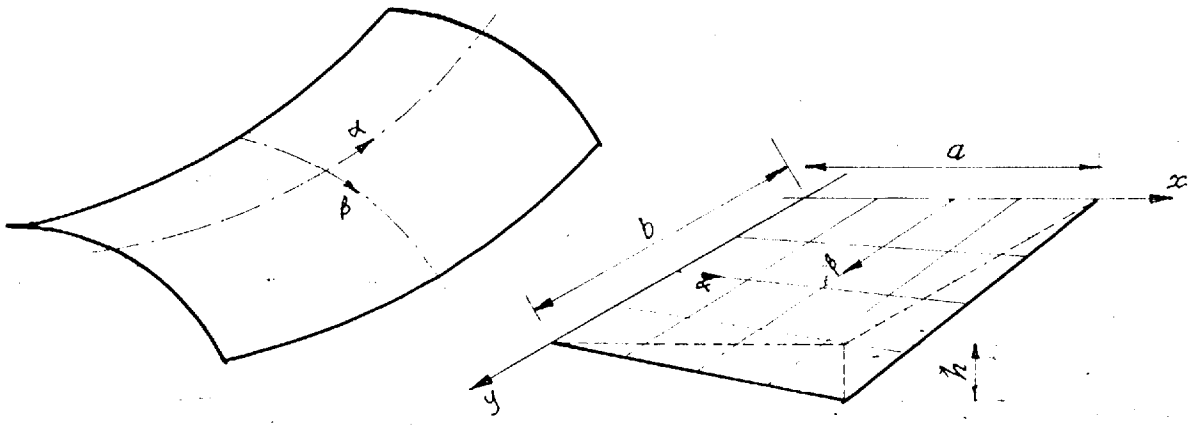
The work in this thesis is concerned with the hyperbolic

paraboloid shell. The hyperbolic paraboloid is the surface generated when a parabola translates on another parabola, their curvatures being opposite in sign. Thus, the product of the principal curvatures, known as the Gaussian Curvature, is a negative quantity; and such shells are therefore referred to as shells of negative Gaussian Curvature.

The classification of hyperbolic paraboloid shells, for purposes of this thesis, is based on the shape of the edges. In translational shells (Fig. 1.1 (a)), the edges coincide with the parabolic generators of the surface, while ruled surface shells are bounded by straight lines. The basic unit of the ruled surface shell is shown on Fig. (1.1 (b)), from which it can be seen that the ruled surface may also be generated by a straight line traversing two other skewed straight lines. There are many ways in which this basic unit may be combined; some of these are shown in Fig. (1.2). Type 1.2 (c) is the one on which the tests reported in this thesis were carried out.

1.3 GENERAL APPROACH TO SHELL PROBLEMS

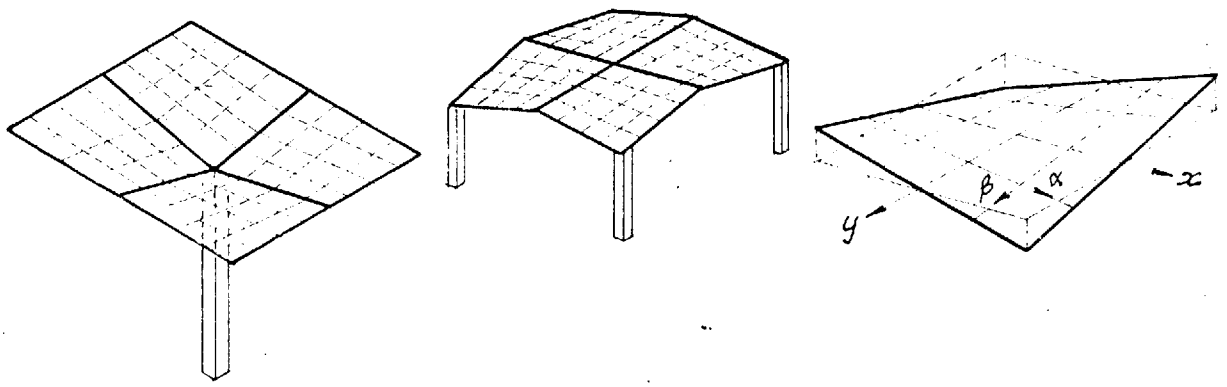
Early attempts at shell analysis were based on the momentless theory, admitting in some cases the existence of bending moments in the edge regions of the shell. However, the limitations of this theory could not be tolerated for long, and hence a general theory has been developed in which bending effects are taken into account. The problem



a. TRANSLATIONAL SURFACE

b. RULED SURFACE

FIG. 1.1



a. b. c.

EXAMPLES OF RULED SURFACE SHELLS

FIG. 1.2.

is necessarily made more complicated and in many cases simplifications have to be introduced in order to achieve a solution.

In applying the momentless theory to the hyperbolic paraboloid shell, there results a second order partial differential equation of hyperbolic type which corresponds to an initial value problem requiring great care with respect to boundary conditions. Generally, these conditions cannot be satisfactorily met, and it is therefore necessary to apply the more complicated bending theory from the beginning. Even then, realistic solutions have been obtained only in the case of translational shells with certain types of edge structure. In the case of hyperbolic paraboloids supported along their straight line generators, no known direct solution exists by which realistic boundary conditions can be satisfied; it is then necessary to introduce approximations in order to arrive at some solution.

The general bending theory of doubly curved shells involving finite displacements yields two fourth order non-linear partial differential equations. On neglecting the non-linear terms the resulting equations can be combined to give an eighth order linear partial differential equation. The non-homogeneous form of this equation gives a solution for surface loading; and any solution thus obtained is called a Particular solution. If the particular solution also satisfies all the boundary conditions, it then becomes the complete solution of the problem. In general, however, this will not be the case, and in order

to satisfy the boundary conditions actions and displacements have to be applied at the edges of the shell. Such actions and displacements are referred to as edge disturbances, and are obtained by considering the complementary solution resulting from the homogeneous form of the eighth order equation. For this reason such a solution is often called the Edge disturbance solution.

An edge disturbance diminishes with increasing distance from the edges; when rapid damping takes place the phenomenon is known as the edge effect. In many cases the momentless solution is a good approximation as a particular solution, and in considering the complementary solution, approximations may be made which effectively reduce the order of the equation and consequently the number of boundary conditions to be satisfied. In view of the requirement of rapid damping associated with the typical edge effect problem it follows that this state of stress is represented by large roots of the characteristic equation. In shells of positive Gaussian curvature an approximation method separates the problem into two parts - a second order elliptic equation (momentless solution) requiring one boundary condition at each edge, and a fourth order equation for which two boundary conditions are specified at each edge, thus simplifying the problem considerably. In hyperbolic paraboloid shells, however, the hyperbolic nature of the equation of the momentless solution precludes the above simplification.

The validity of approximations introduced into the analysis may be checked by controlled tests. Such tests are of particular

significaance in cases where no exact theories have been developed, and may be useful in providing answers to such questions as the relative importance of parameters, effects of edge beams, and importance of different boundary conditions.

1.4 SCOPE OF RESEARCH

1) To study the effects of certain types of edge loading on Ruled Surface shells.

2) Investigation of the Stress Distribution of Ruled Surface shells under uniform loading, with varying edge beam stiffness and tie bar stiffness.

3) To investigate the behaviour of a ruled surface shell tested to failure under uniform loading.

In all cases, comparisons are made between experimental results and those obtained from known approximate solutions.

It was found convenient to adapt the loading system to test the shell under uniform loading over half of the surface, and the results for this case are also reported.

CHAPTER 2

2.1 REVIEW OF THEORETICAL WORK

The Elastic analysis of doubly curved shells is dealt with, special emphasis being placed on shallow, thin shells of negative Gaussian curvature. The historical development is considered under the following headings.

a) The Membrane (Momentless) Theory.

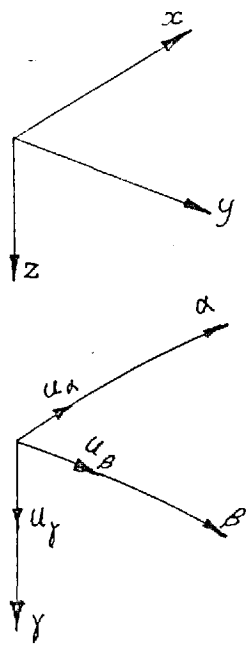
b) The Bending Theory.

c) Approximate Theory.

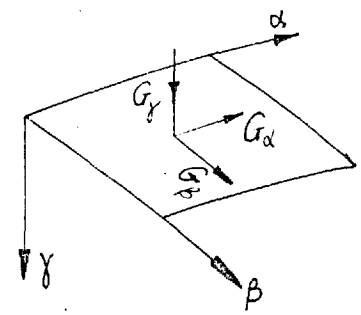
Coordinate axes and loading convention are shown in Figs. (2.1) and (2.2), and (1.1)

2.2. THE MEMBRANE (MOMENTLESS) THEORY

In this context the membrane theory refers to considerations in which the shell is assumed to have negligible bending stiffness. Strictly speaking, the term "momentless" theory should be applied when shells of finite thickness are being considered. As this theory is old, the literature in this field is prolific. When applied to doubly curved shells the following equation is obtained for normal loading :



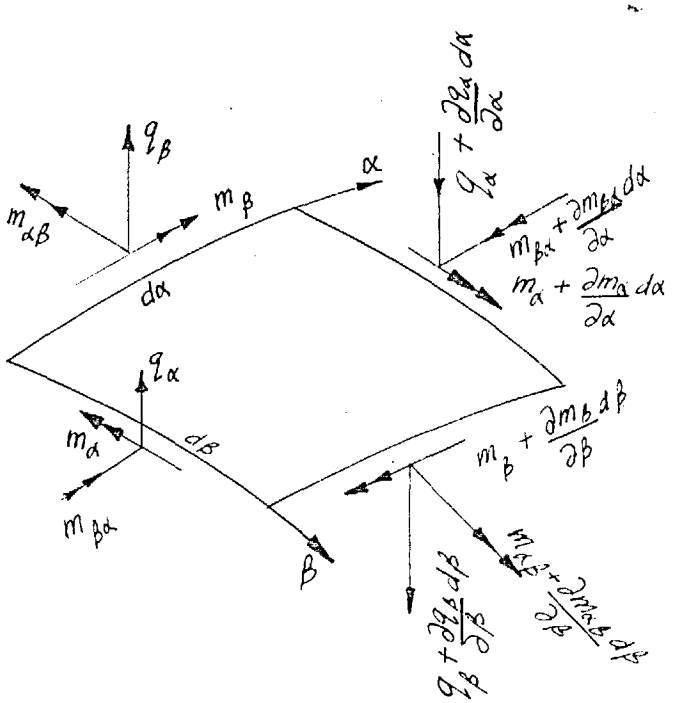
AXES AND DISPLACEMENTS



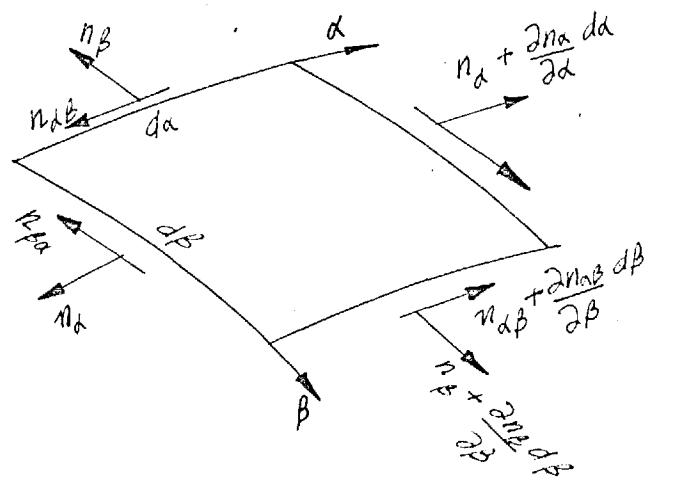
LOADS

AXES
DISPLACEMENTS
AND LOADS

FIG. 2.1



NORMAL INTERNAL ACTIONS.



TANGENTIAL INTERNAL ACTIONS.

POSITIVE ACTIONS

FIG. 2.2.

$$\nabla_R^2 \phi + q_\gamma = 0 \qquad ..(2.1)$$

where ϕ = Airy Stress Function,

$$\nabla_R^2 = \frac{\partial^2 z}{\partial y^2}\frac{\partial^2}{\partial \alpha^2} - 2\frac{\partial^2 z}{\partial x \partial y}\frac{\partial^2}{\partial \alpha \partial \beta} + \frac{\partial^2 z}{\partial x^2}\frac{\partial^2}{\partial \beta^2}$$

In the case of elliptic paraboloid shells whose middle surface is given by :-

$$2z = \frac{x^2}{a^2} + \frac{y^2}{b^2}$$

the equation (2.1) becomes elliptic, and behaves reasonably when boundary conditions are taken into account. In the case of translational hyperbolic paraboloid shells described by :-

$$2z = \frac{x^2}{a^2} - \frac{y^2}{b^2}$$

or of Ruled Surface shells having the equation :-

$$z = kxy$$

equation (2.1) becomes hyperbolic, and as such requires much caution with respect to boundary conditions.

The behaviour of equation (2.1) when applied to shell theory, has been studied by Flugge and Geyling[1]. They have shown that for the elliptic paraboloid shell with simple boundaries the solution is reasonably correct over a large area of the shell. However, when

translational hyperbolic paraboloid shells are considered, it is shown that inextensional deformations are obtained when the ratio $\frac{b}{a}$ has a critical value - a condition which exists for most values of this ratio. When the shell is submitted to normal loading, the solution obtained exhibits severe discontinuities which make such a solution unrealistic. Recourse must therefore be made to the bending theory in order to eliminate these discontinuities.

The momentless theory of Hyperbolic Paraboloid shells, bounded by straight line generators, has been dealt with by several writers including Parme[2] and Vreedenburgh[15] who have suggested that, statically, these shells may be analysed by assuming that the load is divided between a system of intersecting arches and catenaries. The resulting stress system yields compressive forces in the arch direction and tensile forces in the catenary direction. These forces when combined give constant shear $n_{\alpha\beta}$ throughout the shell. This can also be deduced more directly from equation (2.1) by observing that for the Shallow Ruled Surface Shell :-

$$K_\alpha \frac{\partial^2 z}{\partial x^2} = 0 \; ; \quad K_\beta \frac{\partial^2 z}{\partial y^2} = 0 \; ; \quad K_{\alpha\beta} = \frac{\partial^2 z}{\partial x \partial y} = k$$

Hence $$2k \cdot \frac{\partial^2 \phi}{\partial\alpha\partial\beta} = G_\gamma$$

But by definition $$n_{\alpha\beta} = \frac{\partial^2 \phi}{\partial\alpha\partial\beta}$$

Hence $$n_{\alpha\beta} = \text{constant} = \frac{G_\gamma}{2k}$$

The momentless theory of ruled surface shells involving finite displacements has been dealt with by Tottenham[29]. After deriving the two governing non-linear equations, he suggests how variational and successive approximation methods may be applied to solve these equations.

2.3 THE BENDING THEORY

The work in this field for doubly curved shells follows the theory developed by Marguerre in 1938 and later by Vlasov[3] in 1944, which yields two non-linear fourth order partial differential equations. There is no known direct method of solution for such equations, and the tendency has therefore been to disregard the non-linear terms. Thus, Vlasov[3] reduces these equations to the following forms in considering normal loading G_γ.

$$\left.\begin{aligned} \nabla_1^4 \phi + Et \nabla_R^2 u_\gamma &= 0 \\ \nabla_R^2 \phi - \frac{Et^3}{12} \nabla_1^4 u_\gamma &= -G_\gamma \end{aligned}\right\} \quad ..(2.2)$$

where t = thickness of shell

E = Young's modulus of shell material

$$\nabla_1^4 = \frac{\partial^4}{\partial x^4} + 2\frac{\partial^4}{\partial \alpha^2 \partial \beta^2} + \frac{\partial^4}{\partial \beta^4}$$

Vlasov took the α and β coordinates as coinciding with the lines of principal curvature of the middle surface prior to deformation.

Munro[5] derives the General Eighth Order equation for the Linear Analysis of thin, shallow shells in the form :-

$$\nabla_1^8 n_\beta + \frac{12}{t^2}\nabla_R^4 n_\beta = \frac{12}{R_\alpha t^2}\nabla_R^2 \frac{\partial G_\alpha}{\partial \alpha} -$$

$$- \frac{12}{R_\alpha t^2}\nabla_R^2 \frac{\partial G_\beta}{\partial \beta} + \frac{24}{R_{\alpha\beta} t^2}\nabla_R^2 \frac{\partial G_\beta}{\partial \alpha} -$$

$$- \frac{12}{t^2}\nabla_R^2 \frac{\partial^2 G_\gamma}{\partial \alpha^2} + \nabla_1^4 \frac{\partial^3 G_\alpha}{\partial \alpha \partial \beta^2} - \nabla_1^4 \frac{\partial^3 G_\beta}{\partial \beta^3}$$

$$- 2\nabla_1^4 \frac{\partial^3 G_\beta}{\partial \alpha^2 \partial \beta} \qquad ..(2.3)$$

where:

$$\nabla_R^4 = \nabla_R^2 \nabla_R^2$$

$$\nabla_1^8 = \nabla_1^4 \nabla_1^4$$

He employs curvilinear coordinates set on the middle surface of the shell and formed by the projection of the x-y set of a suitable orthogonal Cartesian triad, and derives the Vlasov Equation (2.2) in terms of this curvilinear coordinate system. Particular integral solutions of equation (2.3) are then obtained for translational and ruled surface shells and these compared with the corresponding particular solutions from the membrane theory. Finally, it is shown that in the case of translational shells the particular solution becomes the complete solution when the shell is supported along its parabolic generators by deep, thin, inextensible gables. However, for ruled surface shells supported on their straight line generators a set of unrealistic boundary conditions are necessary for the particular solution to be regarded as the complete solution. For this type of shell, therefore, it is essential to obtain a complementary solution if realistic boundary conditions are to be satisfied.

Ambartsumyan[6] converts the Vlasov equations for thin shallow shells into a different form and employs a stress-displacement function to obtain a solution for translational shells subjected to normal loading and having simply supported boundaries. He expresses the loading in the form of a double Fourier Series and then, following a method first suggested by Khachaturyan, separates the plate solution from the shell solution, thus taking advantage of the rapid convergence of the remainder. A numerical example of an elliptic paraboloid shell is worked out.

After following a method similar to that of Ambartsumyan, Flugge and Conrad[7] give results of worked examples of shells of positive and negative Gaussian Curvature under concentrated load. They infer, in particular, that the stiffness of the hyperboloid is roughly equal to that of the flat plate.

Bouma[8] uses a Levy Type Solution for the complementary function of the eight order equation resulting from the combination of the Vlasov equations (2.2), applied to shells of positive, zero and negative Gaussian Curvature. This solution therefore requires that the shell be supported on deep, thin, inextensible gables on at least two opposite parabolic edges.

As in Bouma's work, a Levy Type solution has been applied by Apeland[10] to solve translational shells supported on two opposite parabolic edges. An influence coefficient method, whereby edge

disturbances are conveniently studied, is developed for solving actual boundary conditions along the other two opposite edges. By plotting the real roots of the characteristic equation against certain shell parameters, it is shown that edge disturbances in hyperbolic paraboloid shells are damped at a much slower rate than shells of positive Gaussian Curvature.

2.4 APPROXIMATE METHODS

2.4a HYPERBOLIC PARABOLOIDS SUPPORTED ALONG PARABOLIC GENERATORS.

After carrying out an exact analysis Bouma[8] approximates the roots of the auxilliary equation of the elliptic and hyperbo paraboloid translational shells. He shows that the method of analysis whereby a solution is obtained by the combination of the membrane theory and the theory of the elastically supported beam is applicable only to the elliptic paraboloid shells supported on four shear diaphragms. An approximate method for use in other cases is suggested.

2.4b HYPERBOLIC PARABOLOID SHELLS SUPPORTED ALONG STRAIGHT LINE GENERATORS.

In considering these shells, Reissner[13] in the first instance, assumes the existence of the typical edge effect. He analyses these

effects for the shell supported on deep, thin, inextensible structures, and concludes that such effects are admissible provided that the ratio of the shell thickness to shell rise is small. However, the bending and membrane stresses in the edge zones are shown to be of comparable order. He points out, however, that the obvious criticism of this approach is the fact that the considerations leading to his conclusions are not rigorous, since it has been assumed that outside the edge zones only the membrane state of stress exists.

Gerard[12] has obtained solutions for three types of Ruled Surface Shells supported on straight lines. The displacement components u_α, u_β, u_γ are assumed in the form of polynomials, which satisfy the boundary conditions only partially. Although Equilibrium conditions are not fulfilled he applies energy methods to determine the constants of the displacement components, and points out that the results of the solution for one type of shell considered compare very favourably with test results. A serious criticism of Gerard's work, is that in meeting boundary conditions he considers the mean value of an error function, instead of the preferable method of minimising the square of this function.

Das Gupta[11] expresses in non-dimensional form the two fourth order equations governing the bending of a Ruled Surface shell. Using Finite Difference methods he obtains a solution for clamped edges and remarks that the results are in agreement with those obtained

from a test reported by Jones[20]. The method could be extended to deal with flexible edges, and more accurate results in the important edge regions, could be achieved by using a closer mesh in these regions.

The Levy Type solution used by Apeland and Popov[9] for translational shells is extended to deal with hyperbolic paraboloids supported on their straight line generators. However, in order to achieve a solution, a set of unrealistic boundary conditions are assumed along one pair of opposite edges. Despite this fact the method proves convenient for studying edge disturbances emanating from the other two edges.

An attempt to study the effects of bending disturbances at the edges of Ruled Surface Shells has been made by Bleich and Salvadori[14] who use Energy Methods to derive the three governing equations. For $G_\alpha = G_\beta = 0$, and assuming the solution in the form $u_\alpha = u_\beta = 0$ the three equations reduce to one similar to that for the plate supported on an elastic foundation. The reduction of this equation to one similar to that of the elastically supported beam is effected by assuming that the disturbances in coordinate directions are independent of each other. As in Reissner's[13] work, the membrane and bending stresses are shown to be of the same order in the edge regions of the shell.

In a brief discussion of bending effects in Ruled Surface

Shells, Vreedenburgh[15], in a manner similar to that of Bleich and Salvadori, reduces the eighth order homogeneous equation to a fourth order one similar to that of the elastically supported beam. It is suggested that for this purpose the shell may in a small region be regarded as a translational surface of circles having radii equal to the principal radii of curvature.

With the assumption that $u_\alpha = u_\beta = 0$, Munro[28] applies the variational method due to Kantarovitch to solve, for certain boundary conditions, the fourth order equation obtained for the hyperbolic paraboloid shell bounded by straight line generators. He compares these solutions with that of the ordinary differential equation resulting when it is assumed that the typical edge effect phenomenon is present, and then shows that the solution obtained for the partial differential equation by using polynomial functions is dependent on the selected polynomial. His work includes the application of Rayleigh functions to solve the fourth order equation by the methods due to Galerkin and Kantarovitch.

In applying an extended Levy Type Solution to a hyperbolic paraboloid shell supported along straight lines, Loof[16] assumes the following boundary conditions:

$$1)\quad u_\alpha = u_\beta = u_\gamma = 0 \quad \text{at all edges}$$

$$2)\begin{cases} \text{(a)}\ u_\alpha = n_\beta = u_\gamma = 0 \quad \text{on } \beta \text{ edges} \\ \text{(b)}\ u_\beta = n_\alpha = u_\gamma = 0 \quad \text{on } \alpha \text{ edges} \end{cases}$$

Also $$\frac{\partial u_\alpha}{\partial \alpha} = 0\ , \qquad \frac{\partial u_\beta}{\partial \beta} = 0 \quad \text{at midpoint of edges}$$

These boundary conditions are more realistic than those used by Apeland and Popov[9], since tangential shear stresses are transmitted to the boundaries. A modified collocation method is used to satisfy the four boundary conditions at six points in the interval of one-half edge and the resulting 24 equations solved on a computer. The behaviour of the edge moment is then examined for large values of a shell parameter, which reveals that the two sets of boundary conditions assumed yield almost identical results. Further, the moments display a highly damped character.

He, therefore, infers the negligible effect of transverse displacement at the edges, and then considers bending disturbances from one edge only, independent of effects from adjacent edges. The results of this approximation give very good agreement with those obtained from the more elaborate collocation method. A rapid method is also proposed for dealing with such factors as tie bar extension and edge beam movements. In this thesis an attempt is made to check the vaidity of this approximate method against test results.

2.5 REVIEW OF EXPERIMENTAL WORK

Up to the present time, very few tests have been reported on shells of negative Gaussian Curvature, and the majority of such tests have been carried out on models as an aid the design of prototype shells.

Leicester and Massey[18] have described tests on a 1 : 16 scaled model of a system of hyperbolic paraboloid shells consisting of six "petals" resting on six supports. The model was made from polyester resin. The results presented are not sufficiently detailed to permit general conclusions. However, they did indicate the presence of quite large bending moments even in regions well removed

from the boundaries of the shell. There was also a marked tendency for the actions to concentrate towards the low corners of the model. An attempt was made by the authors - though with only qualified success - to compare results from the model test with the actual behaviour of the full scale structure.

Flint[19a] has reported tests on a $\frac{1}{8}$ scaled model of one of a set of five separate quasi-hyperbolic paraboloid shells. Different loading conditions were investigated. Their results show that the stresses were not in agreement with the membrane theory, the deformation of the boundaries playing an apparently significant role in the shell behaviour.

A series of tests carried out on three scaled models of hyperbolic paraboloid shells supported on their straight line generators is reported by Rowe[19b]. One of the structures was a multi-shell in the form of an inverted umbrella and another in the form of a grillage of beams. Finally, a shell without edge beams was tested for research purposes. In the multi-shell test, asymmetrical and edge loadings were considered. No attempt was made to compare any of the results with a bending theory, but they showedthat the bending stresses were of the same order as the membrane stresses even at points well removed from the edges. Generally, the membrane theory proved unsatisfactory in predicting the behaviour of these shells.

Included in the report by Rowe[19b] was a test on a one-tenth scale model of a hyperbolic paraboloid shell on straight line generators. The test has been more fully reported by Jones[20]. The model represented one-quarter of the actual structure and as in the prototype the edges were thickened. Two $1\frac{1}{8}$" dia. Lee McCall Bars were used to simulate rigid abutments. Here again, the test showed that bending stresses in the interior of the shell were of the same order as the membrane stresses, both types of stresses increasing rapidly in the vicinity of the edges. An interesting point brought out, was that although the tangential shear stress ($n_{\alpha\beta}$) was not constant throughout the shell, its magnitude in the interior was in reasonable agreement with its value from the membrane theory. This theory, however, when applied to parts near the edges gave results very different from those obtained in the test. The actions tended to concentrate towards the low corners; and the important influence of size of tie bar was bourne out. The main criticism is that the boundary conditions in the model did not conform to those of the prototype. Hence much caution must be exercised when predicting behaviour of the latter from those of the former, since boundary conditions are of such great importance in this type of shell.

Iauletta[19c] reports tests carried out on a brick hyperbolic paraboloid shell supported on straight line generators. The tests were intended to study the statics of this type of shell under uniformly distributed loading. The author infers that the shell behaviour

differed considerably from that predicted by the membrane theory, and approached that of a plate. Another important conclusion is that the state of stress was not influenced to a great extent by change in the rigidity of the edge beam. This, incidentally, was not bourne out in similar tests, reported in this thesis, in which the edge beam rigidity exerted considerable influence on the shell behaviour. On the basis of his test results, Laulotta has proposed an approximate method of design whereby the entire load is assumed carried by the arches having downward concavity, with their ends regarded as hinged. The Bending Moments are then approximately assessed by assuming that the curve of pressure in these arches scarcely reaches the extremity of the inertia's kern.

The first systematic tests reported on shells of negative Gaussian Curvature were made by Munro and Ahuja[19d and 21]. Tests were conducted on two types of hyperbolic paraboloid shells of reinforced concrete mortar, both shells having approximately similar dimensions. The first shell, $8' - 10\frac{1}{4}''$ x $8' - 0''$ x $0.78''$ thick and supported on parabolic generators, was constructed to simulate simply supported boundaries and was tested under various loading conditions. The second shell 8' square, $\frac{3}{4}''$ thick, was supported along straight lines by flexible steel edge beams, and was constructed in such a manner that vertical and horizontal displacements could be imposed at the corners of the shell. Studs were incorporated

in the flexible edge beams, so that edge stiffness could be varied by affixing additional edge beams. In the first shell shrinkage was significant, mainly because of its considerable effect on shell geometry. The main object of the test on the translational shell was to check whether by expressing uniform normal loading in the form of a double Fourier Series the particular solution obtained could be regarded as the complete solution as is the case in theory. It was found that the displacements obtained experimentally showed quite good agreement with theory except near the corners where non-linear tendencies were evident. Test moments and forces, however, did not show such good agreement. The Ruled Surface shell was tested with imposed horizontal and vertical displacements at the low corners and under uniform vertical loading. It was shown also that the shell displacements were almost entirely dependent on the horizontal stiffness of the low corners; and that therfore any form of solution for this shell which does not attempt to satisfy the corner conditions, could not be regarded as satisfactory.

In continuation of the Series of tests being carried out at the Imperial College of Science and Technology, in connection with shells of negative Gaussian Curvature, Scrivener [23] tested a reinforced cement morter hyperbolic paraboloid shell $8' - 10\frac{1}{2}'' \times 7' - 4'' \times \frac{3}{4}''$ thick, and bounded on parabolic generators. The tests were intended to check whether the Levy Type Solution for these shells as reported by Bouma [8] is satisfactory. Thus two opposite edges of the shell were

supported on supports which simulated deep, thin, inextensible diaphragms, while different boundary conditions could be imposed along the other two edges, each of which took the form of a flexible steel edge beam provided with studs to take additional stiffening beams. The experiments showed that the size and shape of the edge beams had considerable effect on the shell behaviour and that any attempt to analyse this type of structure by the membrane theory alone would be grossly inadequate under the boundary conditions of the tests. From the point of view of displacements the theory predicted reasonably the behaviour of the shell.

2.6 DISCUSSION OF PAST RESEARCH

The majority of tests reported so far have been carried out on models as an aid to design. Therefore, these tests were designed to favour investigation of parameters appropriate to the particular problem under consideration. Although the results from such tests have been of great value to the designer, especially in cases where no exact theories exist, it is difficult to formulate on such basis any theory for a problem consisting of so many parameters.

The inadequacy of the membrane theory for shells of negative Gaussian curvature has been confirmed by tests. In some cases, this theory gives an indication of the magnitude of shell stresses in the interior of the shell, but proves useless in the important edge

regions. Only in isolated cases was the typical edge effect observed experimentally. In the majority of the tests the moments, for instance, tended to increase away from the edges of the shell, instead of being rapidly damped.

There were several problems common to all experiments in which electrical resistance strain gauges were used. Their behaviour, particularly in connection with their use on concrete shells, has been so erratic, that any conclusions based on forces and moments deduced from these gauges have been made with much reservation. The formulation of a theory from such results would, therefore, be open to question.

It appears that, as yet, no satisfactory theory exists for hyperbolic paraboloid shells supported on straight line generators and having realistic boundary conditions. All tests on such shells confirm the tendency for the load to be carried by the supports at the low corners. The important influences of corner stiffness, tie bar stiffness, and horizontal foundation movements, on this type of shell, have been amply bourne out by tests. It is significant that the test reported by Lauletta[19c] reveal the relative unimportance of edge beam stiffness; the opposite effect has been observed in tests carried out by the author.

Solutions have been obtained for hyperbolic paraboloid shells supported on their parabolic generators, with simple supports on all

four edges or on two opposite edges only. So far only two sets of experiments have been reported for this type of shell, and the experimental results agree reasonably with theory.

CHAPTER 3

3.1 GENERAL

In the following the general linear theory of shallow, doubly curved, thin shells of constant thickness, and having middle surface of second order, is considered. Particular emphasis is paid to shells of negative Gaussian curvature with special reference to those bounded by straight line generators.

The Coordinate system shown in Figs. (2.1) and (2.2) is that used by Munro[5]

x, y, z is a suitable orthogonal cartesian system

α, β are the curvilinear coordinates on the middle surface of the shell, obtained by projection of the x, y set.

γ is the direction perpendicular to the (α, β) set. In the case of shallow shells, the (α, β, γ) set may be regarded as orthogonal.

For second order surfaces $\frac{\partial^2 z}{\partial x^2}$, $\frac{\partial^2 z}{\partial y^2}$, $\frac{\partial^2 z}{\partial x \partial y}$ have constant values everywhere on the surface, and in the case of shallow

shells the following approximations are valid :-

$$\frac{1}{R_\alpha} = K_\alpha \simeq \frac{\partial^2 z}{\partial x^2}$$

$$\frac{1}{R_\beta} = K_\beta \simeq \frac{\partial^2 z}{\partial y^2}$$

$$\frac{1}{R_{\alpha\beta}} = K_{\alpha\beta} = \frac{\partial^2 z}{\partial x \partial y}$$

where $K_{\alpha\beta}$ = the twist.

R_α and R_β are the radii of curvature of the middle surface in the α and β directions, respectively.

The second order surfaces considered are the hyperbolic paraboloids given as :-

Translational Surface : $2z = \frac{x^2}{a^2} - \frac{y^2}{b^2}$

Ruled Surface : $z = kxy$

3.2 DIFFERENTIAL EQUATIONS

Munro[5] has shown how to derive a linearly independent set

of eleven equations in terms of the eleven variables shown in Fig. (2.1), in which the positive directions and axes are also indicated.

u_α , u_β , u_γ are displacements of the middle surface.

All forces and moments are given per unit length of shell measured in curvilinear coordinate directions.

n_α , n_β , $n_{\alpha\beta}$ are tangential forces.

q_α , q_β are normal shear forces.

m_α , m_β , $m_{\alpha\beta}$ are moments.

G_α , G_β , G_γ are loads per unit area of shell surface.

The eleven equations derived, after neglecting second order terms in expressions obtained from the equilibrium, strain-displacement and stress-strain relations are :-

$$\frac{\partial n_\alpha}{\partial \alpha} + \frac{\partial n_{\alpha\beta}}{\partial \beta} + G_\alpha = 0 \qquad ..(3.1)$$

$$\frac{\partial n_{\alpha\beta}}{\partial \alpha} + \frac{\partial n_\beta}{\partial \beta} + G_\beta = 0 \qquad ..(3.2)$$

$$\frac{\partial m_\alpha}{\partial \alpha} + \frac{\partial m_{\alpha\beta}}{\partial \beta} - q_\alpha = 0 \qquad ..(3.3)$$

$$\frac{\partial m_{\alpha\beta}}{\partial \alpha} + \frac{\partial m_{\beta}}{\partial \beta} - q_{\beta} = 0 \qquad ..(3.4)$$

$$\frac{\partial q_{\alpha}}{\partial \alpha} + \frac{\partial q_{\beta}}{\partial \beta} + \frac{n_{\alpha}}{R_{\alpha}} + \frac{2n_{\alpha\beta}}{R_{\alpha\beta}} + \frac{n_{\beta}}{R_{\beta}} + G_{\gamma} = 0 \qquad ..(3.5)$$

$$n_{\alpha} = Et\left(\frac{\partial u_{\alpha}}{\partial \alpha} - \frac{u_{\gamma}}{R_{\alpha}}\right) \qquad ..(3.6)$$

$$n_{\alpha\beta} = \frac{Et}{2}\left(\frac{\partial u_{\beta}}{\partial \alpha} + \frac{\partial u_{\alpha}}{\partial \beta}\right) - Et\,\frac{u_{\gamma}}{R_{\alpha\beta}} \qquad ..(3.7)$$

$$n_{\beta} = Et\left(\frac{\partial u_{\beta}}{\partial \beta} - \frac{u_{\gamma}}{R_{\beta}}\right) \qquad ..(3.8)$$

$$m_{\alpha} = -\frac{Et^3}{12}\,\frac{\partial^2 u_{\gamma}}{\partial \alpha^2} \qquad ..(3.9)$$

$$m_{\beta} = -\frac{Et^3}{12}\,\frac{\partial^2 u_{\gamma}}{\partial \alpha \partial \beta} \qquad ..(3.10)$$

$$m_{\beta} = -\frac{Et^3}{12}\,\frac{\partial^2 u_{\gamma}}{\partial \beta^2} \qquad ..(3.11)$$

where t = shell thickness

E = Youngs modulus for the shell material

In this thesis only normal loading G_{γ} is considered, i.e., $G_{\alpha} = G_{\beta} = 0$

The eleven equations above, may be combined (5) to give the following eighth order linear equation in terms of n_{β} :-

$$\nabla_1^8 n_\beta + \frac{12}{t^2}\nabla_R^4 n_\beta = -\frac{12}{t^2}\nabla_R^2 \frac{\partial^2 G_\gamma}{\partial \alpha^2} \qquad ..(3.12)$$

where $\nabla_1^8 = \nabla_1^4 \nabla_1^4$

and $\nabla_1^4 = \frac{\partial^4}{\partial \alpha^4} + 2\frac{\partial^4}{\partial \alpha^2 \partial \beta^2} + \frac{\partial^4}{\partial \beta^4}$

The eighth order equation in terms of u_γ, can also be derived as two fourth order equations, viz :-

$$\nabla_R^2 \phi - \frac{Et^3}{12}\nabla_1^4 u_\gamma = -G_\gamma \qquad ..(3.13)$$

$$\nabla_1^4 \phi + Et\,\nabla_R^2 u_\gamma = 0 \qquad ..(3.14)$$

where $\nabla_R^2 = \frac{1}{R_\beta}\frac{\partial^2}{\partial \alpha^2} - \frac{2}{R_{\alpha\beta}}\frac{\partial^2}{\partial \alpha\, \partial \beta} + \frac{1}{R_\alpha}\frac{\partial^2}{\partial \beta}$

ϕ is the Airy Stress Function defined as :

$$n_\alpha = \frac{\partial^2 \phi}{\partial \beta^2}, \quad n_\beta = \frac{\partial^2 \phi}{\partial \alpha^2}, \quad n_{\alpha\beta} = -\frac{\partial^2 \phi}{\partial \alpha \partial \beta}$$

In the case where the α and β axes coincide with the lines of principal curvature, the equations (3.13) and (3.14) give the Vlasov equations

$$\nabla_r^2 \phi - \frac{Et^3}{12}\nabla_1^4 u_\gamma = -G_\gamma \qquad ..(3.15)$$

$$\nabla_1^4 \phi + Et \nabla_r^2 u_\gamma = 0 \qquad ..(3.16)$$

where $$\nabla_r^2 = \frac{1}{R_\beta} \frac{\partial^2}{\partial \alpha^2} + \frac{1}{R_\alpha} \frac{\partial^2}{\partial \beta^2}$$

Bouma[8] further combines these equations to give :-

$$\frac{Et^3}{12} \nabla_1^8 u_\gamma + Et \nabla_r^4 u_\gamma = \nabla_1^4 G_\gamma \qquad ..(3.17)$$

or $$\frac{Et^3}{12} \nabla_1^8 \phi + Et \nabla_r^4 \phi = - Et \nabla_r^2 G_\gamma \qquad ..(3.18)$$

where $$\nabla_r^4 = \nabla_r^2 \nabla_r^2$$

Equations (3.15) - (3.18) apply to translational shells bounded by parabolic generators.

More generally, equations (3.13) and (3.14) combine to give :-

$$\frac{Et^3}{12} \nabla_1^8 u_\gamma + Et \nabla_R^4 u_\gamma = \nabla_1^4 G_\gamma \qquad ..(3.19)$$

For Ruled Surface Shells :-

$$\nabla_R^2 = - 2 K \frac{\partial^2}{\partial \alpha \partial \beta}$$

$$\nabla_R^4 = 4 K^2 \frac{\partial^4}{\partial \alpha^2 \partial \beta^2}$$

and equation (3.19) becomes :-

$$\frac{Et^3}{12}\nabla_1^8 u_\gamma + 4\,Et\,K^2\,\frac{\partial^4 u_\gamma}{\partial\alpha^2\partial\beta^2} = \nabla_1^4 G_\gamma \qquad ..(3.20)$$

3.3 PARTICULAR SOLUTIONS

3.3a Translational Hyperbolic Paraboloids

A particular solution of equation (3.12) is obtained by expressing the loading G_γ in the form :-

$$G_\gamma = \sum_{p=1,3,5}\sum_{q=1,3,5} Z \cos m\alpha \cos n\beta \qquad ..(3.21)$$

where $m = \frac{p\pi}{l_\alpha}$, $n = \frac{q\pi}{l_\beta}$ (p and q odd)

and l_α, l_β are the spans in the α and β directions respectively.

$$Z = \frac{4}{l_\alpha l_\beta}\int_{-\frac{l_\alpha}{2}}^{\frac{l_\alpha}{2}}\int_{-\frac{l_\beta}{2}}^{\frac{l_\beta}{2}} G_\gamma(\alpha,\beta)\cos\frac{p\pi\alpha}{l_\beta}\cos\frac{q\pi\beta}{l_\beta}\,d\alpha\,d\beta$$

$$= \frac{4}{l_\alpha l_\beta}\int_{-\frac{l_\alpha}{2}}^{\frac{l_\alpha}{2}}\int_{-\frac{l_\beta}{2}}^{\frac{l_\beta}{2}} G_\gamma(\alpha,\beta)\cos m\alpha\cos n\beta\,d\alpha\,d\beta$$

For uniform loading G_Y :-

$$Z = \frac{4G_Y}{l_\alpha l_\beta} \int_{-\frac{l_\alpha}{2}}^{\frac{l_\alpha}{2}} \int_{-\frac{l_\beta}{2}}^{\frac{l_\beta}{2}} \text{Cos } m\alpha \text{ Cos } n\beta \, d\alpha \, d\beta$$

which gives :-

$$Z = \frac{16G_Y}{\pi^2 pq} \qquad (\text{p and q odd})$$

Taking the first term of the series gives :-

$$Z = \frac{16G_Y}{\pi^2}$$

Since for <u>translational shells</u> : $\frac{1}{R_{\alpha\beta}} = 0$, then :-

$$\nabla_R^2 = \nabla_r^2 = \frac{1}{R_\beta} \frac{\partial^2}{\partial\alpha^2} + \frac{1}{R_\alpha} \frac{\partial^2}{\partial\beta^2}$$

Equation (3.21) with (3.12) give the particular solution for such shells as :-

$$n_\beta^{\,o} = - \left[\frac{\frac{12m^2}{t^2} \left(\frac{m^2}{R_\beta} + \frac{n^2}{R_\alpha} \right)}{(m^2 + n^2)^4 + \frac{12}{t^2} \left(\frac{m^2}{R_\beta} + \frac{n^2}{R_\alpha} \right)^2} \right] Z \cos m\alpha \text{ Cos } n\beta$$

On examining the forms of the corresponding particular solutions for the other actions and displacements it is observed that the expressions for u_γ, n_α, n_β, n_α and n_β vanish at all edges, while u_α and u_β vanish at the β and α edges respectively. It follows, therefore, that the set of boundary conditions necessary for the particular solution to become the complete solution, are realistic in the case of shells supported along their parabolic generators. These conditions are met by deep, thin inextensible gable supports on all four edges of the shell. The tests carried out by Ahuja[21] confirm that the behaviour of such shells with the above boundary conditions, is reasonably predicted by the particular solution.

3.3b Hyperbolic Paraboloids bounded by Straight line generators

The particular solution of (3.12) becomes :-

$$n_\beta^{\,o} = \frac{-\frac{24}{t^2}\, K_{\alpha\beta}\, m^3 n}{c} \; Z \sin m\alpha \sin n\beta \qquad ..(3.23)$$

where

$$c = (m^2 + n^2)^4 + 48\, \frac{K_{\alpha\beta}^2}{t^2}\, m^2 n^2$$

Eliminating $n_{\alpha\beta}$ from equations (3.1) and (3.2), and substituting in (3.23), gives :-

$$\frac{\partial^2 n_\alpha^{\,o}}{\partial \alpha^2} = \frac{\partial^2 n_\beta^{\,o}}{\partial \beta^2} = \frac{24\, K_{\alpha\beta}^{\,2}\, m^3\, n^3\, Z \sin m\alpha \sin n\beta}{t^2 C}$$

$$n_\alpha^{\,o} = -\frac{24}{t^2}\,\frac{K_{\alpha\beta}\, m\, n^3}{C}\, Z \sin m\alpha \sin n\beta$$

From equation (3.8) with $G_\beta = 0$:-

$$\frac{\partial^2 n_{\alpha\beta}^{\,o}}{\partial \alpha} = -\frac{\partial n_\beta^{\,o}}{\partial \beta} = \frac{24}{t^2}\,\frac{K_{\alpha\beta}\, m^3\, n^2}{C}\, Z \sin m\alpha \cos n\beta$$

$$n_{\alpha\beta}^{\,o} = \frac{24\, K_{\alpha\beta}\, m^2\, n^2}{t^2 C}\, Z \cos m\alpha \cos n\beta$$

Putting $\frac{1}{R_\alpha} = 0$ in (3.6) :-

$$\frac{\partial u_\alpha}{\partial \alpha} = \frac{n_\alpha^{\,o}}{Et}$$

$$u_\alpha^{\,o} = \frac{24\, K_{\alpha\beta}\, n^3}{Et^3 C}\, Z \cos m\alpha \sin n\beta$$

From equation (3.6) :-

$$\frac{\partial u_\beta}{\partial \beta} = \frac{n_\beta}{Et}$$

$$u_\beta^{\,o} = \frac{24\, K_{\alpha\beta}\, m^3}{Et^3 C}\, Z \sin m\alpha \cos n\beta$$

Equations (3.6) and (3.8) combine to give :-

$$Et \nabla_R^2 \frac{\partial^2 u_\gamma}{\partial a^2} = - \nabla_L^4 n_\beta$$

i.e. $$- 2Et K_{\alpha\beta} \frac{\partial^2}{\partial\alpha\partial\beta} \frac{\partial^2 u_\gamma}{\partial a^2} = - \frac{24}{t^2} \frac{K_{\alpha\beta} m^3 n}{C} (m^2 + n^2) Z \sin m\alpha \sin n\beta$$

$$u_\gamma^{\,o} = \frac{12}{Et^3} \frac{(m^2 + n^2)^2}{C} Z \cos m\alpha \cos n\beta$$

Moments are obtained by differentiation from equations (3.9) - (3.11) as follows :-

$$m_\alpha^{\,o} = \frac{m^2(m^2 + n^2)^2}{C} Z \cos m\alpha \cos n\beta$$

$$m_\beta^{\,o} = \frac{n^2(m^2 + n^2)^2}{C} Z \cos m\alpha \cos n\beta$$

$$m_{\alpha\beta}^{\,o} = - \frac{mn(m^2 + n^2)^2}{C} Z \sin m\alpha \sin n\beta$$

Now, on examining the above expressions for actions and displacements, it is seen that for the particular solution to become a complete solution the following boundary conditions must be satisfied :-

At $\alpha = \pm \frac{l_\alpha}{2}$ $\quad u_\gamma = 0$

At $\beta = \pm \frac{l_\beta}{2}$ $\quad u_\gamma = 0$

$$n_\alpha = \frac{\partial^2 u_\gamma}{\partial \alpha^2} = 0 \qquad n_\beta = \frac{\partial^2 u_\gamma}{\partial \beta^2} = 0$$

$$u_\alpha = 0 \qquad u_\beta = 0$$

$$n_{\alpha\beta} = 0 \qquad n_{\alpha\beta} = 0$$

While the first three boundary conditions may together be met in practice, it is difficult to provide for the third and fourth conditions to be fulfilled simultaneously, hence the complementary function must also be determined in order to achieve a complete solution.

The range of edge beams, used in the tests, varied from the very flexible "in-situ" flat section, to the rigid box section, representing almost completely stiff edges. It should therefore be interesting to observe the effect of the changes in the edge structure on the behaviour of the shell to see whether the particular solution is a reasonable complete solution for any of the edge beams.

Although there was a noticeable degree of sagging in the flexible edge beams, due perhaps to shrinkage and dead load, the value of $\Gamma_{\alpha\beta}$ deduced from levels taken by Ahuja[21], after the shell was cured for some time, did not vary appreciably from that obtained from the original shell geometry. The original geometry will therefore be used for calculating actions and displacements as a basis for comparison of theoretical and experimental results.

The loading q_γ is taken as 45 lb/ft^2 = .3125 lb/in^2.

$$K_{\alpha\beta} = \frac{7}{48 \times 48} = 3.038\ 194 \times 10^{-3}\ \text{in}^{-1}$$

$$K_{\alpha\beta}^2 = 9.261\ 005 \times 10^{-6}$$

$$m = n = \frac{\pi}{96} = 3.2725 \times 10^{-2}$$

$$m^2 = n^2 = 10.709\ 256 \times 10^{-4}$$

$$m^3 = n^3 = 3.504\ 60 \times 10^{-4}$$

$$m^2 n^2 = m^4 = 1.146\ 882 \times 10^{-6}$$

$$(m^2 + n^2)^2 = 4m^4 = 4.587\ 528 \times 10^{-6}$$

$$(m^2 + n^2)^4 = 21.045\ 413 \times 10^{-12}$$

$$E = 4.8 \times 10^6 \qquad t = 0.75"$$

$$Et = 3.6 \times 10^6 , \qquad Et^3 = 2.025\ 000 \times 10^6$$

$$C = (m^2 + n^2)^4 + \frac{48\ K_{\alpha\beta}^2}{t^2}\ m^2 n^2$$

$$C = 21.045\ 413 \times 10^{-12} + \frac{48 \times 9.261\ 005 \times 10^{-6} \times 1.146\ 882 \times 10^{-6}}{.5625}$$

which gives :-

$$C = 927.394\ 633 \times 10^{-12}$$

$$w_\gamma^{\ o} = \frac{12}{Et^3} \frac{(m^2 + n^2)^2}{C} Z \cos mx \cos n\beta$$

$$= \frac{12}{2.025 \times 10^{6} \times 927.394\ 633 \times 10^{-12}} \times 4.587\ 528 \times 10^{-6}\ Z \cos m\alpha \ \cos n\beta$$

which gives :-

$$u_{\gamma}^{o} = .029\ 314\ Z \cos m\alpha \ \cos n\beta$$

$$n_{\beta}^{o} = \frac{\frac{-24}{t^2} K_{\alpha\beta} m^3 n}{C} Z \sin m\alpha \ \sin n\beta$$

$$= \frac{-24 \times 3.038\ 194 \times 10^{-3} \times 1.146\ 882 \times 10^{-6}}{0.5625 \times 927.394\ 633 \times 10^{-12}} Z \sin m\alpha \ \sin n\beta$$

$$n_{\beta}^{o} = -.160\ 309\ Z \sin m\alpha \ \sin n\beta$$

$$n_{\alpha}^{o} = -\frac{24}{t^2} \frac{K_{\alpha\beta} m n^3}{C} Z \sin m\alpha \ \sin n\beta$$

$$n_{\alpha}^{o} = -.160\ 309\ Z \sin m\alpha \ \sin n\beta$$

$$n_{\alpha\beta}^{o} = \frac{24}{t^2} \frac{K_{\alpha\beta} m^2 n^2}{C} Z \cos m\alpha \cos n\beta$$

$$n_{\alpha\beta}^{o} = .160\ 309\ Z \cos m\alpha \ \cos n\beta$$

$$u_{\alpha}^{o} = \frac{24}{mt^3} \frac{K_{\alpha\beta} n^3}{C} Z \cos m\alpha \ \sin n\beta$$

$$= \frac{24 \times 3.038\ 194 \times 10^{-3} \times 3.504\ 60 \times 10^{-5}}{2.025\ 000 \times 10^{6} \times 927.394\ 633 \times 10^{-12}} Z \cos m\alpha \ \sin n\beta$$

$$u_{\alpha}^{o} = .136\ 074 \times 10^{-2}\ Z \cos m\alpha \ \sin n\beta$$

$$u_\beta^{\,o} = \frac{24}{Et^3}\,\frac{K_{\alpha\beta}\,m^3}{C}\,Z\ \mathrm{Sin}\,m\alpha\ \mathrm{Cos}\,n\beta$$

$$u_\beta^{\,o} = .136\,074 \times 10^{-2}\ Z\ \mathrm{Sin}\,m\alpha\ \mathrm{Cos}\,n\beta$$

$$m_\alpha^{\,o} = \frac{m^2(m^2+n^2)^2}{C}\,Z\ \mathrm{Cos}\,m\alpha\ \mathrm{Cos}\,n\beta$$

$$= \frac{10.709\,256 \times 10^{-4} \times 4.587\,528 \times 10^{-6}}{927.394\,633 \times 10^{-2}}\,Z\ \mathrm{Cos}\,m\alpha\ \mathrm{Cos}\,n\beta$$

$$m_\alpha^{\,o} = 5.29753\ Z\ \mathrm{Cos}\,m\alpha\ \mathrm{Cos}\,n\beta$$

$$m_\beta^{\,o} = \frac{n^2(m^2+n^2)^2}{C}\,Z\ \mathrm{Cos}\,m\alpha\ \mathrm{Cos}\,n\beta$$

$$m_\beta^{\,o} = 5.29753\ Z\ \mathrm{Cos}\,m\alpha\ \mathrm{Cos}\,n\beta$$

$$m_{\alpha\beta}^{\,o} = \frac{-mn(m^2+n^2)^2}{C}\,Z\ \mathrm{Sin}\,m\alpha\ \mathrm{Sin}\,n\beta$$

$$m_{\alpha\beta}^{\,o} = -5.29753\ Z\ \mathrm{Sin}\,m\alpha\ \mathrm{Sin}\,n\beta$$

For the first term of the series :-

$$Z = \frac{16}{\pi^2}\,q_\gamma = \frac{16}{\pi^2} \times .3125 = .5066\ \mathrm{lb/in^2}$$

The maximum values of the actions and displacements are given

below :-

n_β^o = - .160 309 Z x 10^3 = - 81.2 lb/in. at corners

n_α^o = - .160 309 Z x 10^3 = - 81.2 lb/in. at corners

$n_{\alpha\beta}^o$ = .160 309 Z x 10^3 = 81.2 lb/in. at centre of shell

= zero at edges

u_α^o = .136 074 x 10^{-2} Z = .6894 x 10^{-3} in. at midspan of edge

u_β^o = " = .6894 x 10^{-3} in. "

u_γ^o = .029314 Z = .0149 in. at centre of shell

m_α^o = 5.29753 Z = 2.684 lb. in./in. "

m_β^o = 5.29753 Z = 2.684 lb. in./in. "

$m_{\alpha\beta}^o$ = - 5.29753 Z = -2.684 lb. in./in. at corners

In comparison, the membrane theory, dealt with in the next section, gives :-

$$\left.\begin{aligned} m_\alpha = m_\beta = m_{\alpha\beta} = 0 \\ n_\alpha = n_\beta = 0 \end{aligned}\right\} \quad \text{at all points on the shell}$$

$$n_{\alpha\beta} = -\frac{G_\gamma}{2K_{\alpha\beta}} = -\frac{.3125}{2 \times 3.038\,194 \times 10^{-3}} = -51.43 \text{ lb/in.}$$

Tie Bar Force = $2\, n_{\alpha\beta} \times 96 \cos 45^{\circ}$ = 6981.3 lbs.

3.4 THE MEMBRANE THEORY OF RULED SURFACE SHELLS

This subject has been covered in some of the references cited in the bibliography. However, the theory will be briefly dealt with here in order to show how the shell should behave if the membrane theory is applicable.

With $G_{\alpha} = G_{\beta} = 0$, and neglecting q_{α} and q_{β}, equations (3.1), (3.2) and (3.5) become :-

$$\frac{\partial n_{\alpha}}{\partial \alpha} + \frac{\partial n_{\alpha\beta}}{\partial \beta} = 0 \qquad ..(3.24)$$

$$\frac{\partial n_{\beta}}{\partial \alpha} + \frac{\partial n_{\beta}}{\partial \beta} = 0 \qquad ..(3.25)$$

$$\frac{n_{\alpha}}{R_{\alpha}} + \frac{\partial n_{\alpha\beta}}{R_{\alpha\beta}} + \frac{n_{\beta}}{R_{\beta}} + G_{\gamma} = 0 \qquad ..(3.26)$$

On introducing Airy's Stress Function ϕ the above equations can be reduced to the form :-

$$\nabla_{R}^{2} \phi + G_{\gamma} = 0 \qquad ..(3.27)$$

The Stress - Displacement equations (3.6) - (3.8) may be combined to give :-

$$\nabla_1^4 n_\beta + Et\nabla_R^2 \frac{\partial^2 u_\gamma}{\partial \alpha^2} = 0 \qquad ..(3.28)$$

or $$\nabla_1^4 \phi + Et\nabla_R^2 u_\gamma = 0 \qquad ..(3.29)$$

It is well known, (e.g. (1)), that this equation (3.27) gives acceptable results when applied to shells of positive Gaussian Curvature; in which case the equation is of elliptic type. In the case of shells of negative Gaussian curvature, the equation becomes a hyperbolic one, and it is difficult for general boundary conditions to be met. The solution of the problem is unrealistic, and it is therefore necessary to apply the bending theory.

In particular, for Ruled Surface Shells,

$$K_\alpha = \frac{1}{R_\alpha} = 0 \,, \qquad K_\beta = \frac{1}{R_\beta} = 0 \qquad \text{and}$$

equation (3.27) becomes :-

$$-2K_{\alpha\beta}\frac{\partial^2 \phi}{\partial\alpha\partial\beta} = -G_\gamma$$

or $$\frac{\partial^2 \phi}{\partial\alpha\partial\beta} = \frac{G_\gamma}{2K_{\alpha\beta}} \qquad ..(3.30)$$

$$\frac{\partial \phi}{\partial \alpha} = \frac{G_\gamma}{2K_{\alpha\beta}} \cdot \beta + f(\alpha)$$

$$\phi = \frac{G_\gamma}{2K_{\alpha\beta}} \cdot \alpha\beta + f(\alpha)\, d\alpha + f_2(\beta)$$

The general solution is therefore :-

$$\phi = \frac{G_\gamma}{2K_{\alpha\beta}} \cdot \alpha\beta + f_1(\alpha) + f_2(\beta)$$

where f_1 and f_2 are arbitrary functions of α, and β respectively.

Hence

$$n_\alpha = \frac{\partial^2 \phi}{\partial \beta^2} = \frac{d^2 f_2}{d\beta^2}$$

$$n_\beta = \frac{\partial^2 \phi}{\partial \alpha^2} = \frac{d^2 f_1}{d\alpha^2} \qquad \ldots(3.31)$$

$$n_{\alpha\beta} = -\frac{\partial^2 \phi}{\partial \alpha \partial \beta} = -\frac{G_\gamma}{2K_{\alpha\beta}}$$

In this resultant simple stress system the action n_α, for example, is constant along a particular generator (α), and only varies along the other generator (β). Thus, if at any edge $\alpha = \frac{1_\alpha}{2}$, it is specified that $n_\alpha = 0$ (flexible edge

beam) then it follows that n_α vanishes throughout the shell. The corresponding result also holds for n_β, so that, in the case of flexible edge beams, $n_\alpha = n_\beta = 0$ over the entire shell. In this case the resulting stress system is given by :-

$$\left.\begin{aligned} n_{\alpha\beta} &= -\frac{G_Y}{2K_{\alpha\beta}} \\ n_\alpha &= n_\beta = 0 \end{aligned}\right\} \qquad ..(3.32)$$

It would appear that by trimming the edges of the shell in such a manner that the supportingstructure is able to resist the tangential shear forces $n_{\alpha\beta}$; the membrane state of stress can be achieved. However, if the deformations of the shell and of the edges are such that continued fit is not ensured, then disturbances in the membrane state of stress will develop. This is generally the case in practice.

For purposes of comparison with results of the tests carried out, some important points regarding the membrane behaviour of Ruled Surface Shells are summarised :-

1) When the membrane state of stress exists the tangential stress resultant acting in the direction of a generator is constant along that genorator.

2) The action n_α (or u_β) may assume any arbitrary value

along a particular generator, provided that this arbitrary value is also prescribed at the edges of the shell. In the case of stiff edge beams, for example, since n_α and n_β are not zero at the edges, then these stress resultants should have a value, along a generator, equal to that at the edges. In the case of flexible edge beams (n_α and $n_\beta = 0$ at the edges), these stress resultants should vanish throughout the shell.

3) If the conditions in (3.32) are fulfilled (flexible edge beams) then at an angle of 45° to the generators the principal stress resultants (tension or compression) are everywhere numerically equal to $n_{\alpha\beta}$.

4) As with other shells, in general, the membrane theory admits of small deflections and bending moments,

3.5 APPROXIMATE SOLUTIONS FOR RULED SURFACE SHELLS

It appears that no satisfactory theory has yet been evolved for hyperbolic paraboloid shells bounded by straight line generators, and having realistic boundary conditions. However, a number of attempts have been made at approximate solutions (e.g. [14], [15], [16]). Immediately it must be pointed out that in all cases the boundary conditions assumed in order to achieve a solution, are not realistic. The method proposed by Loof[16] considers approximately the effect of edge beam deformation.

It may, however, be instructive to compare the experimental behaviour of the shell with that predicted from the approximate solutions and for this reason the latter are now considered.

3.5 a Method by Ekelch and Salvadori

The governing equations have been derived by Ekelch and Salvadori[14], using energy methods. These equations are derived below from the set of equations (3.1) - (3.11) for the ruled surface given by :-

$$z = Rxy$$

From equations (3.6), (3.7), (3.8) and (3.1) :-

$$\frac{\partial^2 u_\alpha}{\partial \alpha^2} + \frac{1}{2}\left(\frac{\partial^2 u_\beta}{\partial \alpha \partial \beta} + \frac{\partial^2 u_\alpha}{\partial \beta^2}\right) + G_\alpha = 0 \qquad ..(3.33)$$

$$\frac{\partial^2 u_\beta}{\partial \beta^2} + \frac{1}{2}\left(\frac{\partial^2 u_\beta}{\partial \alpha^2} + \frac{\partial^2 u_\alpha}{\partial \alpha \partial \beta}\right) + G_\beta = 0 \qquad ..(3.34)$$

Equations (3.3) and (3.4) combine with (3.9) - (3.11) to give :-

$$\frac{\partial q_\alpha}{\partial \alpha} + \frac{\partial q_\beta}{\partial \beta} + \frac{Et^3}{12} \nabla_1^4 u_\gamma = 0 \qquad ..(3.35)$$

From (3.35) and (3.5), putting $\frac{1}{R_\alpha} = \frac{1}{R_\beta} = 0$:-

$$\frac{Et^3}{12} \nabla_1^4 u_\gamma - \frac{2n_{\alpha\beta}}{R_{\alpha\beta}} - G_\gamma = 0 \qquad ..(3.36)$$

Substituting from (3.7) into (3.36) gives :-

$$\nabla_1^4 u_\gamma - \frac{12}{t^2} R\left(\frac{\partial u_\beta}{\partial \alpha} + \frac{\partial u_\alpha}{\partial \beta}\right) + \frac{24}{t^2} K^2 u_\gamma = \frac{12}{Et^3} G_\gamma \qquad ..(3.37)$$

Now consider equations (3.33), (3.34) and (3.37) with the solution given by :-

$$u_\alpha = u_\beta = 0, \text{ assuming } G_\alpha = G_\beta = 0.$$

Then (3.33) and (3.34) are satisfied, while (3.37) yields :-

$$\nabla_1^4 u_\gamma + \frac{24}{t^2} K^2 u_\gamma = \frac{12}{Et^3} G_\gamma \qquad ..(3.38)$$

Equation (3.38) is similar in form to that for a plate supported on an elastic foundation, viz:-

$$\nabla_1^4 u_\gamma + \frac{K}{D} u_\gamma = \frac{12}{Et^3} G_\gamma \qquad ..(3.39)$$

which shows that under the assumed conditions the equation for the shallow shell can be deduced from that for the elastically supported plate.

The particular solution of (3.38) is taken in the form :-

$$u_\gamma^{\,o} = \frac{G_\gamma}{2Et K^2} \qquad ..(3.40)$$

If further u_γ is to be zero at the edges of the shell, then by eliminating $u_\gamma^{\,o}$ at the edges bending disturbances are introduced in the shell. Also, if it is assumed that these bending disturbances in a direction at right angles to an edge are affected only to a small extent by those parallel to the edge (i.e. $\frac{\partial^2 u_\gamma}{\partial \beta^2} \ll \frac{\partial^2 u_\gamma}{\partial \alpha^2}$) then equation (3.38) reduces to :-

$$\frac{d^4 u_\gamma}{d\alpha^4} + \frac{24}{t^2} K^2 u_\gamma = \frac{12}{Et^3} G_\gamma \qquad ..(3.41)$$

$$\text{or} \quad \frac{d^4 u_\gamma}{d\alpha^4} + 4\delta^4 u_\gamma = \frac{12}{Et^3} q_\gamma \qquad ..(3.42)$$

where $4\delta^4 = \frac{24R^2}{t^2}$ and $\delta = 1.56\sqrt{\frac{R}{t}}$

It is now seen that equation (3.42) is similar to that for a beam on elastic foundation. The solution of this equation appears in many standard textbooks, e.g. Timoshenko[27].

For the hyperbolic paraboloid shell square in plan equation (3.41) may also be written in the form :-

$$EI \frac{d^4 u_\gamma}{d\alpha^4} + C u_\gamma = q_\gamma \qquad ..(3.43)$$

where C = Foundation Modulus, defined by Vreedenburgh[15]

$= Et(K_1^2 + K_2^2) = 2Et K^2$ in this case.

K_1 and K_2 are local principal curvatures and,

$\frac{t^3}{12} = I$ = Moment of Inertia for unit width of shell.

Equation (3.43) becomes :-

$$\frac{d^4 u_\gamma}{d\alpha^4} + \frac{C u_\gamma}{EI} = \frac{q_\gamma}{Et}$$

or $$\frac{d^4 u_y}{dx^4} + \frac{C}{Et^3/12} = \frac{12\, q_y}{Et^3}$$

By definition, the characteristic length $\frac{1}{\lambda}$ is given by :-

$$\frac{1}{\lambda} = \sqrt[4]{\frac{4Et^3/12}{C}} = \sqrt[4]{\left(\frac{.333Et^3}{2Et\,R^2}\right)}$$

i.e. $$\frac{1}{\lambda} = \frac{0.76\sqrt{t}}{\sqrt[4]{(2R^2)}}$$

or $$\lambda = \frac{\sqrt[4]{2R^2}}{0.76\sqrt{t}}$$

The general solution of equation (3.43) is :-

$$u_y = e^{-\lambda x}(C_1 \cos \lambda x + C_2 \sin \lambda x) + e^{-\lambda x}(C_3 \cos \lambda x + C_4 \sin \lambda x) \quad ..(3.44)$$

where C_1, C_2, C_3 and C_4 are related constants.

If the disturbances from opposite edges are independent of each other, (typical edge effect) then the Constants C_1 and C_2 are zero, and equation (3.44) reduces to :-

$$u_y = e^{-\lambda x}(C_3 \cos \lambda x + C_4 \sin \lambda x) \quad ..(3.45)$$

The boundary conditions to be investigated are those corresponding to hinged edges and clamped edges.

HINGED EDGES

Let P = Shear at Edge. The convention adopted is as shown in Fig. (3.1).

It follows from the definition of Foundation Modulus C that at a great distance from the edge the deflection is given by :-

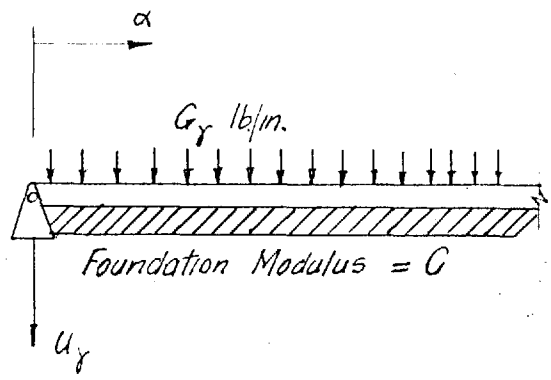
$$u_\gamma^{\,o} = \frac{G_\gamma}{C} \qquad ..(3.46)$$

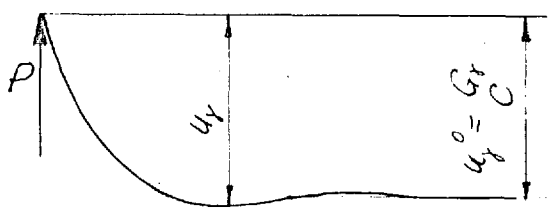
The net deflection u_γ at any point α, may therefore be obtained from the superposition of the constant deflection $u_\gamma^{\,o}$ and the upward deflection caused by the edge shear P alone. Hence the following boundary conditions :-

$$\text{At} \qquad \alpha = 0 : \qquad u_\gamma = 0$$

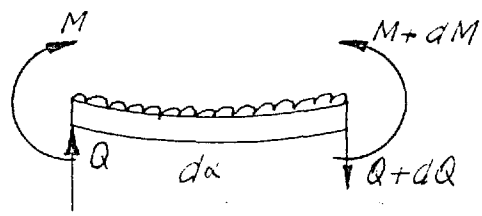
$$\text{Edge Shear} = Q_o = P$$

In the following the solutions for u_γ, P, etc. are derived from expressions given by Hetenyi[25] and Den Hartog[26]. Firstly, the following expressions are defined :-





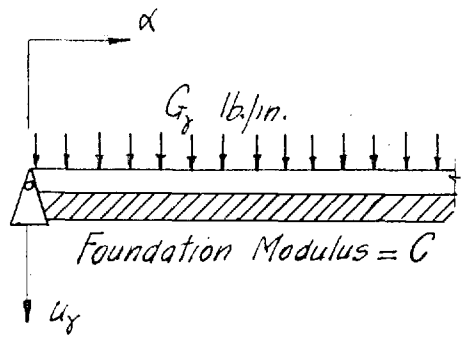
DEFLECTION

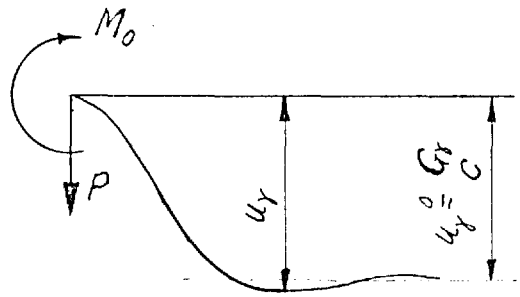


ACTIONS

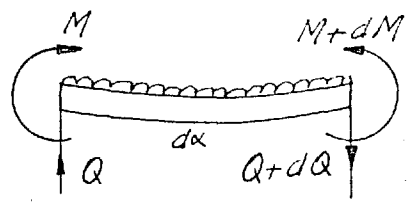
EDGE HINGED

FIG. 3.1.





DEFLECTION



ACTIONS

EDGE CLAMPED

FIG. 3.2

SEMI-INFINITE BEAM ON ELASTIC FOUNDATION

$$F_1(\lambda a) = e^{-\lambda a}(\cos \lambda a + \sin \lambda a) \quad ..(3.47.a)$$

$$F_2(\lambda a) = e^{-\lambda a}(\sin \lambda a) \quad ..(3.47.b)$$

$$F_3(\lambda a) = e^{-\lambda a}(\cos \lambda a - \sin \lambda a) \quad ..(3.47.c)$$

$$F_4(\lambda a) = e^{-\lambda a}(\cos \lambda a) \quad ..(3.47.d)$$

Due to edge shear P :-

$$u_\gamma = -\frac{2\lambda P}{C} F_4(\lambda a) \quad ..(3.48)$$

$$u_{\gamma(net)} = u_\gamma^{\,o} + u_\gamma$$

$$= \frac{G_\gamma}{C} - \frac{2\lambda P}{C} F_4(\lambda a) \quad ..(3.49)$$

From substitution of the boundary conditions :-

$$0 = \frac{G_\gamma}{C} - \frac{2\lambda P}{C} F_4(0)$$

$$\text{Edge Shear} \quad P = \frac{G_\gamma}{2\lambda} \quad ..(3.50)$$

And deflection at any point a is given from (3.49) :-

$$u_\gamma = \frac{G_\gamma}{C} - \frac{G_\gamma}{C} F_4(\lambda a)$$

$$\text{i.e.} \quad u_{\gamma(\text{net})} = \frac{G_\gamma}{C}\left[1 - F_4(\lambda a)\right] \qquad ..(3.51)$$

$$\frac{du_\gamma}{da} = -\frac{G_\gamma}{C}\frac{d}{da}F_4(\lambda a)$$

$$= \frac{G_\gamma \lambda}{C} F_1(\lambda a)$$

$$\text{Moment} = -EI\frac{d^2u_\gamma}{da^2} = 2\lambda^2 G_\gamma \frac{EI}{C} F_2(\lambda a)$$

But by definition $\frac{EI}{C} = \frac{1}{4\lambda^4}$

$$M = \frac{G_\gamma}{2\lambda^2} F_2(\lambda a) \qquad ..(3.52)$$

The maximum B.M. occurs at $\lambda a = \frac{\pi}{4}$, i.e. $a = \frac{\pi}{4\lambda}$.

This gives $F_2(\lambda a) = .3224$

$$\text{Max B.M.} = .3224\frac{G_\gamma}{2\lambda^2} = \frac{0.16\, G_\gamma}{\lambda^2} \qquad ..(3.53)$$

CLAMPED EDGES

This case has been worked by Timoshenko[27]. With the convention shown in Fig. (3.2)

$$u_\gamma = \frac{e^{-\lambda a}}{2\lambda^3 EI}\left[P \cos \lambda a - \lambda M_o (\cos \lambda a - \sin \lambda a) \right]$$

$$\text{i.e.} \quad u_\gamma = \frac{1}{2\lambda^3 EI}\left[P F_4(\lambda a) - \lambda M_o F_3(\lambda a) \right] \qquad ..(3.54)$$

$$\frac{du_\gamma}{da} = -\frac{1}{2\lambda^2 EI}\left[P F_1(\lambda a) - 2\lambda M_o F_4(\lambda a) \right] \qquad ..(3.55)$$

If there were no edgeforces the deflection everywhere would be :-

$$u_\gamma^{\,o} = \frac{G_\gamma}{C} \qquad ..(3.56)$$

Now impose edge actions to bring the resultant deflection, and slope of the edge to zero, i.e., the following boundary conditions :-

$$\left.\begin{array}{lll} \text{At} \quad a = 0 & u_\gamma = -\dfrac{G_\gamma}{C} & \\ & \dfrac{du_\gamma}{da} = 0 & \end{array}\right\} \qquad ..(3.57)$$

Substituting from (3.57) into (3.54) and (3.55) gives :-

$$\left.\begin{array}{l} M_o = -\dfrac{G_\gamma}{2\lambda^2} \\ P = -\dfrac{G_\gamma}{\lambda} \end{array}\right\} \qquad ..(3.58)$$

Combining the Particular solution (3.56) and (3.54) :-

$$u_{y_{(not)}} = \frac{q_y}{c}\left[1 - F_1(\lambda a)\right] \qquad ..(3.59)$$

From (3.59) :-

$$M = -EI\frac{d^2u_y}{da^2}$$

$$M = -\frac{q_y}{2\lambda^2}F_3(\lambda a) \qquad ..(3.60)$$

The expression (3.60) may be written in the form :-

$$M = -\frac{q_y}{2\lambda^2}\sqrt{2}\,e^{-\lambda a}\cos\left(\lambda a + \frac{\pi}{4}\right) \qquad ..(3.61)$$

Equation (3.61) is the expression for M given by Vreedenburgh[15].

N.B.

Two important assumptions have been made in order to arrive at a solution. These are :-

(1) $u_\alpha = u_\beta = 0$ at all edges, which gives a fourth order equation, instead of the eighth order one which would result from combination of equations (3.33), (3.34) and (3.37).

(2) Disturbances from one edge are assumed to be rapidly damped and independent of those emanating from adjacent edges.

This condition could be fulfilled, when considering disturbances from the α-edges, in the case of a rectangular hyperbolic paraboloid shell having the span (l_α) much greater than the other (l_β). By this assumption the partial differential equation is reduced to an ordinary one.

Numerical Calculations From Section (3.3 b)

$K = 3.038\,194 \times 10^{-3}$ in^{-1}

$K^2 = 9.261\,005 \times 10^{-6}$

$C = 2Et\,K^2 = 66.679\,236$ $lb./in^2$.

$$\lambda = \frac{\sqrt[4]{2K^2}}{.76\sqrt{t}} = \frac{\sqrt[4]{18.522\,010 \times 10^{-6}}}{0.76 \times .866025} = 9.9673 \times 10^{-2}$$

$$\frac{G_Y}{\lambda} = \frac{.3125}{.099673} = 3.135\,252$$

$$\frac{G_Y}{2\lambda} = 1.567\,626 \qquad \frac{G_Y}{2\lambda^2} = \frac{.3125}{.019870} = 15.727\,226$$

$$u_Y^{\,o} = \frac{G_Y}{C} = \frac{.3125}{66.679\,236} = .0047 \text{ ins.}$$

Hence the following results :-

CLAMPED EDGES

$$\text{Edge Moment } M_o = \frac{G_\gamma}{2\lambda^2} = 15.73 \text{ lb in./in.}$$

$$M_a = 15.73 \; F_3(\lambda a)$$

$$\text{Edge Shear } Q_o = \frac{G_\gamma}{\lambda} = 3.14 \text{ lb/in.}$$

$$u_\gamma = .0047 \left[1 - F_1(\lambda a) \right]$$

HINGED EDGES

$$M_o = 0$$

$$M_{max} = \frac{.3224 \, G_\gamma}{2\lambda^2} = 5.07 \text{ lb in./in.}$$

$$M_a = 15.73 \; F_2(\lambda a)$$

$$Q_o = \frac{G_\gamma}{2\lambda} = 1.57 \text{ lb/in.}$$

$$u_\gamma^{\,o} = \frac{G_\gamma}{C} = .0047 \text{ ins.}$$

$$u_\gamma = .0047 \left[1 - F_4(\lambda a) \right]$$

The Numerical values of expressions for the actions and

displacements derived in this section have been tabulated in Tables Nos. (1) and (2). They have been plotted in Fig. (3.3). Instead of moments the curves are plotted for differential strains, i.e. $(\varepsilon_1 - \varepsilon_2)$,

where ε_1 = strain in extreme bottom fibre.

ε_2 = strain in extreme top fibre.

$$M = K_1 (\varepsilon_1 - \varepsilon_2) \quad \text{where} \quad K = .2227 \times 10^6$$

In Microstrains, $$\varepsilon_1 - \varepsilon_2 = \frac{M \times 10^6}{222667} = \underline{4.491\ M.}$$

This facilitates comparison with experimental results.

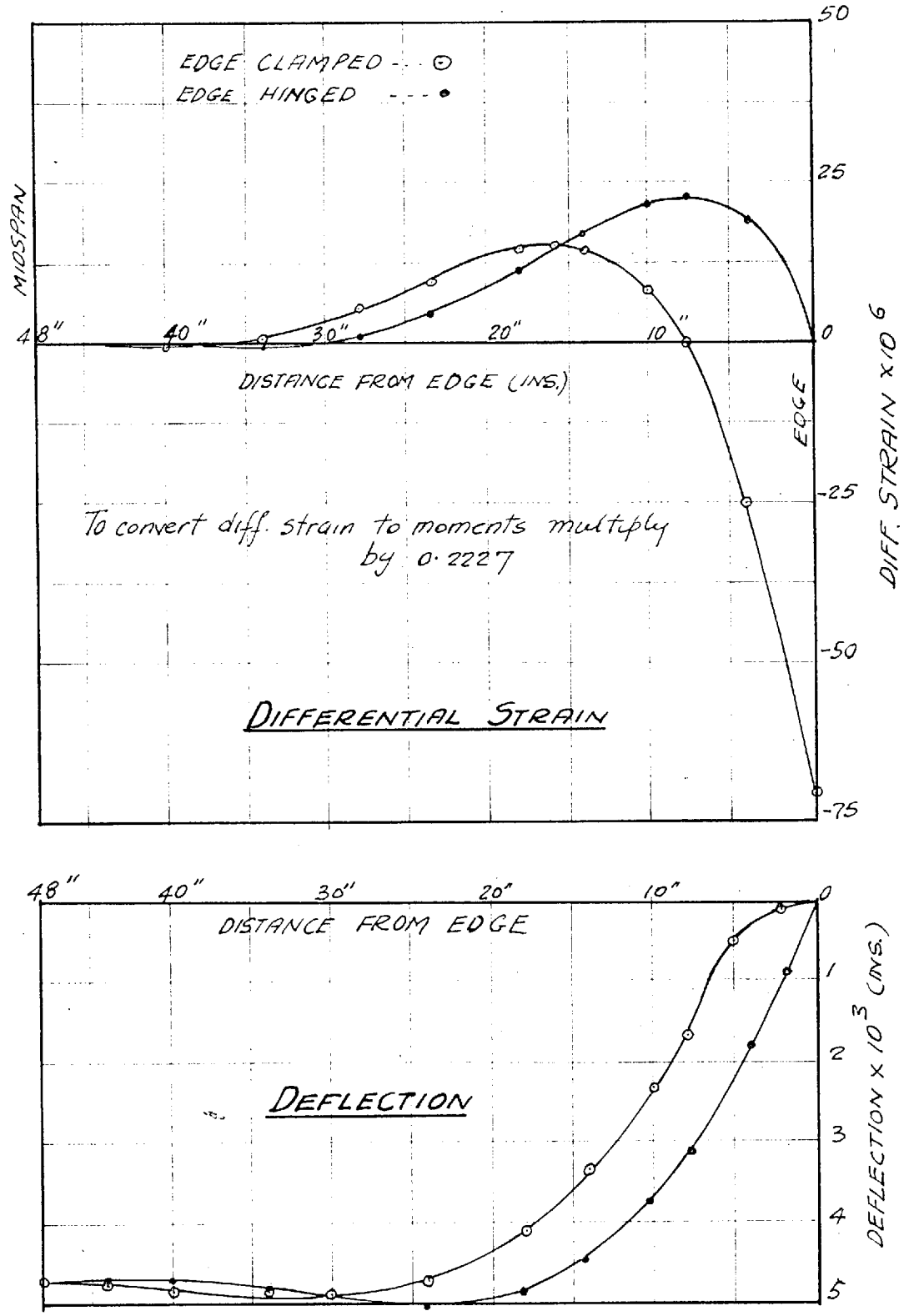
TABLE NO. 1 - MOMENTS

		EDGES CLAMPED			EDGES HINGED		
λa	a(ins) $=10.033\lambda a$	$F_3(\lambda a)$	M_a (lb.in./in)	Diff. strain $(\varepsilon_1-\varepsilon_2)\times10^6$	$F_2(\lambda a)$	M_a (lb.in./in)	Diff. strain $(\varepsilon_1-\varepsilon_2)\times10^6$
0	0	1.000	15.73	70.64	0	0	0
.4	4.013	.356	5.60	25.14	.261	4.14	18.46
$\pi/4$	7.85	0	0	0	.3224	5.07	22.77
.8	8.026	-.009	-0.14	-0.63	.322	5.07	22.77
1.0	10.033	-.111	-1.75	-7.86	.310	4.88	21.92
1.4	14.046	-.201	-3.16	-14.19	.243	3.82	17.16
$\pi/2$	15.70	-.2079	-3.27	-14.69	.2079	3.27	14.69
1.8	18.059	-.199	-3.13	-14.06	.161	2.53	11.36
2.0	20.066	-.179	-2.82	-12.66	.123	1.93	8.67
$3\pi/4$	23.55	-.1342	-2.11	-9.48	.0671	1.06	4.76
2.4	24.079	-.128	-2.01	-9.03	.061	0.96	4.31
2.8	28.092	-.078	-1.23	-5.52	.020	0.31	1.39
3.0	30.099	-.056	-0.88	-3.95	.007	0.11	0.49
3.4	34.112	-.024	-0.38	-1.71	-.009	-0.14	-0.63
3.8	38.125	-.004	-0.06	-0.27	-.014	-0.22	-0.99
4.0	40.132	+.002	+0.03	0.13	-.014	-0.22	-0.99
4.4	44.145	+.008	+0.12	0.53	-.012	-0.19	-0.85
4.8	48.158	+.008	+0.12	0.53	-.008	-0.13	-0.58
5.0	50.165	+.008	+0.12	0.53	-.007	-0.11	-0.49

Note : The sign convention of the moments for clamped edges in the above table is opposite to that used in experiments. To compare theoretical and experimental results, reverse the signs for M above.

TABLE NO. 2 - DEFLECTIONS (u_y)

		EDGES CLAMPED		EDGES HINGED	
$\lambda\alpha$	α	$[1 - F_1(\lambda\alpha)]$	u_y (ins) $= .0047(1-F_1(\alpha))$	$[1 - F_4(\lambda\alpha)]$	u_y (ins.)
0	0	0	0	0	0
0.2		0.035	$.16\times10^{-3}$	0.198	0.93×10^{-3}
0.4	4.016	.122	.57	.385	1.80×10^{-3}
0.6		.237	1.11 "	.547	2.57 "
$\pi/4$	7.85	.3552	1.67 "	.6776	3.18 "
0.8	8.032	.365	1.72 "	.686	3.22 "
1.0	10.04	.492	2.31 "	.801	3.75 "
1.4	14.06	.715	3.36 "	.958	4.50 "
$\pi/2$	15.70	.7921	3.72 "	1.000	4.70 "
1.8	18.07	.877	4.12 "	1.038	4.88 "
2.0	20.08	.933	4.39 "	1.056	4.96 "
2.4	24.10	1.006	4.73 "	1.067	5.01 "
2.8	28.11	1.037	4.87 "	1.057	4.97 "
3.0	30.12	1.042	4.90 "	1.049	4.93 "
3.4	34.14	1.041	4.90 "	1.032	4.85 "
3.9		1.031	4.85 "	1.018	4.78 "
4.0	40.16	1.026	4.82 "	1.012	4.76 "
4.4	44.18	1.016	4.78 "	1.004	4.72 "
4.8	48.20	1.008	4.74 "	.999	4.70 "
5.0	50.21	1.005	4.72 "	.998	4.70 "
∞		1	4.7 "	1	4.70 "



SOLUTION BY BLEICH AND SALVADORI'S METHOD

FIG. 3.3.

3.3 b METHOD BY LOOF

In this method[16], a rather simplified approach has been used in order to achieve a solution of two fourth order equations. The problem will now be examined more fully.

Consider equation (3.19) rewritten below :-

$$\frac{Et^3}{12} \nabla_1^8 u_\gamma + Et \nabla_R^4 u_\gamma = \nabla_1^4 G_\gamma \qquad ..(3.19)$$

By assuming that the bending stiffness of the shell is small, that is $\frac{Et^3}{12} \to 0$, then equation (3.19) becomes :-

$$Et \nabla_R^4 u_\gamma = \nabla_1^4 G_\gamma \qquad ..(3.62)$$

Equation (3.62) can be derived directly from the membrane theory by eliminating ϕ from equations (3.27) and (3.29).

In many shell problems the solution of equation (3.62) may be taken as the particular solution of (3.19). The remainder of the problem then constitutes the solution of the homogeneous form of (3.19), i.e. of the edge disturbance problem represented by :-

$$\frac{Et^3}{12} \nabla_1^8 u_\gamma + Et \nabla_R^4 u_\gamma = 0$$

or

$$\nabla_1^8 u_\gamma + \frac{12}{t^2} \nabla_R^4 u_\gamma = 0 \qquad ..(3.63)$$

The bending effects in Ruled surface shells has been studied by Loof[16] in an approximate method which is more refined than that of Bleich and Salvadori. Again, for purposes of comparison with experimental results the method will be outlined.

Consider equation (3.20), viz :-

$$\frac{Et^3}{12}\nabla_1^8 u_\gamma + 48\frac{k^2}{t^2}\frac{\partial^4 u_\gamma}{\partial\alpha^2\partial\beta^2} = \nabla_1^4 G_\gamma \qquad ..(3.20)$$

The particular solution is taken in the form :-

$$u_\gamma^{\,o} = \frac{G_\gamma}{2Etk^2}$$

In considering the homogeneous form of (3.20) Loof assumes the following solution, which takes symmetry into account :-

$$u_\gamma = \sum A_n\left[\left\{e^{-\rho\beta} + e^{-(1-\beta)}\right\}\sin m\alpha + \left\{e^{-\rho\alpha} + e^{-(1-\alpha)}\right\}\sin m\beta\right] \qquad ..(3.64)$$

where $m = \frac{n\pi}{l}$ $\qquad (n = 1, 3, 5, \text{---})$

The edges are assumed clamped so that :-

$$u_\alpha = u_\gamma = \frac{\partial u_\gamma}{\partial\beta} = 0, \text{ along a } \beta\text{-edge}$$

$$u_\beta = u_\gamma = \frac{\partial u_\gamma}{\partial\alpha} = 0, \text{ along an } \alpha\text{-edge.}$$

The following two alternatives are considered for the fourth boundary condition :-

(1) $u_\beta = 0$ along a β-edge

$u_\alpha = 0$ along an α-edge

(2) $n_\beta = 0$ along a β-edge

$u_\alpha = 0$ along an α-edge

A modified collocation method is then employed to satisfy the boundary conditions at six points within the interval of one-half edge.

The second set of boundary conditions given above are not realistic; but since they permit the transmission of tangential shear at the edges, they are more realistic than those used in Apeland and Popov's work[9].

The solution of the twenty-four equations resulting from the above were carried out by Loof on a computer, and the clamping moment derived at the midpoint of an edge, yields only slightly different results for the alternative sets of boundary conditions. Further the bending moment displays a highly damped character for large values of the parameter $p = \frac{kl^2}{t}$. In view of this it is considered justifiable, in considering a bending disturbance

originating from the midpoint of a β-edge, to take the solution in the form :-

$$w_\gamma = \sum A_n e^{-\rho\beta} \sin m\alpha \qquad ..(3.65)$$

where $m = \frac{n\pi}{l}$ $(n = 1, 3, 5, \text{---})$

and for rapid damping only large values of ρ need be considered. Substituting (3.65) into the homogeneous form of (3.20) gives :-

$$(\rho^2 - m^2)^4 - 48 \frac{K^2}{t^2} m^2 \rho^2 = 0$$

or $$(\frac{\rho^2}{m^2} - 1)^4 - 48 \frac{K^2}{t^2 m^4} (\frac{\rho^2}{m^2}) = 0 \qquad ..(3.66)$$

Equation (3.66) may be written :-

$$\xi^4 - 48 \frac{K^2}{t^2 m^4} (\xi + 1) = 0$$

or $$\xi^4 - A (\xi + 1) = 0 \qquad ..(3.67)$$

$$\left.\begin{aligned} \text{where} \quad \xi &= (\frac{\rho^2}{m^2} - 1) \\ \text{and} \quad A &= \frac{48K^2}{t^2 m^4} \end{aligned}\right\} \qquad ..(3.67.a)$$

The relationship between A and ξ is shown in the graph in Fig. (3.4). In this case equation (3.67) is written in the form :-

$$A = \frac{\xi^4}{1 + \xi}$$

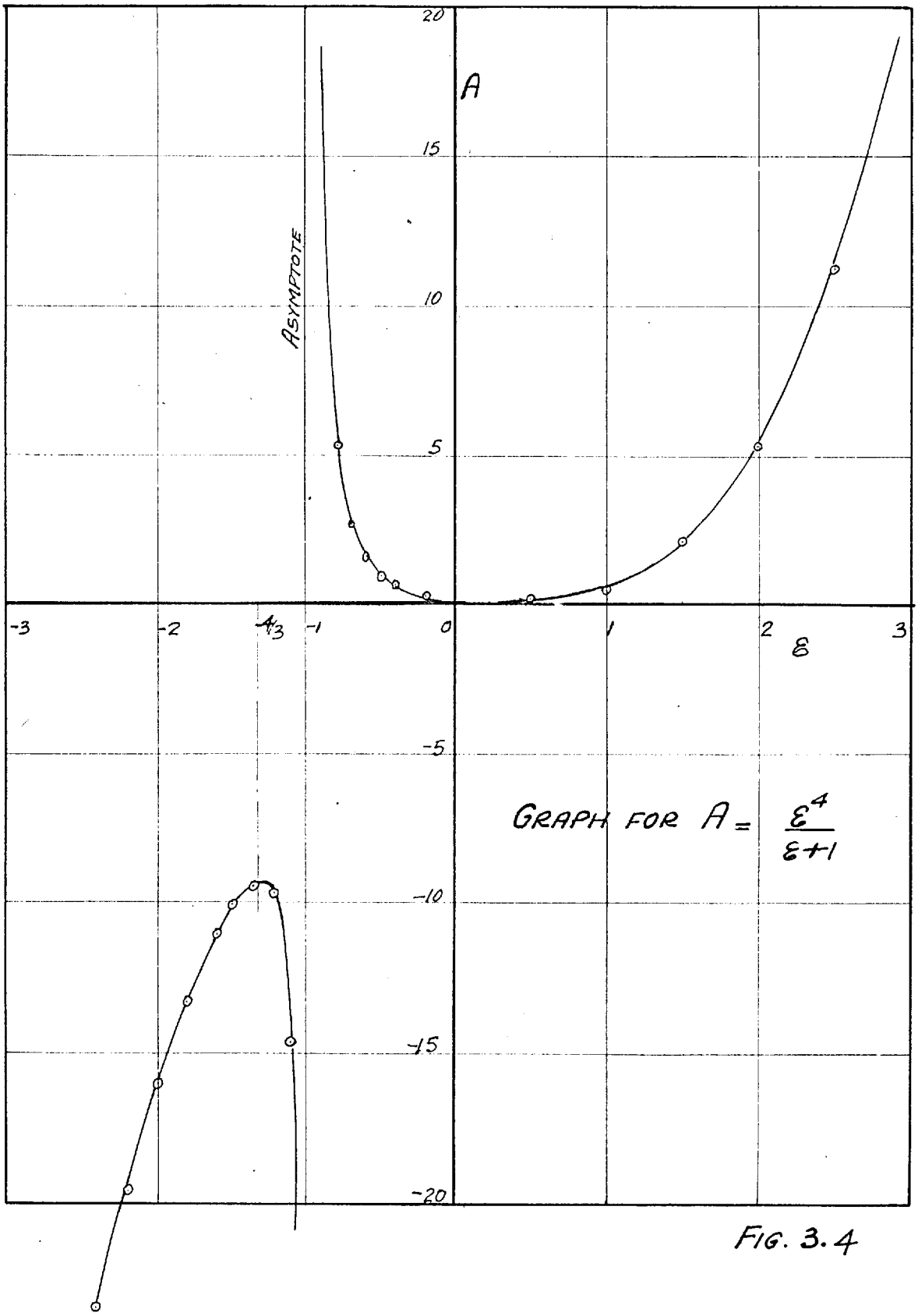


FIG. 3.4

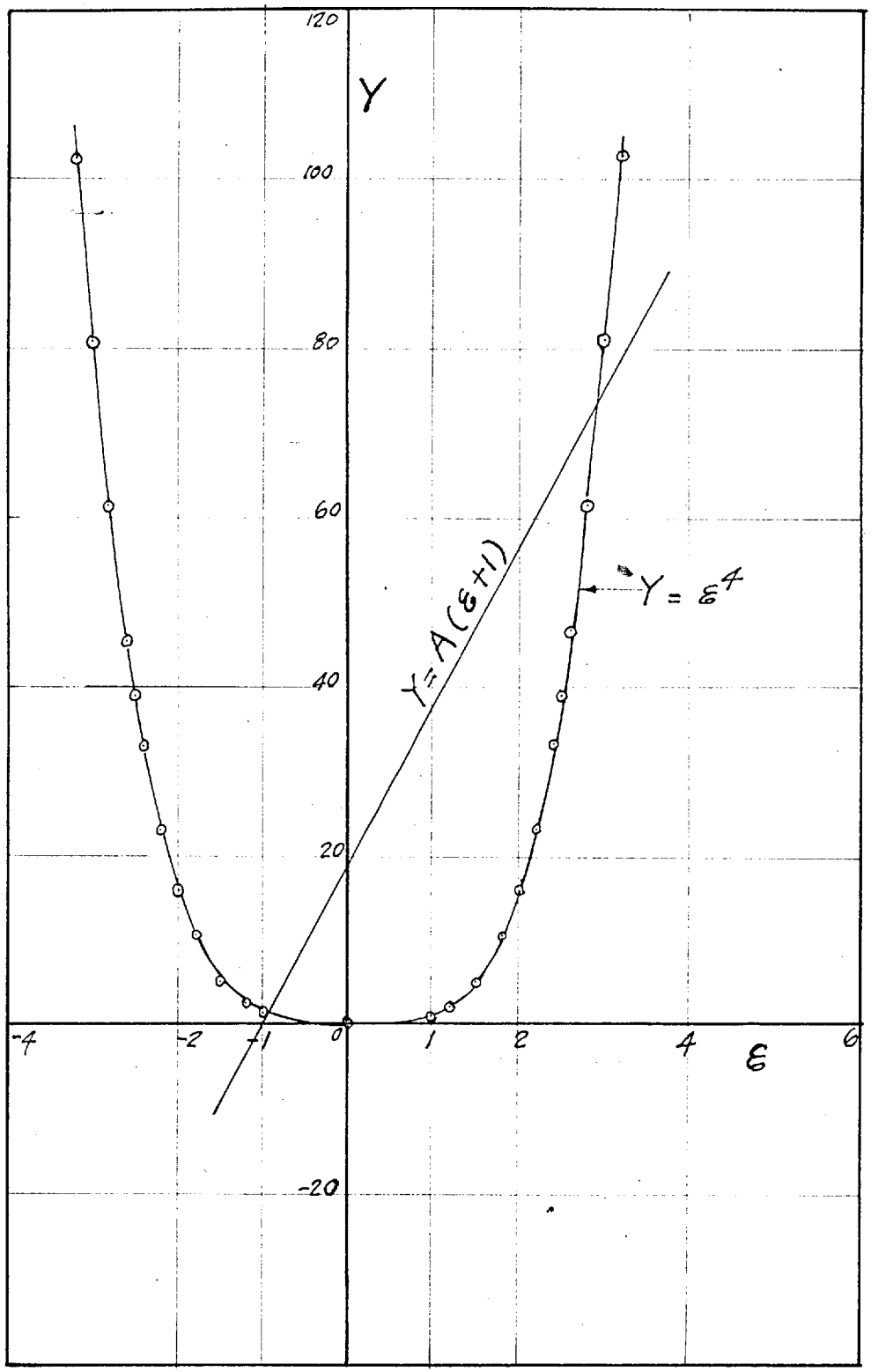


FIG. 3.5

It is seen that for large values of ξ, A becomes large. The line $\xi = -1$ is an asymptote, and turning points occur at $\xi = 0$, and $\xi = -4/3$.

Further observations can also be made regarding the roots of equation (3.67), by examining the points of intersection of the following curves :-

$$Y = \xi^4$$

$$Y = A(\xi + 1)$$

These are plotted in Fig. (3.5). The two curves have one point of intersection in the vicinity of $\xi = -1$, which is therefore a first approximation to a solution of equation (3.67).

But $$\frac{\rho^2}{m^2} = 1 + \xi$$

$$\frac{\rho^2}{m^2} \to 0 \quad \text{when} \quad \xi \to -1 \text{ from above.}$$

hence two of the roots of equation (3.66) are very small. In view of the rapidly damped character of the bending disturbances for large values of $\rho = \frac{kl^2}{t}$, then these small roots may be neglected when considering the typical edge effect. Also, since disturbances are being considered from one edge only, then one of the four boundary conditions at this edge may also be neglected. The more elaborate collocation method employed by Loof shows that the effect of

transverse displacement on bending moment is negligible, hence the boundary condition $\mu_\beta = 0$, may be neglected when considering a bending disturbance at the edge $\beta = 0$.

Now consider the solution of equation (3.67) for large values of p: This equation may be written in the form :-

$$\xi^4 - A\xi + A = (\xi^2 + q\xi + r)(\xi^2 - q\xi + s) \qquad ..(3.67.b)$$

$$\xi^4 - A\xi + A = \xi^4 + (r + s - q^2)\xi^2 + q(s - r)\xi + rs$$

Equating coefficients :-

$$\left.\begin{aligned} r + s - q^2 &= 0 \\ q(s - r) &= -A \\ rs &= A \end{aligned}\right\} \qquad ..(3.67.c)$$

giving :-

$$\begin{aligned} r + s &= q^2 \\ r - s &= \frac{A}{q} \end{aligned}$$

$$\left.\begin{aligned} 2r &= q^2 + \frac{A}{q} \\ 2s &= q^2 - \frac{A}{q} \end{aligned}\right\} \qquad ..(3.67.d)$$

Substituting from (3.67.d) in (3.67.c) :-

$$(q^2 + \frac{A}{q})(q^2 - \frac{A}{q}) = 4A$$

or $(q^3 + A)(q^3 - A) = -4Aq^2$

$$q^6 + 4Aq^2 - A^2 = 0 \qquad ..(3.67.e)$$

This is a cubic in q^2 viz :

$$(q^2)^3 + 4A(q^2) - A^2 = 0 \qquad ..(3.67.f)$$

Now every equation of odd degree and having real coefficients has at least one real root whose sign is opposite to that of the last term; therefore it follows from that (3.67.f) has one real positive root.

The Discriminant of (3.67.f) is :-

$$\triangle = -(27A^4 + 64A^3) \text{ which is -ve.} \quad \text{where } A = \frac{48k^2}{t^2m^4}$$

Hence equation (3.67.f) has <u>one</u> real, positive root, and <u>two</u> complex roots.

The real root of (3.67.f) can be written as :-

$$K^2 = c + d$$

where :-

$$c = \left[\frac{A^2}{2} + \sqrt{\frac{A^4}{4} + \frac{64}{27} A^3} \right]^{\frac{1}{3}}$$

$$d = \left[\frac{A^2}{2} - \sqrt{\frac{A^4}{4} + \frac{64}{27} A^3} \right]^{\frac{1}{3}}$$

Putting $M = \sqrt{\left(\frac{A^4}{4} + \frac{64}{27} A^3\right)}$, $= \frac{A^2}{2}\left(1 + \frac{256}{27A}\right)$

$$K^2 = \left[\frac{A^2}{2} + M\right]^{\frac{1}{3}} + \left[\frac{A^2}{2} - M\right]^{\frac{1}{3}} \qquad ..(3.67.g)$$

The problem of solving (3.67.f) therefore resolves into the solution of the following two equations :-

$$\xi^2 + q\xi + \tfrac{1}{2}\left(q^2 + \frac{A}{K}\right) = 0 \qquad ..(3.67.h)$$

and

$$\xi^2 - q\xi + \tfrac{1}{2}\left(q^2 - \frac{A}{K}\right) = 0 \qquad ..(3.67.j)$$

From the last equation :-

$$\left.\begin{matrix}\xi_1 \\ \xi_2\end{matrix}\right\} = \frac{-q \pm \sqrt{q^2 - 2\left(q^2 - \frac{A}{q}\right)}}{2}$$

or $$\left.\begin{matrix}\xi_1 \\ \xi_2\end{matrix}\right\} = \tfrac{1}{2}\left[-q \pm \sqrt{\left(-q^2 - \frac{2A}{q}\right)}\right] \qquad ..(3.67.k)$$

Similarly from (3.67.h) :-

$$\left.\begin{matrix}\xi_3 \\ \xi_4\end{matrix}\right\} = \tfrac{1}{2}\left[q \pm \sqrt{\left(-q^2 + \frac{2A}{q}\right)}\right] \qquad ..(3.67.l)$$

Now examine the expression for M given by :-

$$M = \frac{A^2}{2}\left(1 + \frac{256}{27A}\right)$$

For large values of A : $M \simeq \frac{A^2}{2}$

$$\text{and} \quad q^2 \simeq \left(\frac{A^2}{2} + \frac{A^2}{2}\right)^{\frac{1}{3}} + \left(\frac{A^2}{2} - \frac{A^2}{2}\right)^{\frac{1}{3}}$$

$$\text{i.e.} \quad q^2 = A^{\frac{2}{3}}$$

$$q = A^{\frac{1}{3}} \; ; \quad \frac{2A}{q} = 2A^{\frac{2}{3}}$$

Substituting for q in (3.67.k) :-

$$\left.\begin{matrix}\varepsilon_1 \\ \varepsilon_2\end{matrix}\right\} = \tfrac{1}{2}\left[-A^{\frac{1}{3}} \pm \sqrt{-A^{\frac{2}{3}} - 2A^{\frac{2}{3}}}\right]$$

$$= \tfrac{1}{2}\left[-A^{\frac{1}{3}} \pm \sqrt{1^2\, 3A^{\frac{2}{3}}}\right]$$

$$\left.\begin{matrix}\varepsilon_1 \\ \varepsilon_2\end{matrix}\right\} = A^{\frac{1}{3}}\left[-\tfrac{1}{2} \pm \tfrac{1}{2} i\sqrt{3}\right] \qquad ..(3.67.m)$$

Similarly :-

$$\left.\begin{matrix}\varepsilon_3\\ \varepsilon_4\end{matrix}\right\} = \left\{\begin{matrix}A^{\frac{1}{3}}\\ 0\end{matrix}\right\} \qquad ..(3.67.n)$$

But $\varepsilon = \frac{\rho^2}{m^2} - 1$.

$$\rho^2 = m^2(\varepsilon + 1), \qquad \rho = m\sqrt{\varepsilon + 1}$$

(taking +ve root)

also $A = \frac{48\,k^2}{t^2 m^4}$

Substituting in (3.67.m) :-

$$\varepsilon_1 = \left(\frac{48\,k^2}{t^2 m^2}\right)^{\frac{1}{3}} \left(-\tfrac{1}{2} + \tfrac{1}{2} i\sqrt{3}\right)$$

i.e. $\left(\frac{\rho^2}{m^2} - 1\right) = \left(\frac{48\,k^2\,l^4}{t^2 m^2 \pi^2}\right)^{\frac{1}{3}} \left(-\tfrac{1}{2} + \tfrac{1}{2} i\sqrt{3}\right)$

$$\varepsilon_1 = \left(\frac{\rho^2}{m^2} - 1\right) = \left(\frac{48\,p^2}{n^4 \pi^4}\right)^{\frac{1}{3}} \left(-\tfrac{1}{2} + \tfrac{1}{2} i\sqrt{3}\right)$$

where $p = \frac{kl^2}{t}$

But $\rho_1 = m(\varepsilon_1 + 1)^{\frac{1}{2}}$

$\rho_1 = m\varepsilon_1^{\frac{1}{2}}(1+\frac{1}{\varepsilon_1})^{\frac{1}{2}}$ which for large values of ε_1, may

be written :-

$$\rho_1 \simeq m\sqrt{\varepsilon_1} = \frac{n\pi}{l}\sqrt{\varepsilon_1}$$

$$\rho_1 = \frac{n\pi}{l}\left(\frac{48\,p^2}{n^4\pi^4}\right)^{\frac{1}{6}}\left(-\tfrac{1}{2}+\tfrac{1}{2}i\sqrt{3}\right)^{\frac{1}{2}}$$

$$= \frac{(48\,p^2 \times n^2\pi^2)^{\frac{1}{6}}\,l^{-1}}{2}\left[\frac{1}{\sqrt{2}}(1+i\sqrt{3})\right]$$

$$= \frac{(48\,n^2\pi^2)^{\frac{1}{6}}}{2}\,p^{\frac{1}{3}}\,l^{-1}\left(1+i\sqrt{3}\right)$$

$$\rho_1 = (\tfrac{3}{4}\,n^2\pi^2)^{\frac{1}{6}}\,p^{\frac{1}{3}}\,l^{-1}\left(1+i\sqrt{3}\right)$$

Similarly

$$\rho_2 = (\tfrac{3}{4}\,n^2\pi^2)^{\frac{1}{6}}\,p^{\frac{1}{3}}\,l^{-1}\left(1-i\sqrt{3}\right)$$

Similarly from (3.67.m) :-

$$\rho_3 = (48\,n^2\pi^2)^{\frac{1}{6}}\,p^{\frac{1}{3}}\,l^{-1}$$

$$= 2(\tfrac{48}{64}\,n^2\pi^2)^{\frac{1}{6}}\,p^{\frac{1}{3}}\,l^{-1}$$

$$\rho_3 = 2\left(\tfrac{3}{4} n^2\pi^2\right)^{\frac{1}{6}} p^{\frac{1}{3}} l^{-1}$$

$$\rho_4 = 0$$

Putting $\mu = \left(\tfrac{3}{4} n^2\pi^2\right)^{\frac{1}{6}} p^{\frac{1}{3}} l^{-1}$ in the above expressions, gives :-

$$\left.\begin{aligned} &\rho_1 \\ &\rho_2 \end{aligned}\right\} = \mu\,(1 \pm i\sqrt{3})$$

$$\rho_3 = 2\mu$$

$$\rho_4 = 0$$

..(3.68)

These are the roots given in Loofs paper[16].

It is interesting to note that the expressions given in (3.68) are also the roots of the equation :-

$$\rho^6 - 48\,\frac{k^2}{t^2}\,m^2 = 0$$

This is the characteristic equation for :-

$$\frac{\partial^6 u_\gamma}{\partial\beta^6} + \frac{48\,k^2}{t^2}\,\frac{\partial^2 u_\gamma}{\partial\alpha^2} = 0 \qquad ..(3.69)$$

when the solution is taken as (3.65).

Equation (3.69) may be obtained from (3.63) by neglecting $\frac{\partial^n}{\partial \alpha^n}$ compared with $\frac{\partial^n}{\partial \beta^n}$ in the expression for ∇_1^8.

This is equivalent to the Schorer type approximation used in cylindrical shell analysis. Thus (3.63) becomes :-

$$\frac{\partial^8 u_Y}{\partial \beta^8} + 48 \frac{k^2}{t^2} \cdot \frac{\partial^4 u_Y}{\partial \alpha^2 \partial \beta^2} = 0$$

giving : $$\frac{\partial^6 u_Y}{\partial \beta^6} + 48 \frac{k^2}{t^2} \frac{\partial^2 u_Y}{\partial \alpha^2} = 0$$

which is the same as (3.69).

Thus, the original eighth order equation is reduced to one of sixth order requiring three boundary conditions at each edge. However, the more elaborate method by Loof indicates which of the four boundary conditions at an edge may be neglected, without much effect on the bending moment in the shell.

From the roots (3.68) of the characteristic equation it is inferred that the complementary solution is :-

$$u_Y = \left[A_1 e^{-\mu(1 + i\sqrt{3})\beta} + A_2 e^{-\mu(1 - i\sqrt{3})\beta} + A_3 e^{-2\mu\beta} \right] \sin m\alpha,$$

where A_1, A_2 and A_3 are arbitrary constants.

The solution for u_γ may also be written in the form :-

$$u_\gamma = \left[A e^{-2\mu\beta} + B e^{-\mu\beta} \operatorname{Cos}(\mu\sqrt{3}\beta + \phi) \right] \operatorname{Sin} m\alpha \qquad ..(3.70)$$

where the third constant is absorbed in the phase angle ϕ.

ACTIONS AND DISPLACEMENTS

The actions and displacements necessary to establish the boundary conditions for clamped and hinged edges will now be derived. These are u_α, $\frac{\partial u_\gamma}{\partial \beta}$, and $\frac{\partial^2 u_\gamma}{\partial \beta^2}$.

From (3.70) :-

$$\frac{\partial u_\gamma}{\partial \beta} = \left[-2\mu\, A e^{-2\mu\beta} + B \left\{ -\mu\, e^{-\mu\beta} \operatorname{Cos}(\mu\beta\sqrt{3} + \phi) \right\} \right.$$
$$\left. -\mu\sqrt{3}\, e^{-\mu\beta} \operatorname{Sin}(\mu\beta\sqrt{3} + \phi) \right] \operatorname{Sin} m\alpha$$

This may alternatively be expressed in the form :-

$$\frac{\partial u_\gamma}{\partial \beta} = -2\mu \left[A e^{-2\mu\beta} + B e^{-\mu\beta} \operatorname{Cos}(\mu\beta\sqrt{3} + \phi - \tfrac{\pi}{3}) \right] \operatorname{Sin} m\alpha$$

Similarly :-

$$\frac{\partial^2 u_\gamma}{\partial \beta^2} = 4\mu^2 \left[A\, e^{-2\mu\beta} + B\, e^{-\mu\beta} \cos\left(\mu\beta\sqrt{3} + Q - \frac{2\pi}{3}\right) \right] \sin m\alpha$$

It is obvious therefore that each successive differentiation of u_γ merely multiplies the result of the previous differentiation by -2μ while the phase angle is decreased by $\frac{\pi}{3}$.

$$\frac{\partial^3 u_\gamma}{\partial \beta^3} = -8\mu^3 \left[A\, e^{-2\mu\beta} + B\, e^{-\mu\beta} \cos\left(\mu\beta\sqrt{3} + Q\right) \right] \sin m\alpha$$

Differentiating (3.7) twice w.r.t. α and from equation (3.1) with $G_\alpha = 0$:-

$$-\frac{\partial^2 n_\beta}{\partial\alpha\partial\beta} = \frac{\partial^2 n_{\alpha\beta}}{\partial\alpha^2} = \frac{Et}{2}\left(\frac{\partial^3 u_\beta}{\partial\alpha^3} + \frac{\partial^3 u_\alpha}{\partial\alpha^2\partial\beta}\right) - \frac{Et}{R_{\alpha\beta}}\frac{\partial^2 u_\gamma}{\partial\alpha^2}$$

Similarly from (3.8) (with $\frac{1}{R_\alpha} = \frac{1}{R_\beta} = 0$)

$$\frac{\partial^3 u_\beta}{\partial\alpha^3} + \frac{\partial^3 u_\alpha}{\partial\alpha^2\partial\beta} - \frac{2}{R_{\alpha\beta}}\frac{\partial^2 u_\gamma}{\partial\alpha^2} = -2\frac{\partial^3 u_\beta}{\partial\alpha\partial\beta^2}$$

Differentiating thrice w.r.t. β :

$$\frac{\partial^6 u_\beta}{\partial\alpha^3\partial\beta^3} + \frac{\partial^6 u_\alpha}{\partial\alpha^2\partial\beta^4} - 2K\frac{\partial^5 u_\gamma}{\partial\alpha^2\partial\beta^3} = -\frac{2\partial^6 u_\beta}{\partial\alpha\partial\beta^5}$$

But from (3.1) and (3.2) :-

$$\frac{\partial^2 n_\alpha}{\partial \alpha^2} = \frac{\partial^2 n_\beta}{\partial \beta^2}$$

Substituting in the preceding expression and then integrating twice ω.r.t. α gives :-

$$\nabla_1^4 u_\alpha = 2K \frac{\partial^3 u_\gamma}{\partial \beta^3}$$

Since the solution has been assumed rapidly damped (large values of p) in the β - direction, then near the midpoint of an edge it may be assumed that derivatives ω.r.t. α are negligible. ∇_1^4 then becomes $\frac{\partial^4}{\partial \beta^4}$ and the last expression becomes :-

$$\frac{\partial^4 u_\alpha}{\partial \beta^4} = 2K \frac{\partial^3 u_\gamma}{\partial \beta^3}, \quad \text{giving}$$

$$u_\alpha = 2K \int u_\gamma d\beta$$

Substituting from (3.70) for u_γ, gives :-

$$u_\alpha = \left[-\frac{k}{u} A e^{-2\mu\beta} + 2KB \int e^{-\mu\beta} \cos(\mu\sqrt{3}\beta + \phi)\, d\beta \right] \sin m\alpha. \quad ..(3.71)$$

Now consider the integral on the right-hand side of

(3.71), integrating by parts :-

$$\int e^{-\mu\beta} \operatorname{Cos}(\mu\beta\sqrt{3} + \phi)\, d\beta$$

$$= -\frac{1}{\mu} e^{-\mu\beta} \operatorname{Cos}(\mu\beta\sqrt{3} + \phi) - 3\int e^{-\mu\beta} \operatorname{Sin}(\mu\beta\sqrt{3} + \phi)\, d\beta$$

Again integrating by parts :-

$$\int (\quad) = -\frac{1}{\mu} e^{-\mu\beta} \operatorname{Cos}(\mu\beta\sqrt{3} + \phi) + \frac{\sqrt{3}}{u} e^{-\mu\beta} \operatorname{Sin}(\mu\beta\sqrt{3} + \phi)$$

$$- 3\int e^{-\mu\beta} \operatorname{Cos}(\mu\beta\sqrt{3} + \phi)\, d\beta$$

$$4\int e^{-\mu\beta} \operatorname{Cos}(\mu\beta\sqrt{3} + \phi)\, d\beta = -\frac{1}{\mu} e^{-\mu\beta}\left[\operatorname{Cos}(\mu\beta\sqrt{3} + \phi) - \sqrt{3} \operatorname{Sin}(\mu\beta\sqrt{3} + \phi)\right]$$

$$= 2e^{-\mu\beta} \operatorname{Cos}(\mu\beta\sqrt{3} + \phi + \tfrac{\pi}{3})$$

Substitution in (3.71) gives :

$$u_\alpha = -\frac{k}{u}\left[A e^{-2\mu\beta} + B e^{-\mu\beta} \operatorname{Cos}(\mu\beta\sqrt{3} + \phi + \tfrac{\pi}{3})\right] \operatorname{Sin} m\alpha$$

Hence summarising :

$$\left.\begin{aligned} u_\gamma &= \left[A e^{-2\mu\beta} + B e^{-\mu\beta} \operatorname{Cos}(\mu\sqrt{3}\,\beta + \phi)\right] \operatorname{Sin} m\alpha \\ \frac{\partial u_\gamma}{\partial\beta} &= -2\mu\left[A e^{-2\mu\beta} + B e^{-\mu\beta} \operatorname{Cos}(\mu\sqrt{3}\,\beta + \phi - \tfrac{\pi}{3})\right] \operatorname{Sin} m\alpha \end{aligned}\right\} \quad ..(3.72)$$

$$\left.\begin{aligned}
\frac{\partial^2 u_\gamma}{\partial \beta^2} &= 4\mu^2 \left[A\, e^{-2\mu\beta} + B\, e^{-\mu\beta} \cos\left(\mu\sqrt{3}\,\beta + \phi - \frac{2\pi}{3}\right) \right] \sin m\alpha \\
\frac{\partial^3 u_\gamma}{\partial \beta^3} &= -8\mu^3 \left[A\, e^{-2\mu\beta} + B\, e^{-\mu\beta} \cos\left(\mu\sqrt{3}\,\beta + \phi\right) \right] \sin m\alpha \\
u_\alpha &= -\frac{k}{p} \left[A\, e^{-2\mu\beta} + B\, e^{-\mu\beta} \cos\left(\mu\sqrt{3}\,\beta + \phi + \frac{\pi}{3}\right) \right] \sin m\alpha
\end{aligned}\right\} \quad ..(3.72)$$

Loof has derived the expressions for moments in the cases of clamped and of hinged edges may be in the form of a series, as follows :-

CLAMPED EDGES

$$m_\beta = -\sqrt[3]{\frac{2}{9\pi}}\, G_\gamma\, l^2\, p^{-\frac{4}{3}} \sum_{n=1,3,5..} n^{-\frac{1}{3}} \left[e^{-2\mu\beta} + 2e^{-\mu\beta} \cos\left(\mu\beta\sqrt{3} + \frac{\pi}{3}\right) \right] \times$$

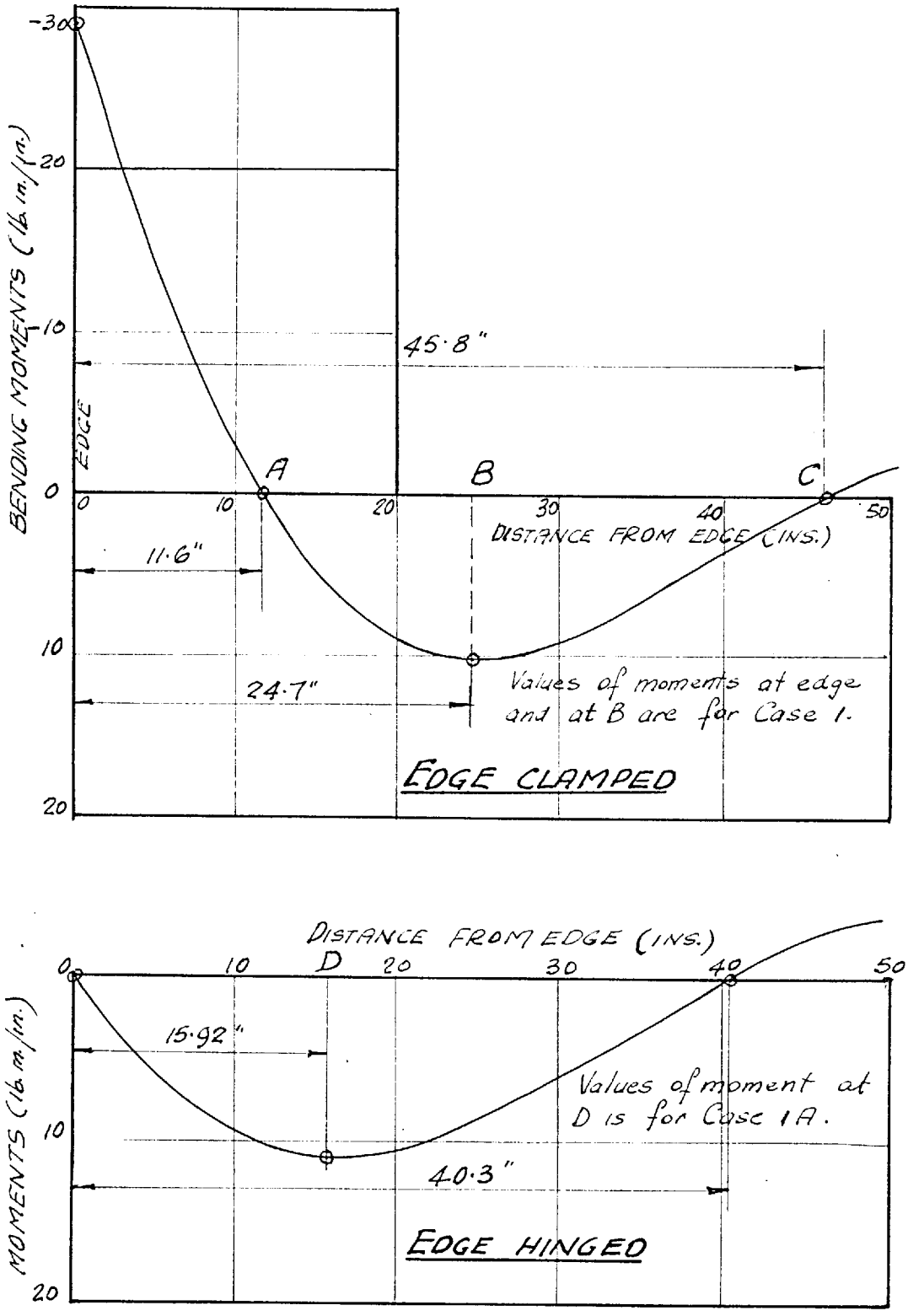
$$\times \sin m\alpha$$

$$\text{At } \alpha = \frac{1}{2}$$

The edge moment $m_{edge} = -0.511\, G_\gamma\, l^2\, p^{-\frac{4}{3}}$

This moment is first reduced to zero at a distance from the edge given by :-

$$\beta = 0.40\, p^{-\frac{1}{3}}\, l.$$



PATTERN OF MOMENTS (LOOF'S METHOD)

FIG. 3.6.

Then follows positive moment up to a distance given by :-

$$\beta = 1.58\, p^{-\frac{1}{3}}\, l.$$

Max. positive moment $= .167\, G_\gamma\, l^2\, p^{-\frac{4}{3}}$ occurring at

$$\beta = 0.85\, p^{-\frac{1}{3}}\, l.$$

$$\text{Edge shear} = 1.732\, G_\gamma\, l\, p^{-1}$$

HINGED EDGES

$$m_\beta = \frac{2}{3}\sqrt{\frac{4}{3\pi^2}}\, G_\gamma\, l^2\, p^{-\frac{4}{3}} \sum_{1,3,5} n^{-\frac{1}{3}}\, e^{-\mu\beta} \sin \mu\beta\sqrt{3} \sin m\alpha$$

with $\alpha = 1/2$:

At $\beta = 0.55\, p^{-\frac{1}{3}}\, l$, $m_{max} = + .149\, G_\gamma\, l^2\, p^{-\frac{4}{3}}$

The moment first becomes zero at $\beta = 1.39\, p^{-\frac{1}{3}}\, l.$

$$\text{Edge shear} = 0.577\, G_\gamma\, l\, p^{-1}$$

Note

It is important to observe that in this approximate analysis it has been assumed that the bending disturbance in the vicinity of an edge is unaffected by disturbances from the other edges.

The analysis is aimed mainly at determination of moments and normal shear forces. The boundary conditions assumed are not realistic, especially in the case of hinged edges, and the solutions obtained are restricted to large values of a parameter $p = \frac{kl^2}{t}$.

EDGE BEAM DEFORMATION

Loof has proposed an approximate method for taking into account the possibility of edge beam deformation. The moments deduced in the case of rigid edges are multiplied by a magnification factor A defined as :

$$A = 1 + \frac{1}{u_{\gamma 0}} \left[\frac{u_{\alpha 1} - u_{\alpha 3}}{2kb} + \frac{u_{\beta 2} - u_{\beta 4}}{2ka} - \frac{1}{4}(u_{\gamma 1} + u_{\gamma 2} + u_{\gamma 3} + u_{\gamma 4}) \right] \quad ..(3.73)$$

where the points 1 and 3, 2 and 4, represent the midpoints of the β edges, and α edges, respectively (see Fig. 3.7), and the above deflections refer to those at the edge structure regarded as separate from the shell.

In the case of rigid edges, A = 1.

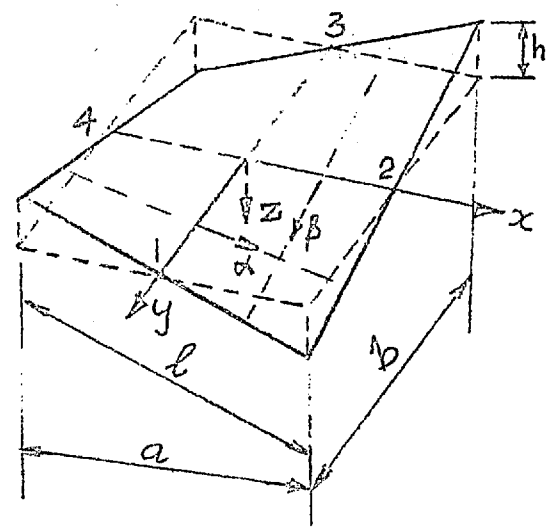


Fig. 3.7.

The above expression for A, which has not yet been ~~checked~~ compared experimentally, takes into account such displacements as those due to tie bar extension, settlement of supports and self weight of edge beams. In view of the several combinations of edge beam and tie bar stiffness in the tests there was ample data from which to check the validity of the formula proposed for A, though only for one particular value of the parameter p.

The procedure is first to determine the proportion of the load carried by slab action alone and then to regard the remainder as carried by membrane action.

Calculations based on Loof's method have been carried out in the appendix, for the shell tested. The results of these calculations are summarised in the next section.

TABLE NO. 3

SUMMARY OF NUMERICAL CALCULATIONS BASED ON LOOF'S WORK

CONDITIONS	Edge Beam Force at midspan (lbs)	Deflection at midspan (in.)	B.M. near mid span of beam (lb.in.)	Value of A.	Division of Load		Max. B.M. in shell (lb.m./in.)	Case No.
					Slab Action	Membrane Action		
Restrained Edges Box Section Beams Edge Beam Supported No Corner movement	2709 (2005)	0	0 (4024)	2.4694	.4571	.5429	-29.04 edge 10.06 at B	1
Hinged Edges Box Sections Edge Beam Supported No Corner movement	4012 (2005)	0	0 (4024)	3.1759	.1959	.8041	10.89 at D	1A
Restrained Edges Channel Sections Beam Supported No Corner movement	2192.5 (2194)	0	0 (3108)	3.0285	.5606	.4394	-35.61 edge 12.34 at B	2
Hinged Edges Channel Sections Beam Supported No Corner movement	3477 (2194)	0	0 (3108)	4.9360	13045	.6955	17.14 at D	2A
Restrained Edges Box Sections Beam Unsupported No Corner movement	3685 (2005)	.0078	1284 (4024)	1.4128	.2615	.7385	-16.61 edge 5.34 at B	3A
Hinged Edges Box Sections Beam Unsupported No Corner movement	4491 (2005)	.0089	490 (4024)	1.6189	.0999	.9001	5.55 at D	3B
Restrained Edges Channel Sections Beam Unsupported No L. Corner movement	4063 (2194)	.0103	912.4 (3108	1.0038	.1858	.8142	-11.80 edge 3.80 at B	4A
Hinged Edges Channel Sections Beam Unsupported No L. Corner movement	4650 (2149)	.0114	334.1 (3108)	1.1306	.0681	.9319	3.78 at D	4B

N.B: Experimental results in brackets

TABLE NO. 3 (Con'd.)

CONDITIONS	Force (lbs) at midspan of beam.	Defln. (ins) at midspan of beam.	B.M. (lb-in) near midspan of beam.	Value of A.	Division of Load		Max. B.M. in Shell (lb-in/in)	Case No.
					Slab Action.	Membrane action.		
Restrained Edges Box Sections Beam Unsupported Movement at L.C.	2539	.0146	166.6	2.6531	.4911	.5089	-31.20 edge 10.19 at B	5A
Hinged Edges Box Sections Beam Unsupported Movement at L.C.	4049	.0168	-2612.7	3.0563	.1886	.8114	10.48 at D	5B
Restrained Edges Channel Sections Beam Unsupported Movement at L.C.	2578 (2460)	.0235	-46.7 (5758)	2.2862	.4232	.5768	-26.89 edge 8.79 at B	6A
Hinged Edges Channel Sections Beam Unsupported Movement at L.C.	4166 (2460)	.0276	-2873.9 (5758)	2.6754	.1651	.8349	9.18 at D	6B
Restrained Edges Flexible Edge Beam Beam Unsupported No Movement at L.C.	.4770 (1835)	.0152	40.1 (790)	.2385	.0441	.9559	2.80 edge 0.9 at B	7A
Hinged Edges Flexible Edge Beam Beam Unsupported No Movement at L.C.	4194 (1835)	.0156	13.3 (790)	.2440	.0151	.9849	0.15 at D	7B
Restrained Edges Flexible Edge Beam Beam Unsupported Movement at L.C.	2756 (2150)	.1545	-239.5 (1395)	2.4182	.5524	.4476	-28.44 edge 8.09 at B	8A
Hinged Edges Flexible Edge Beam Beam Unsupported Movement at L.C.	4118 (2150)	.1809	-2784.6 (1395)	2.8310	.1747	.8253	9.71 at D	8B

L.C. = Low Corner

TIE BAR FORCE

From the membrane theory :-

Tie Bar Force = 6981.3 lbs.

If the total load is considered as taken by slab and membrane action, then,

Theoretical Tie Bar Force = 6981.3 x (Portion of Load carried by membrane action)

The resulting theoretical tie bar force for the different cases dealt with are summarised below :-

TABLE NO. 4

CASE NO.	1	1A	2	2A	3A	3B	4A	4B
Portion carried by membrane action	.5429	.8041	.4394	.6955	.7385	.9001	.8142	.9319
Theoretical Tie Bar Force	3790.1	5613.7	3067.6	4855.5	5155.7	6283.9	5684.2	6505.9
Experimental Tie Bar Force	2237	2237	2535	2535	2236	2236	2535	2535

CASE	5A	5B	6A	6B	7A	7B	8A	8B
Portion carried by membrane action	.5089	.8114	.5768	.8349	.9559	.9849	.4476	.8253
Theoretical Tie Bar Force	3552.8	5664.6	4026.8	5828.7	6673.4	6875.9	3124.8	5761.7
Experimental Tie Bar Force	719	719	889	889	2843	2843	1252	1252

3.6 FLAT PLATE SOLUTIONS

The deflections and moments observed experimentally were considered very high for the shell. The moments in particular, were quite large in the central region. It was therefore considered advisable to compare the behaviour of the shell with that of a plate having similar dimensions and with different types of boundary conditions.

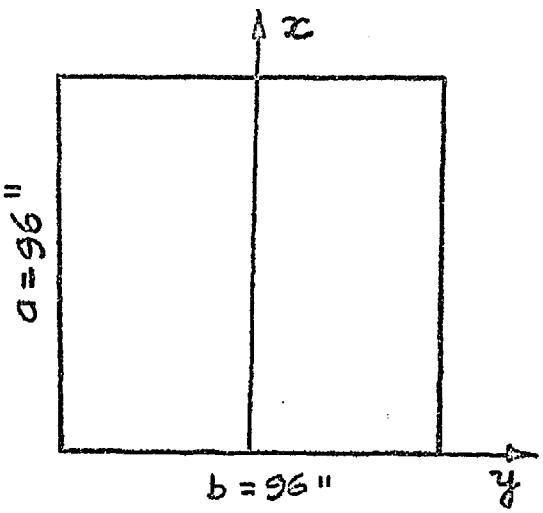
The well-known plate equation is :-

$$\nabla_1^4 u_Y = \frac{G_Y}{Et^3/12} \qquad ..(3.74)$$

3.6.a PLATE WITH SIMPLY SUPPORTED EDGES

The solution is given for a uniform loading of $G_Y = 45 \text{ lb/ft}^2$ ($.3125 \text{ lb/in}^2$).

This case has been considered by Timoshenko[27] who employs a Levy type solution to give the following results:



Deflection

$$u_\gamma = \frac{4G_\gamma a^4}{\pi^5 D} \sum_{1,3,5} \left[1 - \frac{\alpha_m \tanh \alpha_m + 2}{2 \cosh \alpha_m} \cosh \frac{2\alpha_m y}{b} + \frac{\alpha_m}{2 \cosh \alpha_m} \cdot \frac{2y}{b} \cdot \sinh \frac{2\alpha_m y}{b} \right] \sin \frac{m\pi x}{a} \quad ..(3.75)$$

where $\alpha_m = \frac{m\pi b}{2a} = \frac{\pi}{2}$, $D = \frac{Et^3}{12}$

Taking the first term of the series (i.e. m = 1) and for y = 0 :-

$$u_\gamma = \frac{4G_\gamma a^4}{\pi^5 D} \left[1 - \frac{\alpha_m \tanh \alpha_m + 2}{2 \cosh \alpha_m} \right] \sin \frac{\pi x}{a}$$

For the square plate : $(\alpha_m = \frac{\pi}{2})$

$$u_\gamma = \frac{4G_\gamma a^4}{\pi^5 D} \left[1 - \frac{\frac{\pi}{2} \tanh \frac{\pi}{2} + 2}{2 \cosh \frac{\pi}{2}} \right] \sin \frac{\pi x}{a}$$

i.e.

$$u_\gamma = \delta \frac{G_\gamma a^4}{D} \sin \frac{\pi x}{a}$$

where δ is taken from Table No. 8 of Timoshenko's book[27] to be 0.00406.

$$\therefore \quad u_\gamma = .00406 \frac{G_\gamma a^4}{D} \sin \frac{\pi x}{a}$$

Putting $D = \frac{Et^3}{12} = 1.67 \times 10^5$ and substituting for values of G_γ and a :-

$$u_\gamma = \frac{.00406 \times .3125 \times (96)^4}{1.67 \times 10^5} \text{ Sin } \frac{\pi x}{a}$$

$$\text{i.e. } u_\gamma = .6457 \text{ Sin } \frac{\pi x}{a}$$

$u_{\gamma(max)}$ = .6457 inch. at midspan

TABLE NO. 5

DEFLECTIONS

$\frac{x}{a}$	$180 \frac{x}{a}$ (Degrees)	Sin $\frac{\pi x}{a}$	u_γ (ins)
0.1	18°	.30902	.1997
0.2	36°	.58778	.3795
0.3	54	.80902	.5224
0.4	72	.95106	.6141
0.5	90	1.00000	.6457

MOMENTS

Moments are derived from Table No. 6 of Timoshenko[27] for $\frac{b}{a} = 1$ and at $y = 0$.

$M_y = \beta^1 q_y a^2$, where values of β^1 are given in the Table referred to above.

$$M_y = \beta^1 \times .3125 \times (96)^2 = 2880\ \beta^1$$

Similarly :

$$M_x = \beta_1^1 \times .3125 \times (96)^2 = 2880\ \beta_1^1$$

TABLE NO. 6

$\frac{x}{a}$	β^1	β_1^1	M_y (lb. in/in.)	DIFF. STRAIN $= 4.491M$
0.1	.0209	.0168	60.20	270.4
0.2	.0343	.0303	98.78	443.6
0.3	.0424	.0400	122.10	548.4
0.4	.0466	.0459	134.20	602.7
0.5	.0479	.0479	137.95	619.5

3.6.b PLATE WITH CLAMPED EDGES

This case has also been worked out by Timoshenko[27]. The previous case of simply supported edges is used as the particular solution.

Particular Solution

$$u_\gamma^{\,o} = .6457 \cos \frac{\pi x}{a}$$

On this must be superimposed the deflections due to moments applied at the edges of the plate, these moments being adjusted in such a manner to satisfy the boundary condition. Firstly, the deflection due to moments applied along two opposite edges of the plate, is obtained. This is

$$u_\gamma^{(1)} = \left\{ -\frac{a^2}{2\pi^2 D} \sum_{1,3,5}^{\infty} E_m \frac{(-1)^{\frac{m-1}{2}}}{m^2 \cosh \alpha_m} \cos \frac{m\pi x}{a} \left(\frac{m\pi y}{a} \sin \frac{m\pi y}{a} - \alpha_m \tanh \alpha_m \cosh \frac{m\pi y}{a} \right) \right\} \qquad ..(3.76)$$

The coefficients E_m are taken from Timoshenko[27] page 201.

$$\alpha_m = \frac{m\pi b}{2a} = \frac{m\pi}{2} \quad \text{for square plate.}$$

At $x = 0$:-

$$u_y^{(1)} = -\frac{a^2}{2\pi^2 D} \sum_{1,3,5,7}^{\infty} E_m \frac{(-1)^{\frac{m-1}{2}}}{m^2 \cosh \alpha_m} \left(\frac{m\pi y}{a} \sinh \frac{m\pi y}{a} - \alpha_m \tanh \alpha_m \cosh \frac{m\pi y}{a} \right) \quad ..(3.77)$$

where $E_1 = 0.3722\ K$. $\quad E_3 = -0.0380\ K$.

$E_5 = -0.00178\ K$. $\quad E_7 = -0.0085\ K$.

and $\quad K = -\frac{4G_y a^2}{\pi^3}$

The value of the series (3.77) has been calculated for different values of y/a, and for $m = 1, 3, 5, 7$. The results are given below :

TABLE NO. 7

EVALUATION OF SERIES 3.77

$$u_y^1 = -\frac{a^2}{2\pi^2 D} \sum_{1,3,5,7} m$$

y/a	S for m=1 (S_1)	S for m=3 (S_3)	S for m=5 (S_5)	S for m=7 (S_7)	$\sum S_m$..
0	-.21369K	-.00036K	small	small	-.21405K
0.2	-.19479K	-.000745K			-.19554K
0.4	-.10523K	-.000156K			-.10538K
0.5	0	0			0

The total deflection along a line, say $x = 0$, is the sum of the deflections due to moments applied at both edges, $x = \pm \frac{a}{2}$, $y = \pm \frac{b}{2}$.

$$\text{i.e.} \quad u_\gamma = u_\gamma^{(1)} + u_\gamma^{(2)}$$

$\therefore$ Along $x = 0$:-

$$u_\gamma = u_\gamma^{(1)} + u_{\gamma\,(max)}^{(2)} \cos \frac{m\pi y}{a}$$

$$u_{\gamma\,(max)}^{(2)} = -.21405\, K x \left(-\frac{a^2}{2\pi^2 D} \right)$$

$$= -.21405 \left(-\frac{4 G_\gamma a^2}{\pi^3} \right) \left(-\frac{a^2}{2\pi^2 D} \right)$$

$$u_{\gamma\,(max)}^{(2)} = \frac{-.42810\, G_\gamma a^4}{\pi^5 D} = -.00140 \frac{G_\gamma a^4}{D}$$

This compares exactly with the value given in Timoshenko[27].

Due to $u_\gamma^{(1)}$:-

$$\text{Deflection at } y/a = 0.2 = -.19554K \left(\frac{-a^2}{2\pi^2 D} \right)$$

$$= \frac{-.39108\, G_\gamma a^4}{\pi^5 D} = -.00128 \frac{G_\gamma a^4}{D}$$

$$\text{Deflection at } y/a = 0.4 = -.10538K\left(-\frac{a^2}{2\pi^2 D}\right)$$

$$= \frac{-.21076G_\gamma a^4}{\pi^5 D} = \frac{-.00069G_\gamma a^4}{D}$$

Deflection at $y/a = 0.5 = 0$

Total deflection due to moments applied at all edges is

$$u_\gamma = u_\gamma^{(1)} + u_{\gamma(max)}^{(2)} \cos\frac{m\pi y}{a}$$

The values of u_γ due to edge moments are given in the table below :-

TABLE NO. 8

y/l	0	0.2	0.4	0.5
$u_\gamma^{(1)}$	-.00140	-.00128	-.00069	0
$u_{\gamma(max)}^{(2)}$ Cos mπy/a	-.00140	-.00113	-.00043	0
Sum	-.00280	-.00241	-.00112	0
Sum x $\frac{G_\gamma a^4}{D}$ (ins)	-.44532	-.38330	-.17813	0
Particular Solution	+ .6457	.5224	.1997	0
Net DEFLECTION	.2004	.1391	.0216	0

$$G_\gamma a^4/D = \frac{.3125 \times 96^4}{1.67 \times 10^5} = 159.04379$$

On taking symmetry into account, the net deflections are as follows, along the axes and diagonal :-

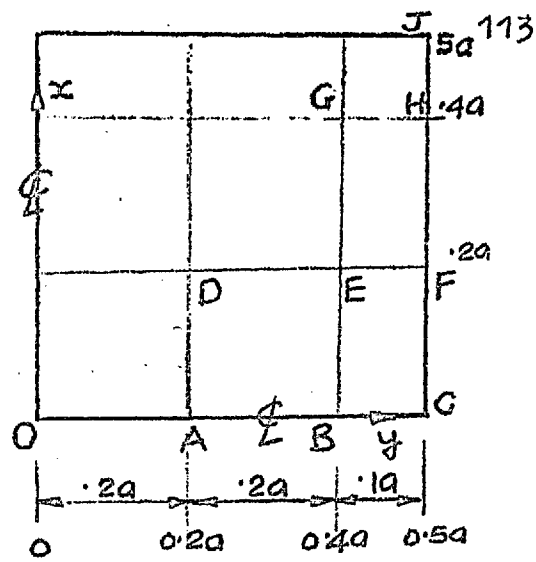


TABLE NO. 9

Point	A	B	C	D	E	O
Deflection(net)	.1391"	.0216"	0	.1216"	.0069"	.2004"

Bending Moments

From Table 35, Timoshenko[27], page 202 :-

Moment at midspan of shell $= .0231\ G_\gamma a^2$

$= .0231 \times .3125\ (96)^2 = 66.53$ lb.in/in.

Moment at midspan of edges $= -.0513\ G_\gamma a^2 = -147.74$ lb.in/in.

3.6.c PLATE SIMPLY SUPPORTED ON ELASTIC EDGES

The theory covering this case has been fully dealt with by Wood[23] and [24] who employs a finite difference method to solve the plate equation with the appropriate boundary conditions, viz:

(a) Equal and opposite reactions between slab and edge beams.

(b) Zero moment at edges of the slab.

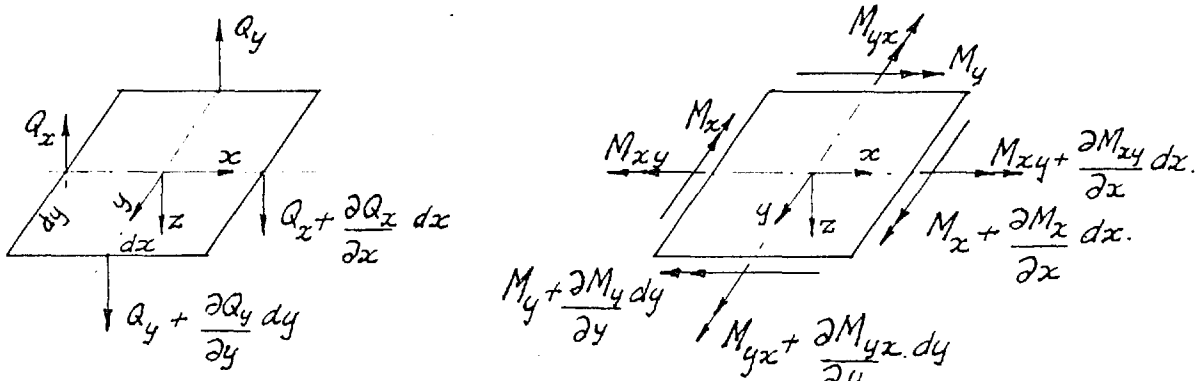
The work is carried out in non-dimensional form, which reduces the biharmonic plate equation to the form :-

$$\nabla_1^4 W = \frac{q_Y L^3}{D} = \lambda \qquad ..(3.78)$$

where $$\nabla_1^4 W = \frac{\partial^4 W}{\partial X^4} + 2\frac{\partial^4 W}{\partial X^2 \partial Y^2} + \frac{\partial^4 W}{\partial Y^4}$$

$$X = \frac{x}{L}, \quad Y = \frac{y}{L}, \quad W = \frac{w}{L}$$

and L is a convenient representative length (e.g. short span of a rectangular slab). In this case w is used instead of u_Y to represent deflection. The convention used is shown in Fig. (3.8).

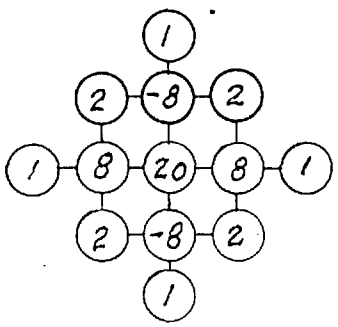


SHEAR FORCES

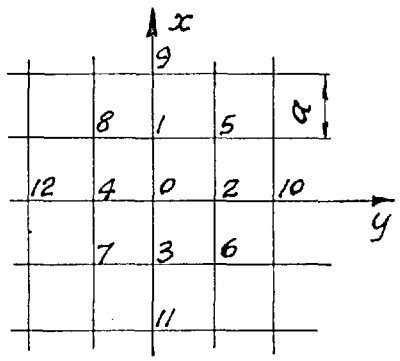
MOMENTS

CONVENTION FOR PLATE SOLUTION

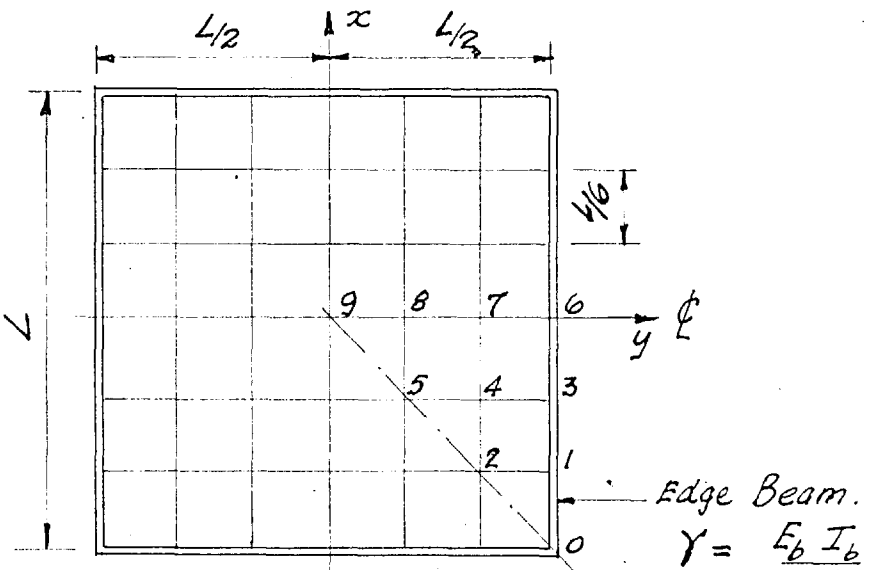
FIG. 3.8.



FINITE DIFFERENCE PATTERN



MESH FOR FINITE DIFF. APPROXIMATIONS



6x6 MESH FOR SYMMETRICAL LOADING.

PLATE SUPPORTED ON ELASTIC EDGES.

FIG. 3.9.

For a mesh length a :

$$\nabla_1^4 w = \frac{1}{a^4}\left[20w_o - 8(w_1 + w_2 + w_3 + w_4) + 2(w_5 + w_6 + w_7 + w_8) + (w_9 + w_{10} + w_{11} + w_{12})\right] = \frac{G_y}{D} \quad ..(3.79)$$

Equation (3.79) may be expressed in the following non-dimensional form :-

$$\frac{G_y}{D} = \frac{1}{L^3\Lambda^4}\left[20w_o - 8(w_1 + w_2 + w_3 + w_4) + 2(w_5 + w_6 + w_7 + w_8) + (w_9 + w_{10} + w_{11} + w_{12})\right]$$

$$\text{or } A^4\lambda = 20w_o - 8\,w_{1,2,3,4} + 2\,w_{5,6,7,8} + w_{9,10,11,12} \quad ..(3.80)$$

where, in the usual manner, (Fig. 3.7) the point 0 is at the centre of the pattern.

The procedure is, therefore, to apply the finite difference pattern shown in Fig. (3.9) at each of the mesh points into which the slab surface is divided; thus giving an equation of the form (3.80) at each point. The only real difficulty lies in the satisfaction of boundary conditions. At, or in the vicinity of an edge, the finite

difference pattern has to be adjusted in order to take the boundary conditions into account. The variation of the pattern in such cases is given by Wood[23 and 24].

Thus, in considering a 6 x 6 mesh shown in Fig. 3.7, after taking symmetry into account, nine linearly independent equations are obtained, in terms of $W = \frac{w}{L}$. The stiffness of the edge beams and slab are included in the parameter $\gamma = \frac{E_b I_b}{D L/2}$, in the case of the square panel with four identical edge beams.

The following are the nine equations obtained :-

At 9: $20W_9 - 32W_8 + 4W_7 + 8W_5 + 0W_4 + 0W_2 + 0W_6 + 0W_3 + 0W_1 = A^4\lambda$

At 8: $-8W_9 + 25W_8 - 8W_7 - 16W_5 + 6W_4 + W_6 = A^4\lambda$

At 7: $W_9 - 8W_8 + 19W_7 + 4W_5 - 16W_4 + 2W_2 - 6W_6 + 4W_3 = A^4\lambda$

At 5: $2W_9 - 16W_8 + 4W_7 + 22W_5 - 16W_4 + 2W_2 + 2W_3 = A^4\lambda$

At 4: $3W_8 - 8W_7 - 8W_5 + 22W_4 - 8W_2 + 2W_6 - 6W_3 + 3W_1 = A^4\lambda$

At 2: $2W_7 + 2W_5 - 16W_4 + 18W_2 + 4W_3 - 12W_1 = A^4\lambda$

At 6: $2W_8 - 12W_7 + 8W_4 + (16 + 36\gamma)W_6 - (16 + 48)W_3 + (2 + 12\gamma)W_1 = A^4\lambda$

At 3: $4W_7 + 2W_5 - 12W_4 + 4W_2 - (8 + 24\gamma)W_6 + (17 + 42\gamma)W_3 - (8 + 24\gamma)W_1 = A^4\lambda$

At 1: $6W_4 - 12W_2 + (1 + 6\gamma)W_6 - (8 + 24\gamma)W_3 + (19+30\gamma) = A^4\lambda$

..(3.81)

The nine equations were solved by inversion of the matrix on a computer, for different values of γ corresponding to those in the tests carried out on the ruled surface shell. The programme was checked for results for the known case of $\gamma = 1$ [23]. It was found convenient to consider two different values of D, namely $D = .086 \times 10^6$ and $D = 1.67 \times 10^5$. The former was obtained from the Moment-Deflection relationship of the test slab; while the latter was obtained from the strain-moment relationship.

For a 6 x 6 mesh :

$$\Lambda = \frac{a}{L} = \frac{1}{6}$$

$$A^4\lambda = \frac{A^4 G_\gamma L^3}{D} = \frac{1}{1296} \frac{G_\gamma L^3}{D}$$

For $D = 0.086 \times 10^6$, $G_\gamma = .3125$ lb/in^2 :

$$A^4\lambda = \frac{1}{1296} \times \frac{.3125 \times (96)^3}{0.86 \times 10^5} = \underline{2.480620 \times 10^{-3}}$$

i.e. $A^4\lambda L = .238140$

For $D = .167 \times 10^6$

$$A^4\lambda = \frac{1}{1296} \times \frac{.3125 \times 96^3}{0.86 \times 10^5} = \underline{1.277445 \times 10^{-3}}$$

Also $A^4\lambda L =$

$$\gamma = \frac{2E_b I_b}{DL} = \frac{1}{48\,D} (E_b I_b)$$

TABLE NO. 10

VALUES OF γ INVESTIGATED

EDGE BEAMS	$E_b I_b$	$D = .086 \times 10^5$		$D = 1.67 \times 10^5$	
		$\frac{1}{48D}$	γ	$\frac{1}{48D}$	γ
"In-situ" beam	7.1190×10^6	$\frac{1}{41.28 \times 10^5}$	1.734 560	$\frac{1}{80.16 \times 10^5}$	0.888 099
"In-situ" + Channel	6.1719×10^7		14.951 308		71699 476
"In-situ" + Box Section	11.6319×10^7		28.178 050		14.510 853

N.B. All figures in lbs-in units

In the calculations the right hand side of equation (3.81) was put equal to unity in all cases so that the output obtained for the deflection (W) had to be multiplied by $A^4\lambda^2$ to obtained the actual deflections (w).

MOMENTS IN SLAB

Consider, for example, the point O shown in Fig. (3.7). Then :-

$$(M_x)_o = -D\left(\frac{\partial^2 w}{\partial x^2}\right)_o = -\frac{D}{a^2}(w_1 - 2w_o + w_3)$$

$$\therefore (M_x)_o = -\frac{D}{A^2L}(W_1 - 2W_o + W_3)$$

Since calculations have been carried out in terms of $\frac{W}{A^4\lambda}$,

Then :

$$(M_x)_o = -\frac{D}{A^2L}\left[\frac{W_1}{A^4\lambda} - \frac{2W_o}{A^4\lambda} + \frac{W_3}{A^4\lambda}\right]\frac{A^4G_yL^3}{D}$$

i.e. $$(M_x)_o = -\frac{G_yL^2}{36}\left[\frac{W_1}{A^4\lambda} - \frac{2W_o}{A^4\lambda} + \frac{W_3}{A^4\lambda}\right]$$

Similarly :

$$(M_{xy})_o = \frac{G_yL^2}{144}\left[\frac{W_5}{A^4\lambda} - \frac{W_6}{A^4\lambda} + \frac{W_7}{A^4\lambda} - \frac{W_8}{A^4\lambda}\right]$$

MOMENTS IN BEAMS

For the beams parallel to the x axis :-

$$(M_b)_o = -E_bI_y\left(\frac{\partial^2 w}{\partial x^2}\right)_o = -\frac{E_bI_b}{A^2L}\left(\frac{\partial^2 W}{\partial X^2}\right)_o A^4\lambda$$

i.e.:

$$(M_b)_o = -\frac{E_bI_y}{DL}\left[\frac{W_1}{A^4\lambda} - 2\frac{W_o}{A^4\lambda} + \frac{W_3}{3}\right]\times A^2G_yL^3$$

The results of the above calculations are given in the Tables Nos. 11 and 12.

TABLE NO. 11

RESULTS FOR $D = .086 \times 10^6$ lb.in.

γ	Point	W	w (ins.)	M_x (lb. (lb.in./in).	M_y (lb.) (lb.in./in.)	Moment in Edge beam (lb.in.)
	9	13.527 575	3.221 457	156.41	156.41	
	8	12.550 031	2.988 664	152.40	140.51	
	7	9.817 336	2.337 900	141.05	90.43	
γ = 1.724 560	5	11.597 519	2.761 833	136.74	136.74	10334.7
Flat alone	4	8.935 769	2.127 964	126.13	88.01	(at midspan)
	2	6.477 544	1.542 562	80.55	80.55	
	6	5.954 197	1.417 932		0	
	3	5.173 902	1.232 113		0	
	1	3.012 401	0.717 373		0	
	9	6.489 997	1.545 528	111.74	111.74	
	8	5.791 599	1.379 211	99.93	103.56	
	7	3.798 695	0.904 621	72.87	66.52	
14.951 308	5	5.167 056	1.230 485	92.77	92.77	1565.4
(Channels + Flat)	4	3.382 918	0.805 608	61.82	65.76	(at midspan)
	2	2.194 361	0.522 565	44.40	44.40	
	6	0.894 957	0.213 125		0	
	3	0.776 765	0.184 979		0	
	1	0.450 865	0.107 369		0	
	9	5.918 793	1.409 501	108.12	108.12	
	8	5.243 070	1.248 585	95.65	100.58	
	7	3.310 018	0.788 272	60.43	71.47	
28.178 030	5	4.645 239	1.106 217	89.20	89.20	846.80
Flat + Box	4	2.932 421	0.698 327	56.59	63.98	(at midspan)
	2	1.847 361	0.439 931	41.49	41.49	
	6	0.463 840	0.110 222		0	
	3	0.419 905	0.099 996		0	
	1	0.243 674	0.058 039		0	

TABLE NO. 12

RESULTS FOR $D = 1.67 \times 10^5$

Y	Point	W	w(ins.)	M_x (lb.in/in)	M_y (lb.in/in)	Moment in Edge Beam (lb.in)
	9	18.145 569	2.225 282	185.67	185.67	
	8	16.985 117	2.082 970	186.62	164.72	
	7	13.765 614	1.688 146	189.31	102.33	
	5	15.818 738	1.939 931	165.60	165.60	
	4	12.582 400	1.543 043	168.13	102.91	
0.888 099	2	9.297 567	1.140 207	104.72	104.72	8234.3 lb.in.
Flat alone	6	9.266 938	1.136 451	193.16	0	(at midspan)
	3	8.059 663	0.988 397	171.89	0	
	1	4.703 763	0.576 846	107.83	0	
	9	7.574 754	0.928 930	118.63	118.63	
	8	6.833 302	.838 002	108.04	109.23	
	7	4.726 512	.579 636	78.08	75.54	
	5	6.158 067	.755 195	99.54	99.54	
7.699 476	4	4.238 521	.519 791	71.76	69.16	13070.12 lb.in
Flat +	2	2.853 586	.349 950	49.92	49.92	(at midspan)
Channel	6	1.675 519	.205 477	35.36	0	
	3	1.454 486	.178 371	31.11	0	
	1	0.844 610	.103 579	18.78	0	
	9	6.526 205	0.800 341	111.97	111.97	
	8	5.826 370	.714 517	100.20	103.75	
	7	3.829 666	.469 651	66.91	72.96	
	5	5.200 135	.637 719	92.99	92.99	
14.510 853	4	3.411 476	.418 366	62.15	65.87	13554.85 lb.in.
Flat + Box	2	2.216 361	.271 803	44.58	44.58	(at midspan)
	6	0.921 018	.112 949	19.46	0	
	3	0.799 388	.098 033	17.10	0	
	1	0.464 003	.056 903	10.20	0	

CHAPTER 4

4.1 OBJECTS AND DESIGN OF EXPERIMENTS

The experiments were conducted on a Hyperbolic Paraboloid Shell whose boundaries coincided with straight line generators. All four corners of the shell were supported, and a tie bar was incorporated across the low corners.

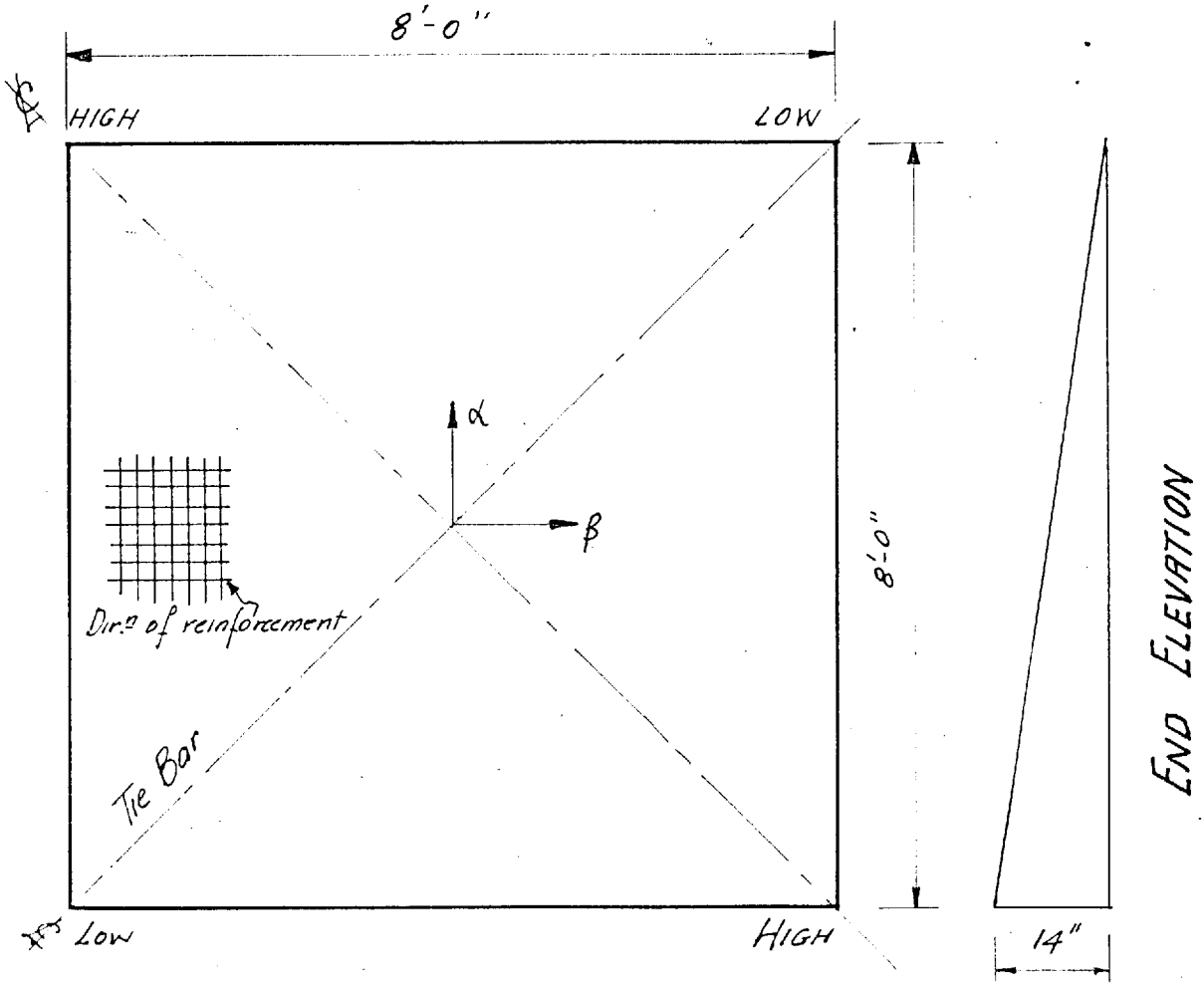
The objects of the experiments were as follows:

(1) To investigate the behaviour of the shell under uniform loading when the stiffnesses of the edge beams and of the tie bar were varied. It was also convenient to study the shell behaviour when uniform loading was applied over half the shell surface.

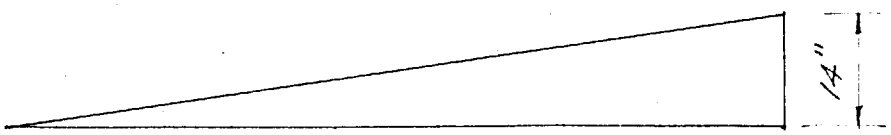
(2) To study the effects of certain edge disturbances.

(3) To study the behaviour of the shell tested to destruction under uniform loading.

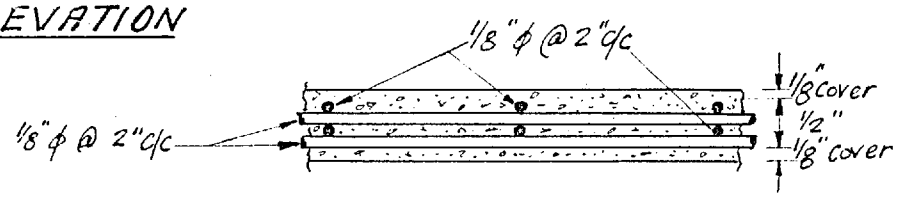
The shell was therefore designed so that different edge beams could be attached at the edges which were originally trimmed with relatively flexible steel beams. The tie bar details were such that the stiffness of the tie could be varied as desired.



PLAN



ELEVATION



SHELL SECTION

SHELL DIMENSIONS

FIG. 4.1.

4.2 DESCRIPTION OF SHELL

The shell, which was of reinforced cement/sand mortar, was constructed by B.M. Ahuja and described in his thesis[21]. Certain preliminary tests carried out by him on this model were alsi reported in his thesis.

4.2 a SHELL DIMENSIONS AND MATERIALS

The shell was 8'0" square by 0.75" thick, with edges stiffened by flexible mild steel edge members. Such members were of course necessary at least to take the tangential shear stresses ($n_{\alpha\beta}$) resulting from the membrane theory.

The rise between the low corner and high corner of the shell was 14 inches, the corners being constructed so that vertical and horizontal movements could be imposed at these points. The rise to span ratio was originally chosen so as to accentuate the bending moments in the shell.

Reinforcement consisted of four layers of 1/4" diameter steel bars at 2" centres. Cover to reinforcement was 1/8". Details of reinforcement and shell dimensions are shown in Fig (4.1).

The aggregate/cement ratio of 3:1 was used in the cement/sand mortar of which the shell was constructed. All particles of the

sand aggregate passed through the No.14 B.S.Sieve. In order to reduce shrinkage to a minimum, a low water/cement ratio of 0.365 was adopted when casting the shell. During curing, elaborate precautions were taken to reduce the shrinkage stresses in the shell.

4.3 LOADING FRAME

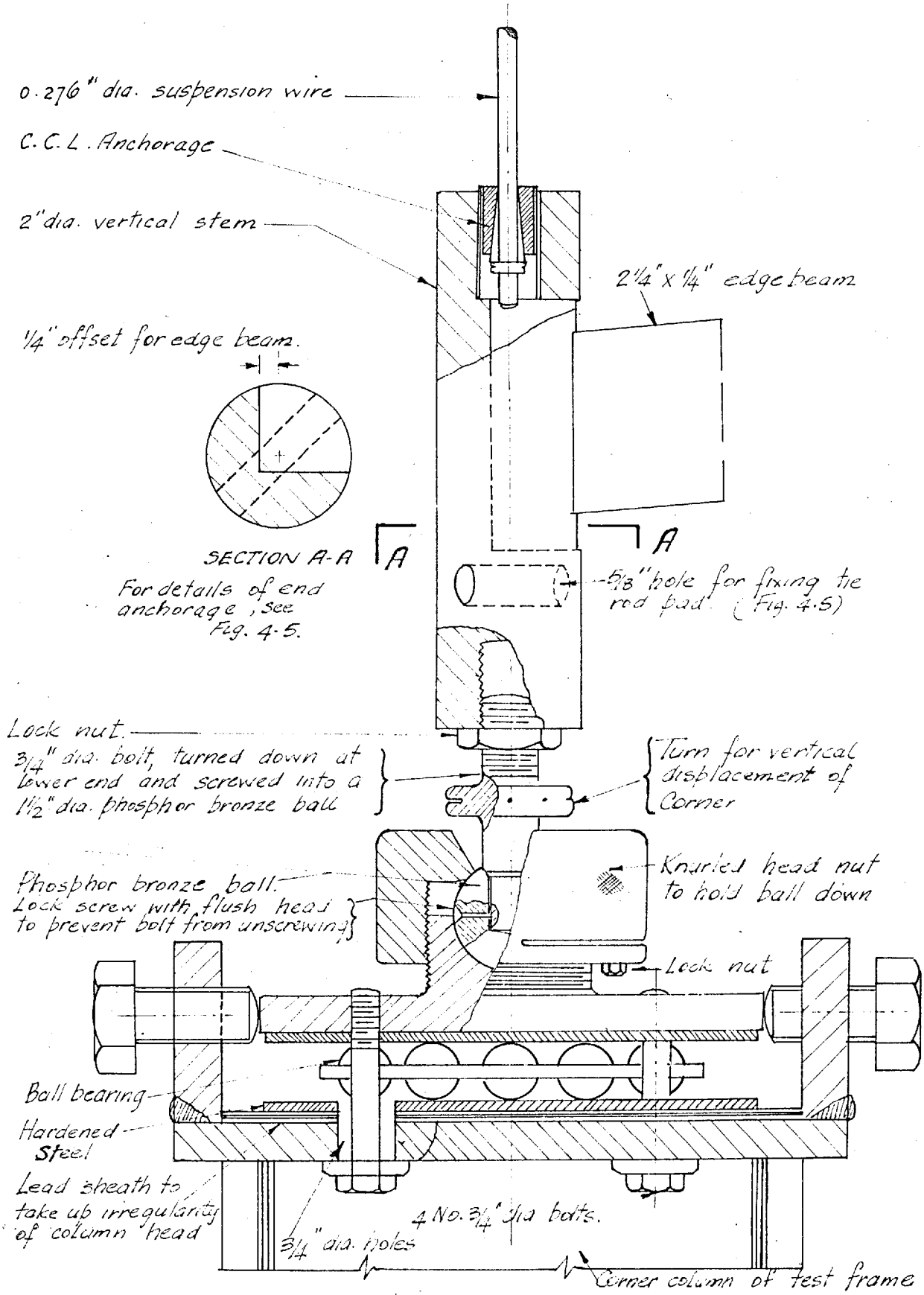
The main part of the loading frame consisted of four R.S.J. columns which took the reaction from the four shell corners. These columns were braced horizontally by two R.S.J.beams running parallel to two opposite shell edges. Spanning horizontally across these beams were four R.S.J's which served as further bracing to the frame, as well as to provide bearing for the hydraulic jacks which were used to apply load to the shell. A flat plate was welded to the head of each column, and by further welding four vertical flat plates to the periphery of this plate, a walled enclosure was formed which contained the ball seating of the shell supports. The horizontal flat plate on each column head was provided with four 3/4" diameter holes through which passed 3/8" diameter bolts. The latter, when tightened, clamped the shell corners in position; and, when slackened, permitted small horizontal movement at the shell corners. The vertical sides of the walled enclosure were provided with tapped holes and screws, so that controlled horizontal corner movements could also be imposed by manipulation of these screws.

The four corners of the shell were kept clamped in position during testing except during stages of the test to destruction. The general arrangement of the test frame is shown in Plates (1) and (6).

4.4 CORNER DETAILS

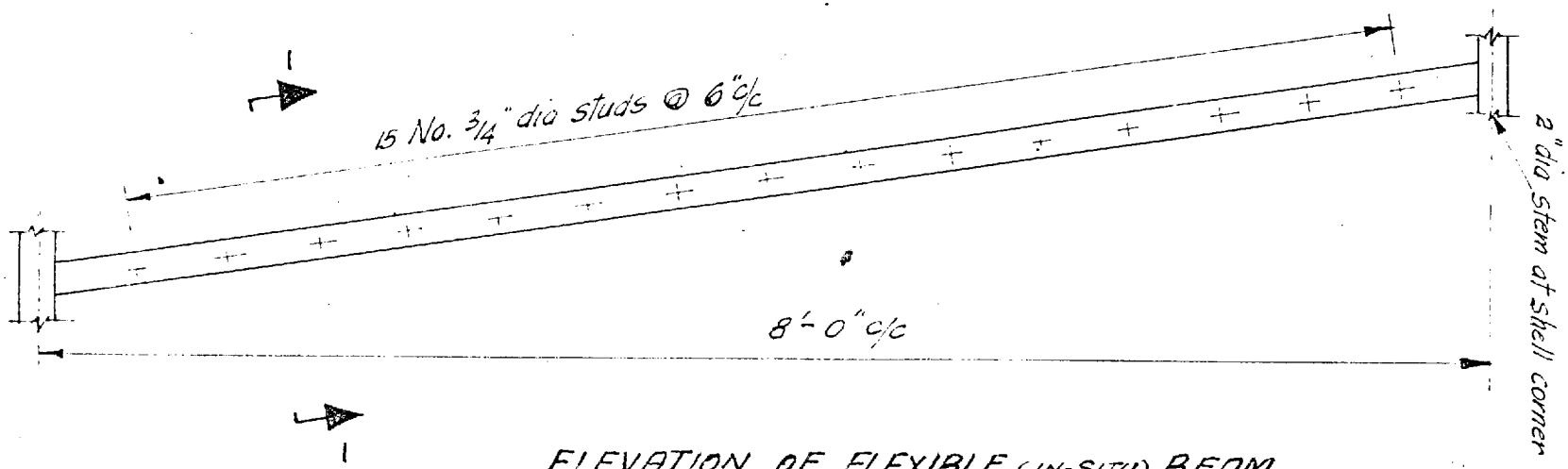
As shown in Fig (4.2) and Plate (2), the corners were elaborately designed to permit both horizontal and vertical movements and rotations as required. Care was taken to reduce friction in the bearings to a minimum. The ends of the four in-situ flexible steel edge beams were welded to a 2" diameter vertical stem, the top of which was provided with a tapped hole. Into this hole was screwed an externally threaded C.C.L. pre-stressing cone. One end of a H.T.S. wire of 0.276" diameter was anchored into the cone, while the other end was supported at a point vertically above the cone by means of a specially made large nut placed on a cantilever-like bracket welded to the column head. By means of the four suspension wires, the shell corners could be lifted vertically, after the bolts clamping the base plates to the column heads were released. This facility however, was not used in the series of tests reported in this thesis.

The lower ends of the 2" diameter stems, which supported the steel edge beams, were provided with a universal ball-jointed seating as shown in Fig (4.2).



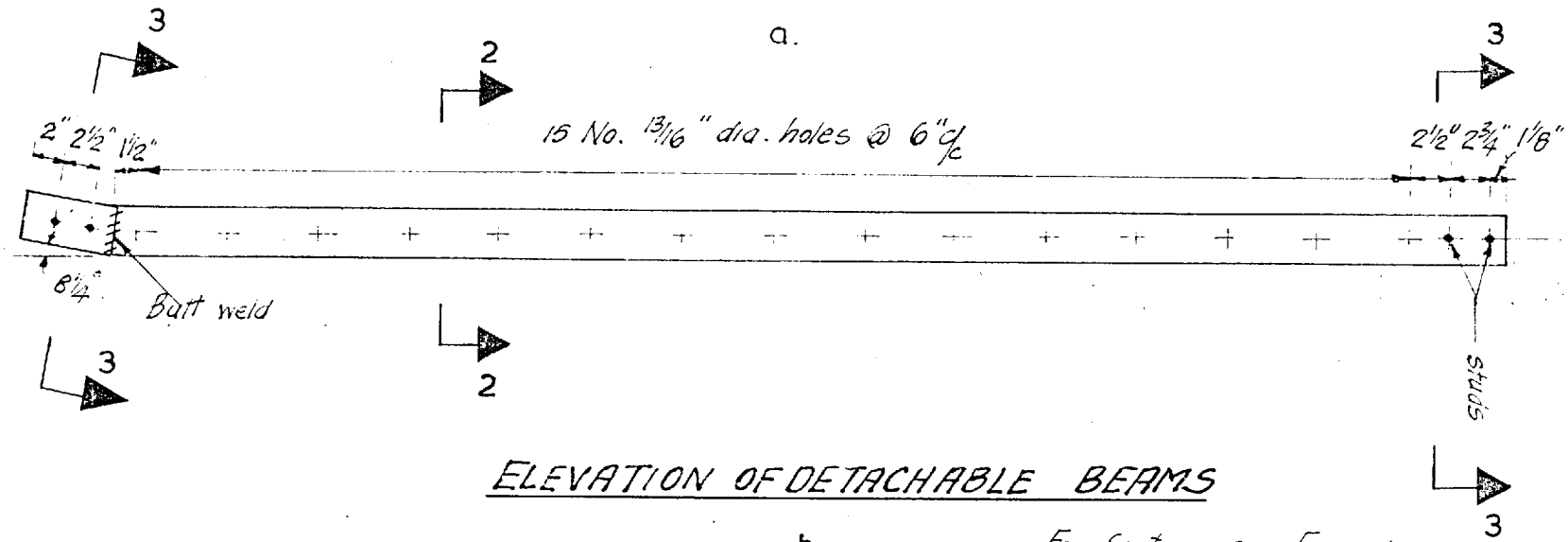
UNIVERSAL BALL JOINT SEATING

FIG. 4.2.



ELEVATION OF FLEXIBLE (IN-SITU) BEAM.

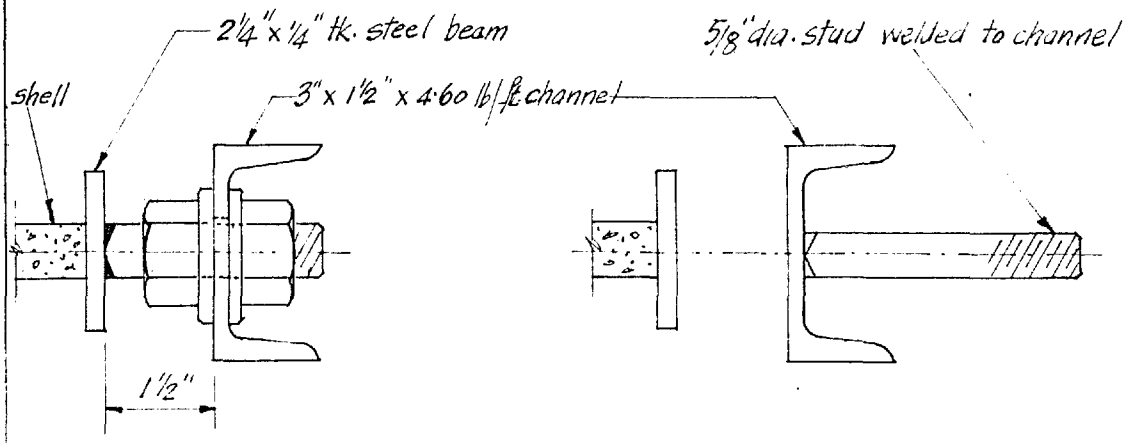
a.



ELEVATION OF DETACHABLE BEAMS

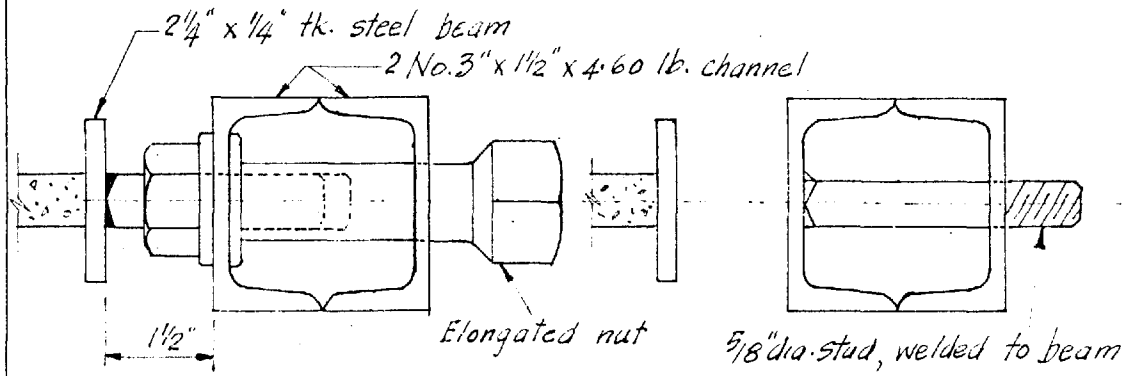
b. For Sections see Fig. 4.4.

FIG. 4.3. DETAIL OF EDGE BEAMS



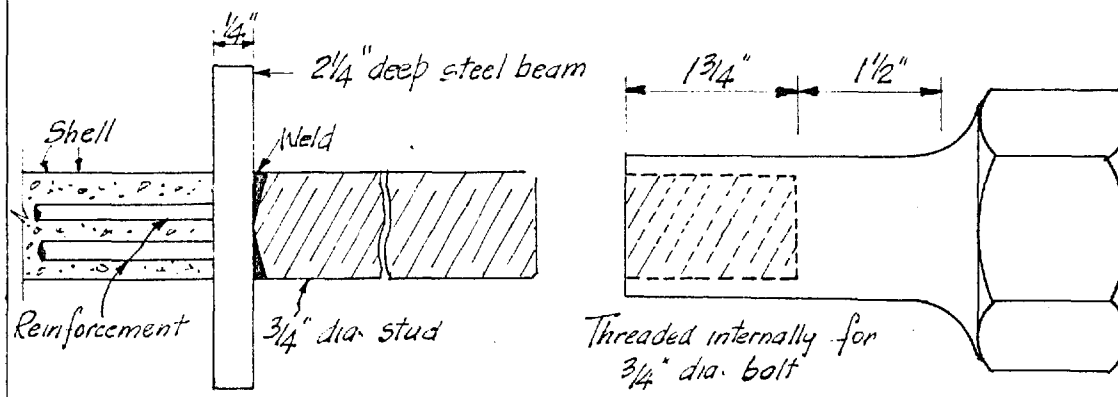
SECTION 2-2 SECTION 3-3

DETAIL OF CHANNEL BEAMS



SECTION 2-2 SECTION 3-3

DETAIL OF BOX - SECTIONED BEAM



SECTION 1-1 DETAIL OF ELONGATED NUT

CROSS SECTIONS OF EDGE BEAMS

FIG. 4.4.

4.5 EDGE BEAM DETAILS

Initially the shell was supported along the edges by flexible steel beams $2\frac{1}{4}$" x $\frac{1}{4}$" thick, the ends of which were welded to the 2" diameter vertical stems at the shell corners. To the outside face of each of these edge beams were welded 3/4" diameter screwed studs which enabled additional stiffening beams to be fixed to the edges. To the other side of the flats were welded two layers of 1/8" diameter mild steel bars 5" long which lapped with the main reinforcement of the shell thus ensuring continuity of reinforcement at the edges.

The variation of edge beam stiffness was achieved by fixing two sets of edge beams to the 3/4" diameter studs provided along the in-situ beam. The additional sections took the form of a 3"x $1\frac{1}{2}$" x 4.60 lb. channel, and a 3"x 3" beam of box section made up from two channels welded toe-to-toe. The details of sections of additional edge beams and their method of fixing are shown in Figs (4.3 and 4.4). In the case of the box sections, the length of the 3/4" diameter studs was inadequate to enable them to be bolted in a manner similar to that of the channels, hence the detail of fixing had to be altered. Elongated nuts were made which passed through enlarged holes on the outer face of the box section and screwed onto the studs which passed through holes in the inner face of the section. An attempt was made, without much success, to establish some degree of continuity at the corners of the additional edge beams, this problem

being made greater by restricted clearances at the shell corners. An L-shaped elbow was made from 4"x 2" channels. These elbows were provided with two slightly elongated holes in each leg, through which passed two studs which were welded to the ends of each edge beam. After being bolted into position, the elbow and edge beams were prevented from moving relative to each other by wedging tapered washes into the spaces between their toes. A view of the elbows is shown in Plate (3) from which it will be seen that the welded joint at the junction of the legs of the elbow was reinforced by plates welded to the webs and toes of the section.

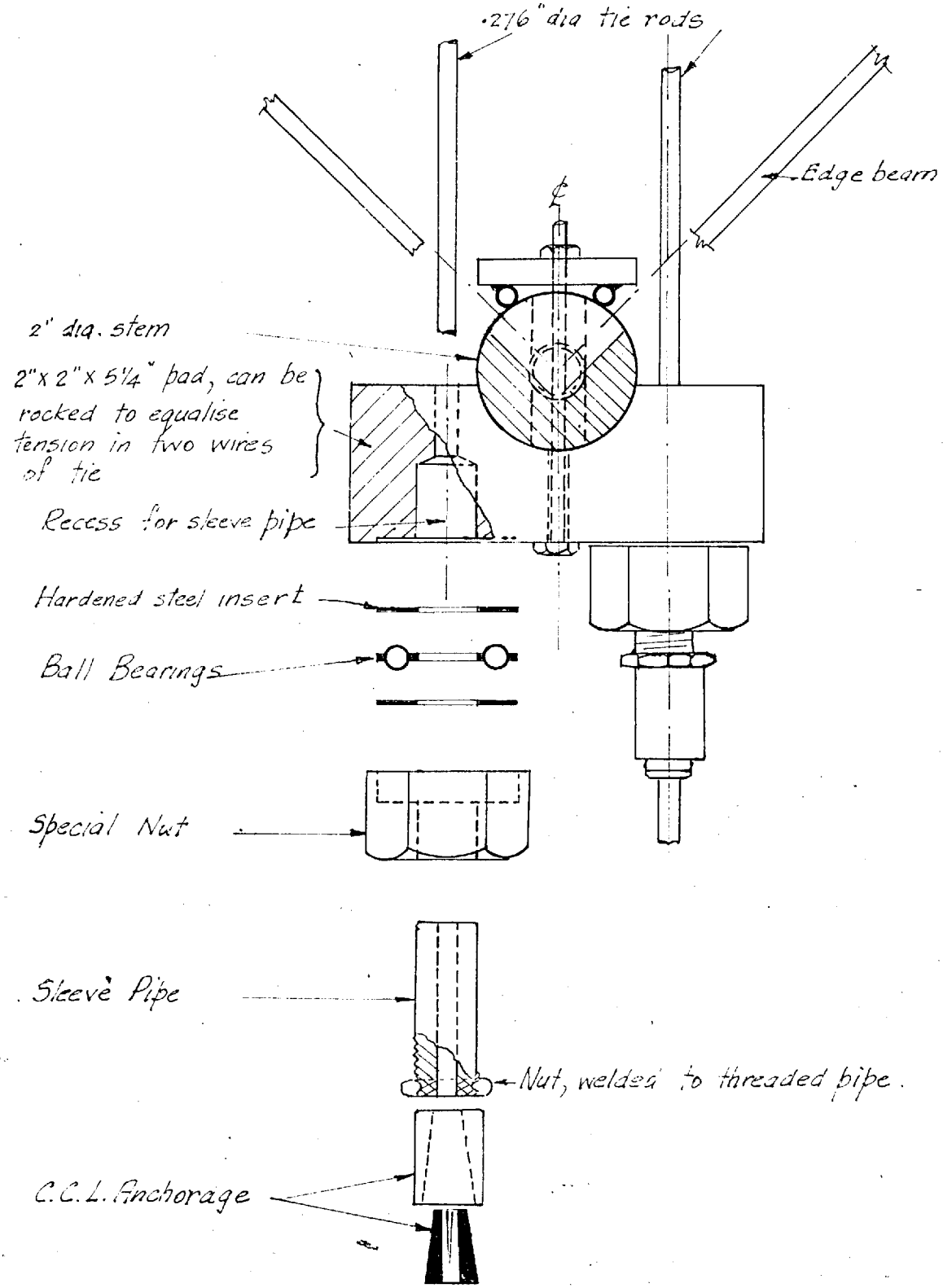
In order to clear the bearing pads at the corners of the shell, it was necessary to weld to the ends of the edge beams special short lengths inclined at an angle to the axis of the beam. This also shown in Plates(4),(4A), and (4B).

4.6 TIE BAR DETAILS

Two different sets of tie bars were used in the experiments. The first were relatively flexible ties comprised of two 0.276" diameter H.T. steel wires, while the second consisted of two $1\frac{1}{8}$" diameter Lee McCall Bars.

4.6 a FLEXIBLE TIE

The two 0.276" diameter H.T.Steel wires spanned across the low corners of the shell. The method of fixing is shown in Fig (4.5)



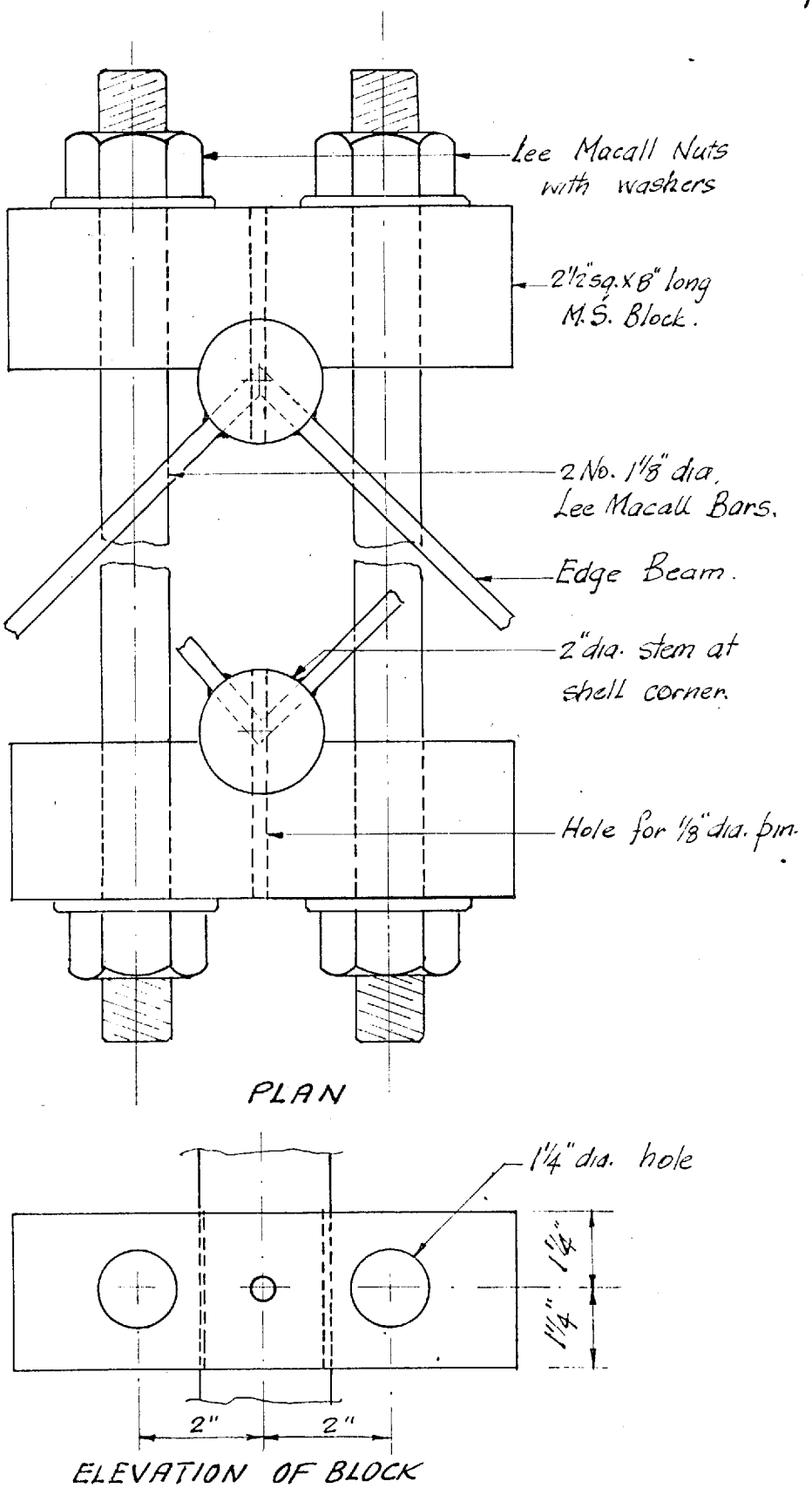
END ANCHORAGE OF FLEXIBLE TIE

FIG. 4.5.

and Plate (2). These tie bars were supported at their ends in such a manner that any tendency to twisting of the tie, when being tightened, was reduced to a minimum. The wires were held by C.C.L. grips supported on sleeve pipes through which the cables passed. These pipes were threaded externally to engage a specially designed large nut. The load in the tie was transferred to a 2"x 2"x $5\frac{1}{4}$" long steel pad via the large nuts by means of a thrust race. The bearing fitted into a special recess provided in the nut which served to protect the bearing from dust. The pad in turn bore centrally on the 2" diameter stem at the shell corner. By means of this arrangement it was possible to apply a force to the tie bar by manually manipulating the large nuts, since the friction in the system was low. The force in the tie bars could be equalised by rocking the steel pad. A similar arrangement was used to support the vertical suspension wires at the shell corners. Throughout the tests these vertical wires were slackened so that all the reaction at the shell corners was transmitted directly to the vertical columns of the loading frame via the steel bearings at the column heads.

4.6 b RIGID TIE

This consisted of two $1\frac{1}{8}$" diameter Lee McCall Bars threaded at the ends to accomodate Lee McCall Nuts. As shown in Fig (4.6) these nuts bore on washers which rested directly onto a $2\frac{1}{2}$" x $2\frac{1}{2}$" x 8" long steel pad. This pad transferred the load to the vertical 2" diameter stem at the shell corner. No special precautions were taken to avoid



ANCHORAGE OF RIGID TIE BARS. FIG. 4.6.

twisting in these wires when the nuts were tightened; but as described in the next chapter, steps were taken to ensure that at the beginning of a test these bars were identically stressed.

4.7 LOADING TECHNIQUE

It was necessary to design the loading system to be as flexible as possible. It should be stable at all stages and should be capable of loading the shell at a rate which could be easily varied, while eliminating at the same time, any possibility of impact loading. The hydraulic system, Fig (4.7), used in the tests met these requirements ideally, especially in view of the restricted headroom in the laboratory.

4.7 a UNIFORM LOADING AND HALF LOADING

This was simulated by point loads applied at 64 points on a 1 foot grid over the shell surface. The load was applied through 16 inter-connected hydraulic jacks, each of which applied load to four loading points on the shell. One end of each jack was fitted with a steel plate which could be clamped to the R.S.J.'s provided in the loading frame to take the thrust of the jacks. The other end of each jack was provided with a screwed fitting, the end of which was recessed to accommodate a 1/2" diameter steel ball. The latter rested in another recess at the central point of a H-Frame comprised of a T-shaped beam resting through a ball joint on the mid-point of another transverse beam.

The four tips of the H-Frame were connected through turnbuckles to four loading points on the shell by means of a looped suspension wire. At the shell end, each suspension wire passed through a small hole provided in the shell, then through a central hole in a 6" square wooden pad and finally around a 6" long, 1/2" diameter steel bar. This bar rested on the wooden pad; thus the thrust from the jacks was distributed equally to four points on the H-Frame and then via the four suspension wires to four points on the shell surface. "Tiluma" cement was used to fix the wooden pads to the shell surface. The arrangement of the jacks, H-Frame, and suspension wires is shown in Plate (5). Levelling of the H-Frame was achieved by manipulating the turnbuckles.

The jacks were connected by 1/4" diameter flexible hosing to a 3/4" diameter ring main. This system was then connected to an electrical pump through a length of flexible hosing and two control valves. The latter served to control the rate at which pressure was built up in the system, and hence, also the rate of loading of the shell. Further, the combination of the large diameter main and flexible rubber hosing absorbed any shock transmitted to the system due to pulsations resulting from the operation of the electrical pump. A constant length of hosing was used to connect the jacks to the ring main, hence the friction loss along the hoses was constant. The two valves incorporated in the ring main made it possible to isolate 8 of the 16 jacks from the pressure system, thus providing loading

over half of the shell surface. Provision was made for "bleeding" air from the system at the point most remote from the inlet. Two calibrated pressure gauges were used to record pressures, one being placed near the inlet and the other near the "bleeding" point. The difference in pressure between these gauge readings represented the friction loss in the system.

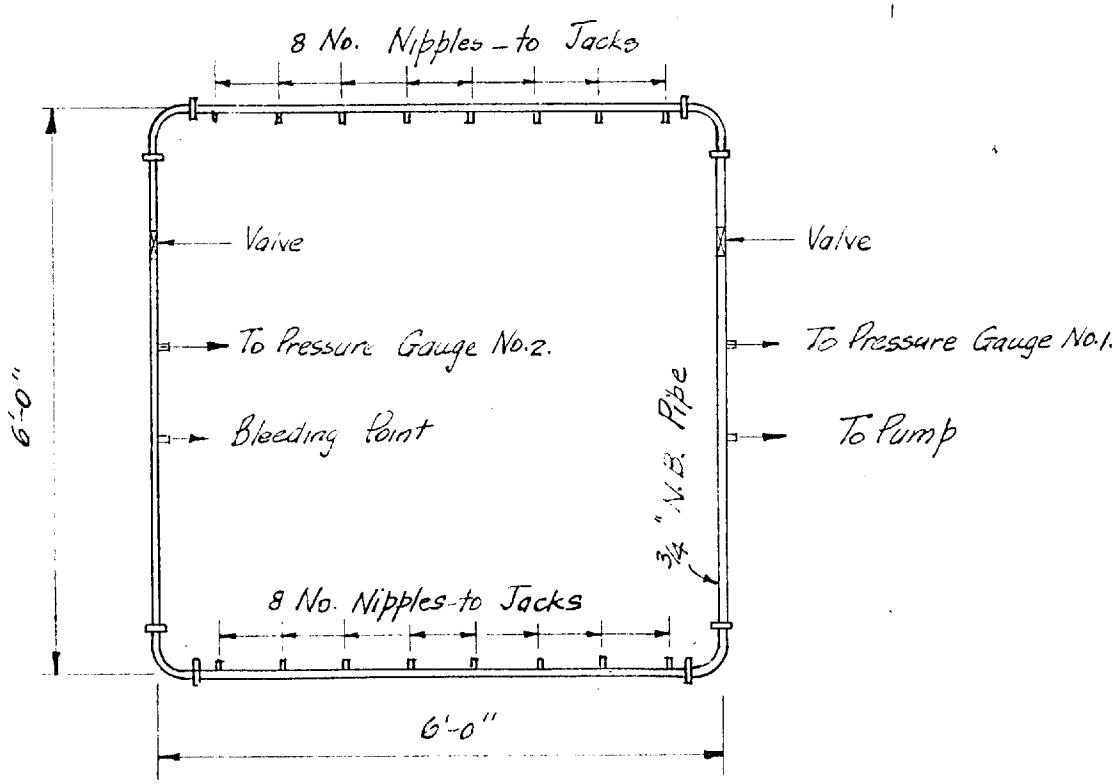
The capacity of the electrical pump was low, therefore, a large capacity hand pump was used initially to fill the entire system with oil at atmospheric pressure. The two pumps were connected through a valve which when closed, isolated the hand pump from the hydraulic system; therefore the electrical pump was used to increase the pressure. Since the capacity of the ring main and jacks was so great relative to that of the electrical pump it was possible to increase the pressure at a slow rate. This rate could be further varied by manipulation of the two valves through which the electrical pump was connected to the hydraulic system; or, if necessary, by using the hand pump.

In order to maintain the hydraulic pressure constant over any period of time it was necessary to rid the system entirely of air. By continuous pumping and then bleeding at each nipple, the ring main was filled with oil at atmospheric pressure. The jacks and connecting hosing, after being filled with oil, were then connected

to the system and then all air removed by further bleeding. Any leaks were easily detected and eliminated. Thus on testing the system under a pressure of 40 psi over a period of eight hours a loss in pressure of only 1 psi resulted.

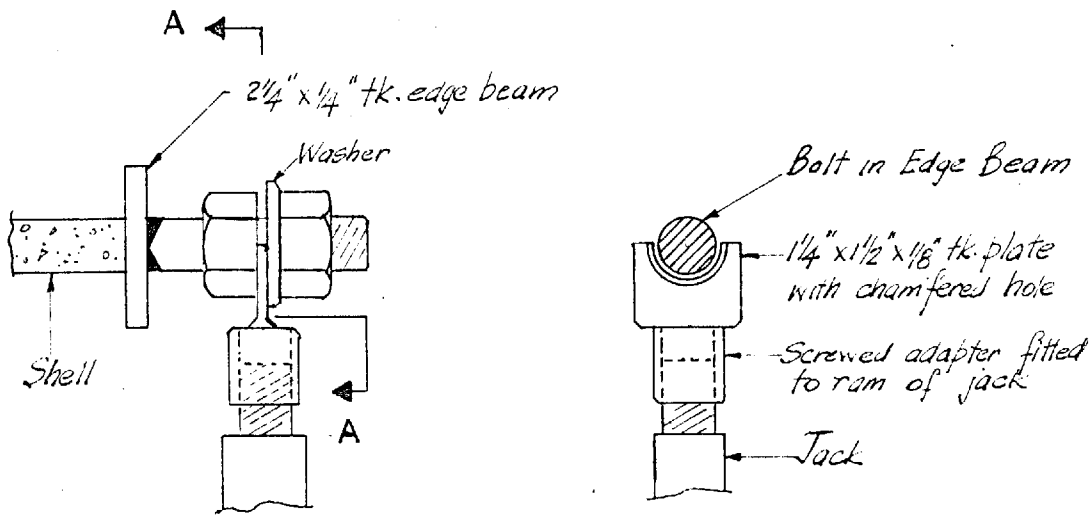
4.7 b EDGE LOADING

The loading of an edge was achieved by jacking against seven of the studs provided along the in-situ flexible edge beams. The base of each jack was supported on a steel ball accurately positioned on a horizontal plate fixed to the testing frame. The other end of the jack bore onto the stud through a 1/4" thick plate having a "U" end formed by cutting diametrically across a chamfered 7/8" diameter hole. This detail is shown in Fig (4.8). It was thus possible to apply a point load to each of the seven studs, either directly against the face of the edge beam or at a predetermined distance from it, thus inducing shear only, or shear together with moment, at the edge. The point on the loading frame vertically below the point at which the loading was to be applied to the shell edge was determined by a plumb-bob. At the commencement of the tests the screwed fittings at the heads of the jacks were adjusted so that the "U" ended plates were just touching the studs on the shell edges. The general arrangement of the edge loading system is shown in Plate (6).



DETAILS OF HYDRAULIC PRESSURE SYSTEM

FIG. 4.7.



METHOD OF APPLICATION OF EDGE LOADING

FIG. 4.8.

4.7 c CALIBRATION OF JACKS AND PRESSURE GAUGES

The pressure gauges used in the tests involving edge loadings of the shell were graduated in 5 psi intervals up to 100 psi. Those used in the uniform loading tests were graduated in 10 psi intervals up to a maximum of 300 psi.

In order to translate pressure gauge reading to the force on the ram of the jack it was necessary to calibrate the gauges against known loading applied to the jack. Each gauge was connected to a jack by means of a flexible rubber hose. Known weights were placed on the jack and the corresponding pressure gauge reading noted, thereby giving a relationship between loading and pressure gauge reading. Results were obtained for each gauge connected in turn to five different jacks and the law obtained in each case showed very little variation. Due mainly to friction in the system, the law obtained with increasing load was different from that obtained for decreasing load, the latter showing greater variation than the former. Consequently it was decided to take readings only with increasing load on the shell. Ideally the pressure gauges should be calibrated in the hydraulic system when all 16 jacks were connected but this obviously was not practicable .

4.8 STRAIN MEASUREMENT

The 214 electrical resistance strain gauges fixed by Ahuja in

his preliminary experiments have been employed in the present tests to measure strain. Of these, four circuits of 48 gauges each were fixed to the shell surface. These were arranged so that the readings of any particular gauge could be checked by at least one other gauge in another position on the shell surface. Symmetry was not assumed. The remaining gauges were attached to the in-situ edge beams and tie bars, and suspension bars. Only one gauge was placed on each tie bar and suspension wires while four gauges were fixed to each edge beam at midspan.

In addition, four strain gauges were attached at midspan of each of the stiffening edge beams used in the series of tests now being reported. The majority of gauges were of Technograph 1" linear foil type of 80 ohm nominal resistance. The six gauges on the suspension wires and flexible tie bars were 1/2" gauges of paper-backed type. Some typical gauges on the concrete were checked for drift which was quite small over a period of several hours, hence it was concluded that no deterioration of the bond had taken place.

The following technique was adopted in fixing the gauges to the shell edge beams: All scale and rust were removed from the surface by means of a wire brush. The surface was then washed clean with acetone and allowed to dry. A thin layer of Araldite MY573 was then applied to the prepared surface, and the gauge was washed in

acetone and left to dry. The back of the gauge was then painted with Araldite and the gauge fixed in position on the surface before the Araldite on both surfaces had commenced to set. Care was taken to ensure that no air bubbles were trapped between the back of the gauge and the surface to which it was fixed. The gauge was finally covered with a strip of polythene sheeting on top of which was placed a rubber pad and weights. The entire assembly was left undisturbed for at least two days, to allow the Araldite to harden. The leads were then soldered to the gauge which was finally covered with a protective layer of Araldite.

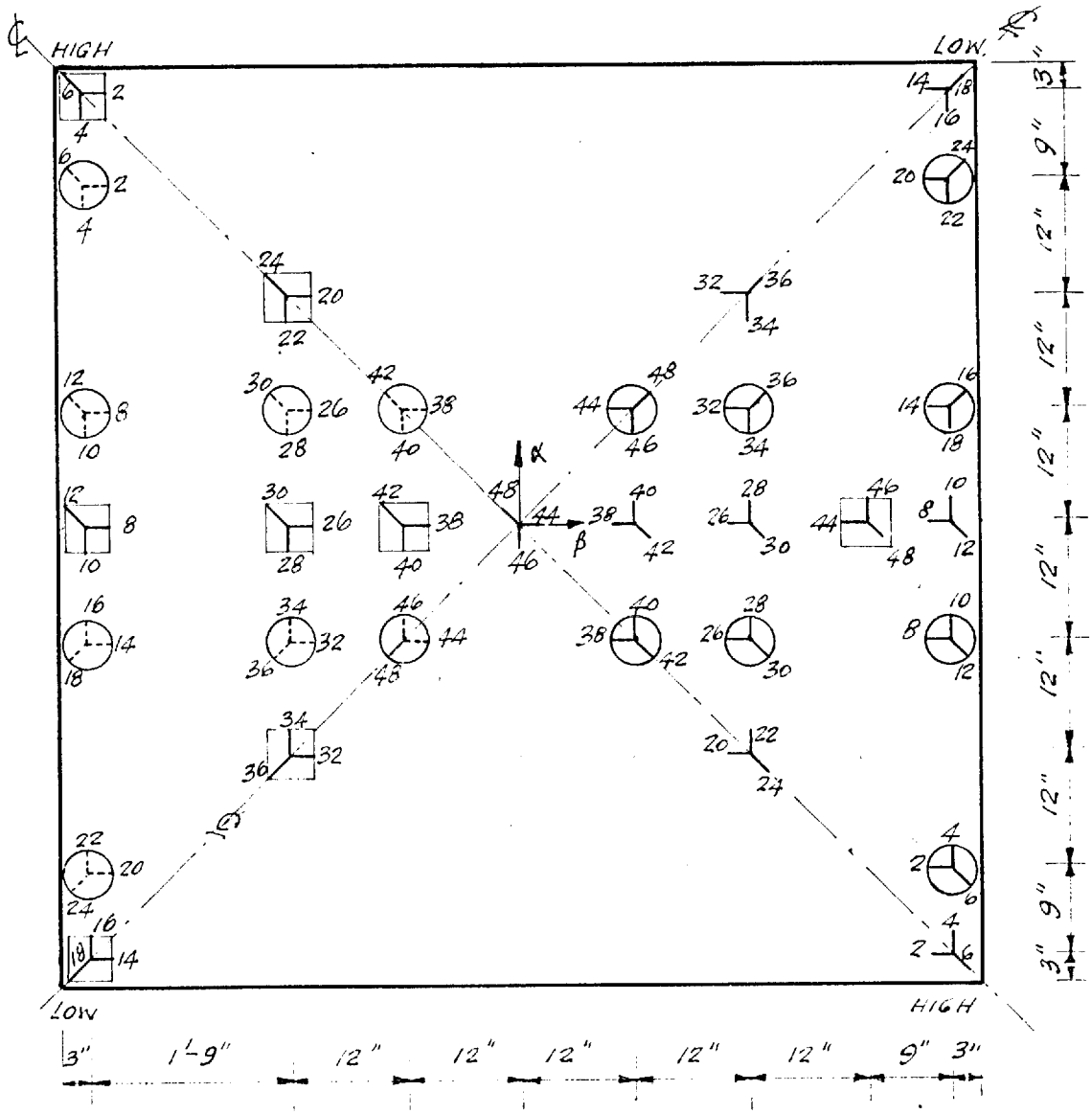
The gauges on both surfaces of the shell were arranged in rosettes so that complete information on sheears, moments, and direct forces could be deduced from readings obtained from gauges at the point concerned. The position of gauges on the shell surface and on the edge beams are shown in Fig (4.9) and (4.10).

For tests with uniform loading, one of the circuits (No.5) was permanently connected to a Peekel 540 DNH Strain Recorder through a 48-way switch box. For the first series of tests with the flexible tie bars the other circuits were in turn connected to a Savage and Parsons 50-way Strain recorder. In order to select any particular circuit for measurement, a Mercury switch box was used in conjunction with the Savage and Parsons recorder. All necessary

LEGEND:

- Circuit No.1
- Circuit No.2
- Circuit No.3
- Circuit No.5

Gauges Nos. 49 & 50 of Circuit No.3, attached to Tie rods are of paper backed type. All other gauges are of foil type.

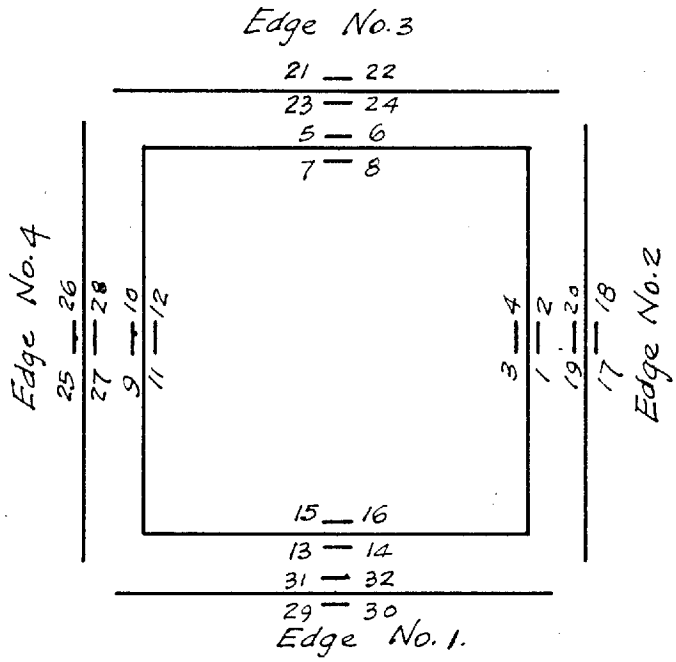


NOTES:

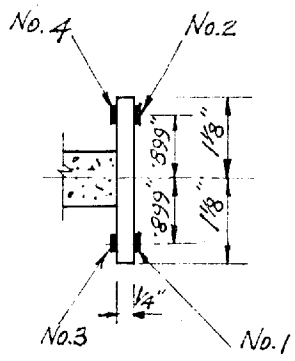
For Circuit No.4 (Edge Beams), see Fig. 4.11.
Circuit No.5 permanently connected to 5 Volt A/c Peekel Strain recorder. Other four circuits connected in turn through 50-way mercury switchbox to Savage and Parsons recorder.

FIG. 4.9.

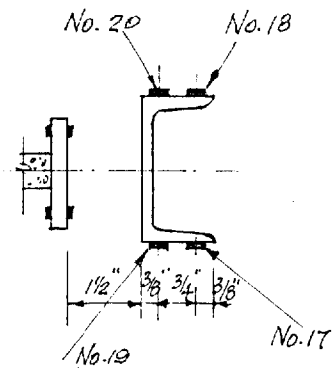
NUMBERING OF STRAIN GAUGES ON TOP SURFACE OF SHELL DURING TESTS NOS. 3 – 6



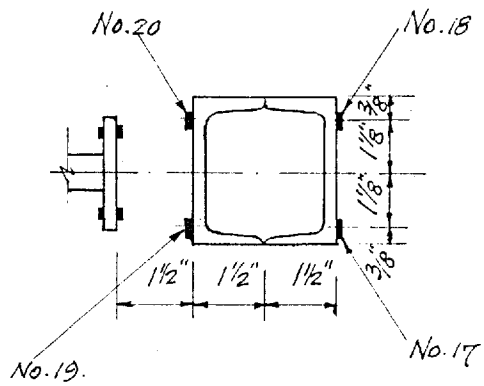
PLAN



FLEXIBLE "IN-SITU BEAM



CHANNEL



BOX SECTION

NUMBERING OF STRAIN GAUGES ON EDGE BEAMS

FIG. 4.10.

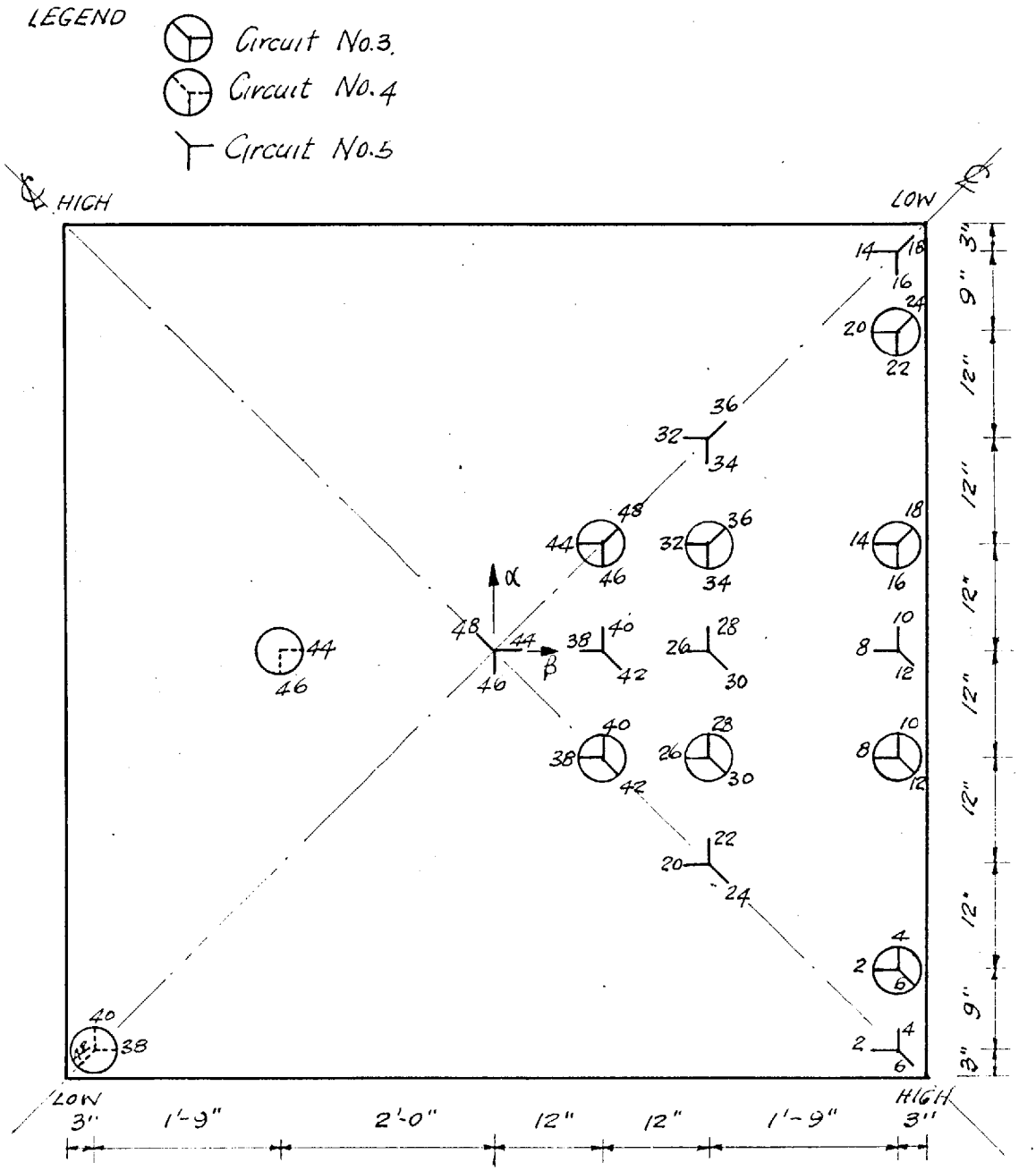
precautions were taken to ensure that the former was not disturbed during testing. It was possible to check the reliability of readings obtained through the mercury switch box by comparing readings obtained from gauges in different circuits during a test repeated on different days. The accuracy of the loading technique and of the readings of the gauges in the permanently connected circuit No.5 could also be checked by comparing readings obtained for this circuit on different days.

In the Savage and Parsons system of strain measurement all the gauges were continuously excited by direct current, the voltage across the bridge being maintained at 5 Volts. Each active gauge required a dummy gauge which was fixed to a slab cast at the same time as the shell. This slab was of the same thickness as the shell, was reinforced similarly and was cured under identical conditions. In the Peekel system of strain measurement, the voltage across the bridge was 5 Volts A.C. and the current passed through one active and one dummy gauge only during measurement, hence only two dummy gauges were required for use with a switch box which was divided into two halves, each taking 24 gauges.

During the first series of tests it was observed that the closing errors of gauges connected to the Savage and Parsons recorder were in most cases so large that the readings obtained were useless.

Since all the gauges in a circuit were tested for drift before measurement commenced the large closing errors were attributed to faults either in the mercury switch box or in the strain recorder or a combination of both. Fortunately however, in the second series of tests involving the rigid tie bars, another type of Peekel strain recorder was available and was used for circuits which were connected to the mercury switch box and Savage and Parsons recorder. In these circuits a set of Peekel transistorised Strain Indicators were used. In this system the Bridge operated on 1 Volt A.C. and 12-way switch boxes were used to select the gauges for measurement. As in the first series of tests the 5 Volt A.C. Peekel Strain recorder was also attached to circuit No.5 permanently. Very good strain readings were obtained with the 1 Volt A.C. Peekel Strain indicator since the drift in this case was considerably reduced owing to the small current passing through the gauges at the time of measurement. The number of these recorders available was very limited and it was necessary to repeat several times the tests in the elastic range in order to cover a reasonable number of gauges. It was therefore decided to eliminate certain gauges and to provide checks on the readings of certain gauges by rearranging the circuits. For this reason only three circuits were used in the second series of tests; these circuits are shown in Fig (4.11).

Precautions were taken to reduce drift in gauges to a minimum.



NOTES.

1. Gauges Nos. 33-36 of Circuit No.4., attached to tie bars.
2. Gauges Nos. 1-32 of Circuit No.4, attached to edge beams (Fig.4.11)
3. Circuit No. 5 permanently connected to 5 Volt A.C. Peekel recorder. Other circuits connected in turn through 23-way and 12-way switchboxes to 1 Volt A.C. Peekel recorder.
4. All gauges of foil type.

NUMBERING OF STRAIN GAUGES ON TOP SURFACE OF SHELL DURING TESTS NOS. 7 - 9

FIG. 4.11.

As far as was possible, tests were carried out on mid-week afternoons when the temperature of the laboratory was practically constant. All lights in the laboratory were switched on from the evening preceding the day of the test and draughts were controlled by closing all doors and by keeping the number of persons in the vicinity of the shell to a minimum. Atmospheric temperature was observed continuously throughout a test by means of two thermometers placed near to two opposite edges of the shell. The temperature changes over a period of testing of about 4 hours were not greater than $\pm$.3 degrees Centegrade. The zero strain readings were taken at the beginning of a test and again at the end; and the difference between the two sets of zero readings was distributed proportionately to the intermediate readings. In some cases, especially when small strains were being measured, the drifts were numerically greater than the strain readings.

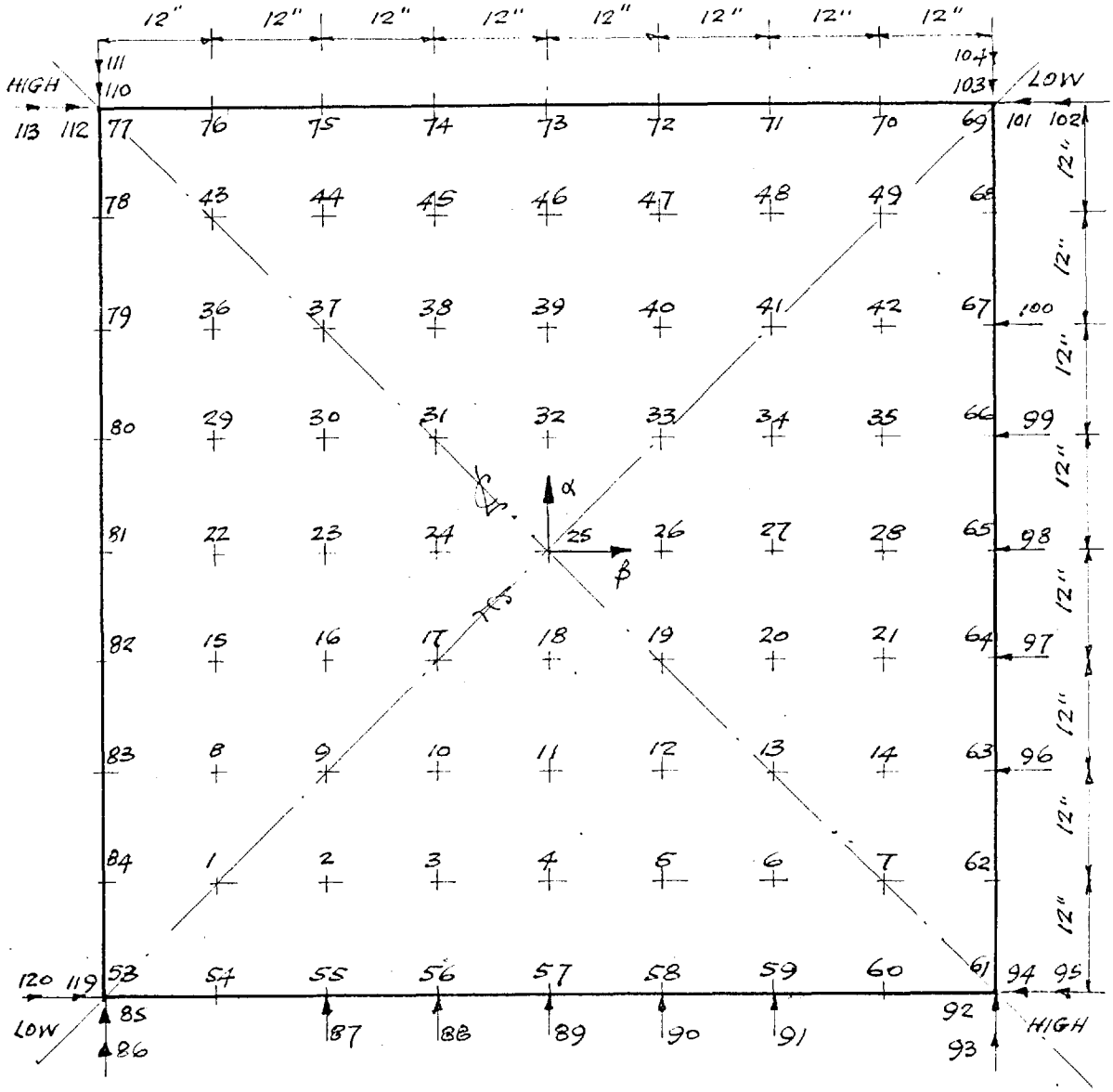
4.9 MEASUREMENT OF DEFLECTIONS

A maximum number of 131 dial gauges were used to measure deflections; all gauges were of the John Bull Type. The gauges Nos. 1-49, measuring vertical deflections over the shell surface, were of 1" travel and graduated to .001 inch. All other gauges were graduated to .0001 inch and had 1/2" travel. The arrangement of dial gauges is shown in Fig (4.12). Vertical deflections along the edge beams and at shell corners were recorded by gauges Nos. 53-84. At each corner of the shell, four dial gauges were used to measure rotational

as well as horizontal movements in coordinate directions. Horizontal movements along the edges were measured in some of the tests by gauges Nos. 87-91 and 96-100. Deflection readings were taken at every loading stage of a test, and since the majority of tests were repeated more than once, there were ample checks on the deflection readings.

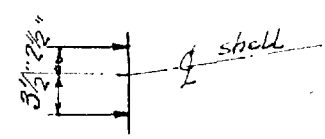
The gauges were supported on a framework of "Handy-angles" with steel flats used to support this framework at its periphery. The entire frame supporting the dial gauges was independent of the shell.

A 1/2" wood screw was fixed with "Durofix" to each point at which deflection was to be measured and the gauge was set by eye to measure deflection in the appropriate direction. The spindle of each gauge was fitted with a specially made flat smooth anvil, which was initially made to rest approximately centrally on the tips of the screws fixed to the deflection points. This ensured that only the component of deflection parallel to the stem of a particular gauge was recorded. Since the gauges remained in position for long periods, the spindles were frequently cleaned to keep them free of dust.



NOTES:

1. Gauges Nos. 1 – 84 measure vertical deflections. Remaining gauges measure horizontal deflections.
2. Gauges Nos. 1 – 49 read to ·001 inch. All other gauges read to ·0001 inch.
3. At the corners the gauges measuring horizontal deflections are numbered so that the gauge having the lower number is nearer the shell base. These gauges placed as shown below



NUMBERING OF DIAL GAUGES

FIG. 4.12.

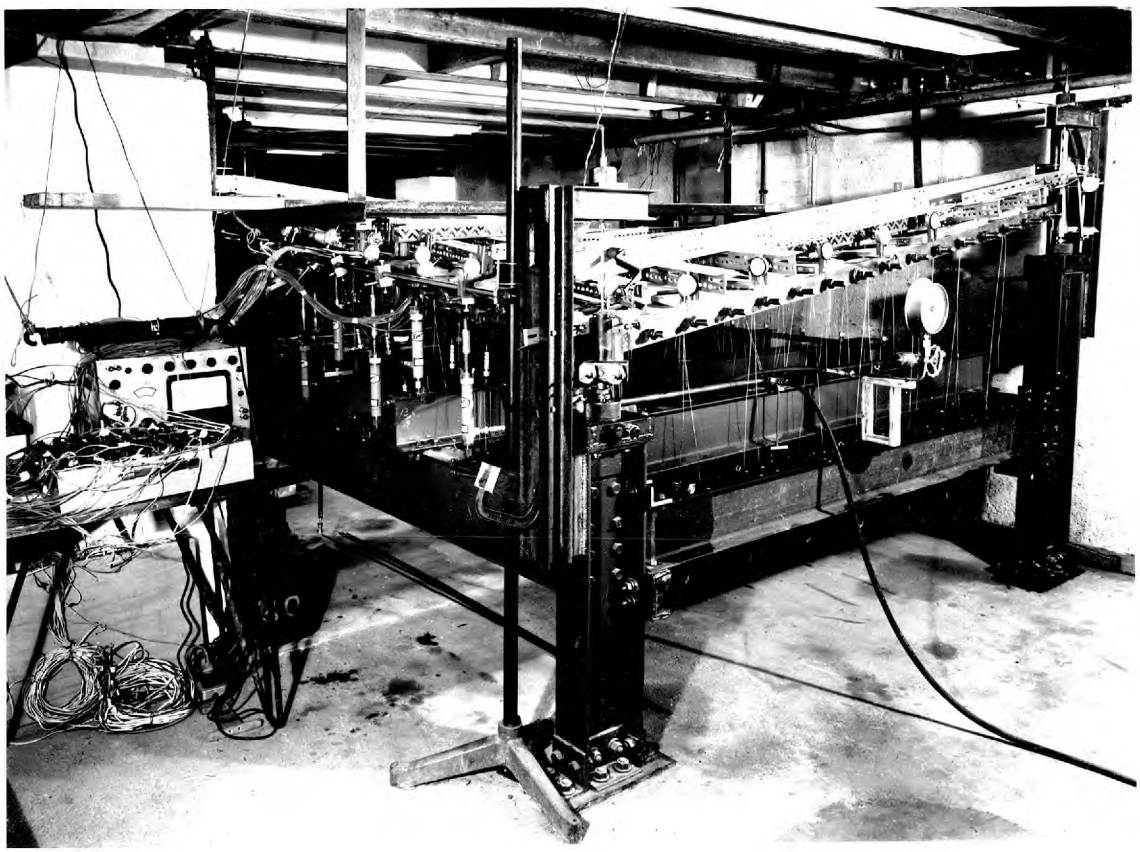


Plate 1. Loading frame.



Plate 2. Shell corner and channel edge beam.

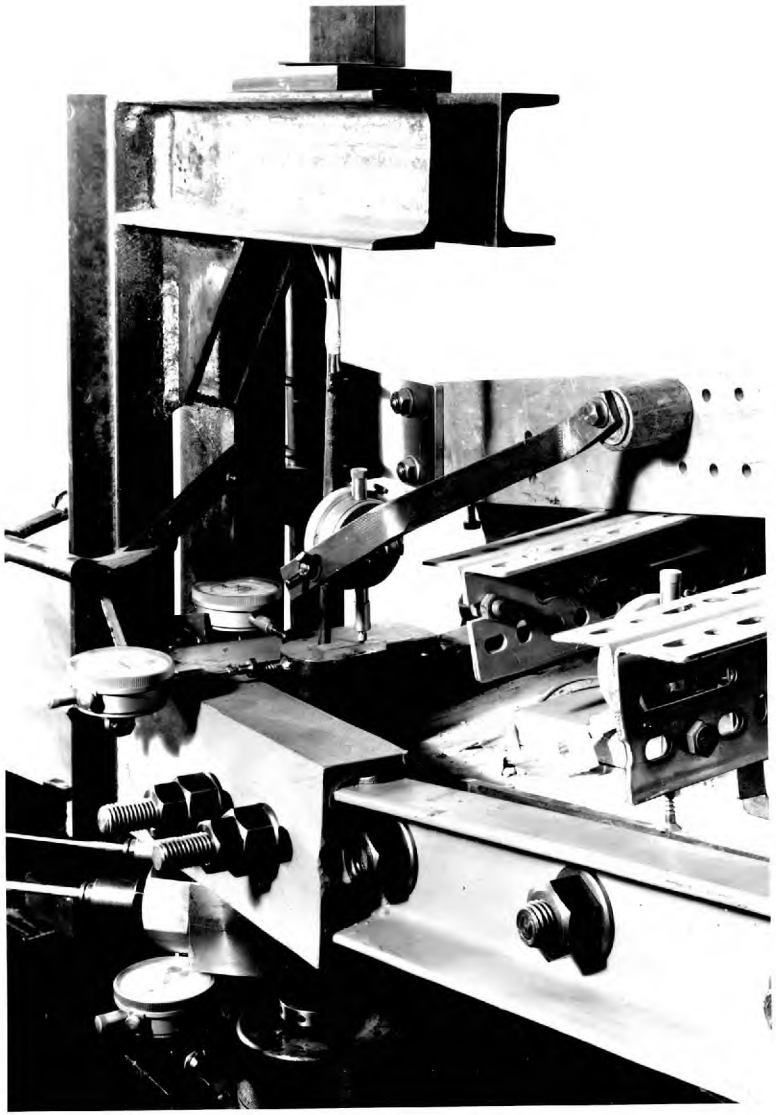


Plate 4. Edge beam junction at corners

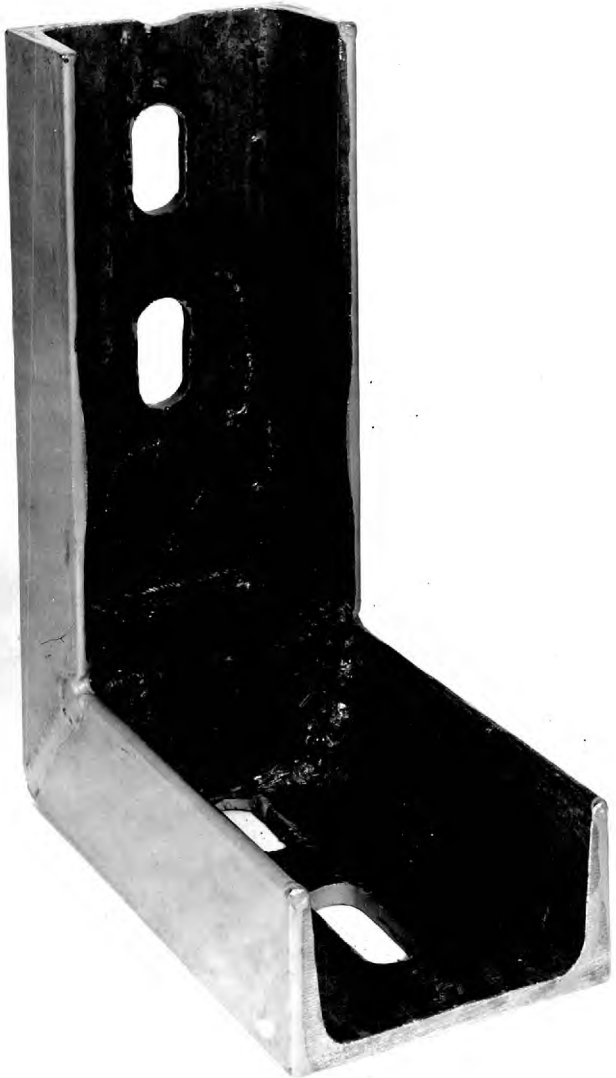


Plate 3. Elbow used at junction of edge beams

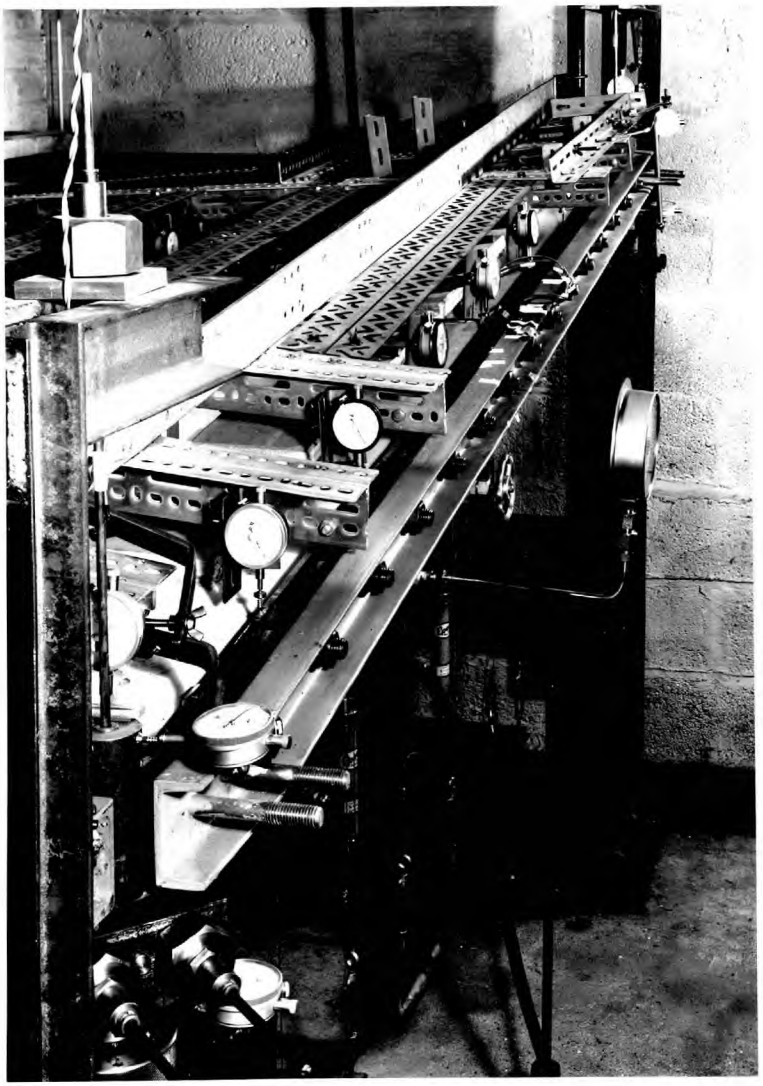


Plate 4b. Channel edge beam

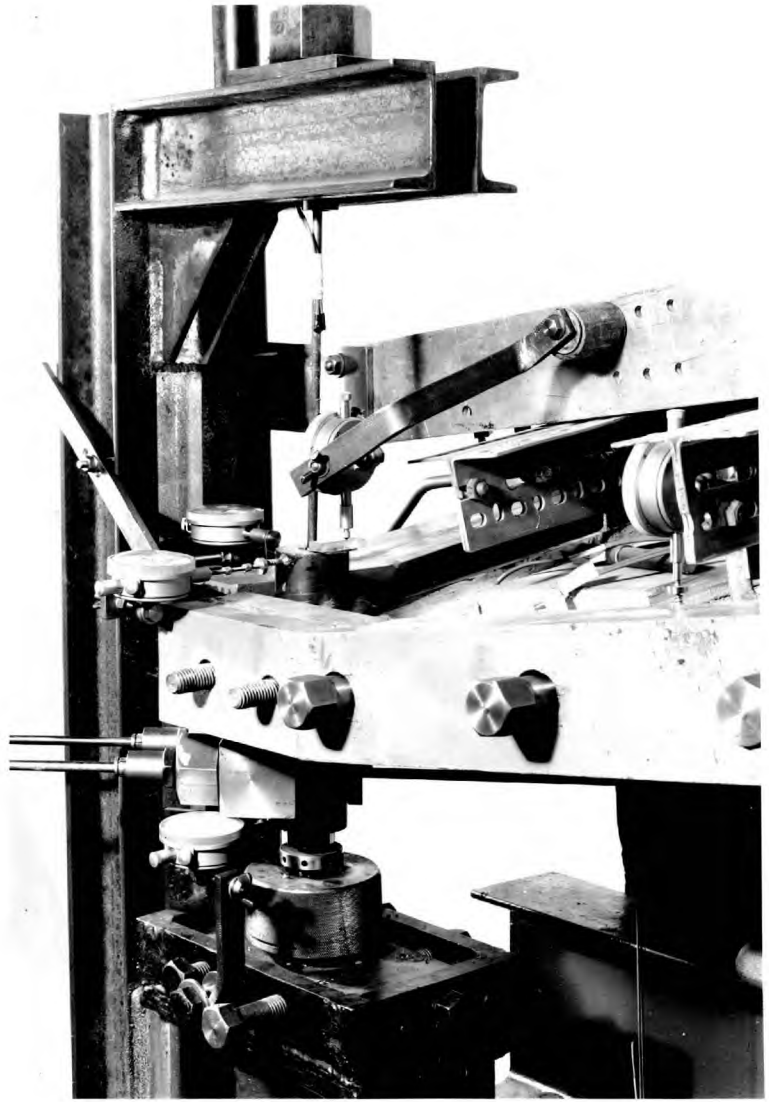


Plate 4a. Box-section edge beam

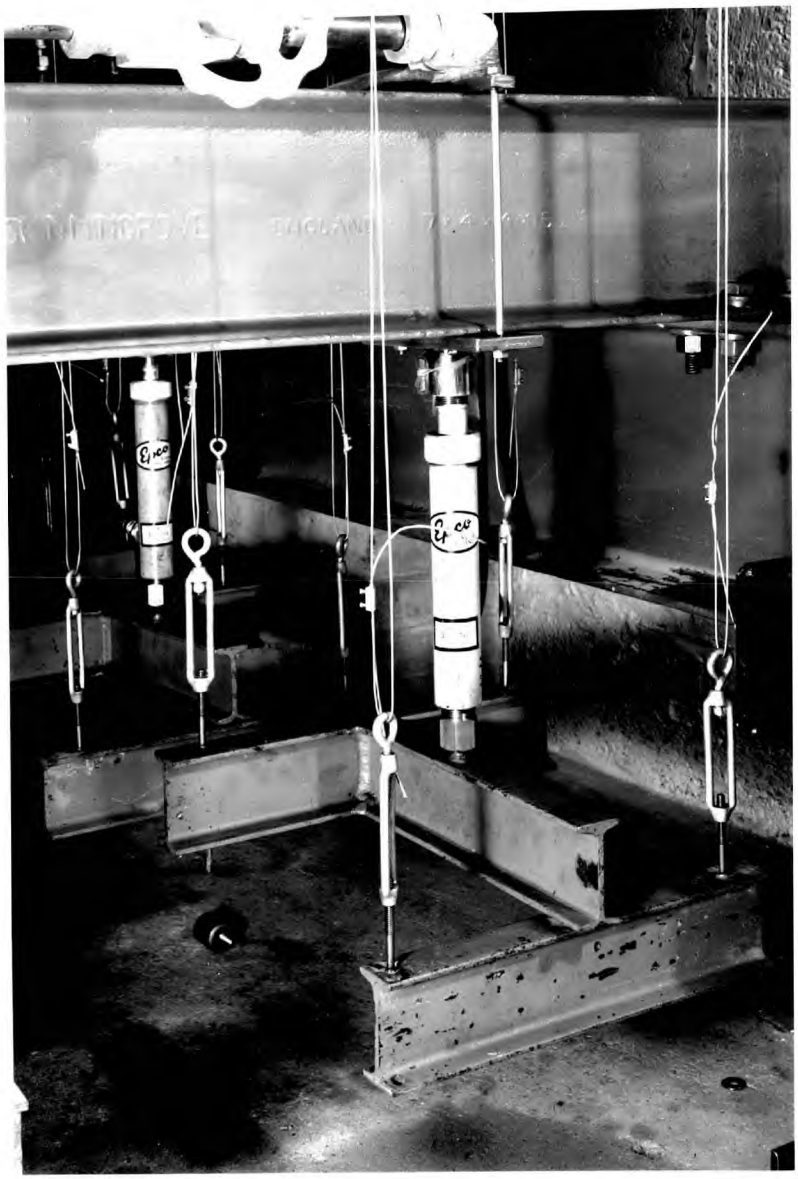


Plate 5. Jacks and H-frames used in loading shell.

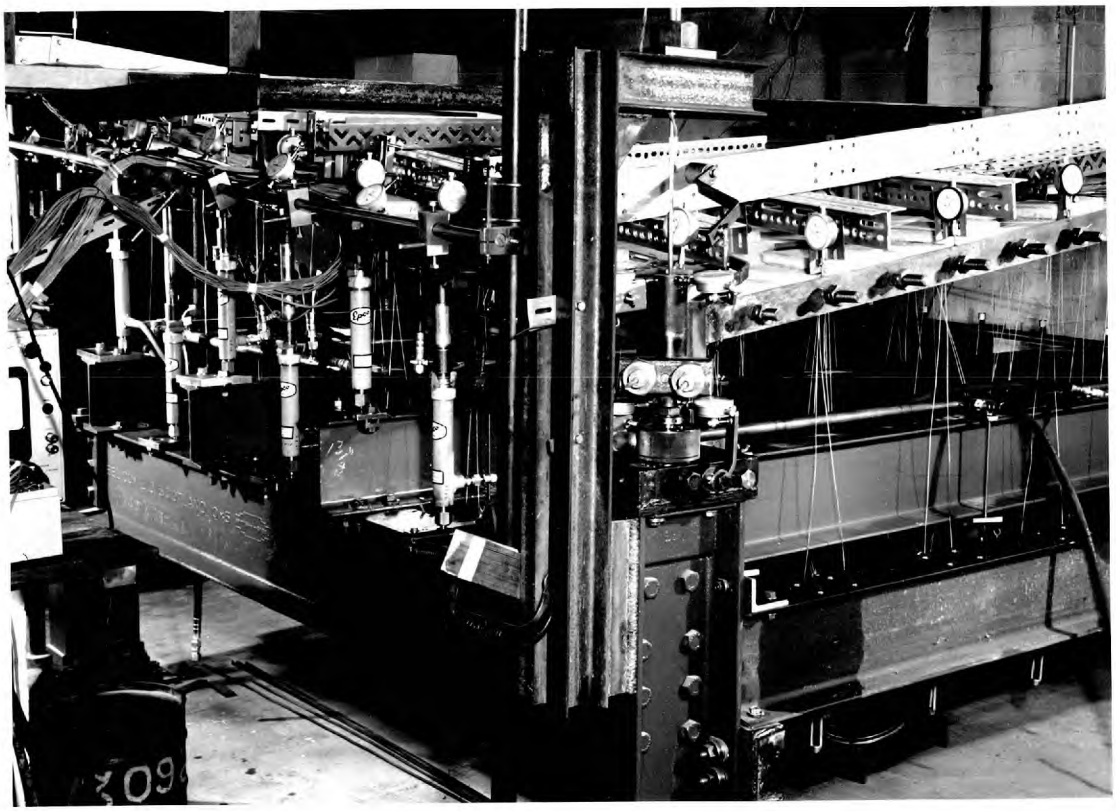


Plate 6. General arrangement for edge loading.

CHAPTER 5

5.1 RANGE OF TESTS

Ten tests were carried out on a hyperbolic paraboloid shell supported along straight line generators. The tests include certain types of edge loading, uniform loading over half the shell, and uniform loading over the entire shell with varying tie bar stiffness and edge beam stiffness. Finally the shell was tested to failure.

The first series of six tests was carried out with the flexible tie described in Chapter 4. In the other four tests, a rigid tie was incorporated between the low corners.

5.2 TESTS WITH FLEXIBLE TIE

5.2(1) TEST No.1: VERTICAL SHEAR APPLIED AT EDGE OF SHELL

The vertical force was applied along edge No. 2 (see Fig 4.10) by jacking against bolts provided in the flexible steel edge beam. This was considered the most convenient method in view of the limited clearance between the shell edge and the horizontal joist of the loading frame.

The method of loading has already been described in Chapter 4. To check on the accuracy of the jacking system and on the symmetrical behaviour of the shell, the experiment was repeated at edge No.1.

The results obtained in both cases compared very favourably. An attempt was made to take strain readings, but except for gauges on the edge beams, the strains were so small as to make them useless.

5.2(2) TEST No.2: SHEAR AND MOMENT AT EDGE No.2

The method of loading adopted was similar to that used in Test No.1, with the jacking force applied at a distance of $1\frac{1}{2}$" from the flexible edge beam.

In both tests involving edge loading, it was essential that the shell should not develop any cracks; hence the maximum load applied at the edges was comparatively low. The base plates at the shell corners were kept clamped in position during these tests.

The results of the first two tests are shown in Figs (6.1-6.8).

5.2(3) TEST No.3: UNIFORM LOADING OVER HALF OF SHELL

This test is useful in assessing the ability of the structure to withstand asymmetrical loading due to wind, snow etc. The load was increased from zero up to 29.5lb/ft^2 and deflection and strain readings were taken at each stage. The results are shown in Fig (6.9 -6.14).

5.2(4) TEST No.4,5, and 6: UNIFORM LOADING WITH VARYING EDGE BEAM STIFFNESS

These tests were intended to assess the effect of variation

of edge beam stiffness on shell behaviour with a flexible tie. The shell bases were kept clamped throughout. The flexible tie was made just taught at the beginning of each test, and the load then increased in four approximately equal stages up to a maximum of about 45 lb/ft^2. This loading was chosen as a standard for comparison of shell behaviour in all tests involving uniform loading. In cases where this standard loading was not exactly attained, the results for this load were obtained by interpolation. After removing the load from the shell, an interval of at least 10 minutes was allowed before final zero readings were taken. This measure ensured that effects of creep were reduced to a minimum.

Each experiment was repeated at least three times on three different days, thus providing checks on deflection and strain readings. The 5-Volt A/C Peekel Strain recorder was permanently connected to Circuit No.5.

Test No.4 was conducted with the shell edges supported by the flexible "in-situ" edge beams only. This test was also done by Ahuja, but it was considered advisable to repeat it because of possible changes having taken place in the structure during the tests involving edge loadings. Further, the loading equipment had been altered, and shrinkage had taken place in the shell since Ahuja carried out his tests. Strain readings were taken over all

five circuits, but the closing errors in the gauges connected through the Mercury switchbox to the Savage and Parsons Strain recorder were in many cases so large as to render their readings worthless. This was also the case in Tests Nos. 5 and 6; in fact, the Savage and Parsons equipment exhibited considerable drift even when observed over a period of about one hour prior to testing on different days.

In Test No.5 the channel beams were fixed to the flexible edge beams and the shell again subjected to uniform loading. Care was taken to ensure that all nuts were screwed up against the edge beams to approximately the same extent. This, together with the fact that the nuts were tightened up just sufficiently to keep the edge beams firmly in position, eliminated the possibility of large direct forces being transmitted to the shell edges.

Beams of box section were added to the flexible edge beams in Test No.6. As the weight of these sections was considerable, care was taken to avoid shock-loading of the shell while the beams were being placed in position.

5.3 TESTS Nos.7,8, and 9: UNIFORM LOADING WITH RIGID TIE AND VARYING EDGE BEAM STIFFNESS

The unreliability of the strains obtained through the Savage

and Parsons strain recorder was fully recognised in the previous tests. Advantage was therefore taken of a 1 Volt A/C Peekel strain recorder which became available together with a 23-way switchbox and a 12-way one. These were used to cover circuits Nos. 3 and 4, and the other circuits Nos.1 and 2 were omitted due to the limited number of switchboxes available.

The size of the tie bars and the details of fixing at their ends were such that torsional stresses might be induced during the tests, and some step had to be taken to eliminate them, or at least, to reduce them to a minimum. Each tie was provided with two strain gauges fixed on opposite sides of its horizontal axis. Prior to testing, the strains in these gauges were observed at stages of increasing load. The nuts at the ends of the bars were adjusted at each stage, until the average strains of both sets of gauges were equal. The process was repeated for loading decreasing down to zero, which became the starting point of a test. This method proved effective in equalising the load transmitted to each of the ties.

Test No.7 involved the in-situ flexible edge beam only, with rigid ties between the low corners of the shell. With the use of a 23-way and of a 12-way switchbox, only 46 gauges could be accommodated from circuit No.4. Switchpoints 1-32 were reserved for the gauges on

edge beams, and 33-36 for those on the tie bars. Points 37-46 were connected to gauges Nos.13-18 and 25-48 of Circuit No.2, thus providing a means of checking the corresponding gauges of Circuit No.5 . However, all 48 gauges in Circuit No.3 were covered since at the time of this test, and subsequently four 12-way switchboxes were available. The latter grouping of strain gauges was adopted for the remaining tests.

In Test No.8 the channel edge beams were added, the rigid tie still being in position.

Test No.9 was carried out after the beams of box section were added to the flexible edge beams.

5.4 TEST No.10: TEST TO FAILURE

The shell was tested to failure under uniform loading, with the edges supported on the flexible steel edge beams. Only after three attempts was it possible to fail the shell.

In the first attempt, all the base plates were clamped in position. Deflection readings were taken on all gauges and strains observed in circuits Nos. 3,4, and 5. The load-deflection relationship at midspan was linear up to a load of 51 lb/ft^2, beyond which the slope of the curve changed abruptly, though the relationship remained

linear up to the maximum load of 134.2 lb/ft^2 which could be applied. Very large rotations were observed especially at the high corners, but only a few minor cracks had formed. The ties were then released but the only effect noticeable was increased rotation at the corners and falling off of the load.

The load was removed from the shell; the ties nominally tightened and all four base plates released before load was then again applied. In this case linearity was observed up to about 40 lb/ft^2 loading, with the load deflection curve up to this point coinciding with that obtained in the first attempt. At the latter loading the slope of the load-deflection relationship again changed abruptly, and with the load at 129.5 lb/ft^2, it was observed that the high corners of the loading frame had lifted some 2" off the floor, which was probably the cause of the abrupt change in slope of the curves referred to above.

The base plates at the high corners of the loading frame were fixed to the floor, and the shell subjected again to uniform load increasing up to a maximum of 200.4 lb/ft^2. The four corners of the shell were released in this attempt at failing the structure. The load-deflection relationship (Fig 6.45) was linear up to 133 lb/ft^2. At the 200.4 lb/ft^2 load, large diagonal cracks, which were audible, appeared on the top surface of the shell, approximately $3\frac{1}{2}$" from the low corners at an angle of about 45 degrees to the edge beams. These

were accompanied by crushing of the shell material along the corresponding lines on the bottom surface.

The load was removed and restored after the ties were completely released. Observations were made on deflection at midspan of the shell and on strains of the tie bars up to a loading of 264 lb/ft^2. At this point, the deflection of the shell was so large that some jacks in the middle region were transmitting no load. However, the pressure of the system was increased, and strains in the tie bars observed until the pressure gauge reading was 1800 psi which would correspond to a distributed loading of 477.6 lb/ft^2. At this point, the ring main failed.

The dial gauge framework and loading equipment were removed and the crack patterns marked out for both surfaces. These are shown in Figs (6.46) and (6.47). Views of the shell after failure are shown in Plates (7) to (12).

5.5 TESTING OF SPECIMENS

5.5 a TEST SLABS

At the time of casting of the shell, a number of slabs 20"x 6"x 3/4" thick had been cast from the shell material. The reinforcement to these slabs, and the conditions of curing were identical to those of the shell. Some of the slabs had been tested at the end of Ahuja's

tests, and the two which remained were tested under uniform bending moment to give the characteriatics of the shell section. The apparatus used for the test is shown in Fig (5.1).

Strains were measured by four strain gauges,- two on each face - fixed longitudinally at midspan. Each slab was supported on rollers 16" apart, and equal point loads were applied at the third points by means of a calibrated jack, thus giving a constant bending moment for a given load over the middle third of the span. Deflection gauges reading to .0001" were set up $2\frac{1}{2}$" on either side of the midspan. In order to minimise friction at the rollers and to facilitate distribution of load, building paper was placed between the slab and the rollers.

Deflection and strain readings were taken at different stages of increasing load. Cracks which were formed in the early stages were audible though not visible. The load was then decreased and new zeros obtained. Readings were then taken for load increasing and decreasing over several cycles. Finally, the slab was tested to failure.

As shown in Figs.(5.2) and (5.3), the equivalent E values obtained for the slab differed considerably for deflections and for strains. In fact, different values of E were obtained for the compression and tension sides of the slabs. Further, these results were different for both slabs. In view of the fact that small cracks were observed

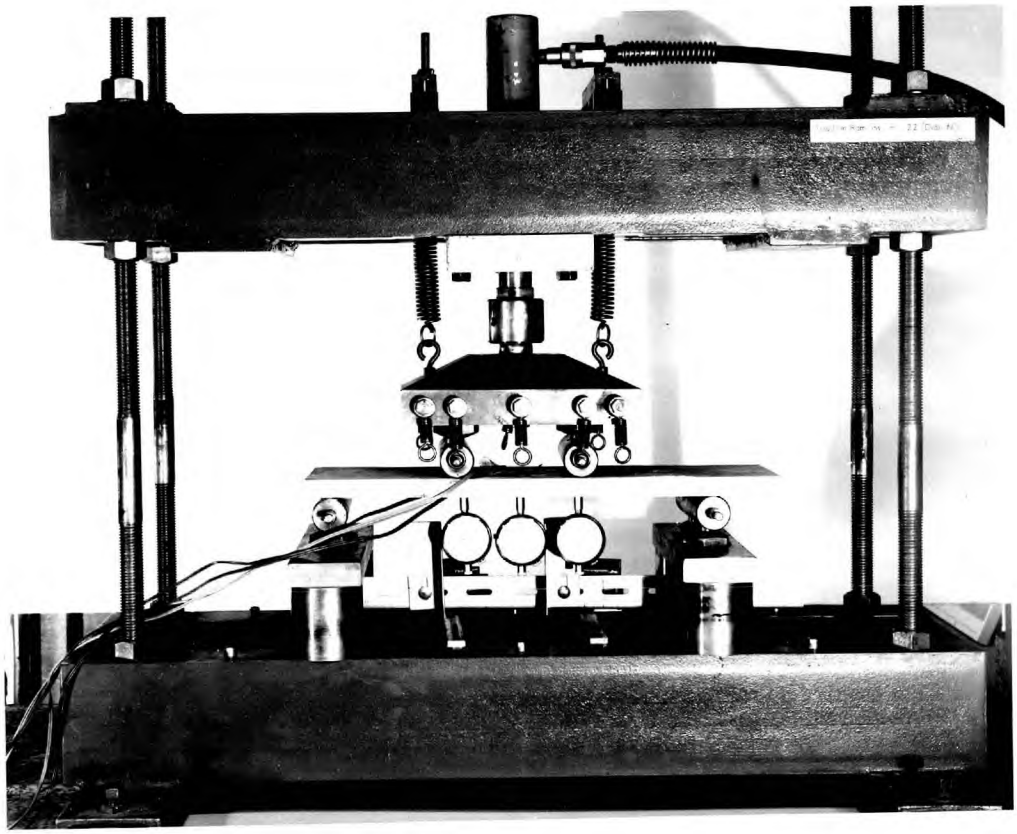
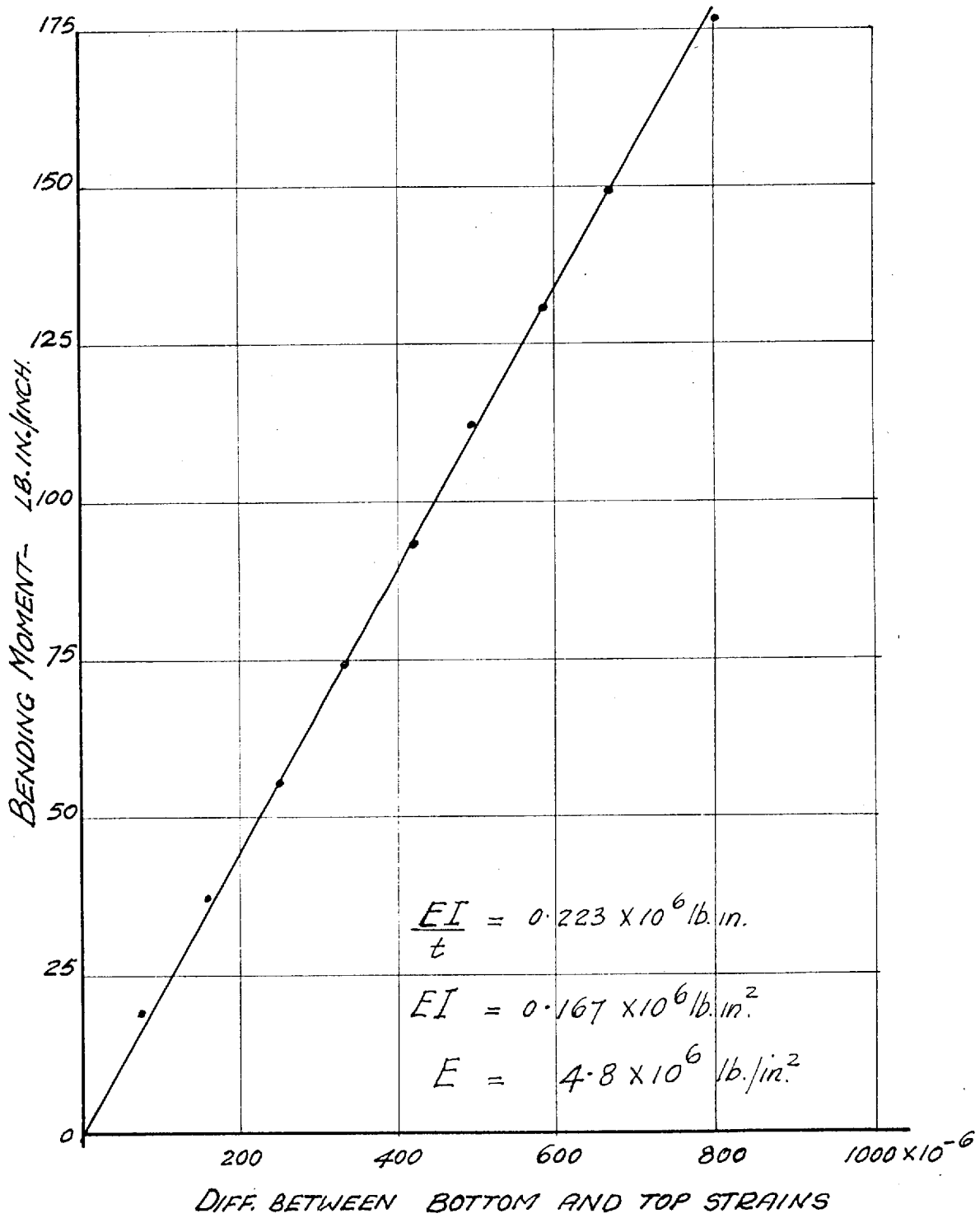
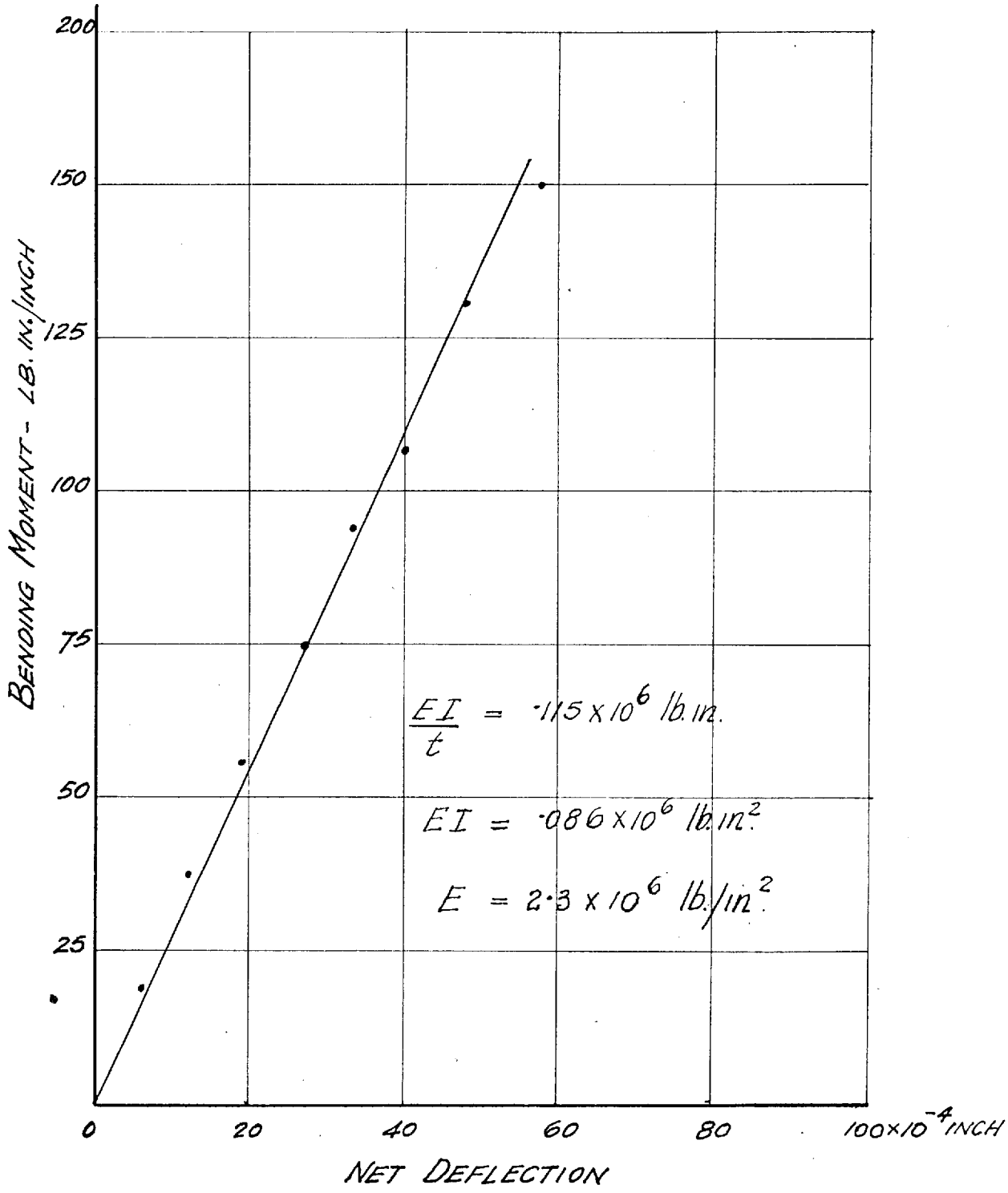


Fig. 5.1. Test slab apparatus.



TEST SLAB.

FIG. 5.2.



TEST SLAB

FIG. 5.3.

prior to testing on both faces of one of the slabs, it was decided to discard the readings for that slab.

The E values varied from 4.8×10^6 lb/in^2 in bending to 2.3×10^6 lb/in^2 for the moment vs. deflection relationship. The former value which was adapted for use in the shell calculations also represented the average of values of E obtained separately from observations of strain on the top and bottom surfaces of the slab. Ideally, slabs should also be tested in tension but no specimens were available for this purpose.

5.5 b TEST CUBES

Four 4" cubes were tested in compression. The average compressive strength was 11,750 lb/in^2.

5.5 c INDIRECT TENSILE TEST

Only one 6" diameter cylinder remained on which to carry out this test. The result obtained was 585 lb/in^2.

5.5 d TEST ON LEE McCALL BAR

A 2 ft. length of Lee McCall Bar was tested in tension to determine an E value for use in the second series of tests. Strains were measured by two gauges fixed at midspan, and the E value of 25.0×10^6 lb/in^2 was obtained over several cycles of loading and unloading. This figure compares favourably with 24.7×10^6 lb/in^2 given by the manufacturers in their handbook. The bar diameter (1.136") is the average of several micrometer readings.

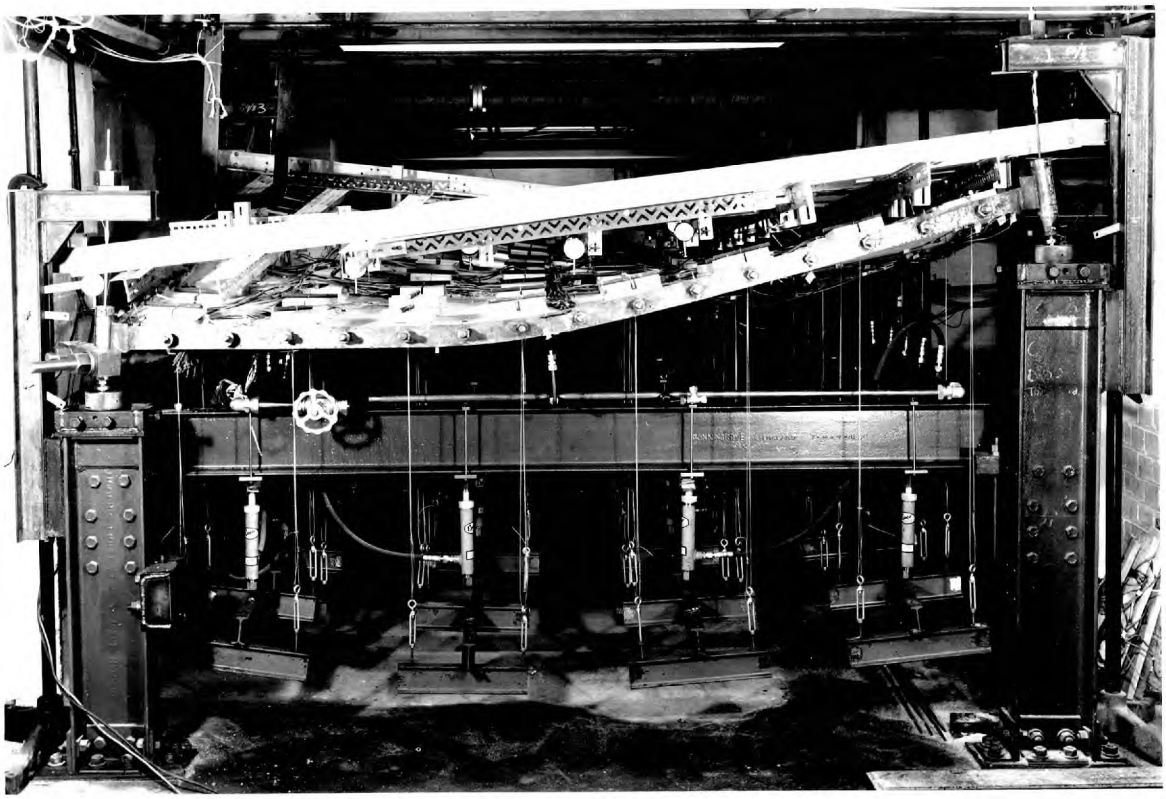


Plate 7. View of shell after failure.

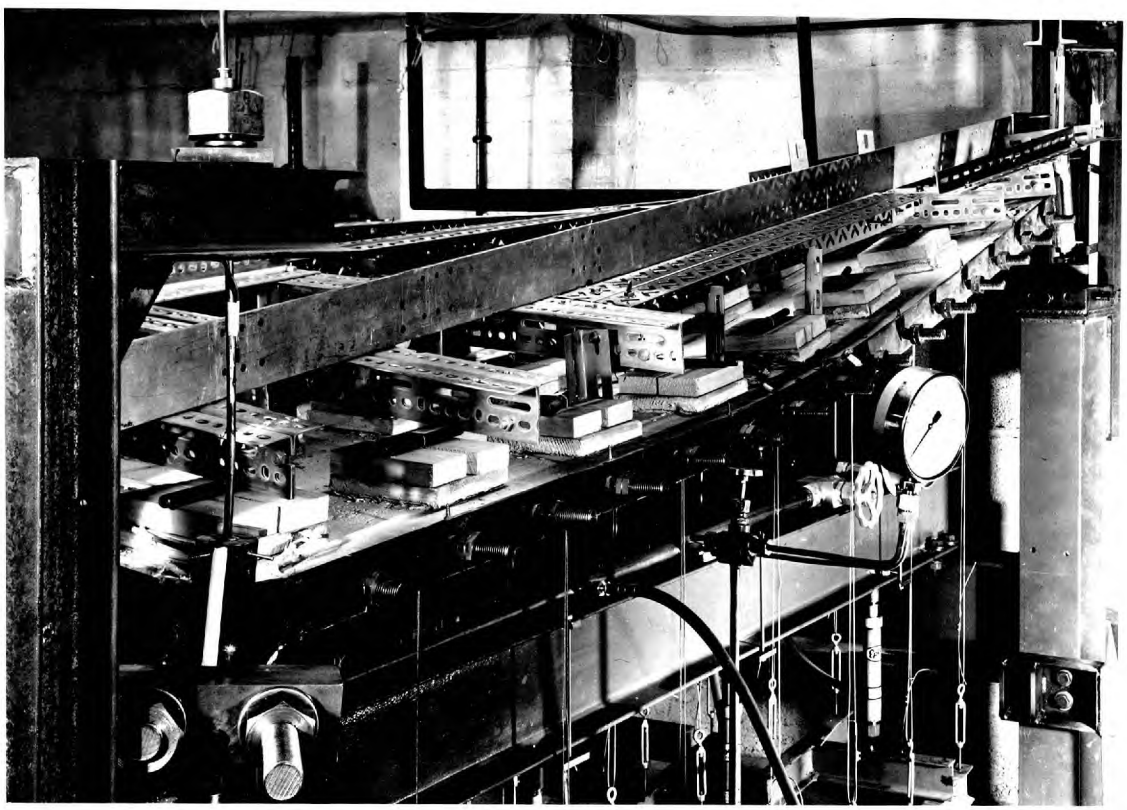


Plate 8. View of shell after failure.

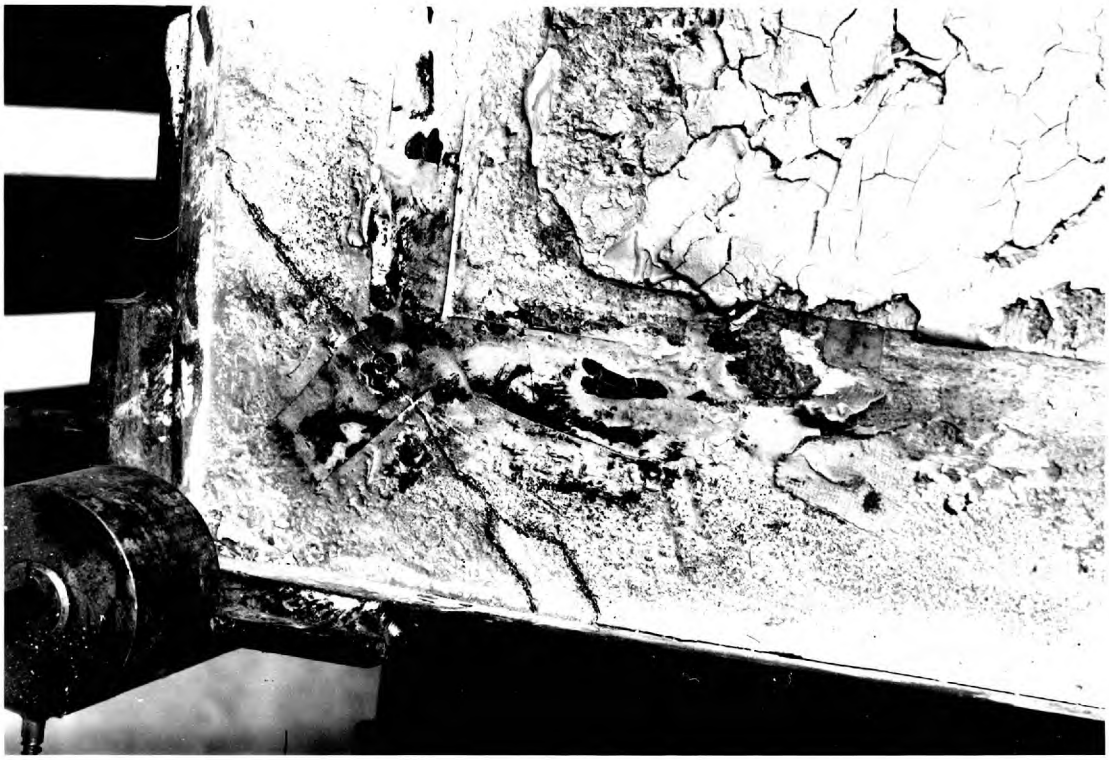


Plate 9. Crack on top face at low corner 1 .



Plate 10. Crushing of mortar on bottom face-low corner 1.



Plate 11. Crack on top face at low corner 3 .



Plate 12. Crushing of mortar on bottom face-low corner 3.

CHAPTER 6

PRESENTATION OF RESULTS

The results of experiment and comparisons with theory are presented in the following manner:

Tests 1 and 2 - All results are based on deflections and are given in Figs 6.1 - 6.8.

Test 3 - Figs 6.9 - 6.14 inclusive. As the strain readings in this case showed definite trends the strain results are included in Figs 6.13 and 6.14.

Tests 4 to 9 - The experimental results for these tests are included in Figs 6.15 - 6.44 inclusive. Each test has been systematically reported as follows:

a) Typical Deflection Profiles

b) Vertical deflections for standard loading of 45 lb/ft^2.

c) Vertical deflection contours for U.D.L. of 45 lb/ft^2. Such diagrams indicate whether or not the structure behaves symmetrically during tests.

d) Average of strains on bottom and top surfaces of the shell from which the force distribution may be derived.

e) Difference of strains in bottom and top surfaces. From these the distribution of moments over the shell can be obtained.

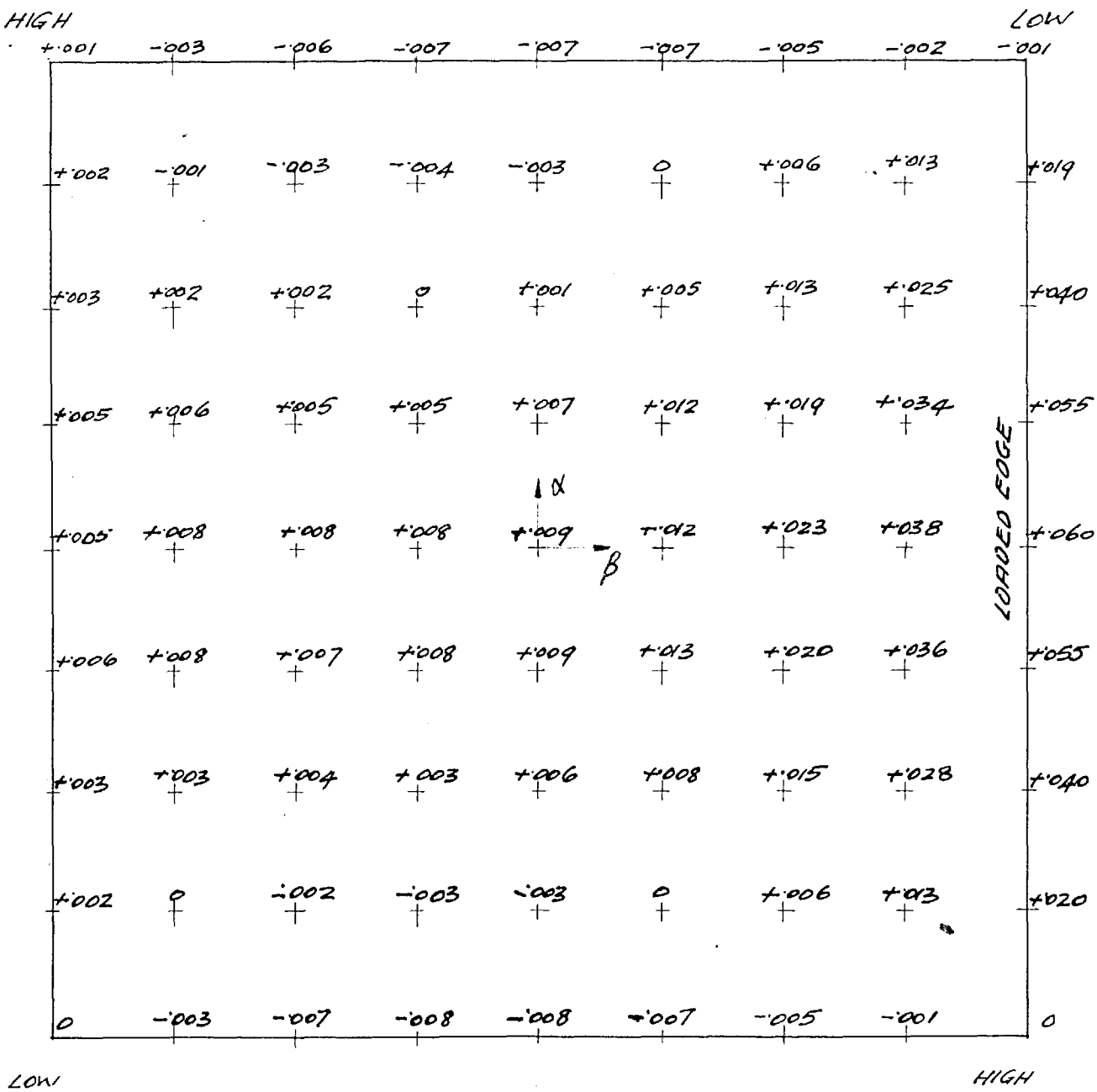
Test 10 - Load deflection curves and cracking patterns at failure are indicated in Figs 6.45 - 6.48.

COMPARISON OF RESULTS

Results for Tests 4 - 6, involving the flexible tie and variation of edge beam stiffness, are compared in Figs 6.48 - 6.54. Similar comparisons are made in Figs 6.55 - 6.60 for Tests 7 - 9 in which the rigid tie was used.

Comparisons of Tests 4 - 9 inclusive are made in Figs 6.61 - 6.67.

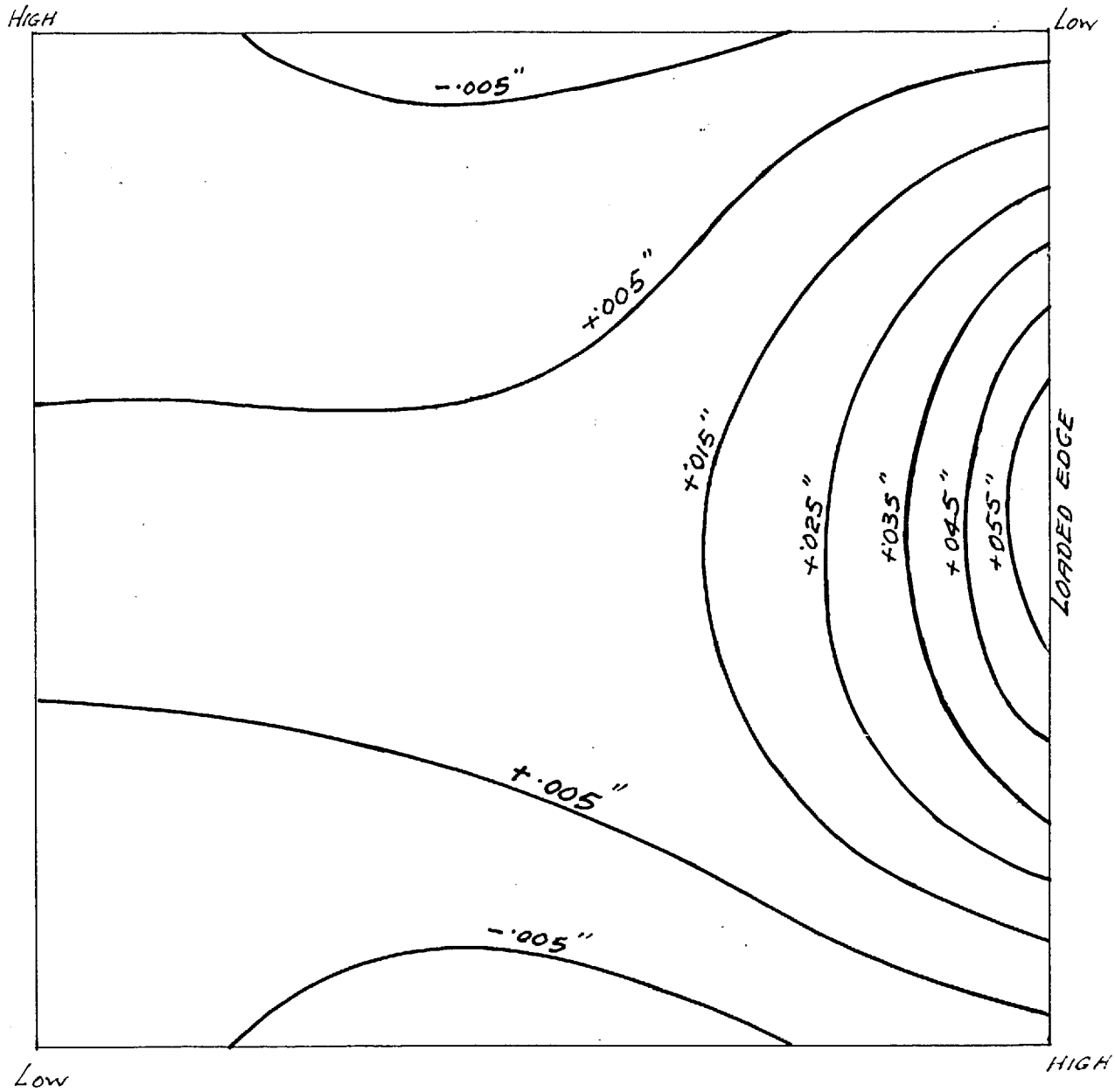
Finally, in Figs 6.68 - 6.71, comparisons are made with the plate solutions.



VERTICAL DEFLECTIONS (INS.)

TEST 1 . SHEAR ONLY AT EDGE 2 = 264 LB/FT.

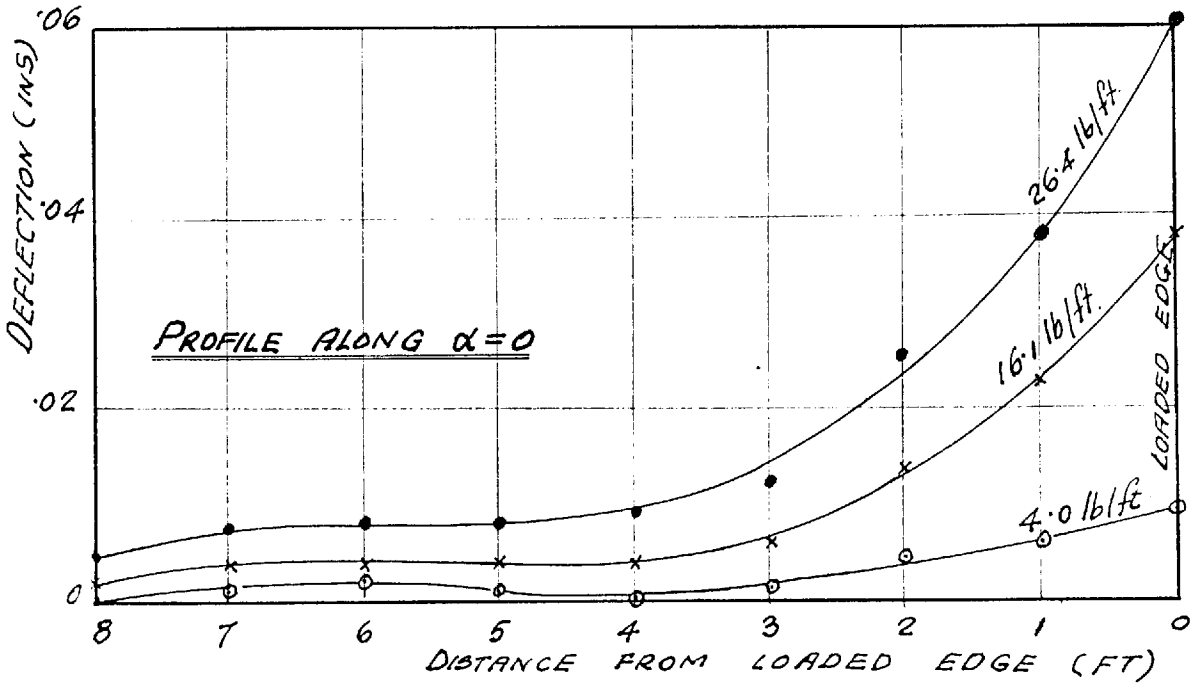
FIG. 6.1.

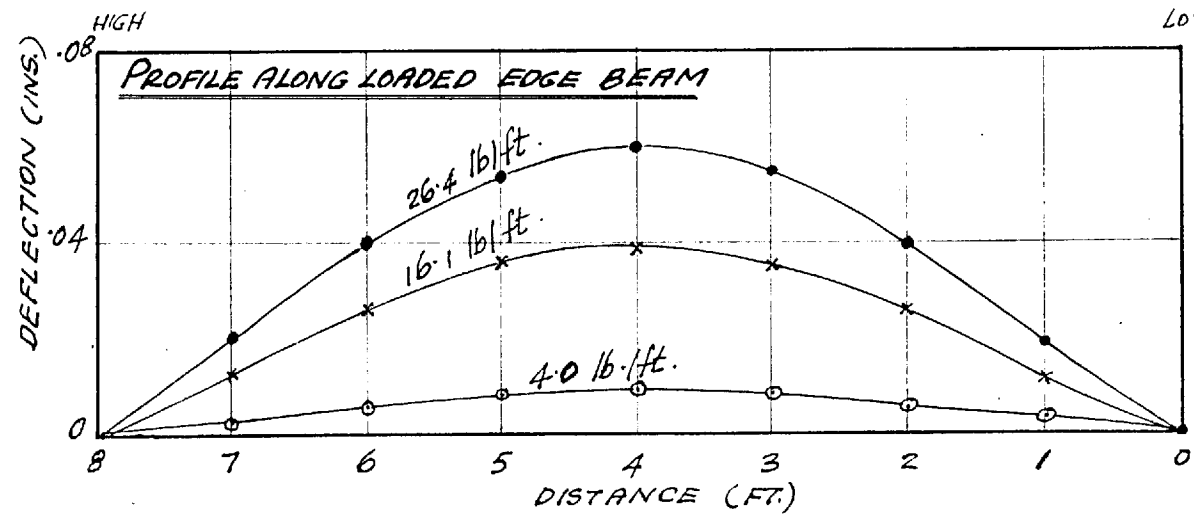


VERTICAL DEFLECTION CONTOURS

TEST 1. SHEAR ONLY AT EDGE 2. = 26·4 LB/FT.

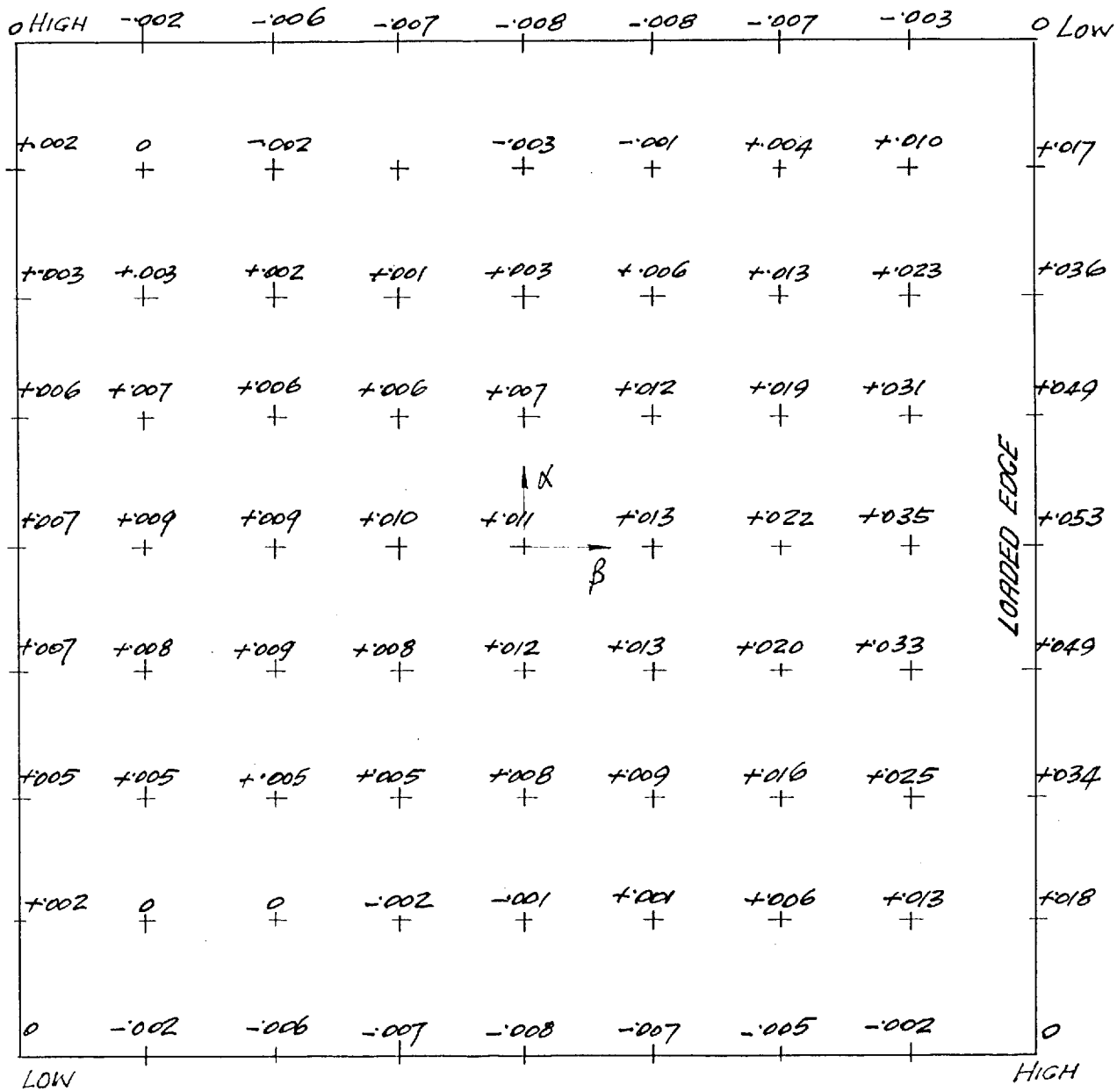
FIG. 6.2.





TEST NO. 1. TYPICAL DEFLECTION PROFILES.

FIG. 6. 3.



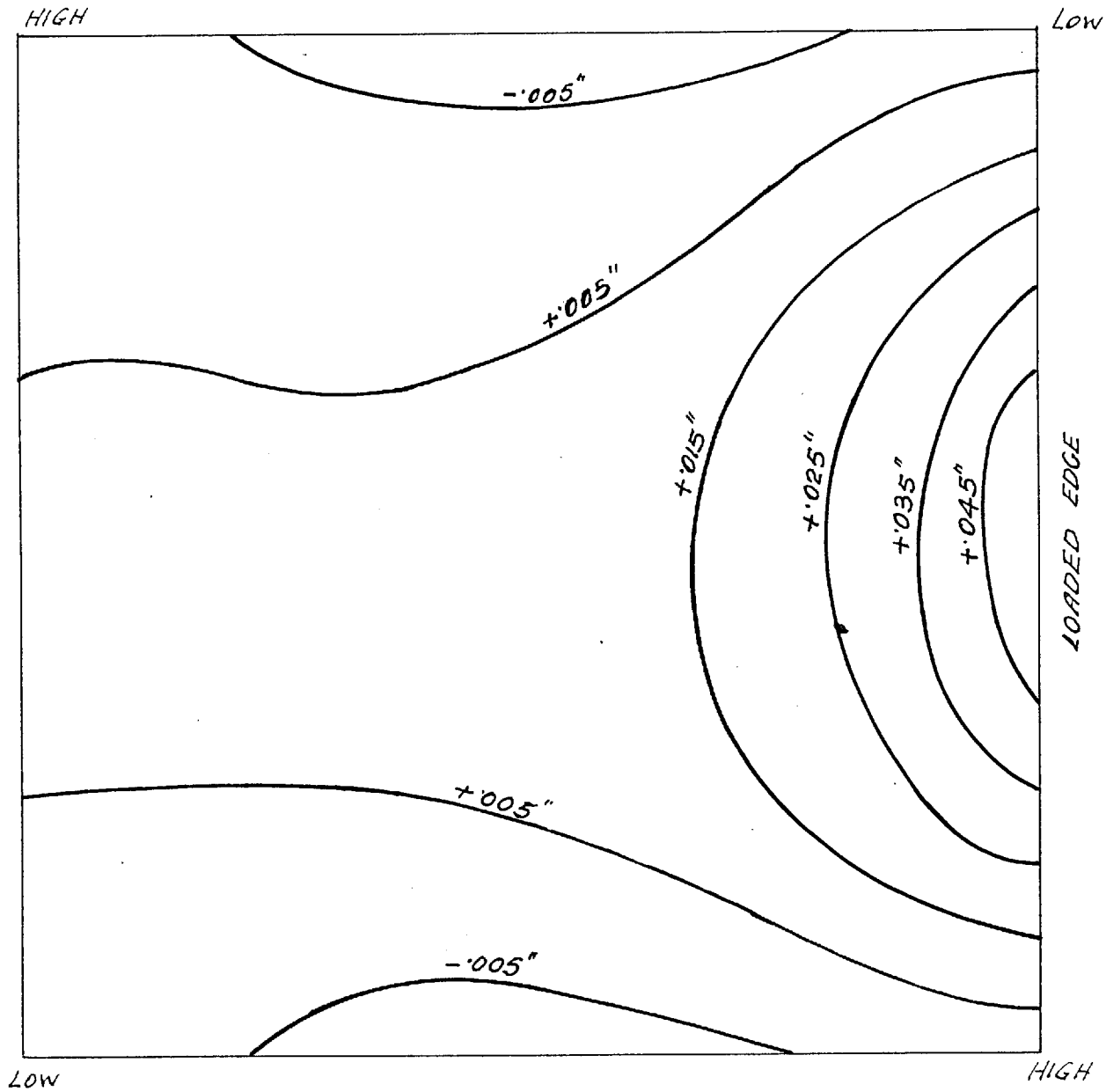
VERTICAL DEFLECTIONS (INS.)

TEST NO.2

SHEAR AT EDGE 2 = 26·4 LB/FT.

MOMENT " " = 39·6 LB.IN./FT.

FIG. 6.4.



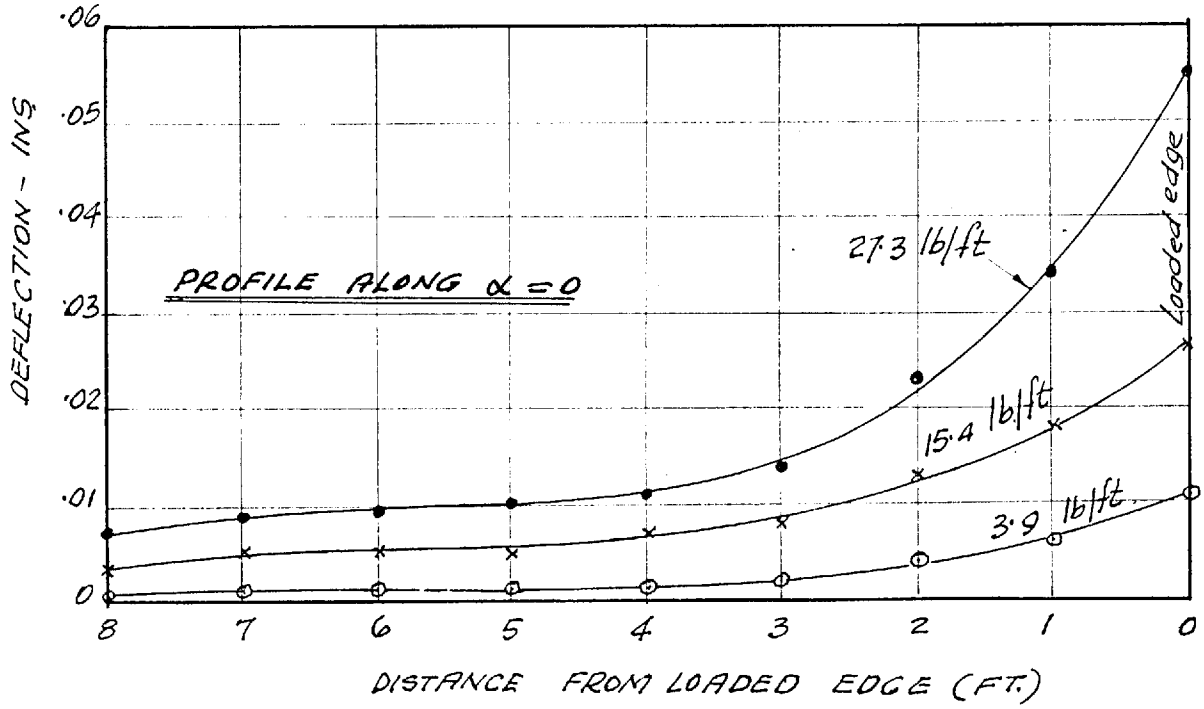
VERTICAL DEFLECTION CONTOURS

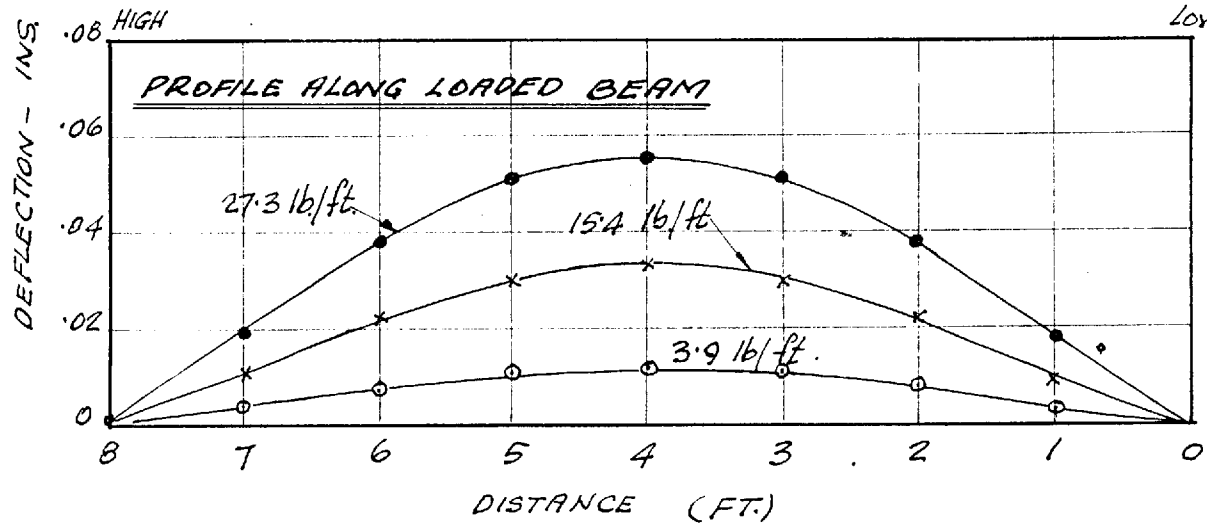
TEST NO.2

SHEAR AT EDGE 2 = ·26·4 LB/FT.

MOMENT " " = 39·6 LB.IN./FT.

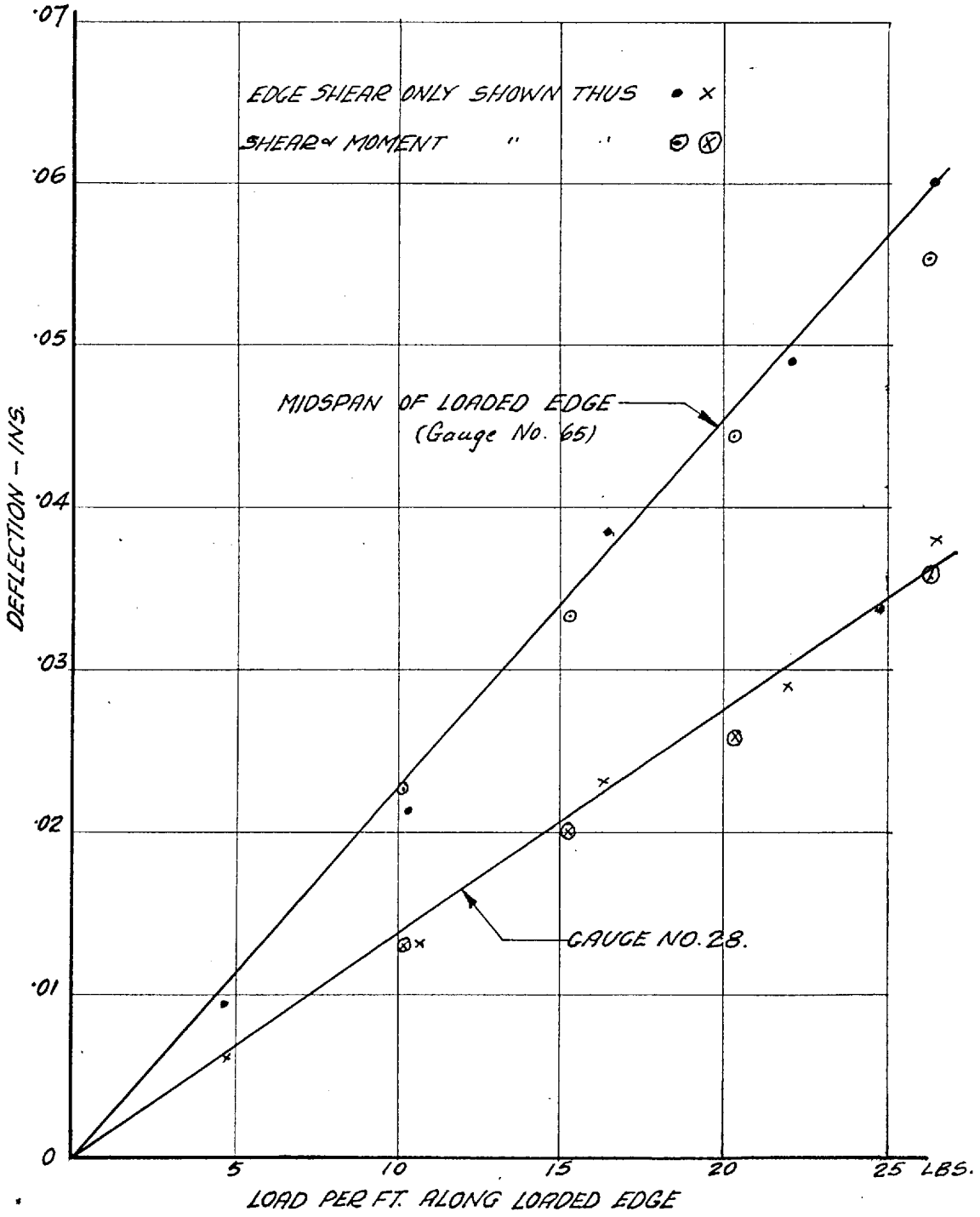
FIG. 6. 5.





TEST NO.2. TYPICAL DEFLECTION PROFILES.

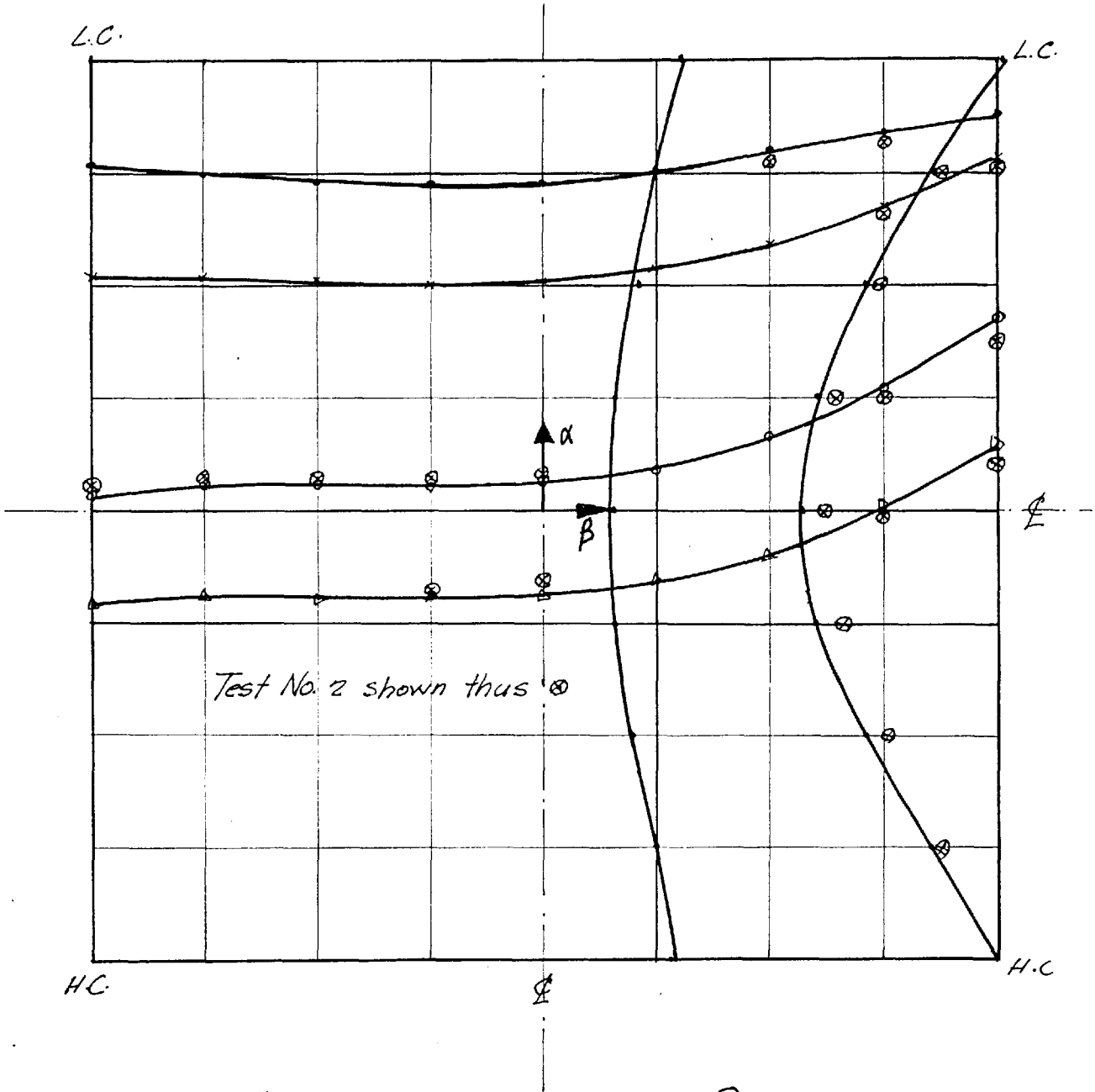
FIG.6.6.



TYPICAL LOAD-DEFLECTION CURVES.

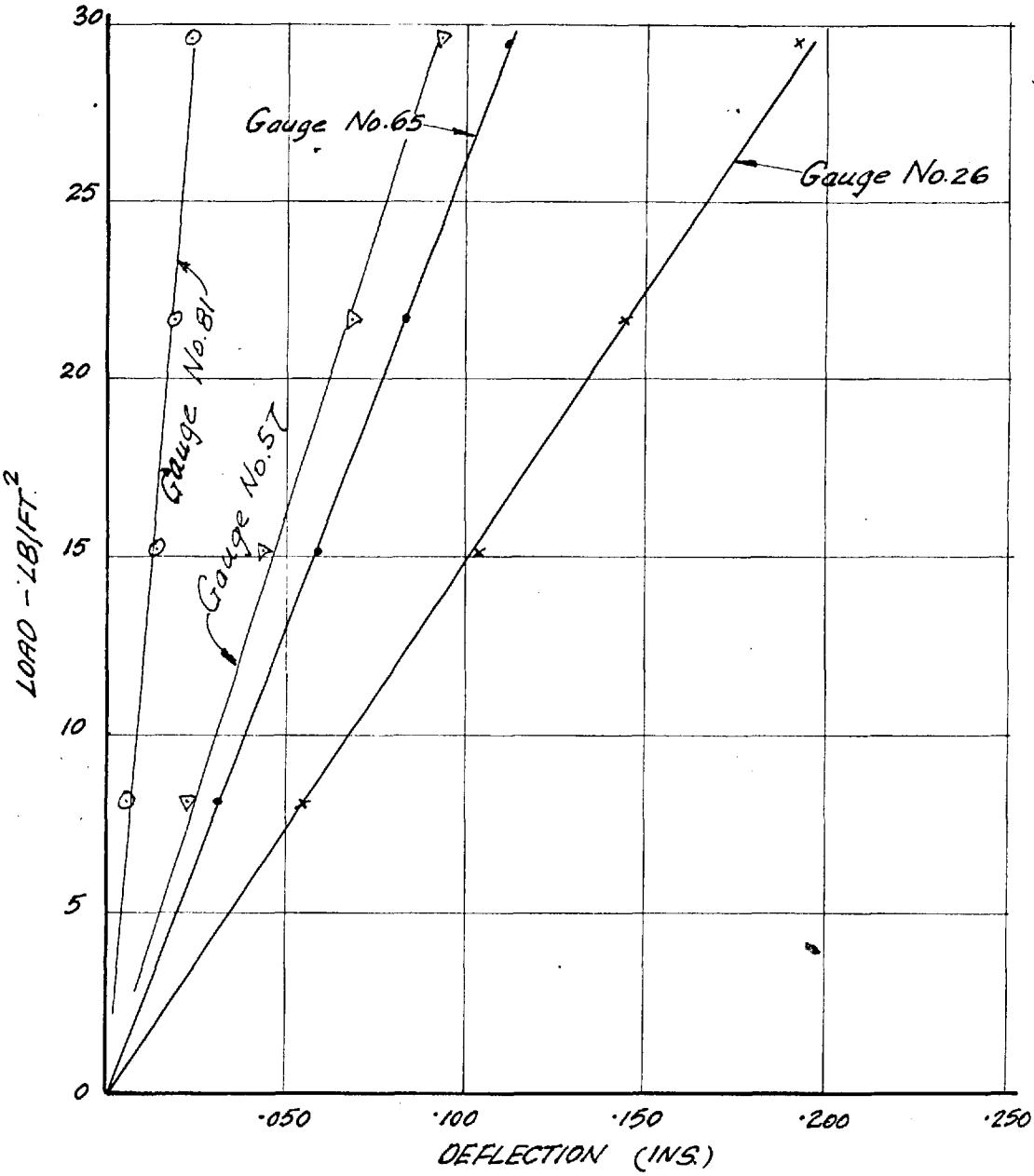
TEST NO.1 – SHEAR ONLY AT EDGE 2
TEST NO.2 – SHEAR & MOMENT " " "

FIG. 6. 7.



TESTS 1 + 2 : DEFLECTION PROFILES (MAX LOAD.)

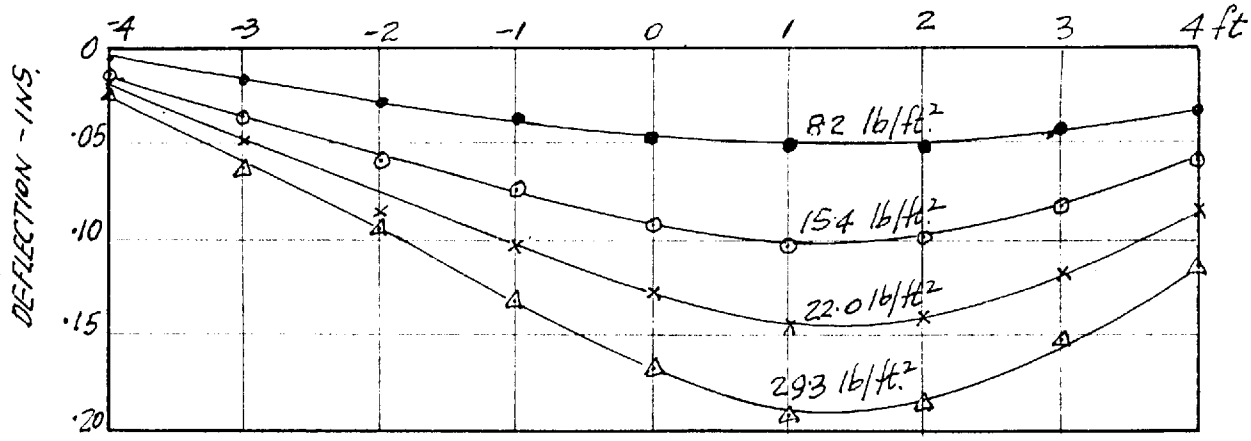
FIG. 6.8



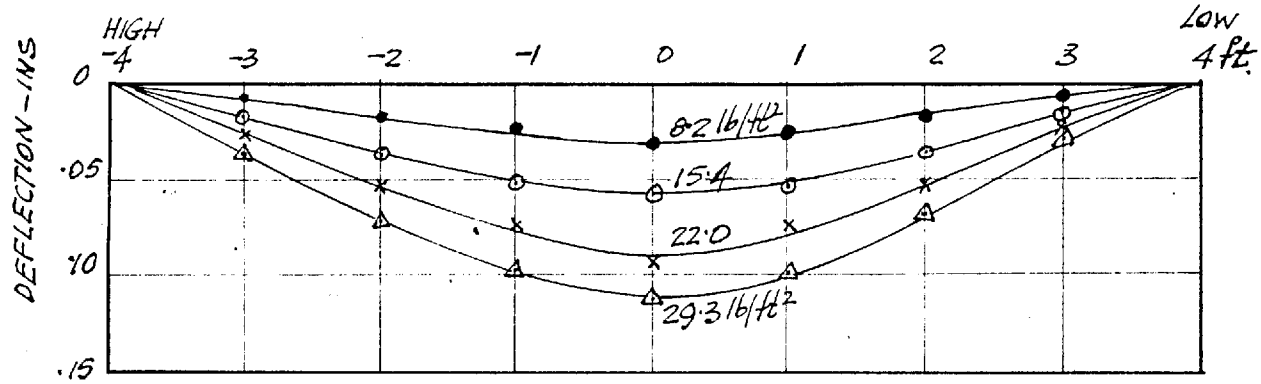
TYPICAL LOAD-DEFLECTION CURVES

TEST NO.3. HALF SHELL LOADED.

FIG. 6.9.



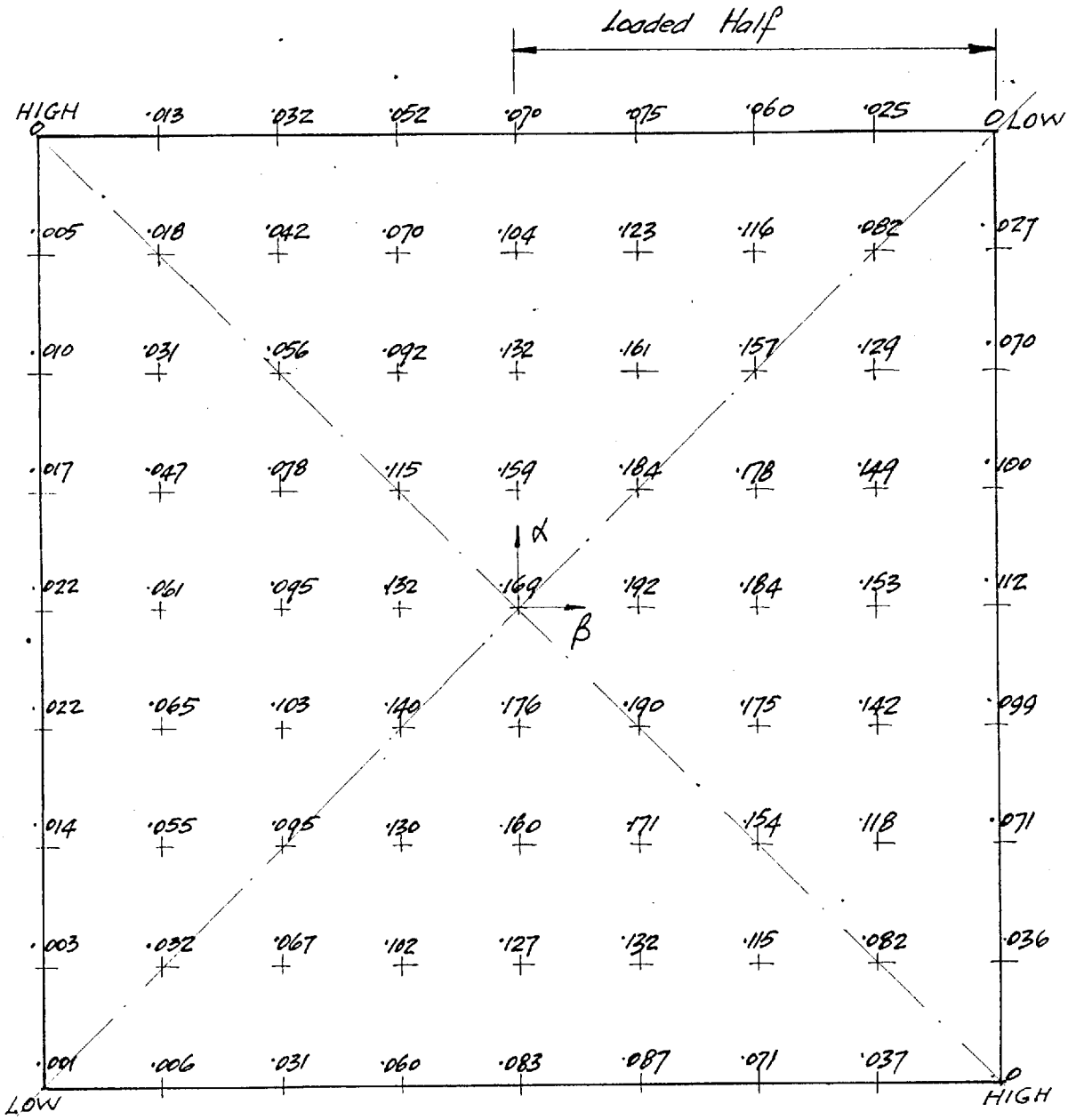
PROFILE ALONG $\alpha = 0$



PROFILE ALONG EDGE BEAM NO. 2 ($\beta = 4'-0"$)

TEST NO. 3. TYPICAL DEFLECTION PROFILES.

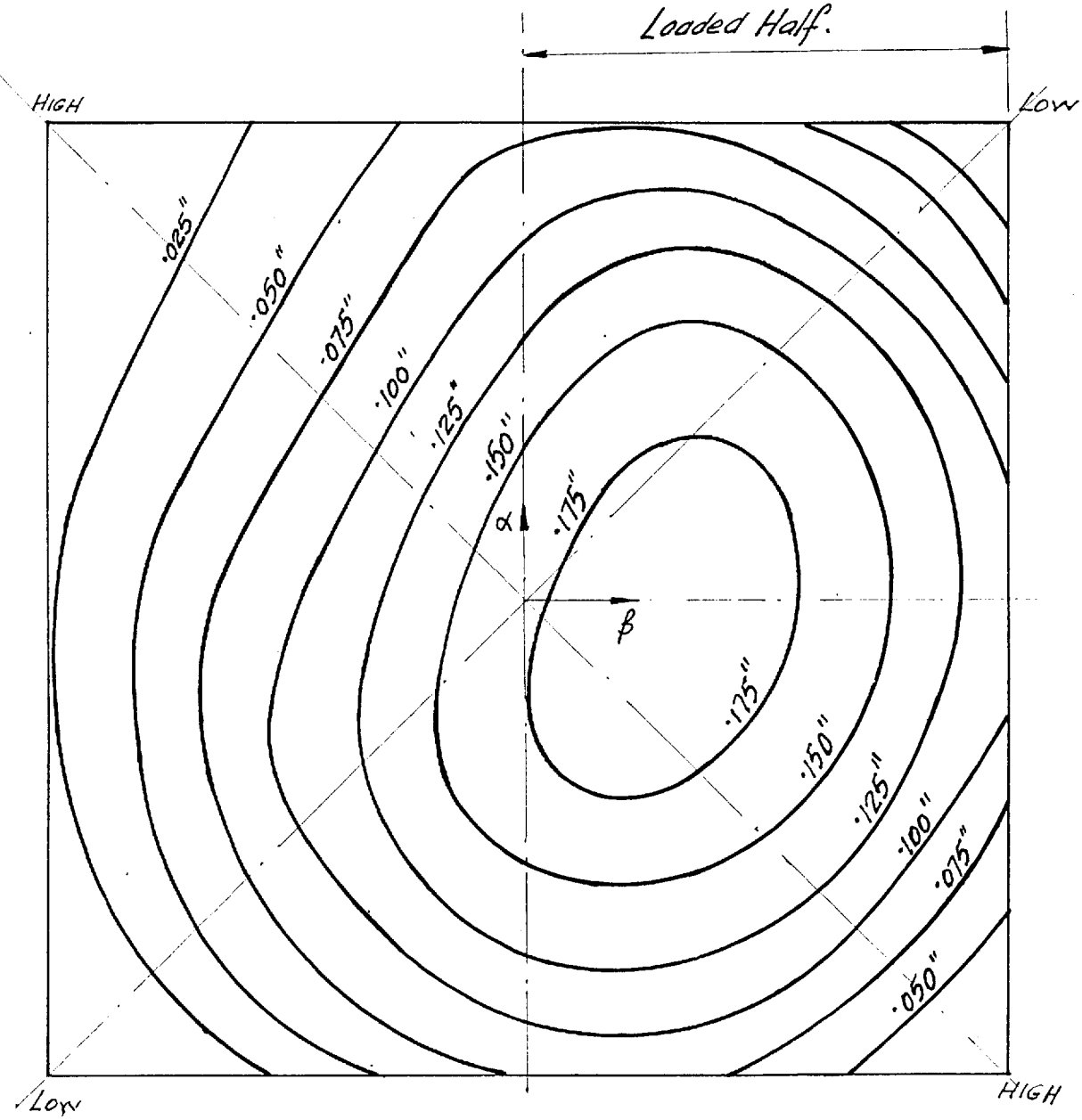
FIG. 6.10.



VERTICAL DEFLECTIONS (INS.) FOR 29·5 LB/FT² ON LOADED HALF

TEST. NO.3. HALF SHELL LOADED.

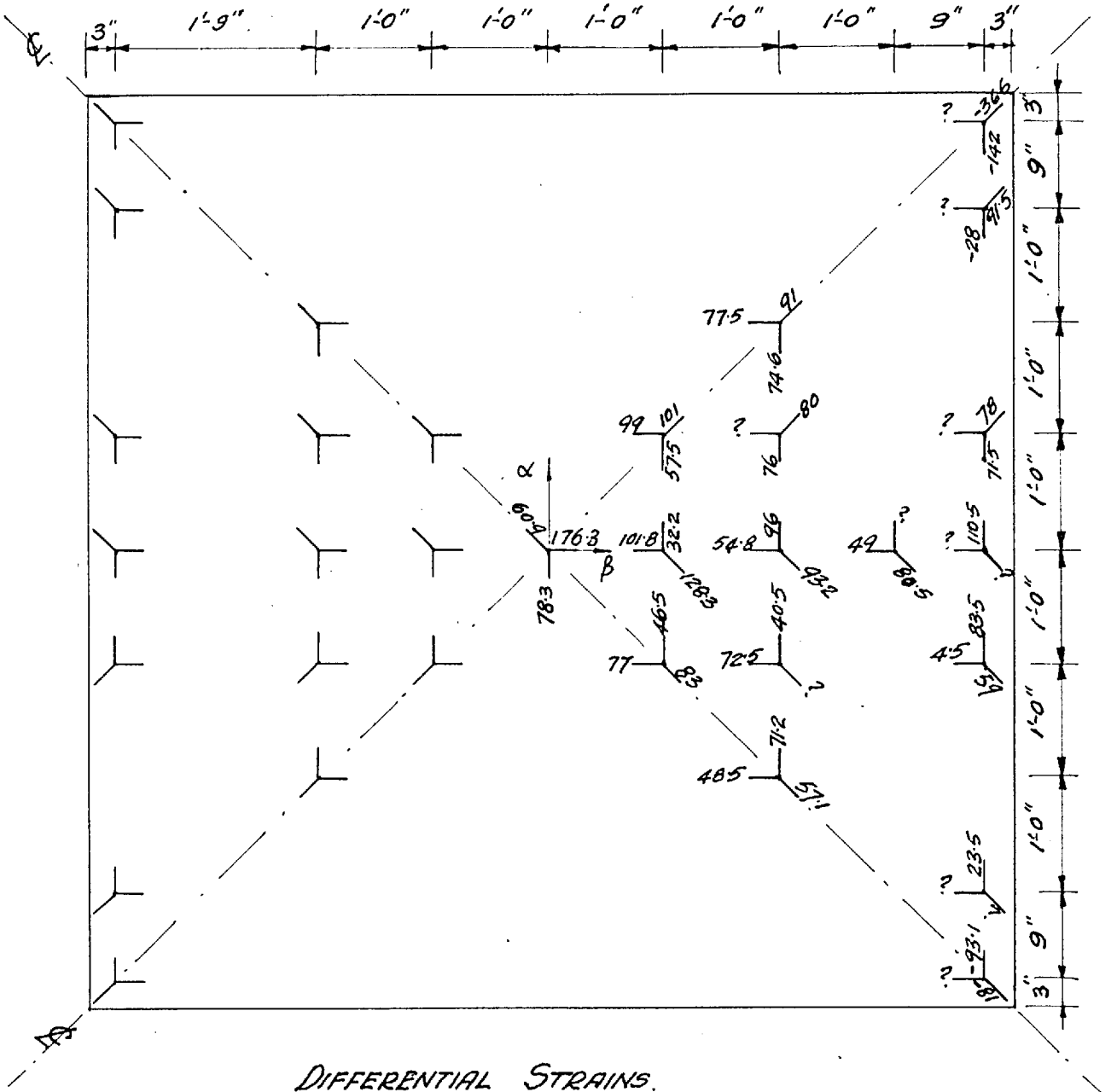
FIG. 6.11.



VERTICAL DEFLECTION CONTOURS FOR LOAD OF 29·5 LB/FT.^{2}

TEST NO.3. HALF SHELL LOADED

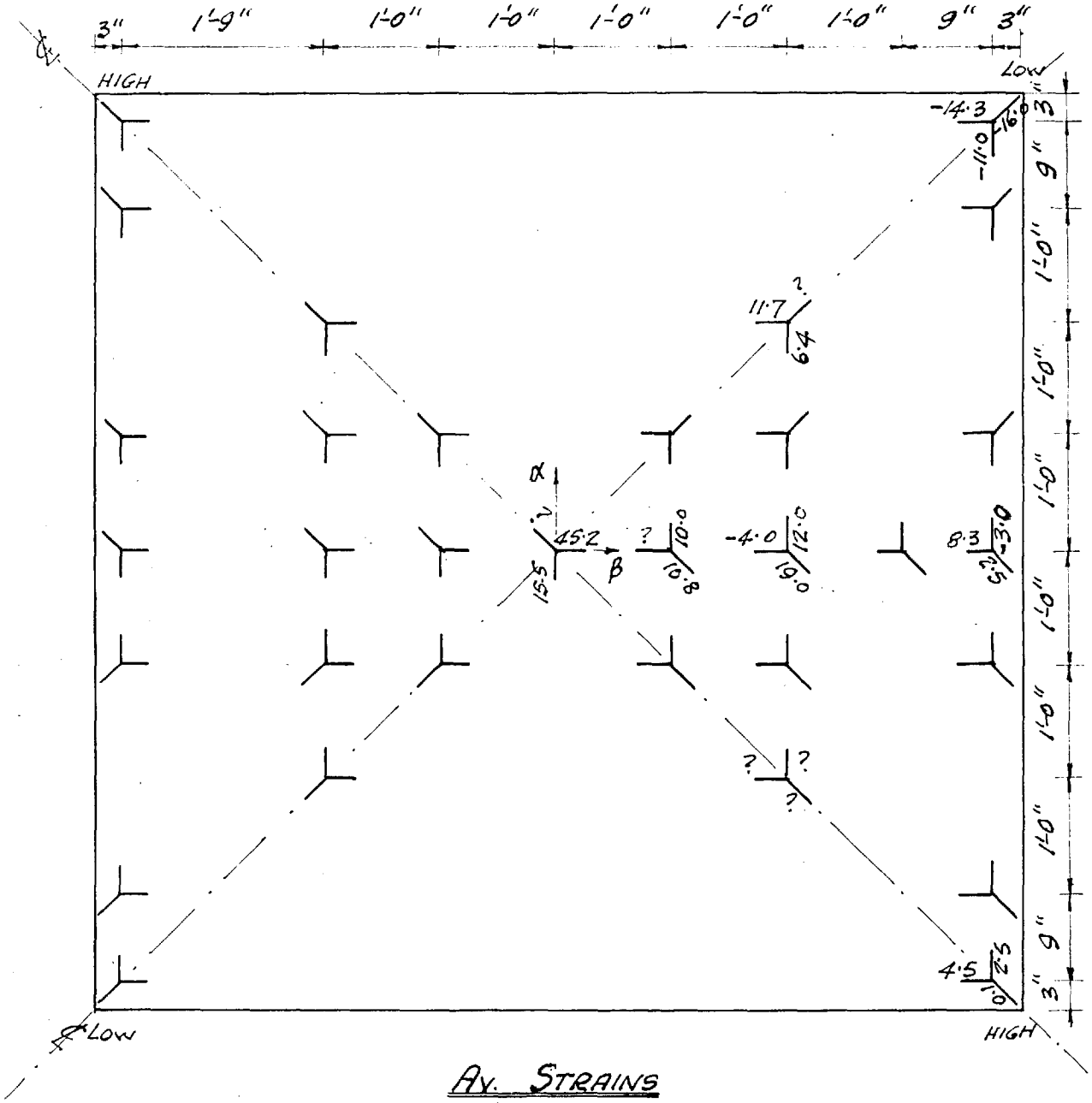
FIG. 6·12.



DIFFERENTIAL STRAINS.

TEST NO.3 HALF SHELL LOADED

FIG. 6·13.

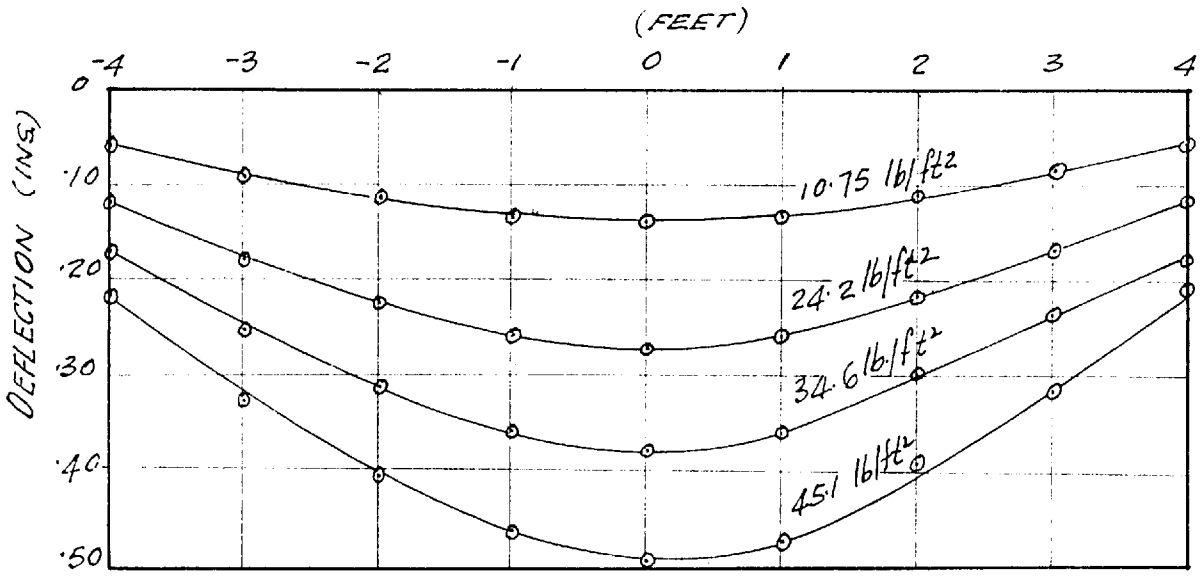


Av. Strains

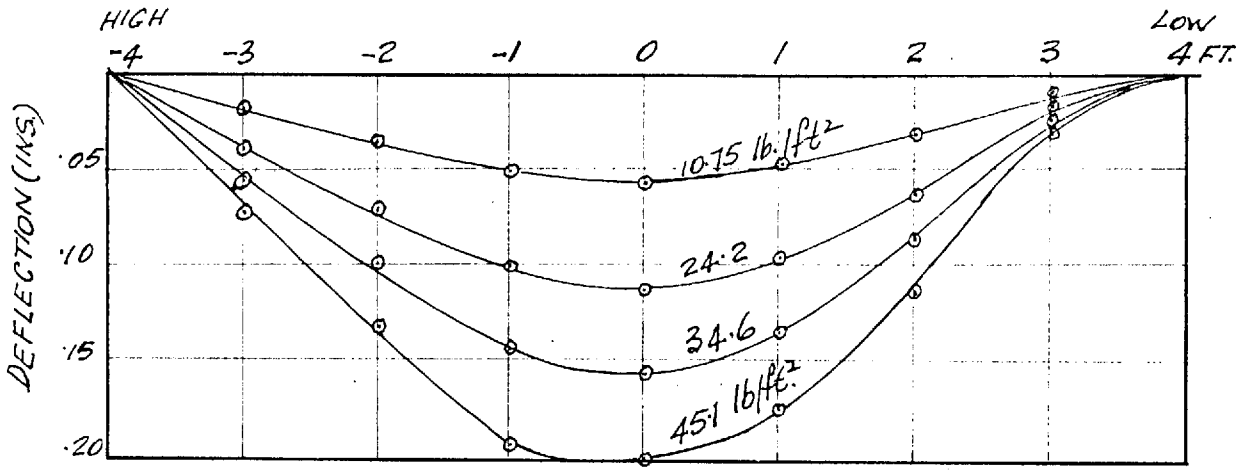
Test No. 3. Half Shell Loaded.

N.B: The av. strains were unreliable in Circuits Nos. 1-3, covered by the Savage & Parsons Strain recorded.

FIG. 6.14.



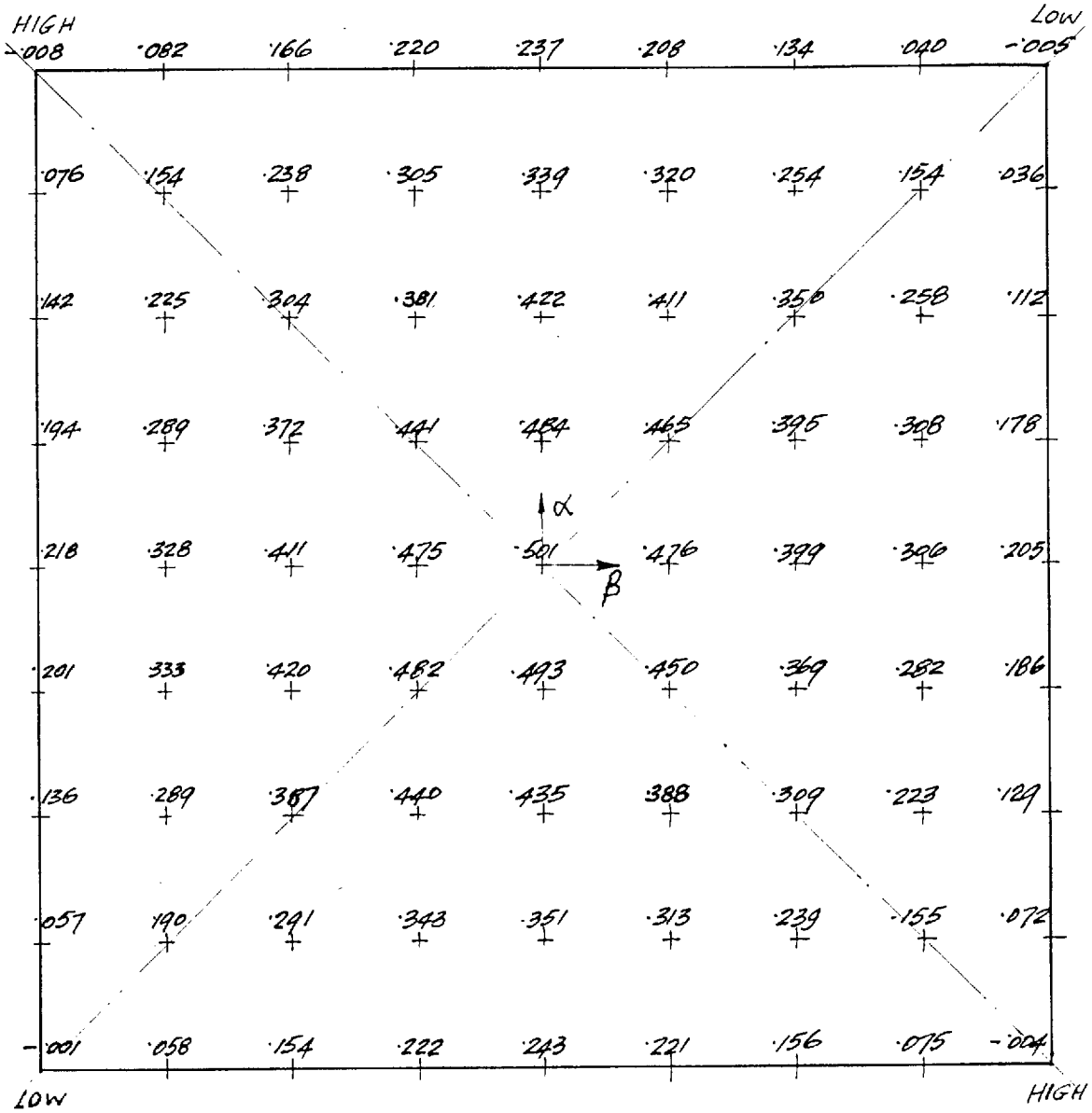
PROFILE ALONG $\alpha = 0$



PROFILE ALONG EDGE BEAM NO.1 ($\beta = 4.0'$)

TEST NO. 4. TYPICAL DEFLECTION PROFILES.

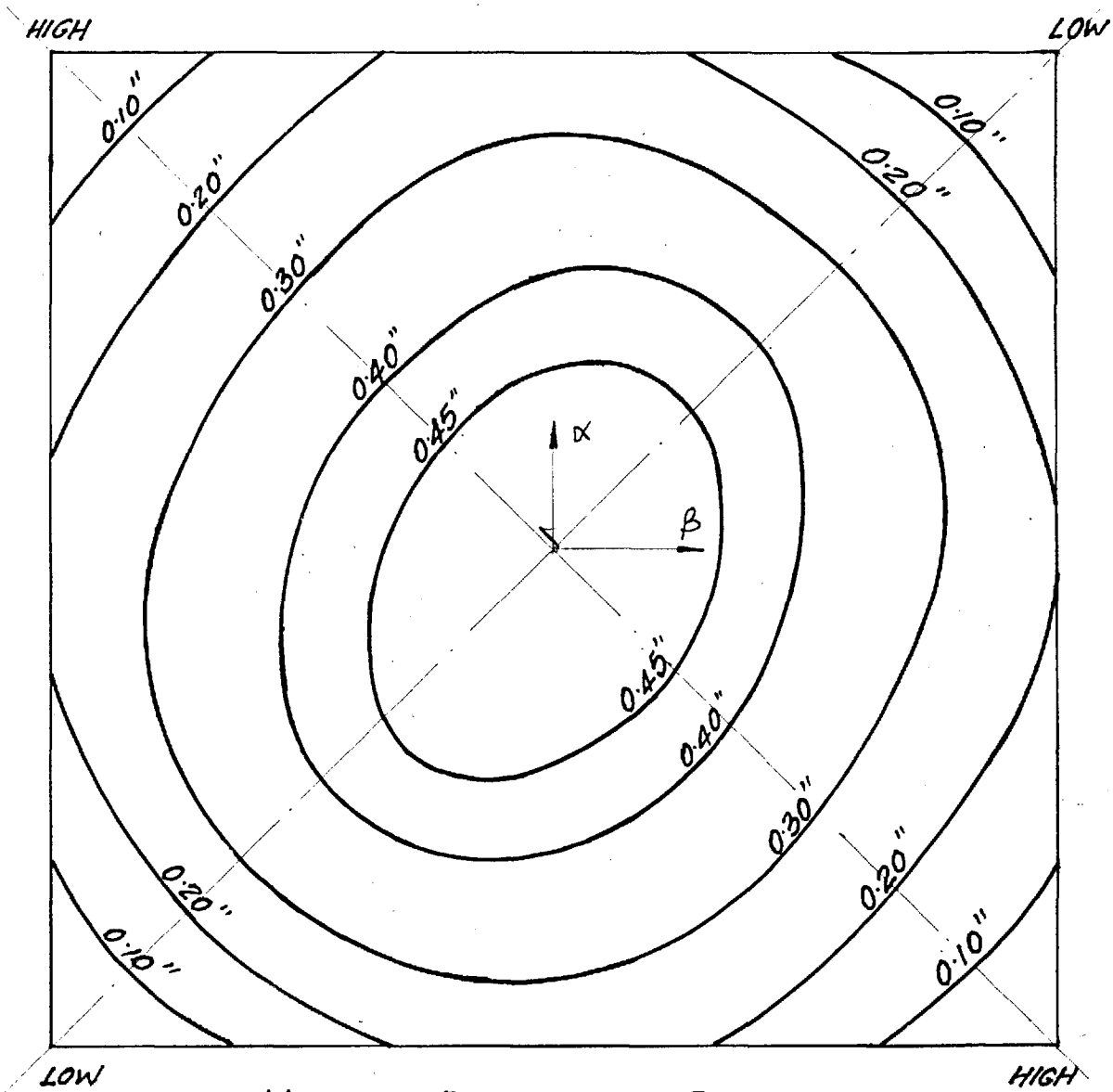
FIG. 6 .15.



VERTICAL DEFLECTIONS - INS.
FOR U.D.L. OF 45 LB/FT².

TEST NO.4 - U.D.L

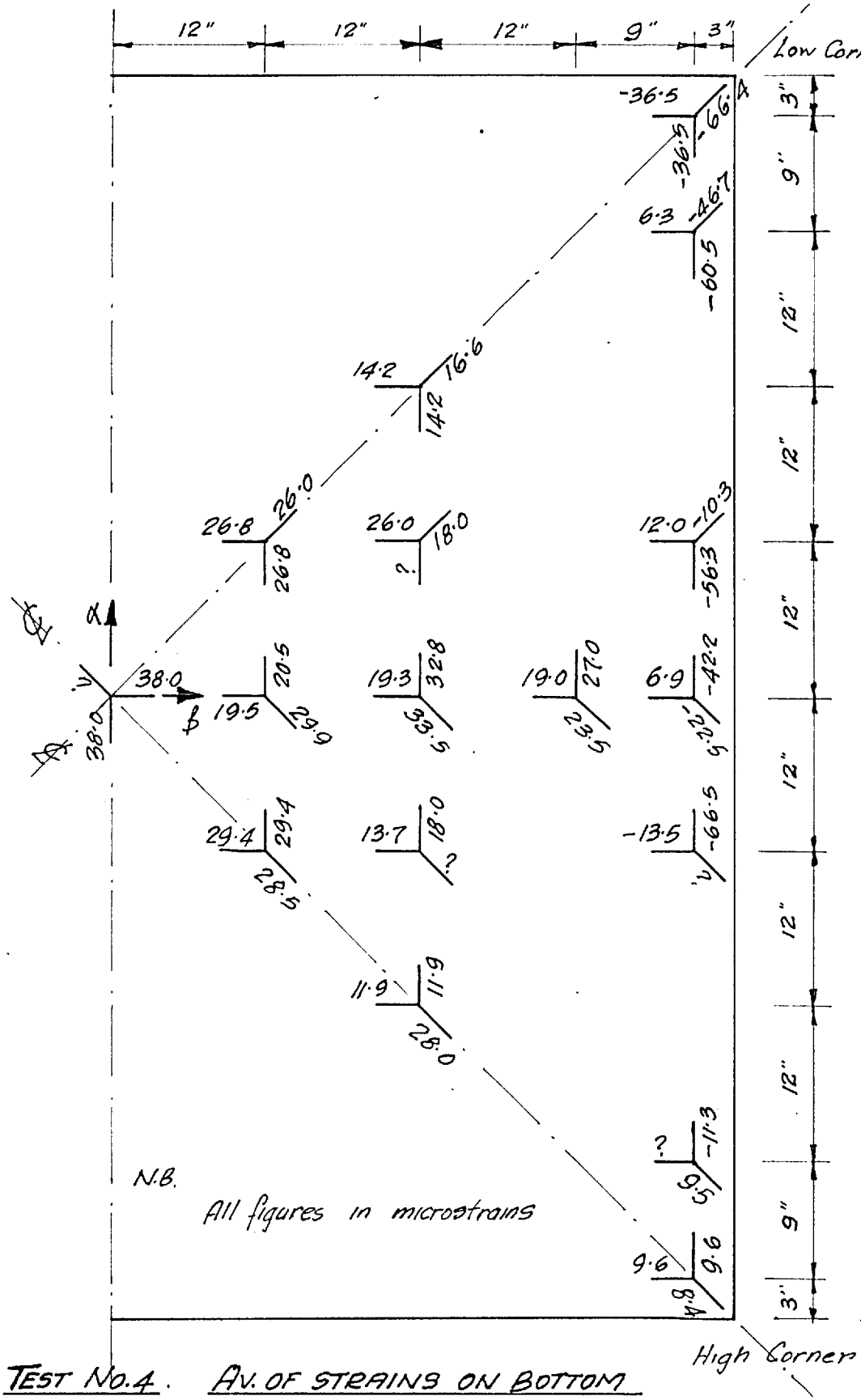
FIG. 6.16.



VERTICAL DEFLECTION CONTOURS
FOR U.D.L. OF 45 LBS/FT.^{2}

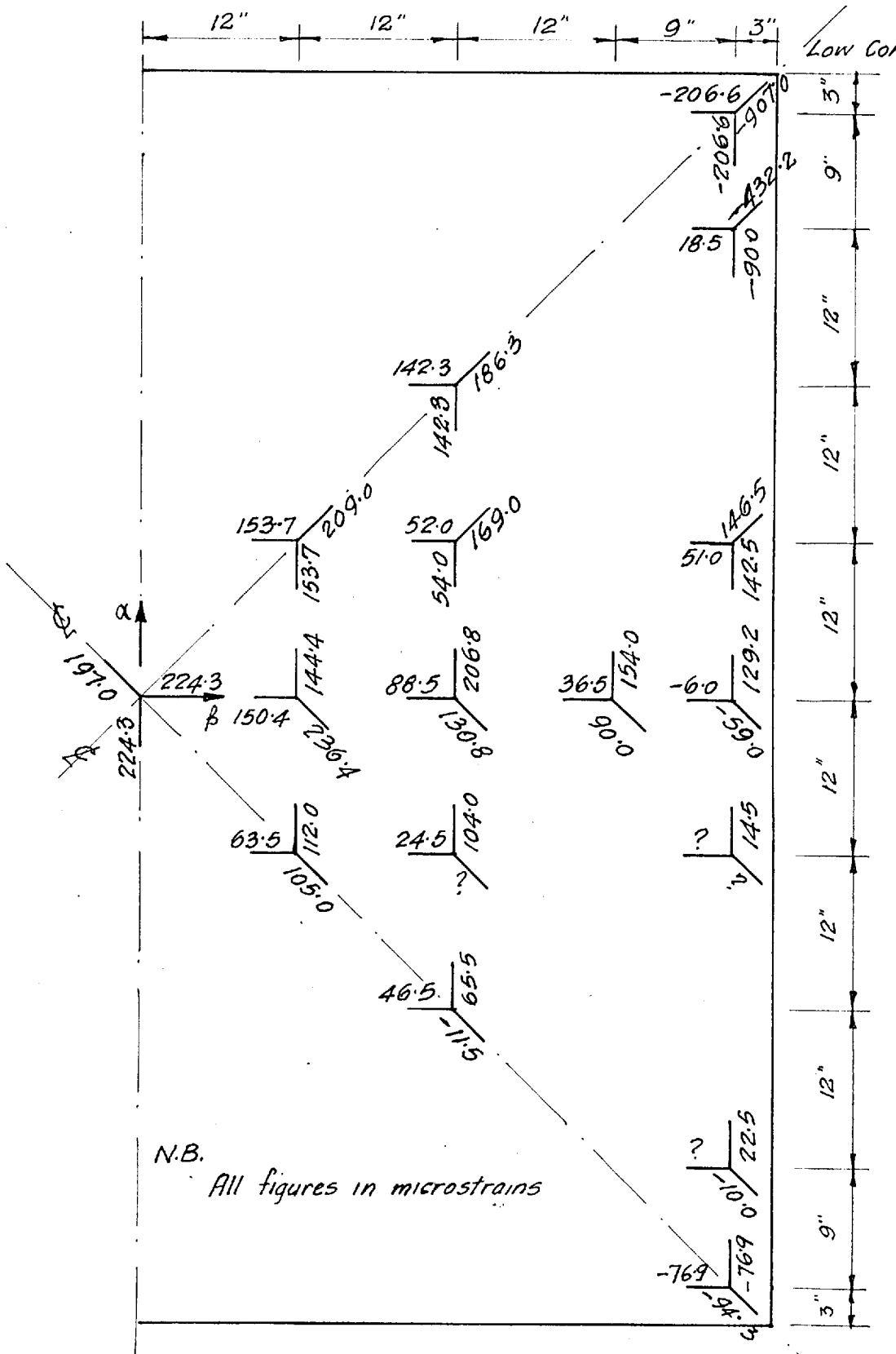
TEST NO.4 - U.D.L.

FIG. 6.17.



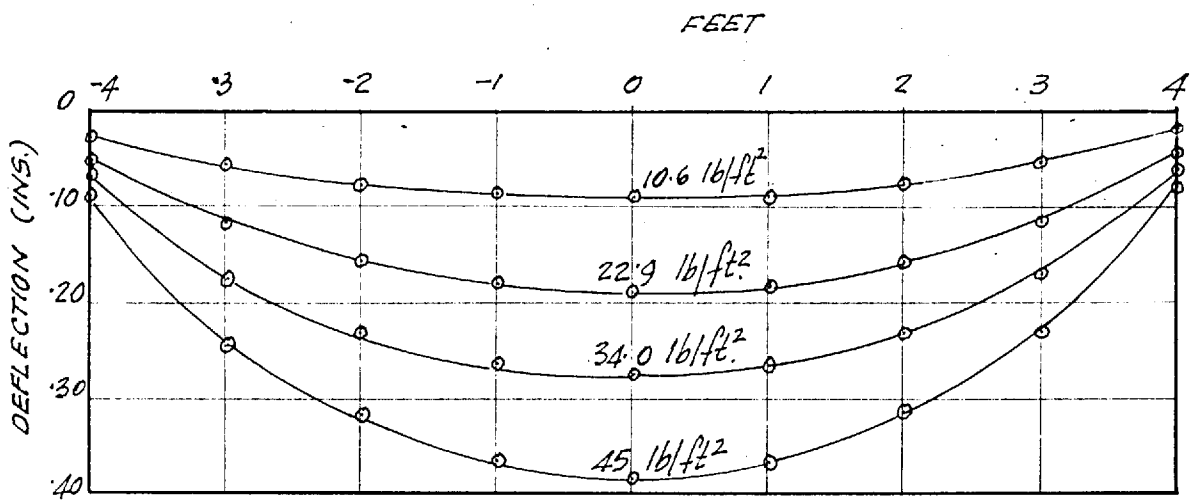
TEST NO.4. AV. OF STRAINS ON BOTTOM AND TOP SURFACES

FIG. NO. 6.18

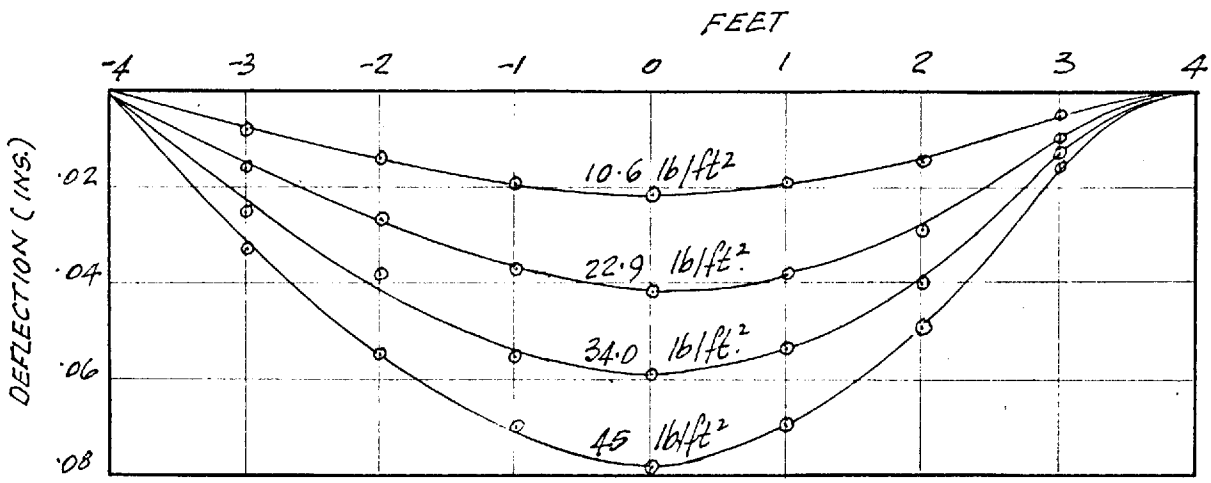


TEST NO.4. DIFF. IN STRAINS ON TOP AND BOTTOM SURFACES

FIG. NO. 6.19.



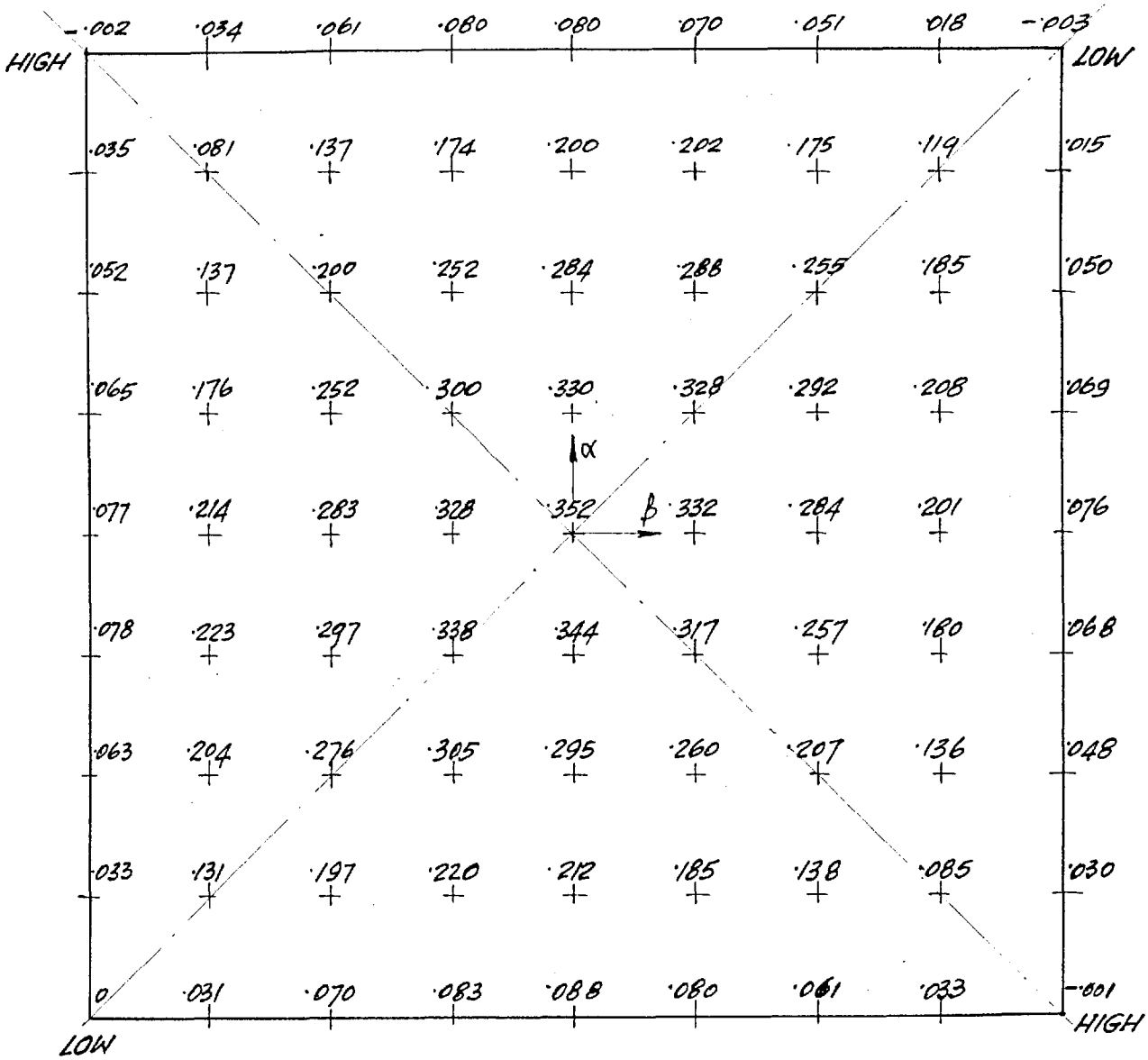
PROFILE ALONG $\alpha = 0$



PROFILE ALONG EDGE BEAM NO.2 ($\beta = 4'$)

TEST NO. 5. TYPICAL DEFLECTION PROFILES

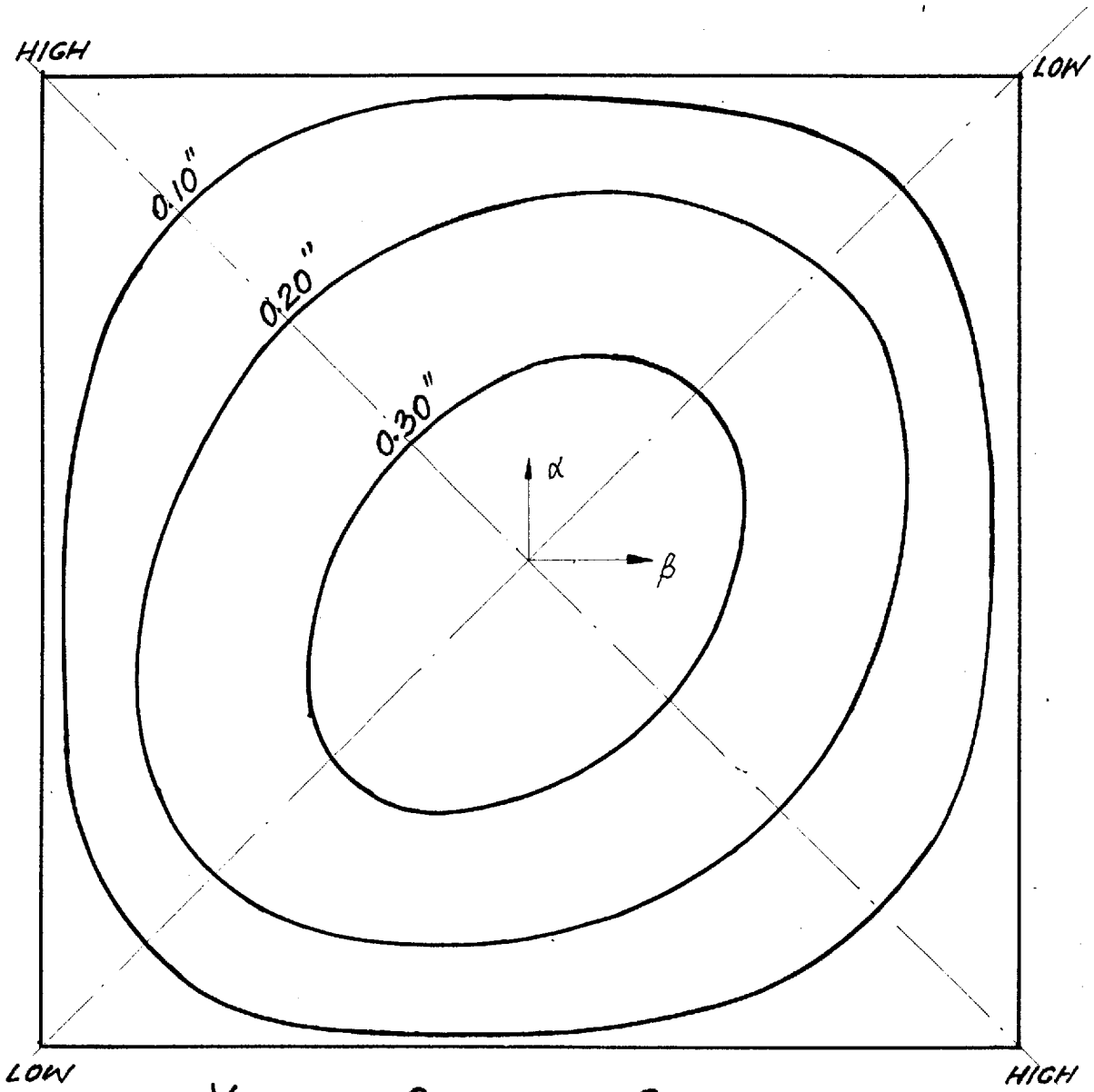
FIG. 6.20.



VERTICAL DEFLECTIONS — INS.

TEST NO. 5 - U.D.L OF 45 LB/FT.^{2}

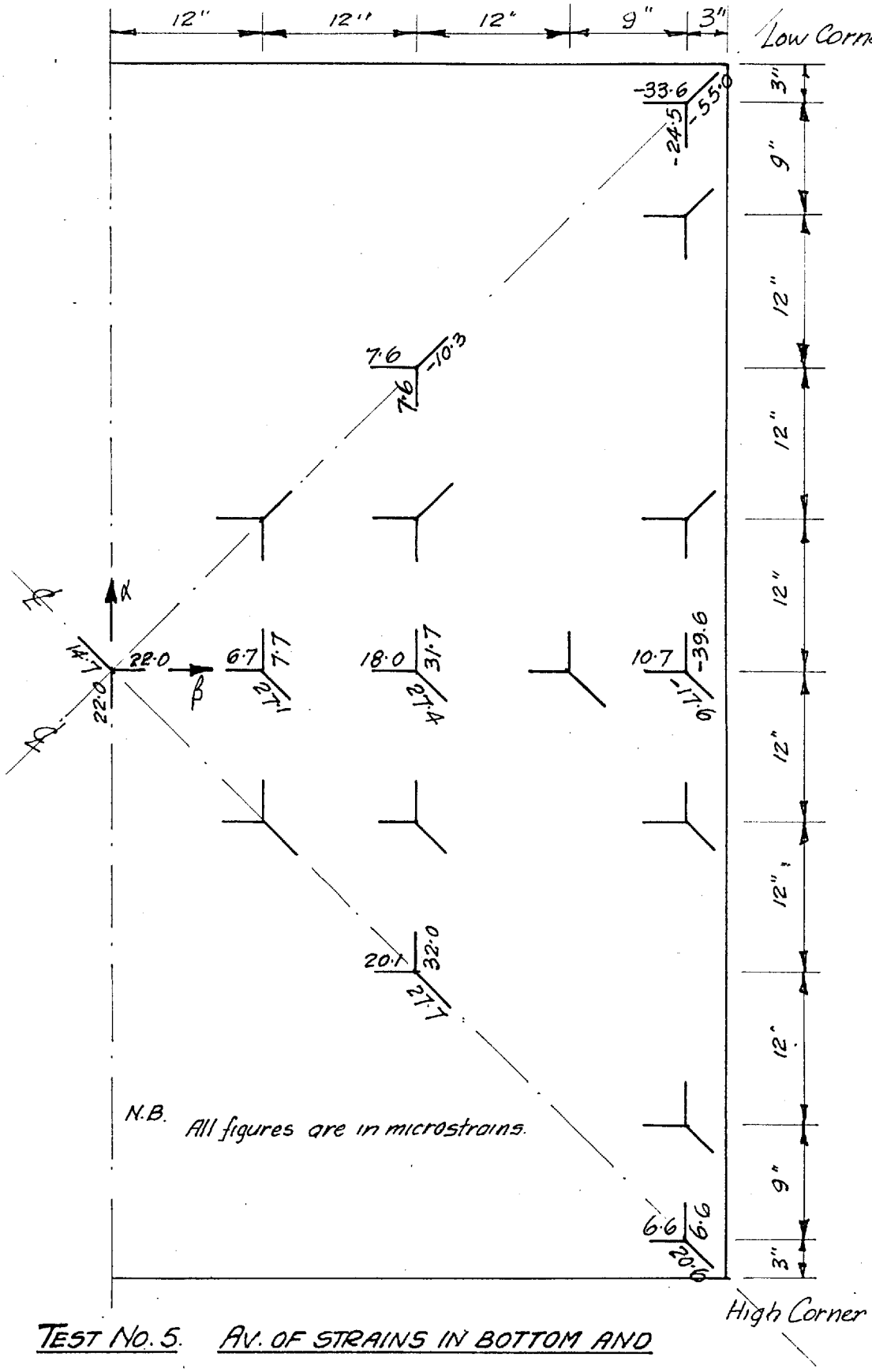
FIG. 6.21



VERTICAL DEFLECTION CONTOURS

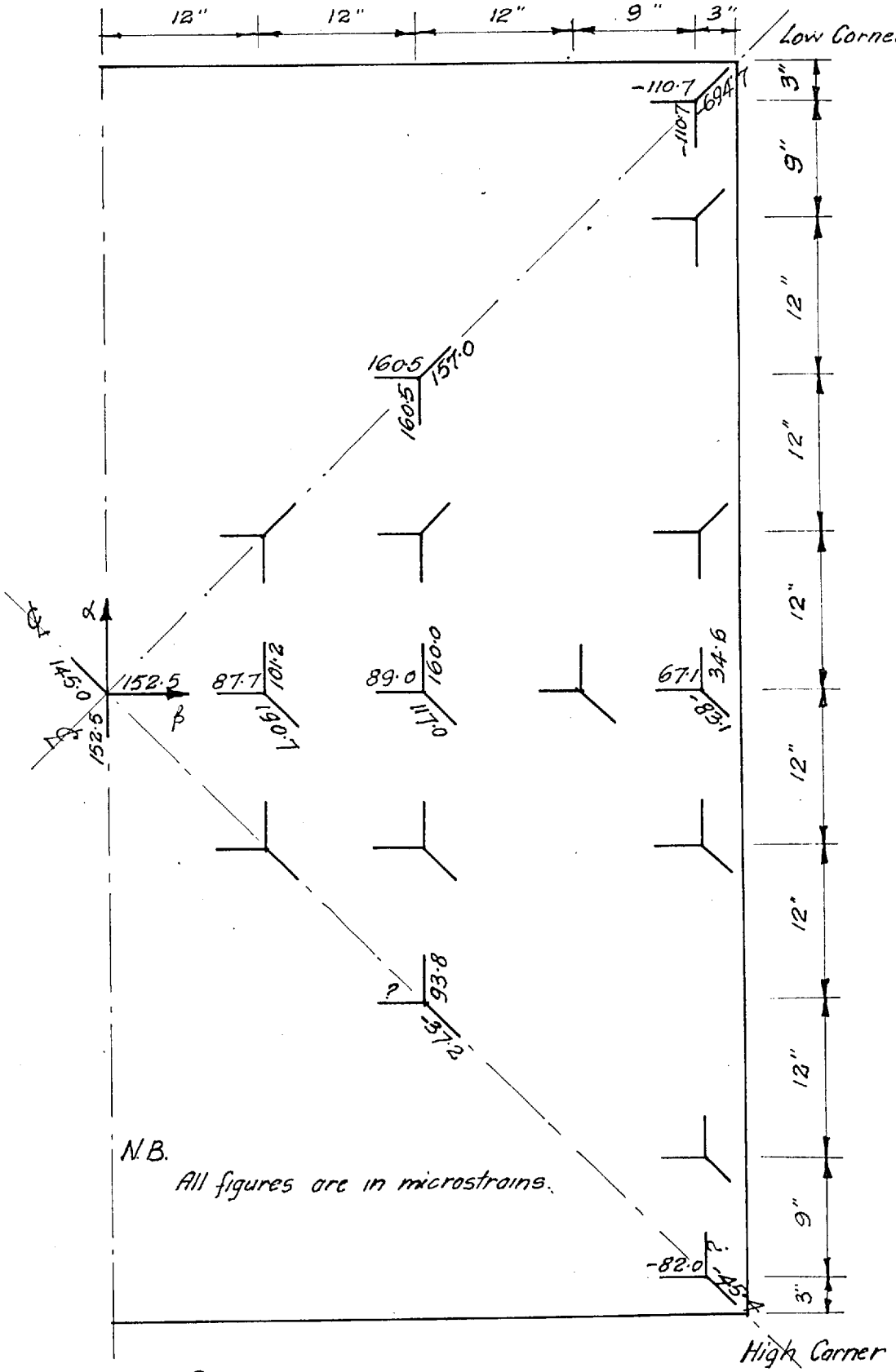
TEST NO.5.

FIG. 6. 22.



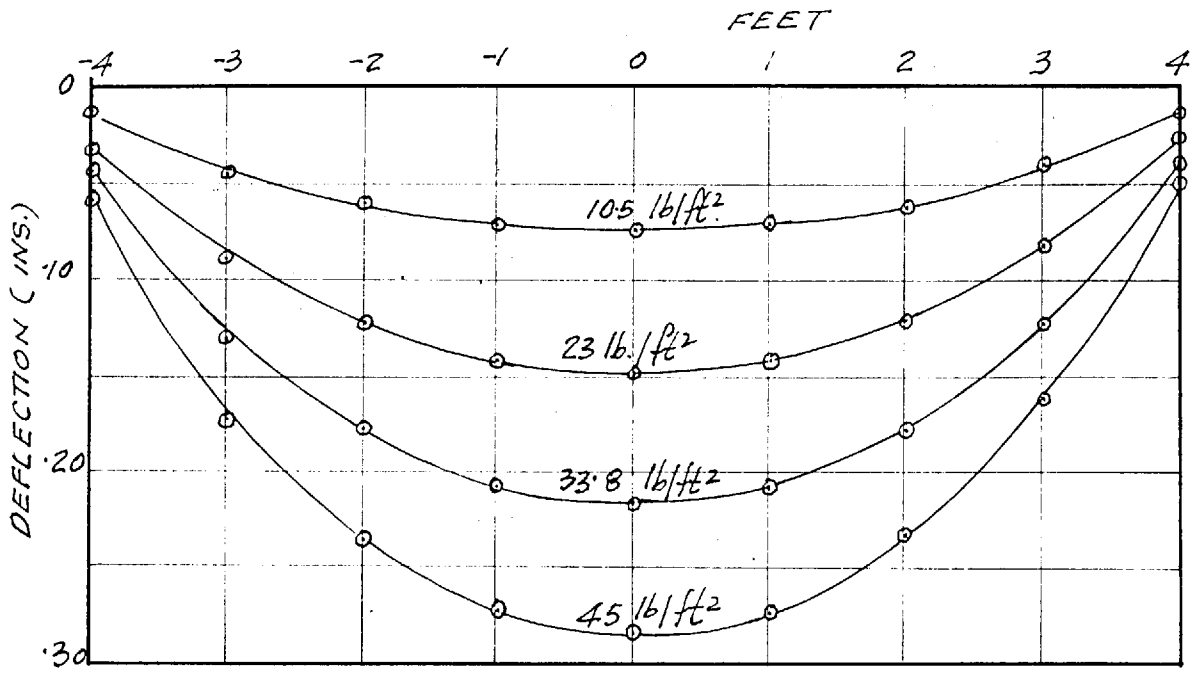
TEST NO. 5. AV. OF STRAINS IN BOTTOM AND TOP SURFACES.

FIG. NO. 6.23

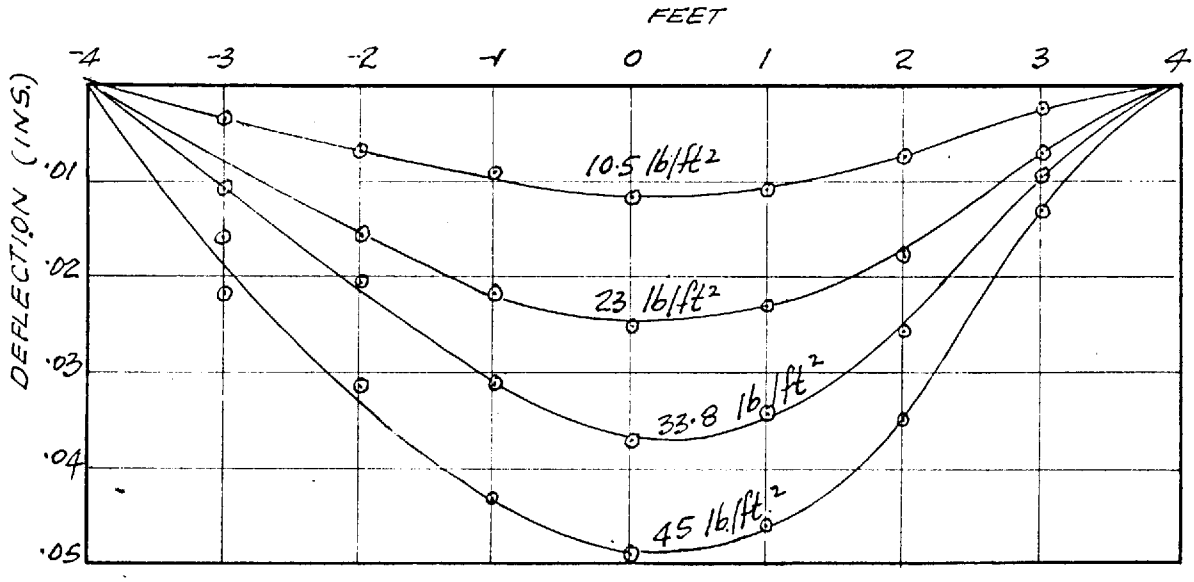


TEST NO.5. DIFF. BETWEEN STRAINS IN BOTTOM AND TOP SURFACES

FIG. NO. 6.24



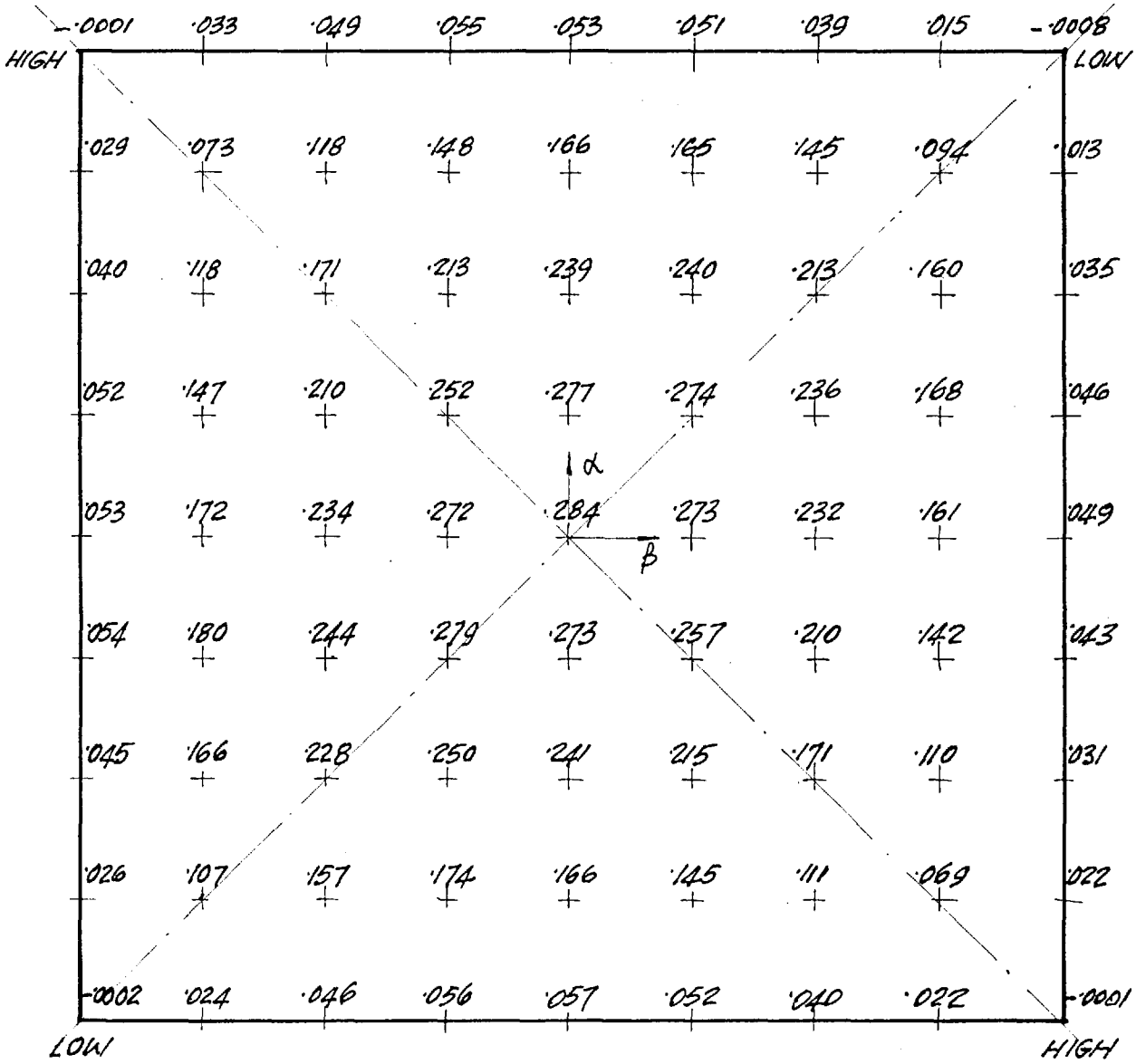
PROFILE ALONG $\alpha = 0$



PROFILE ALONG EDGE BEAM NO.2 ($\beta = 4'\text{-}0''$)

TEST NO. 6. TYPICAL DEFLECTION PROFILES.

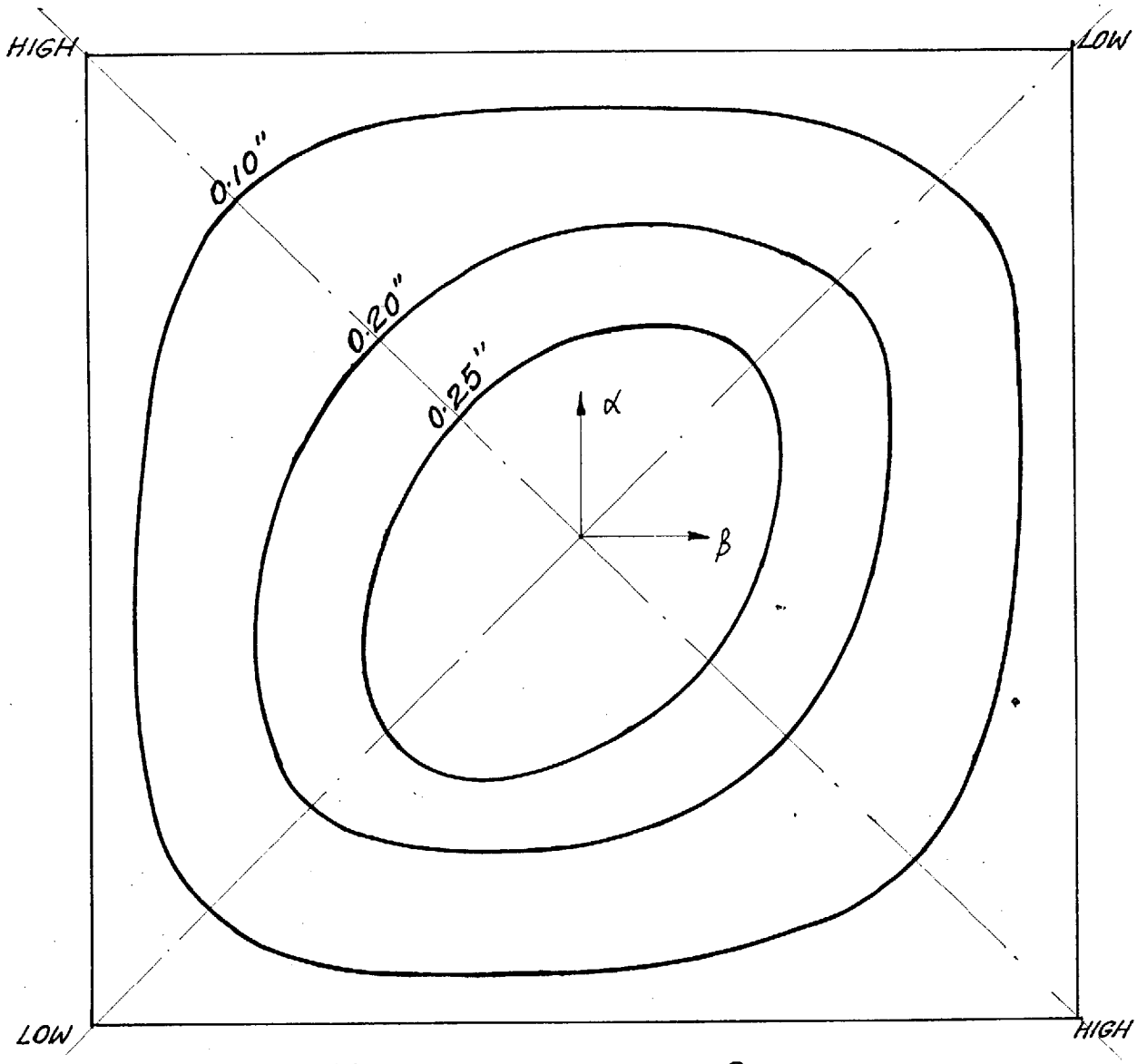
FIG. 6. 25.



VERTICAL DEFLECTION – INS.

TEST NO. 6 – U.D.L. OF 45 LB/FT.^{2}

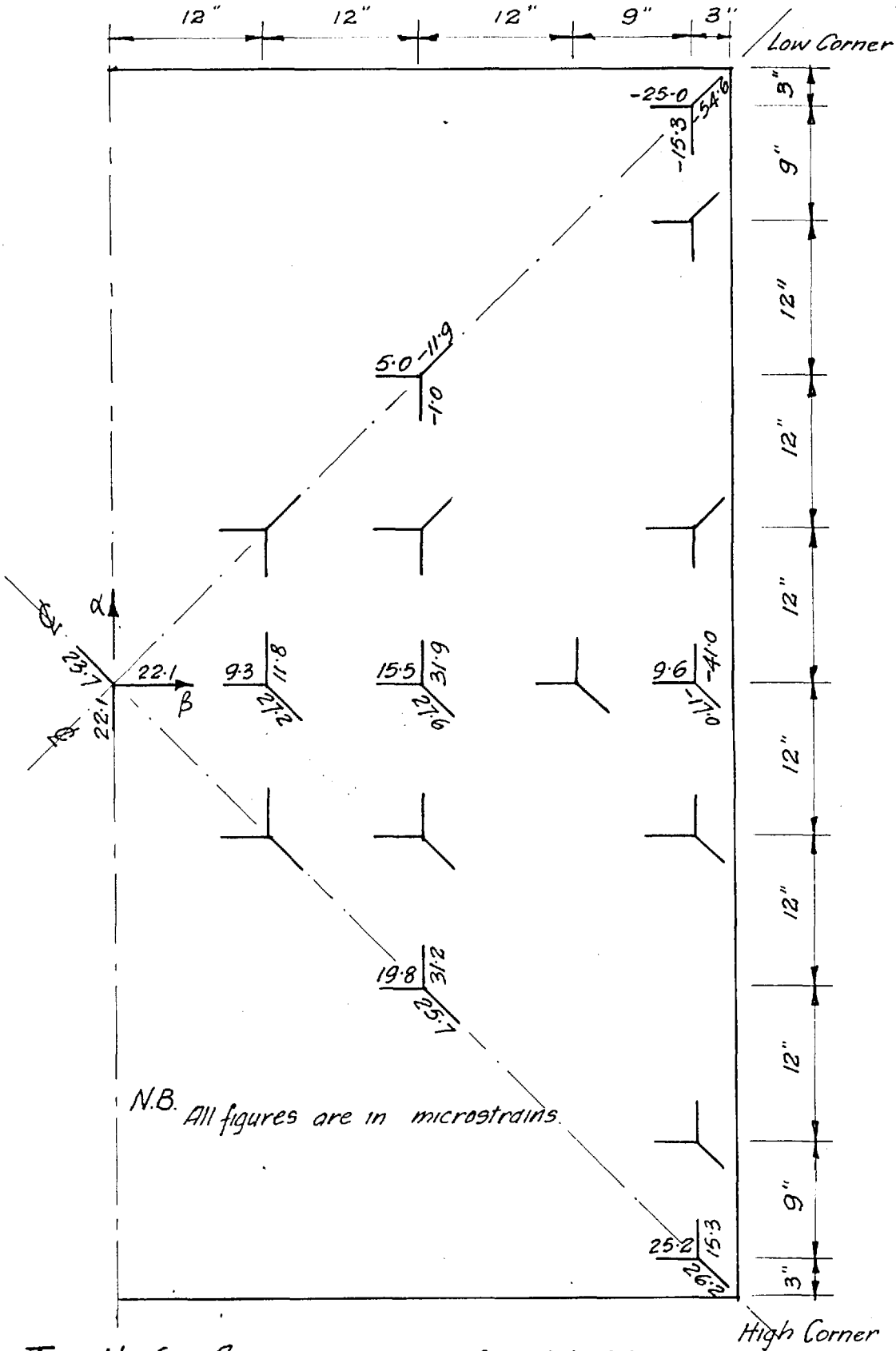
FIG. 6.26.



VERTICAL DEFLECTION CONTOURS
FOR U.D.L. OF 45 LB/FT.^{2}

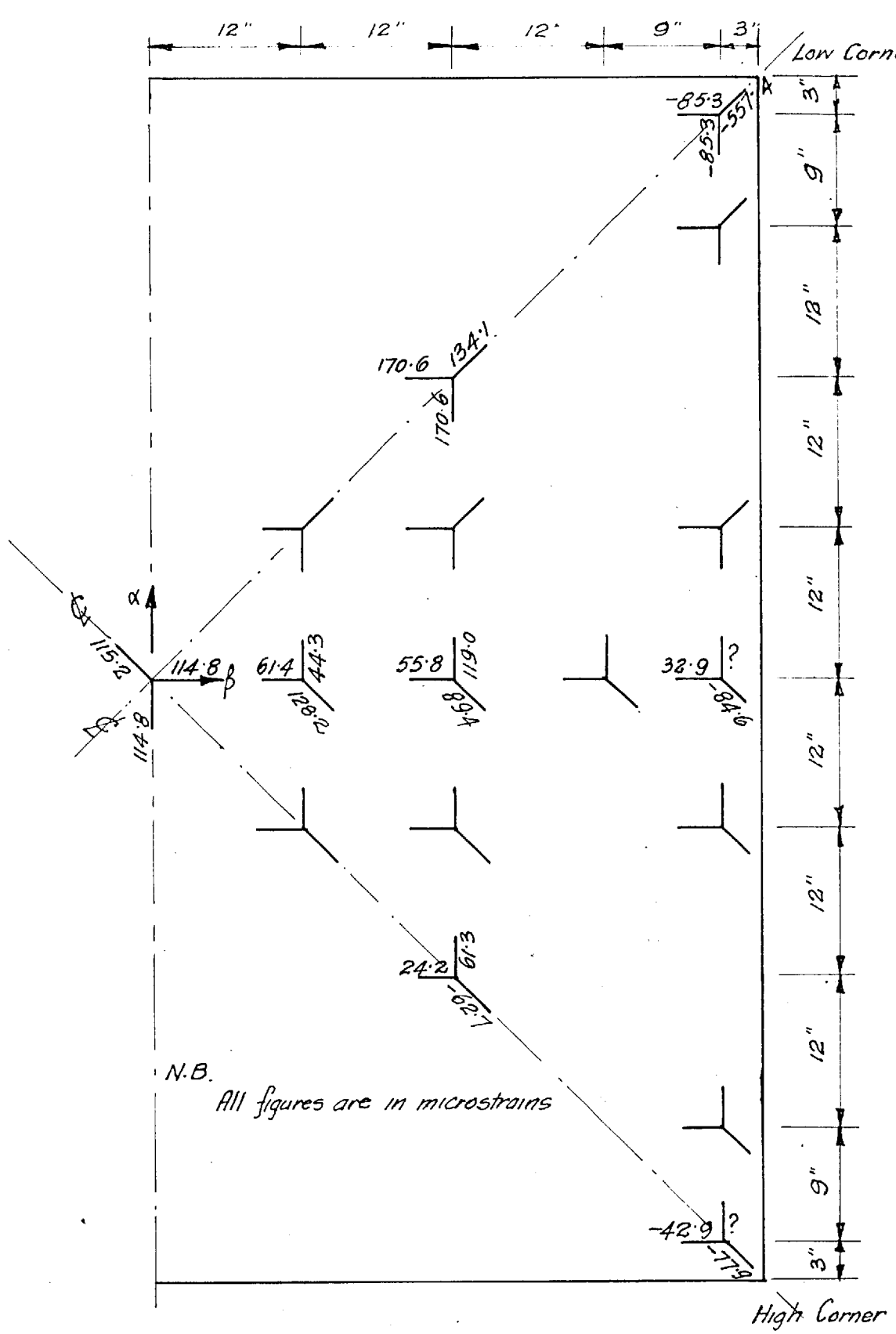
TEST NO. 6.

FIG. 6.27.



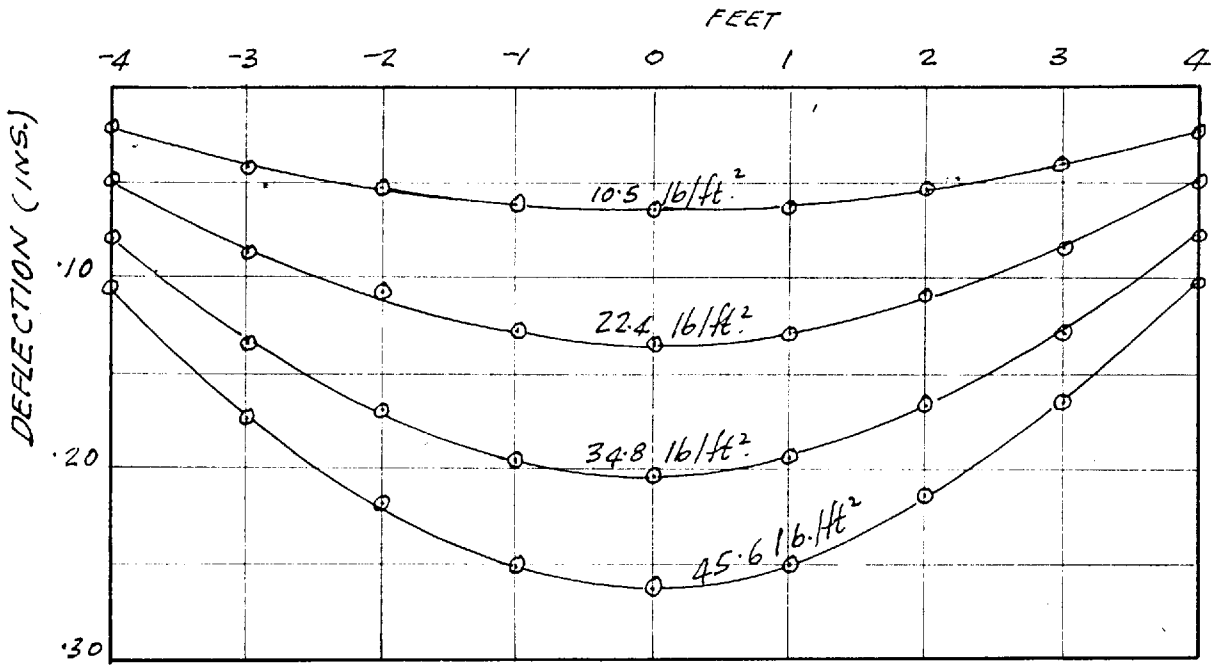
TEST NO. 6. AV. OF STRAINS IN BOTTOM AND TOP SURFACES

FIG. 6.28

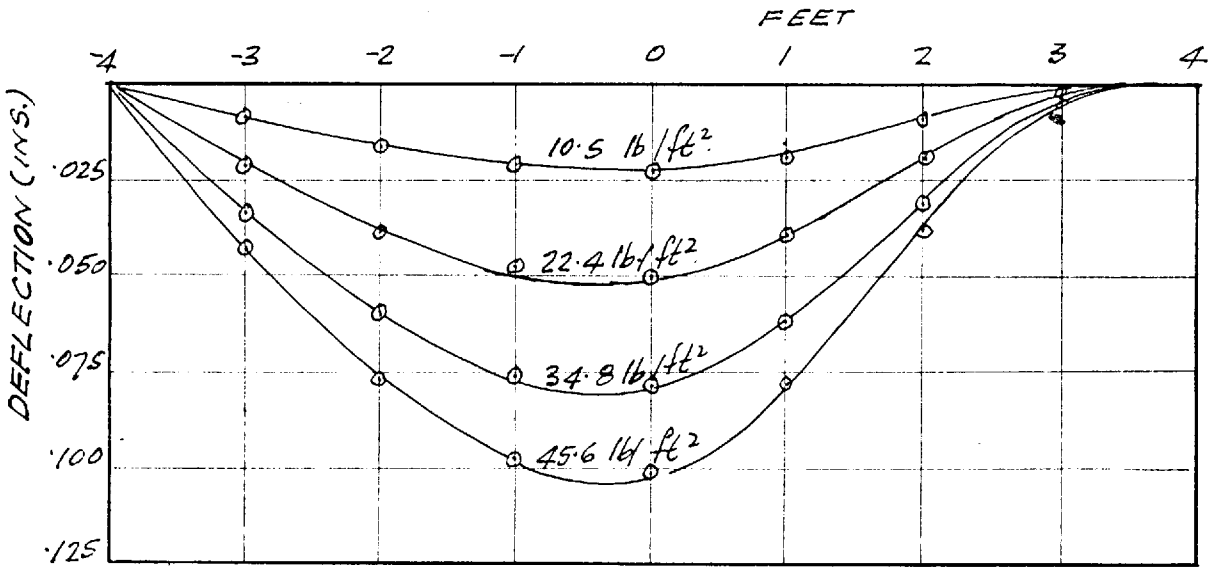


TEST NO.6 DIFF. BETWEEN STRAINS IN BOTTOM AND TOP SURFACES.

FIG. NO. 6.29.



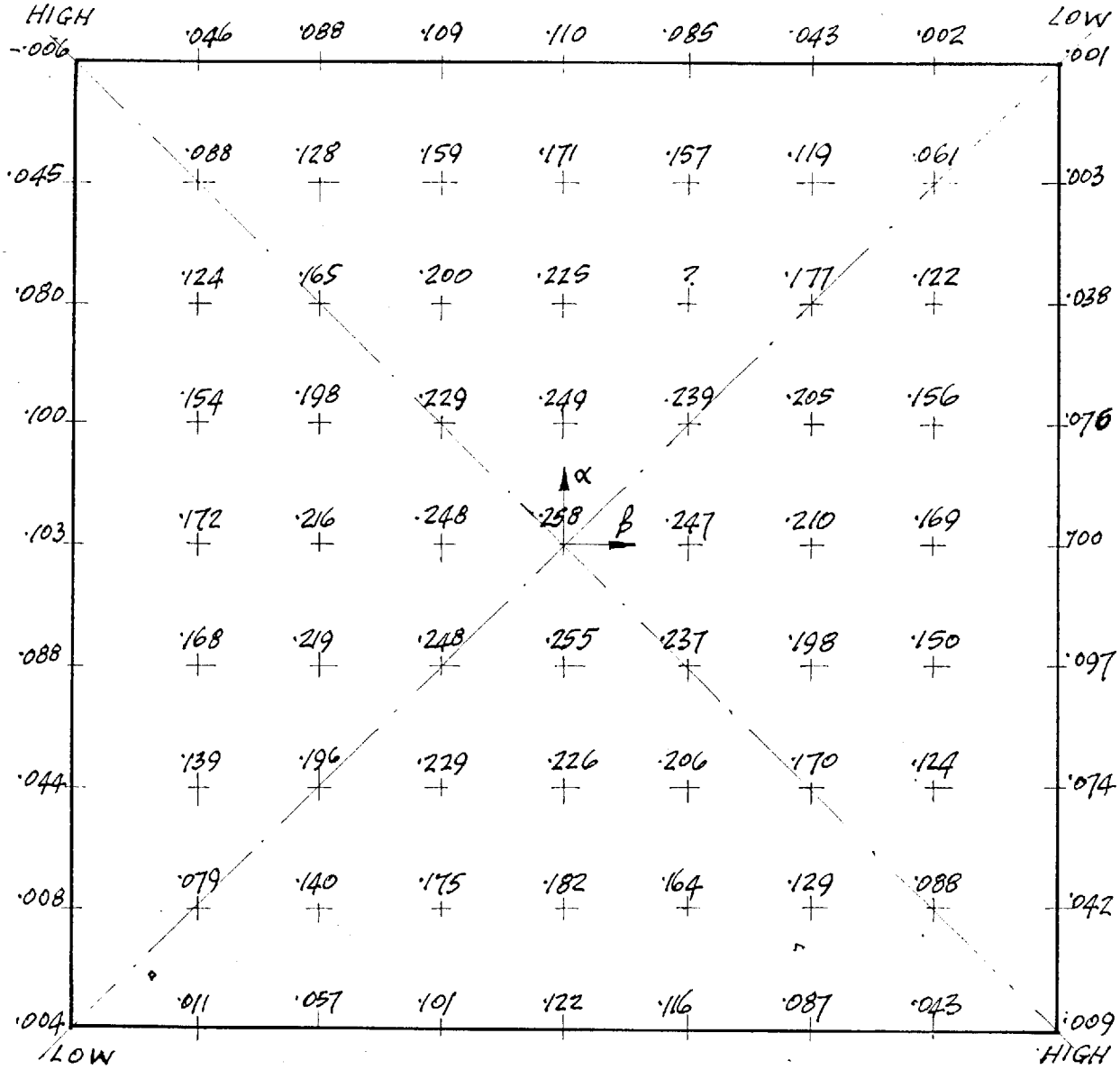
PROFILE ALONG $\alpha = 0$



PROFILE ALONG EDGE BEAM No. 2 ($\beta = 4'\text{-}0''$)

TEST NO.7. TYPICAL DEFLECTION PROFILES.

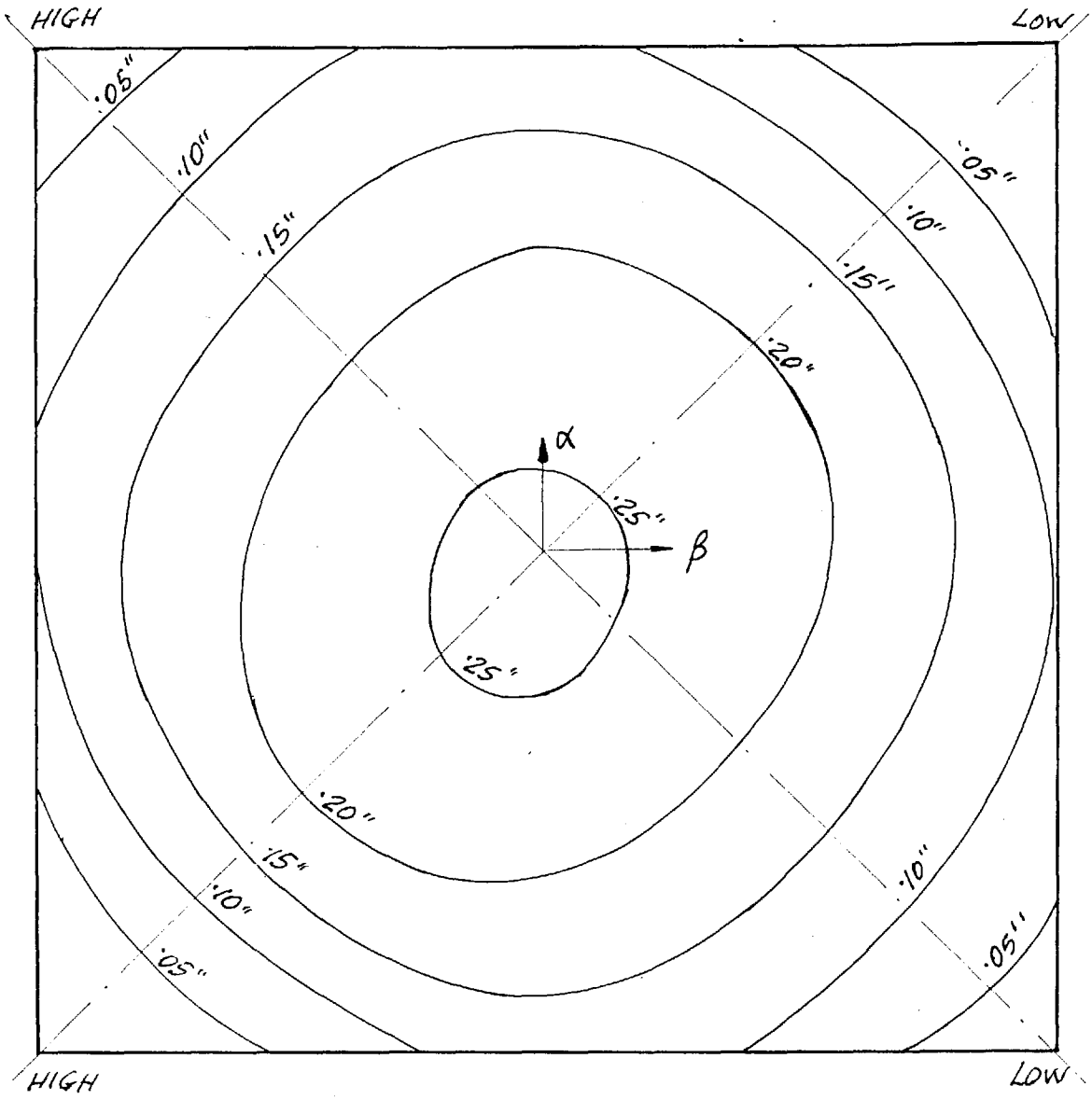
FIG. 6.30.



VERTICAL DEFLECTION (INS.) – U.D.L. OF 45 LB/FT^2.

TEST NO. 7.

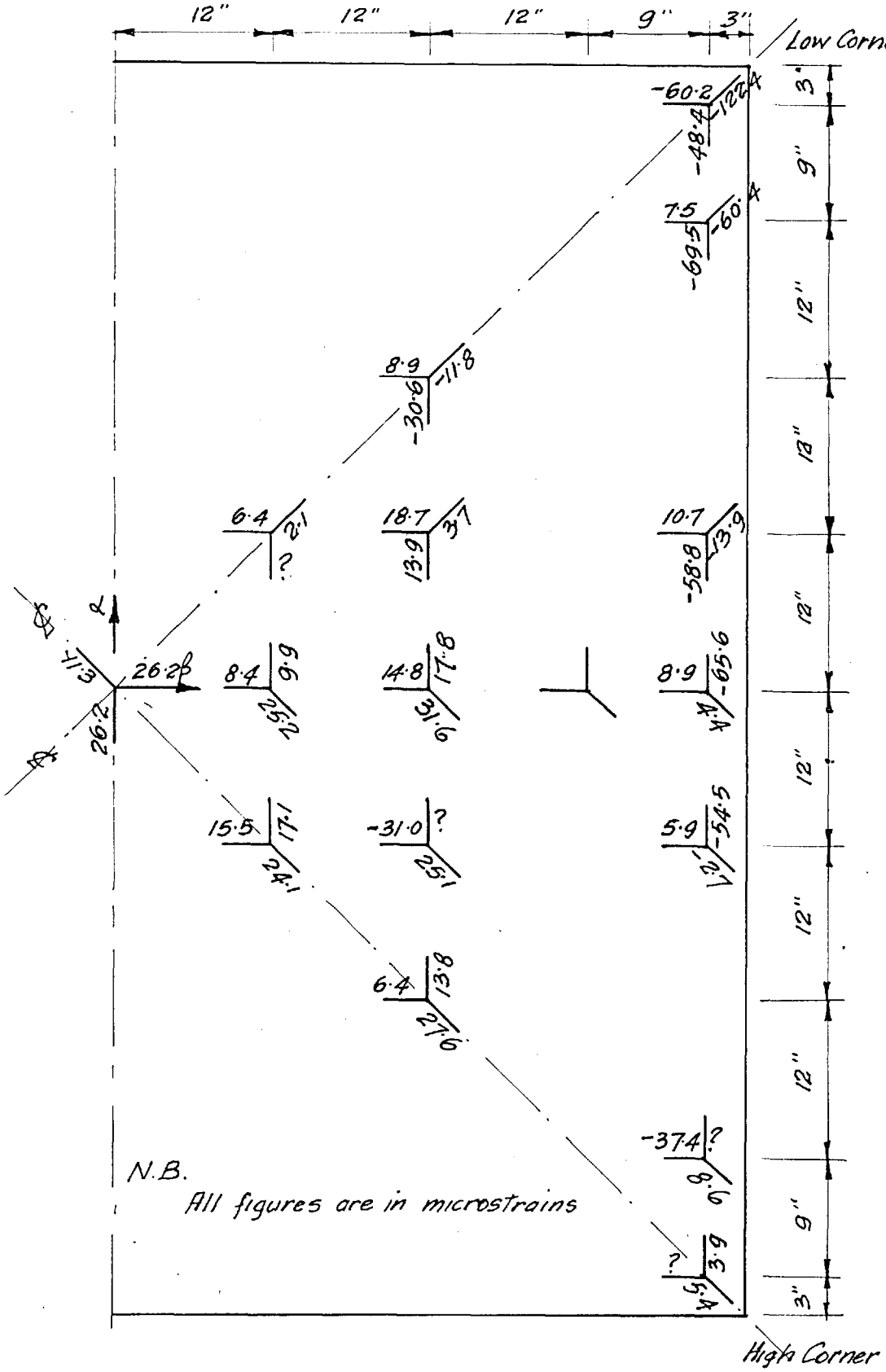
FIG. 6.31.



VERTICAL DEFLECTION CONTOURS

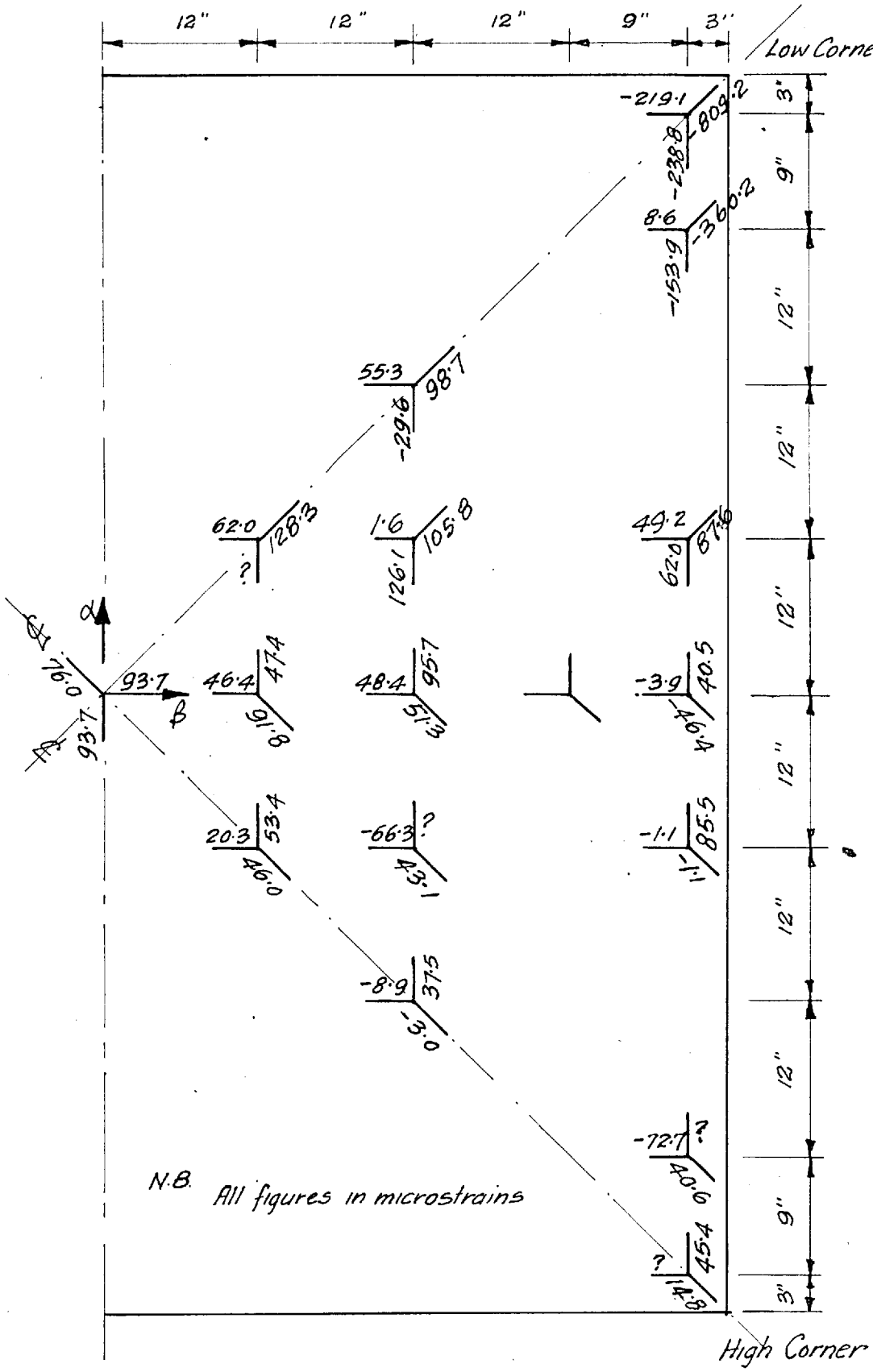
TEST NO. 7.

FIG. 6.32.



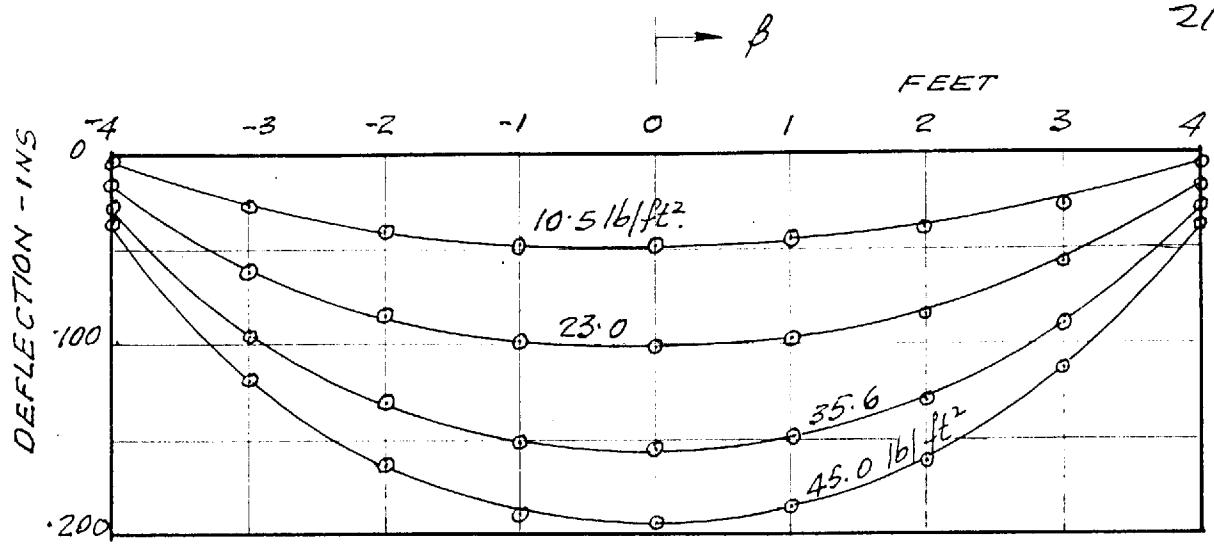
TEST NO. 7. AV. OF STRAINS IN BOTTOM AND TOP SURFACES.

FIG. NO. 6.33

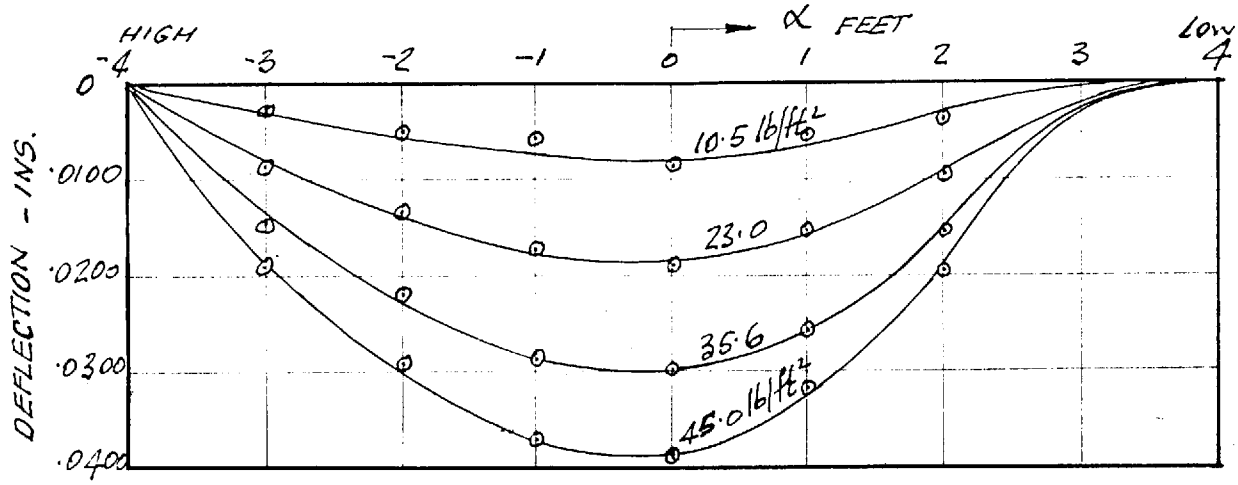


TEST NO.7. DIFF. BETWEEN STRAINS IN BOTTOM AND TOP SURFACES.

FIG. NO.6·34



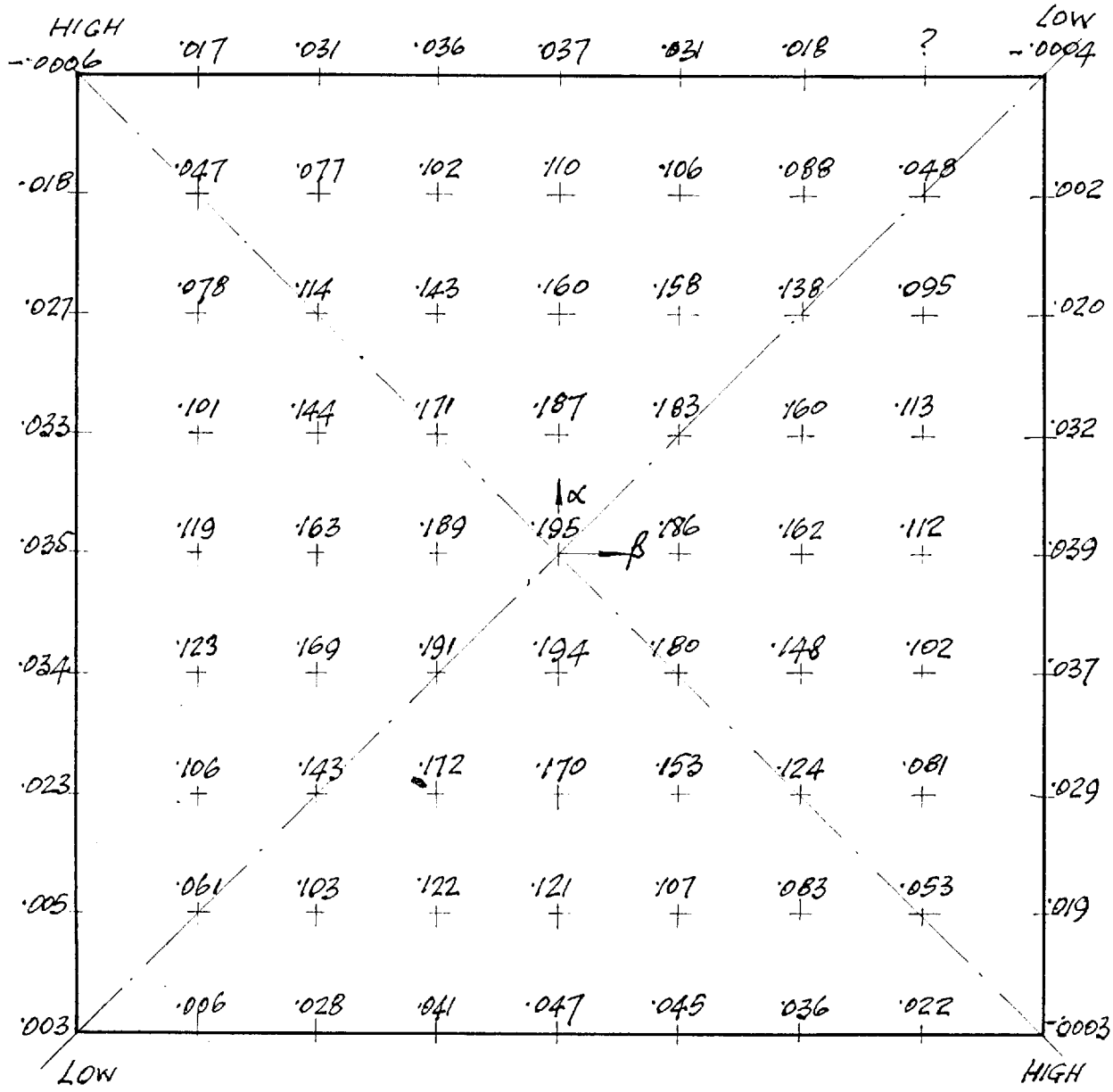
PROFILES ALONG $\alpha = 0$



PROFILES ALONG EDGE BEAM NO.2 ($\beta = 4'\text{-}0''$)

TEST NO.8. TYPICAL DEFLECTION PROFILES.

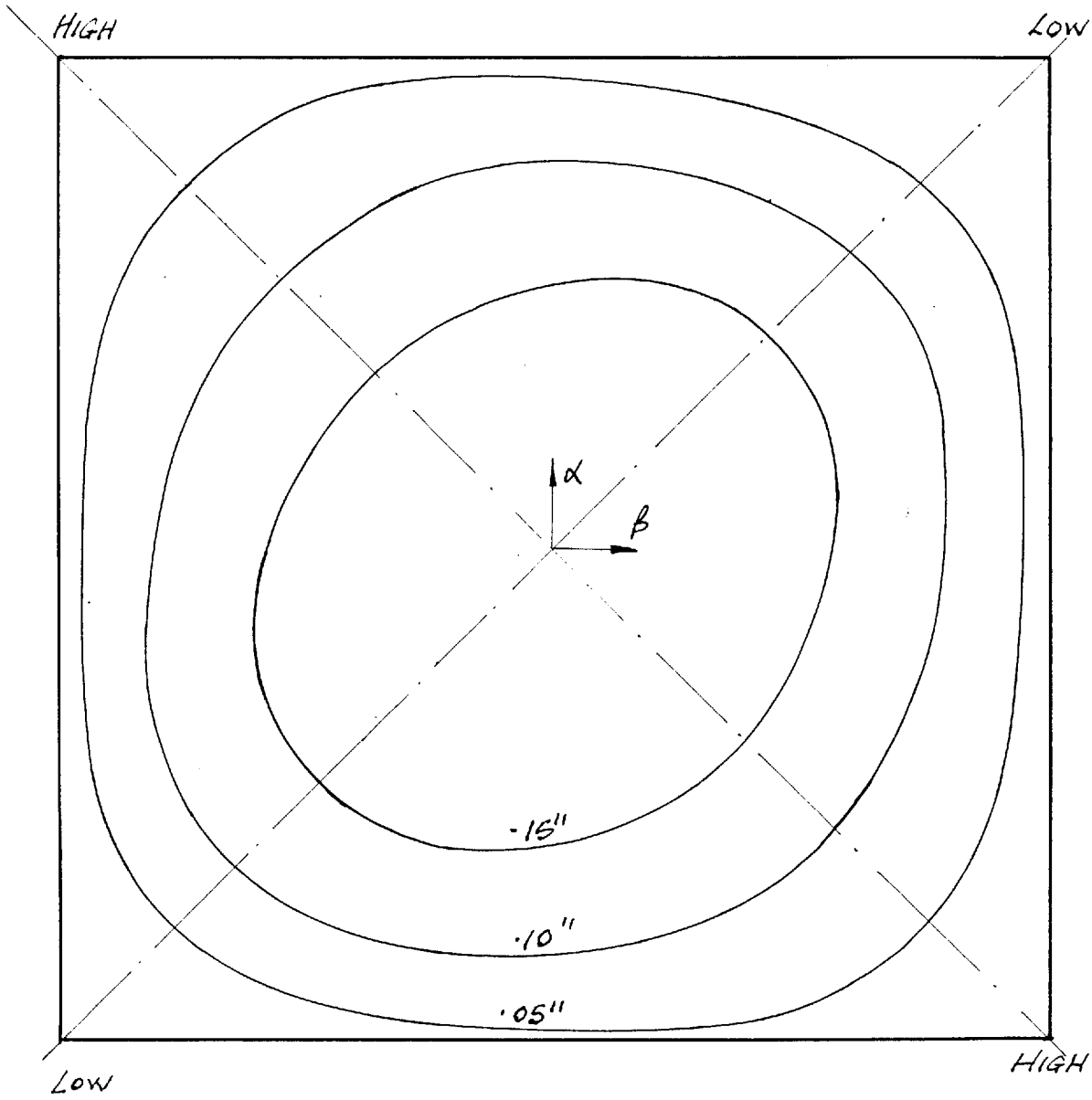
FIG.6.35.



VERTICAL DEFLECTION (INS.) – U.D.L. OF 45 LB/FT.²

TEST NO. 8.

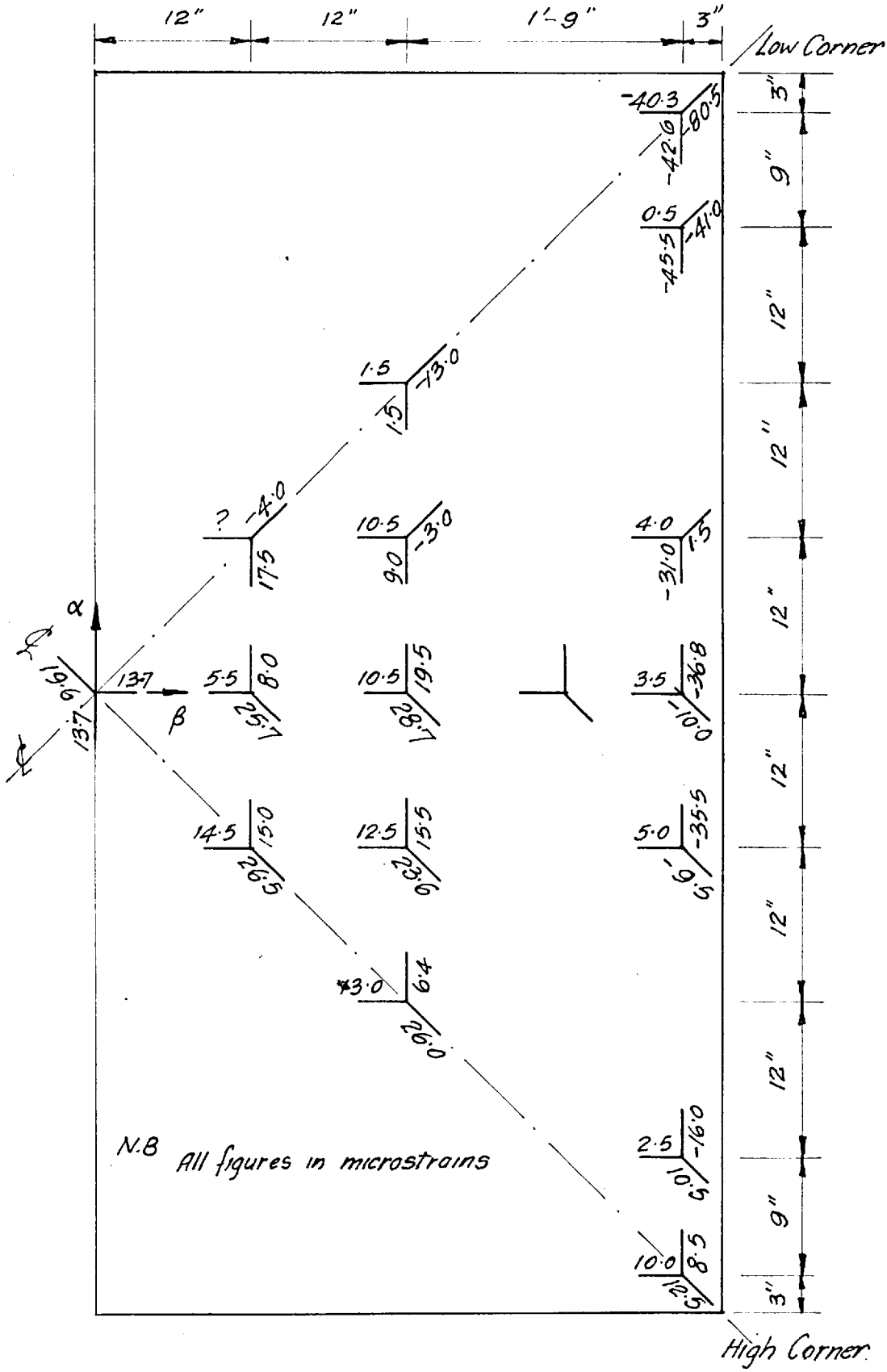
FIG. 6.36.



VERTICAL DEFLECTION CONTOURS.

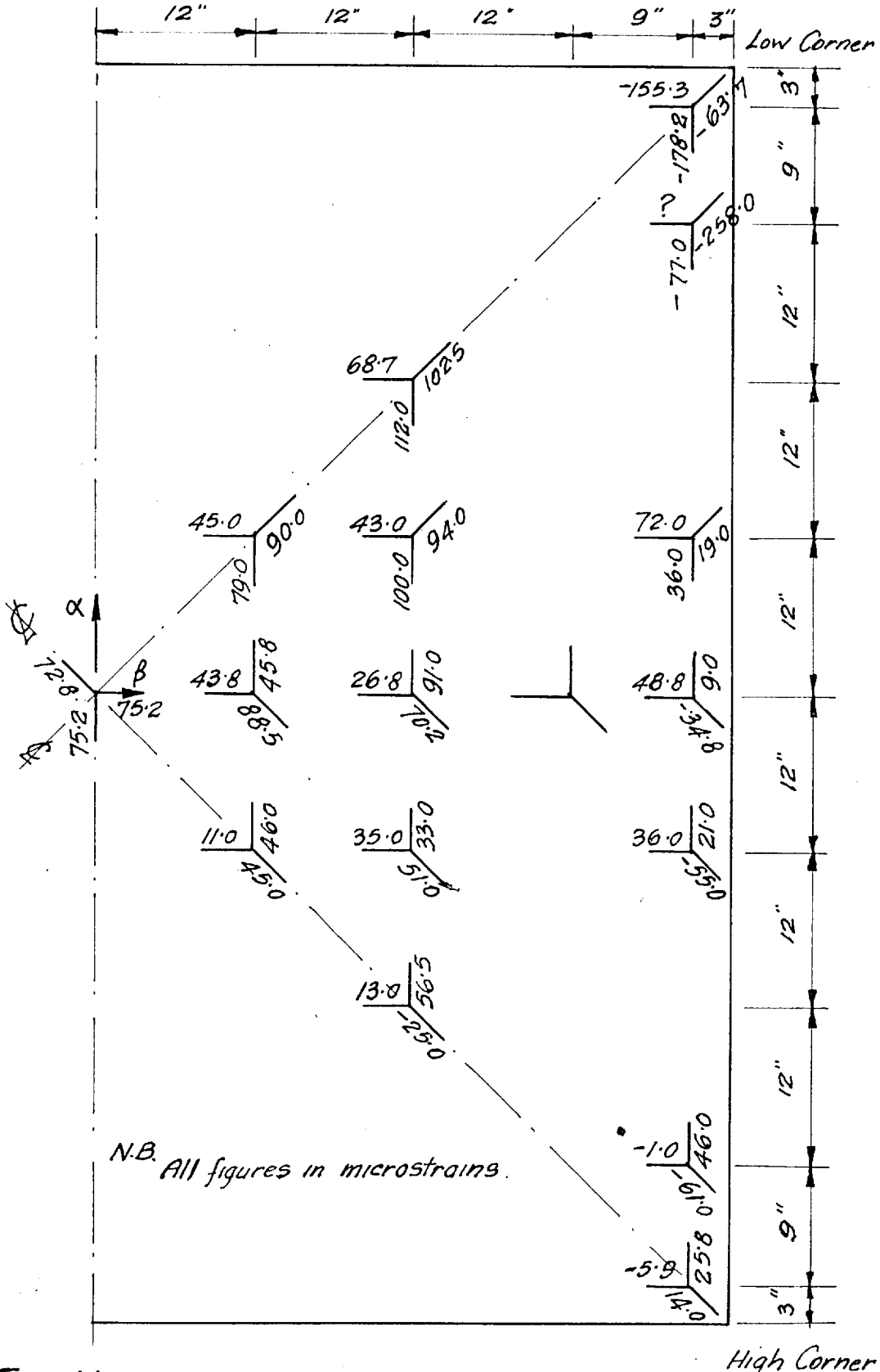
TEST NO. 8.

FIG. 6.37.



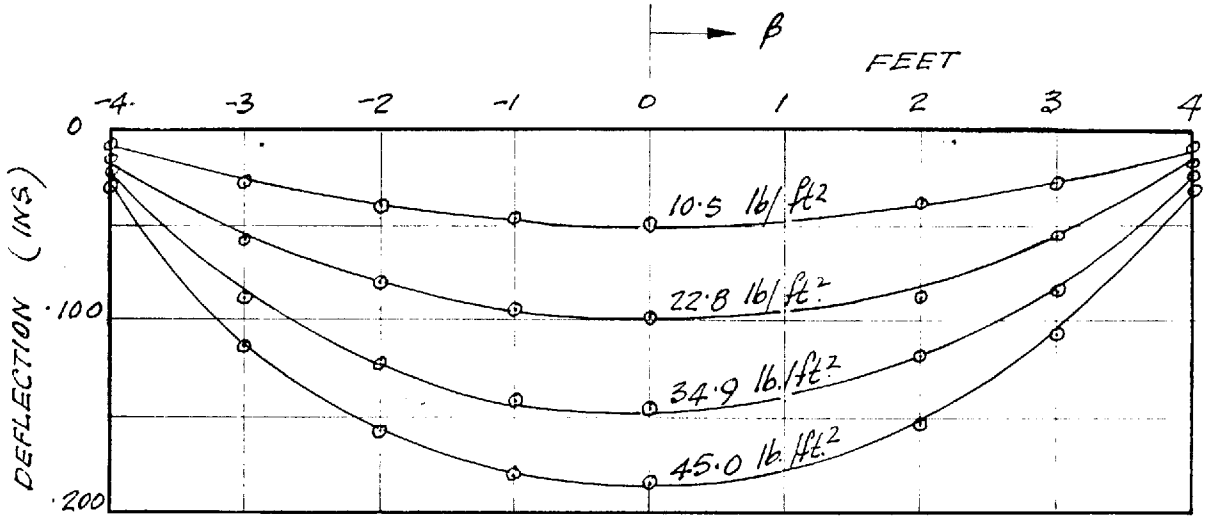
TEST NO.8. AV. OF STRAINS IN BOTTOM AND TOP SURFACES.

FIG. NO. 6.38.

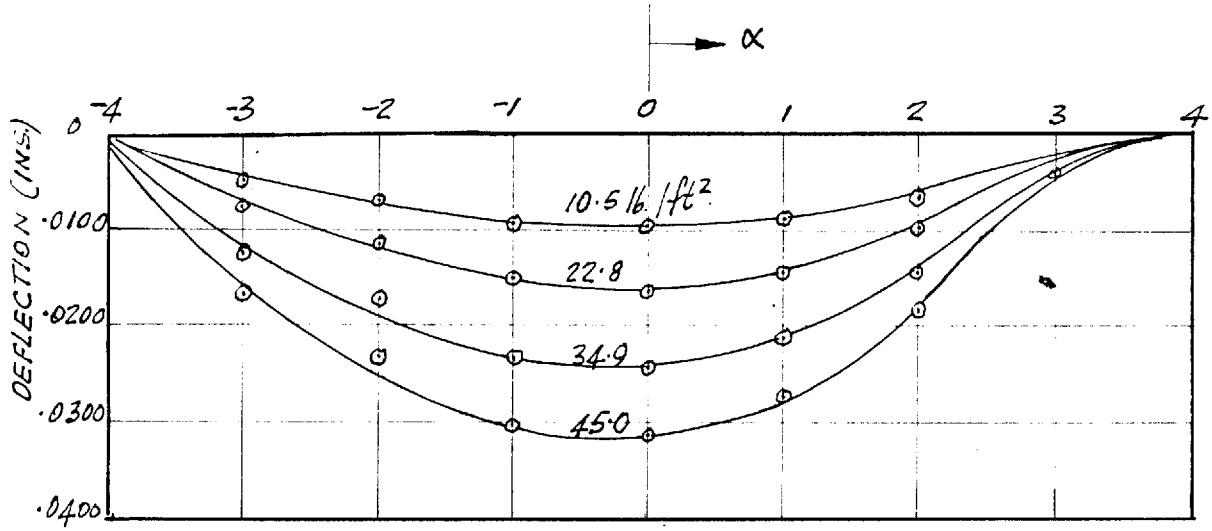


TEST NO. 8. DIFF. BETWEEN STRAINS IN BOTTOM AND TOP SURFACES.

FIG. NO. 6. 39.



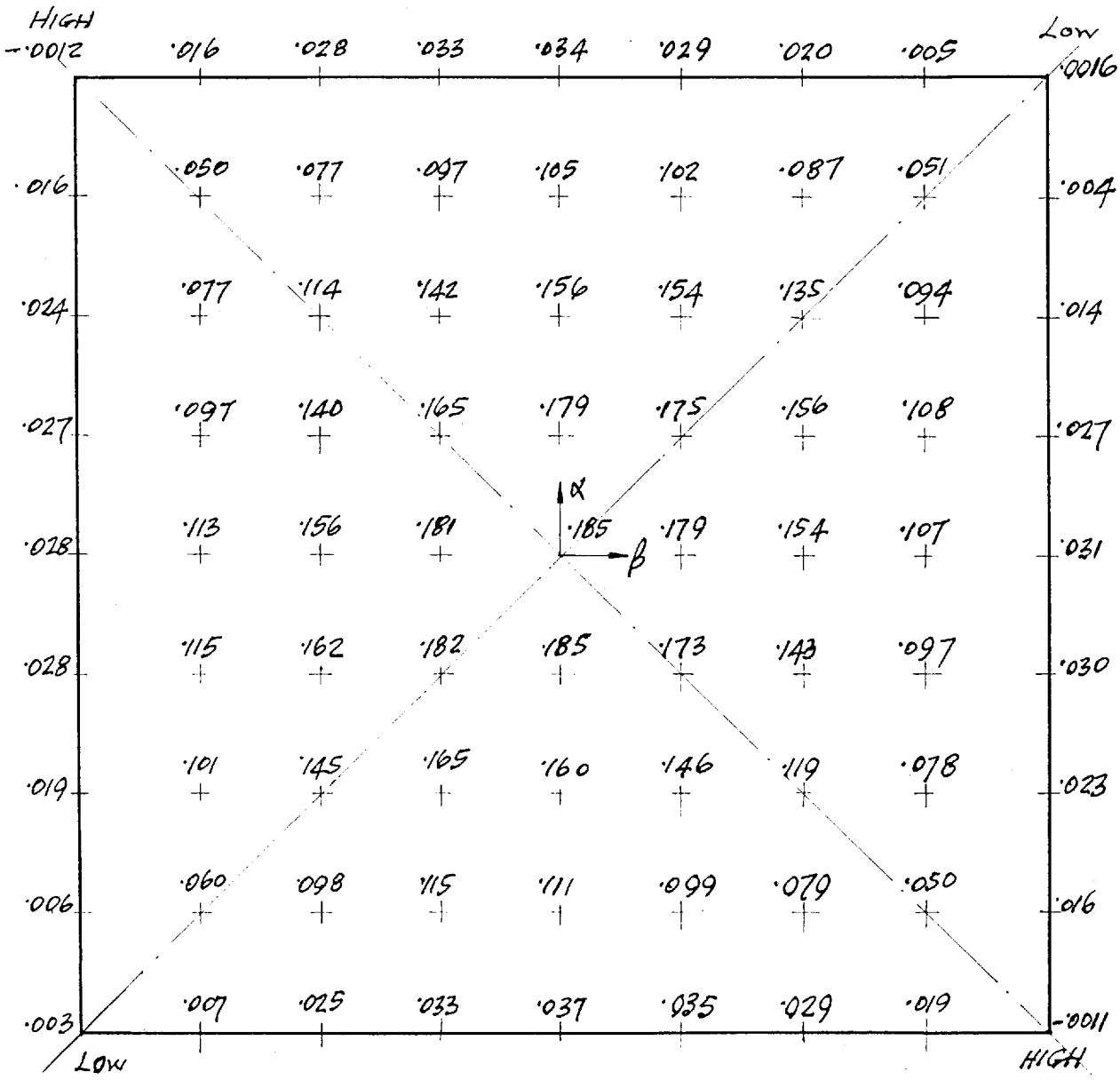
PROFILES ALONG $\alpha = 0$



PROFILES ALONG EDGE BEAM NO. 2 ($\beta = 4'\text{-}0''$)

TEST NO. 9.

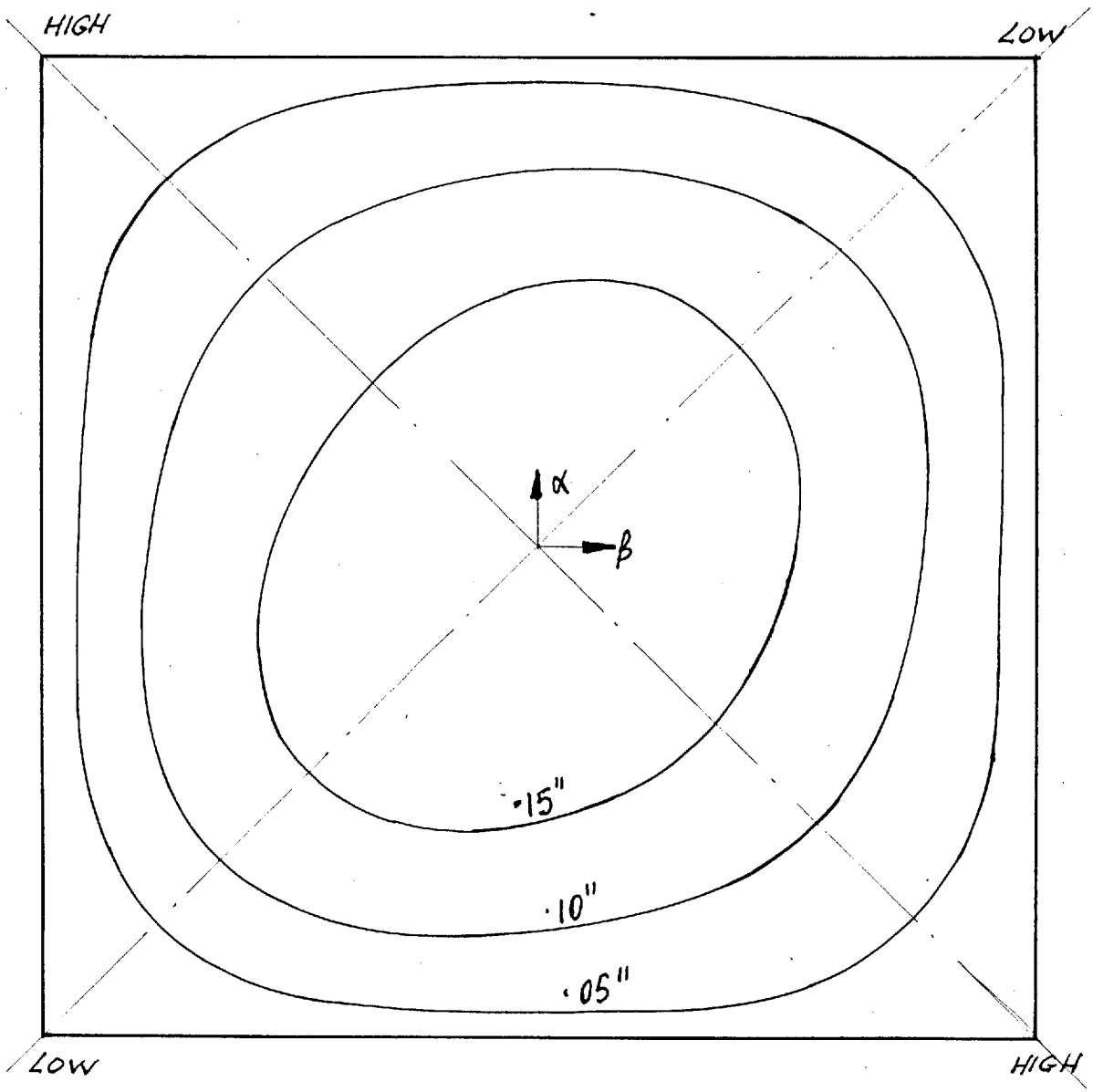
FIG. 6.40.



VERTICAL DEFLECTIONS(INS.) FOR U.D.L OF 45 LB/FT.^{2}

TEST NO. 9.

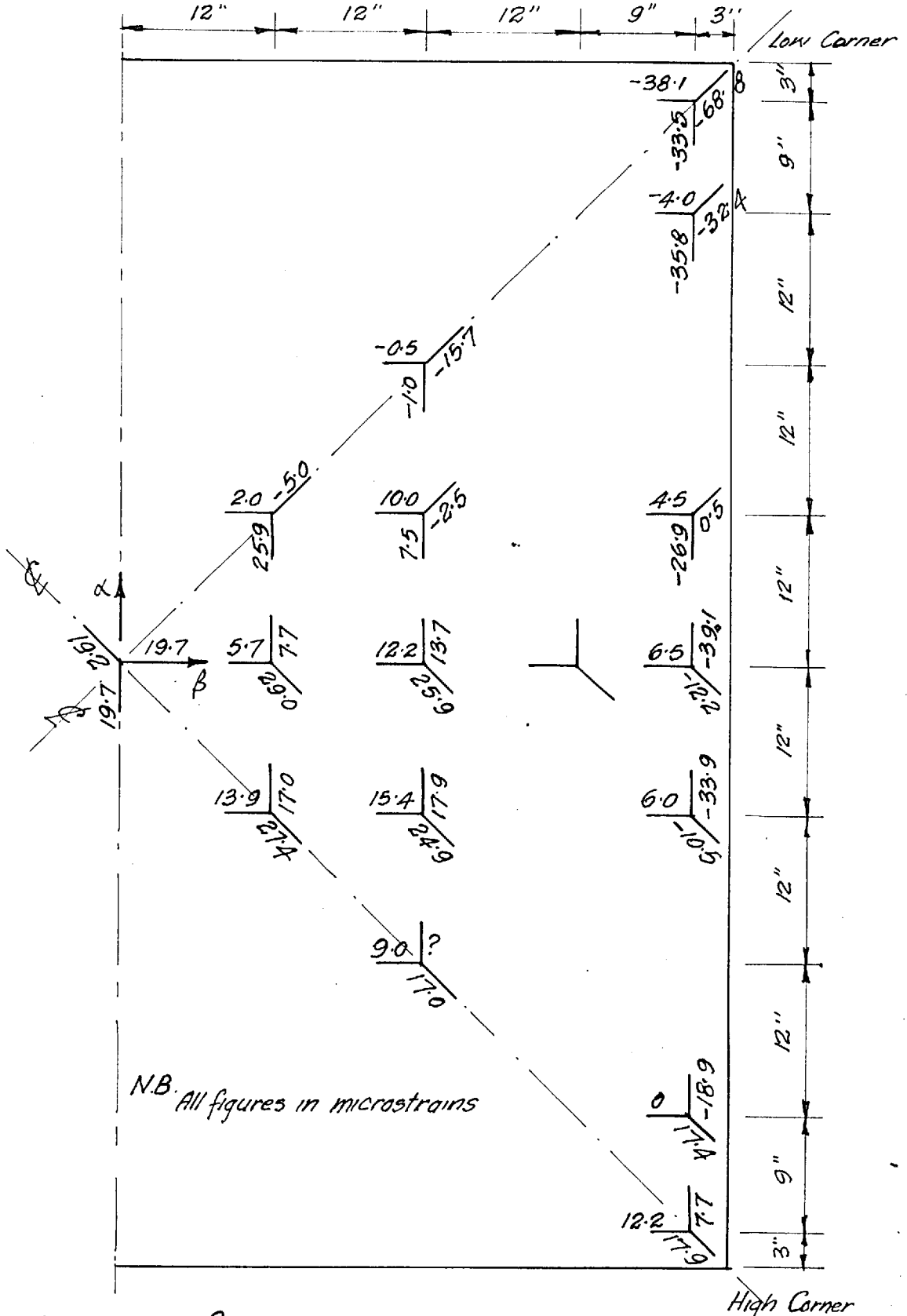
FIG. 6.41.



VERTICAL DEFLECTION CONTOURS

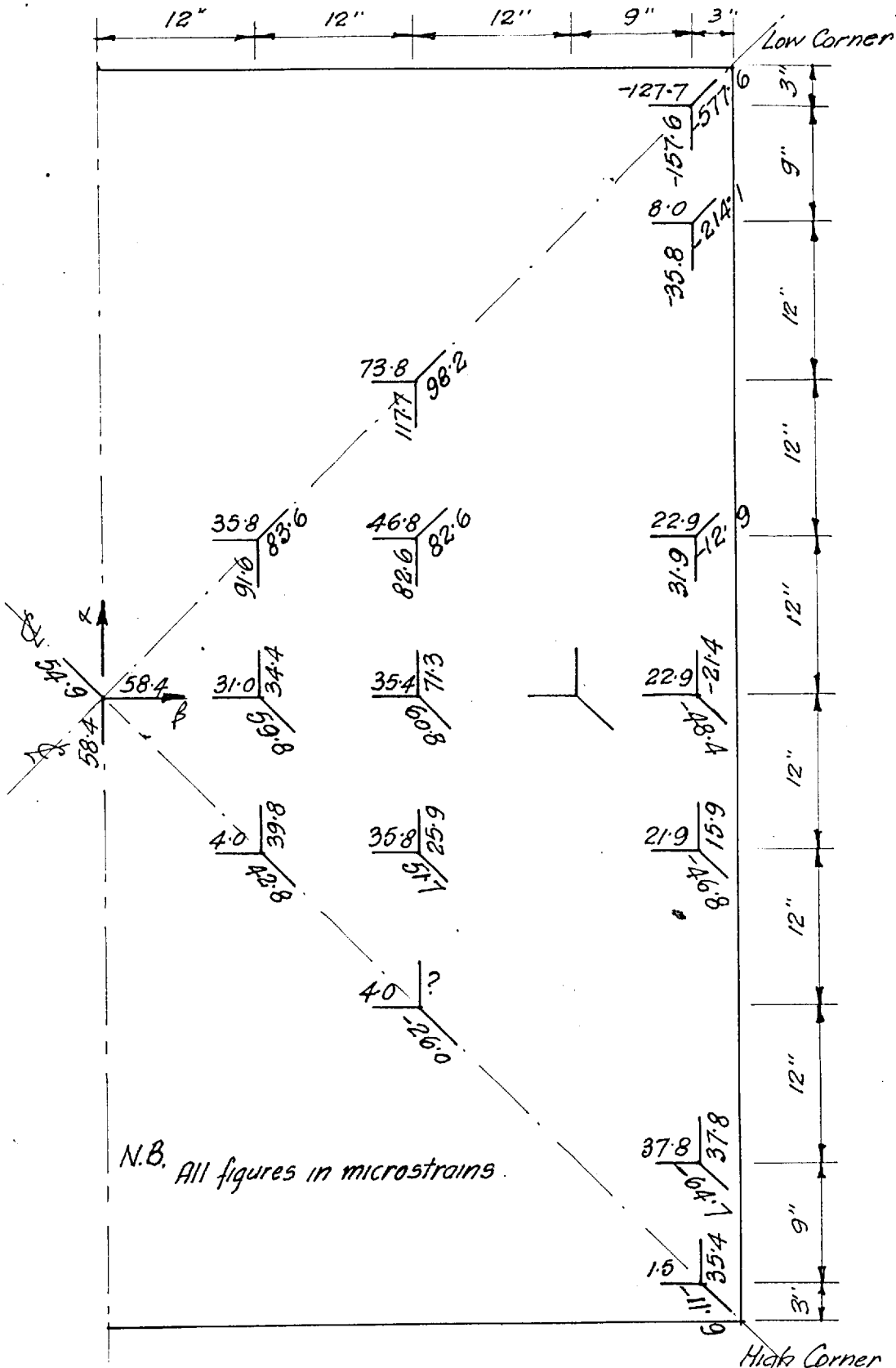
TEST NO. 9.

FIG. 6.42.



TEST NO. 9. AV. OF STRAINS IN BOTTOM AND TOP SURFACES

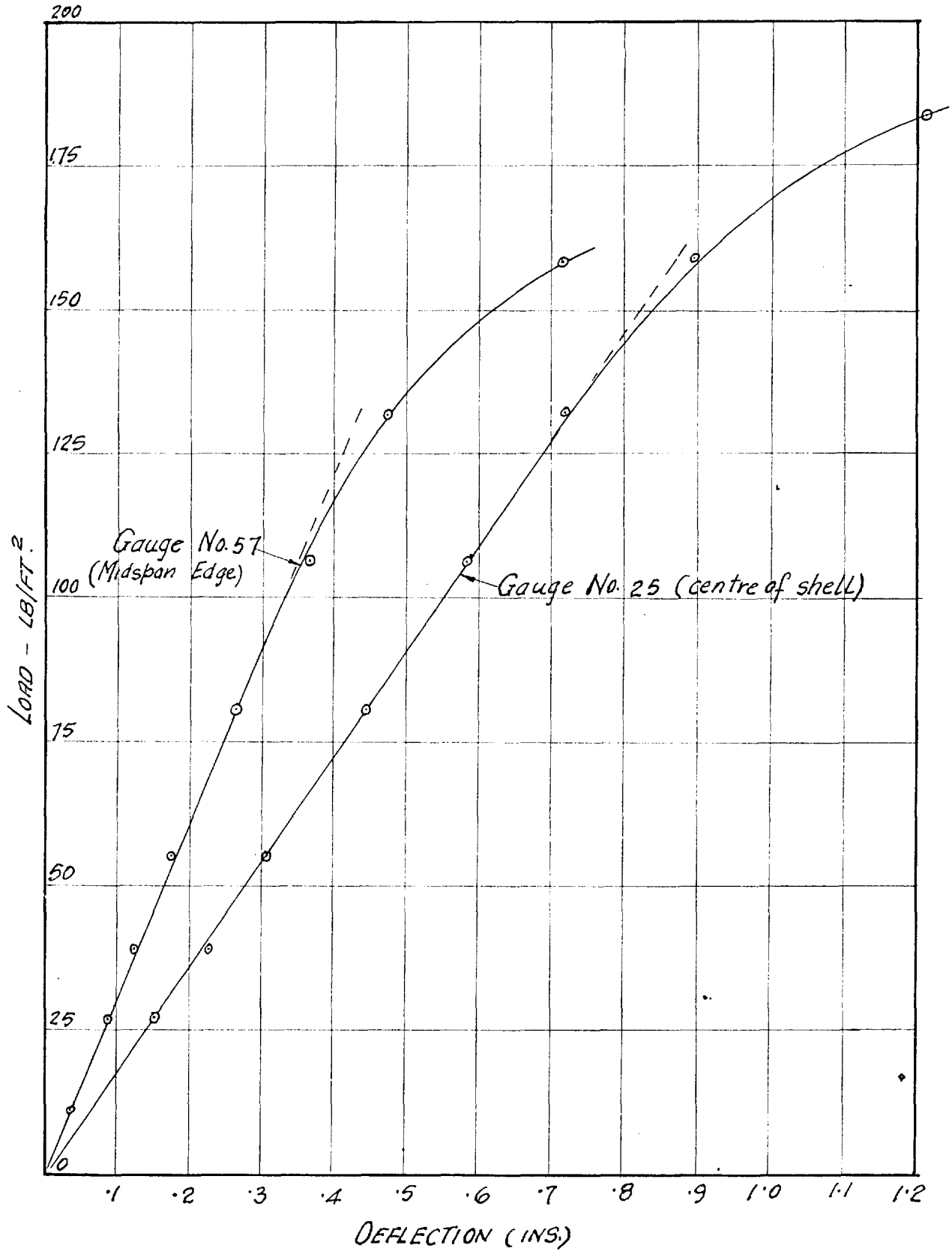
FIG. NO. 6.43.



N.B. All figures in microstrains.

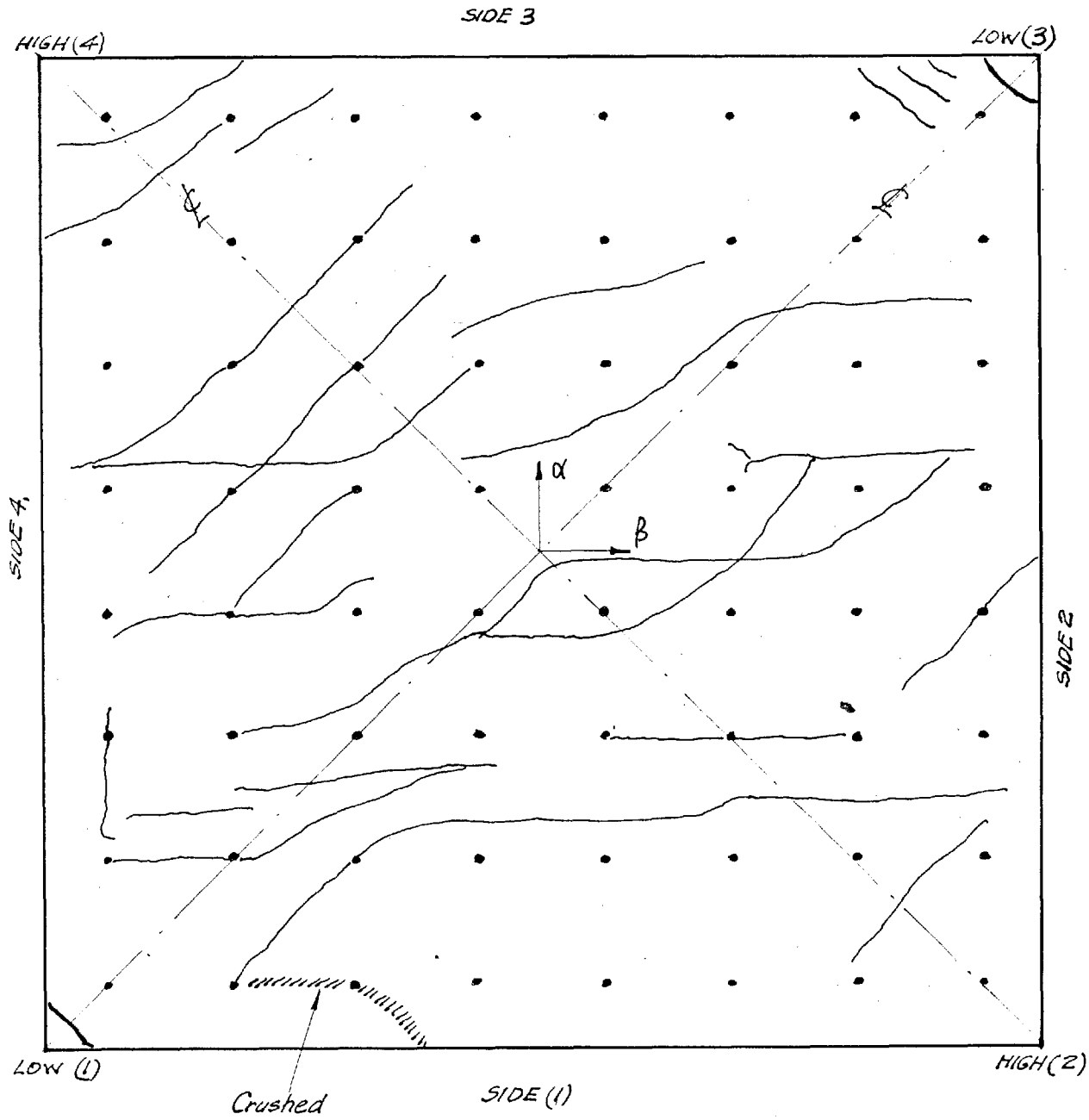
TEST NO. 9. DIFF. BETWEEN STRAINS IN BOTTOM AND TOP SURFACES

FIG. NO. 6.44.



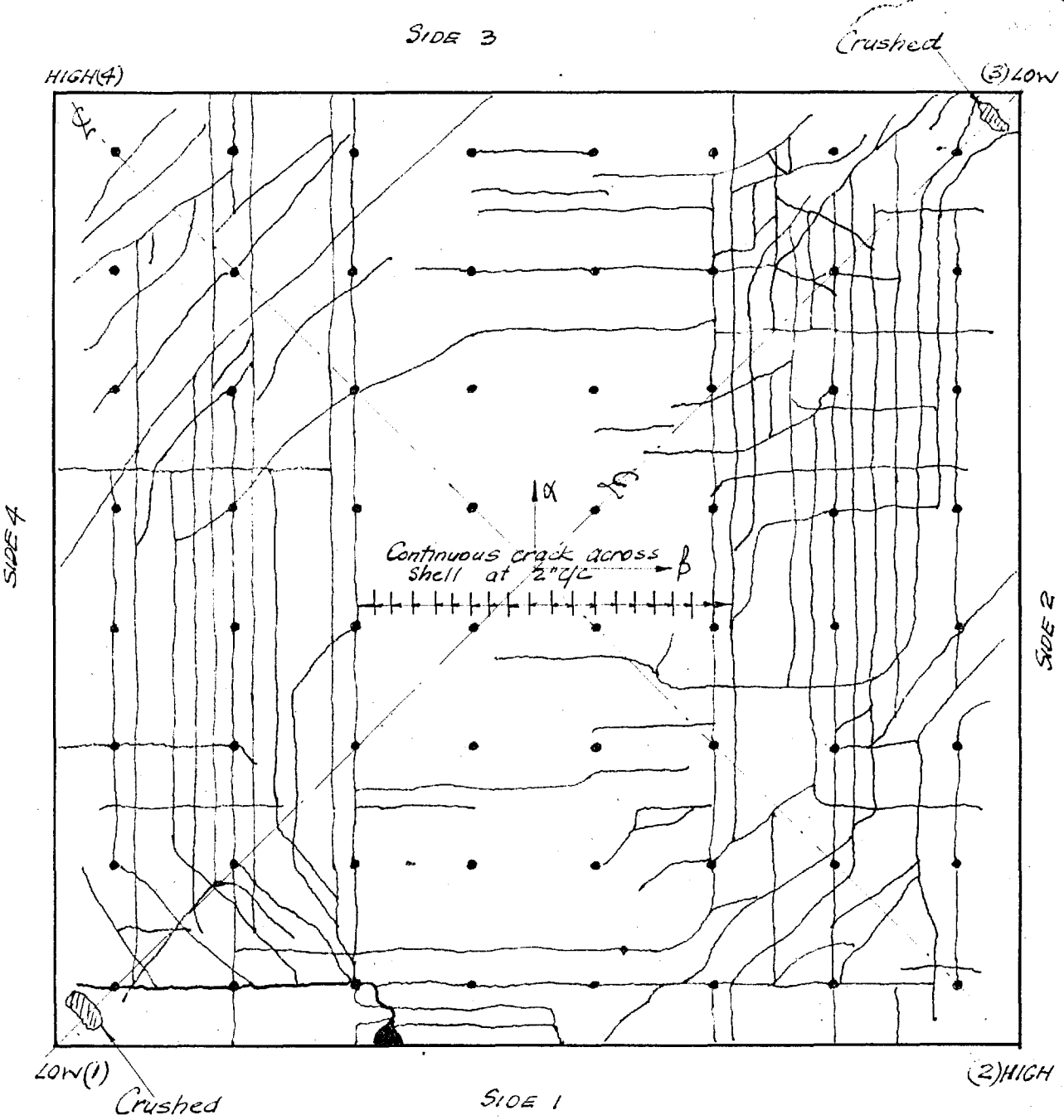
TEST NO. 10. TEST TO FAILURE.

FIG. 6.45.



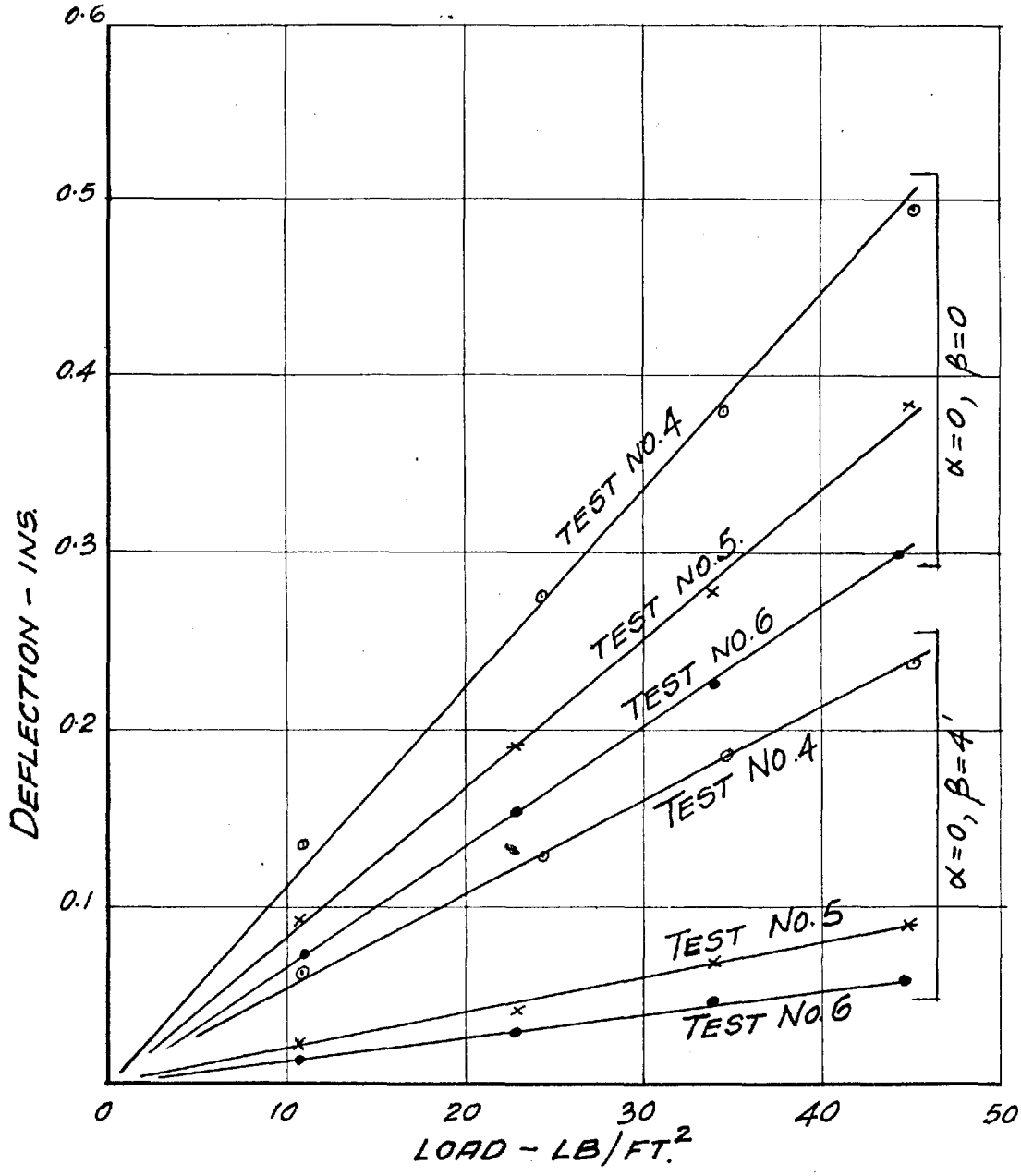
TEST NO. 10. CRACKS ON TOP SURFACE.

FIG. 6.46.



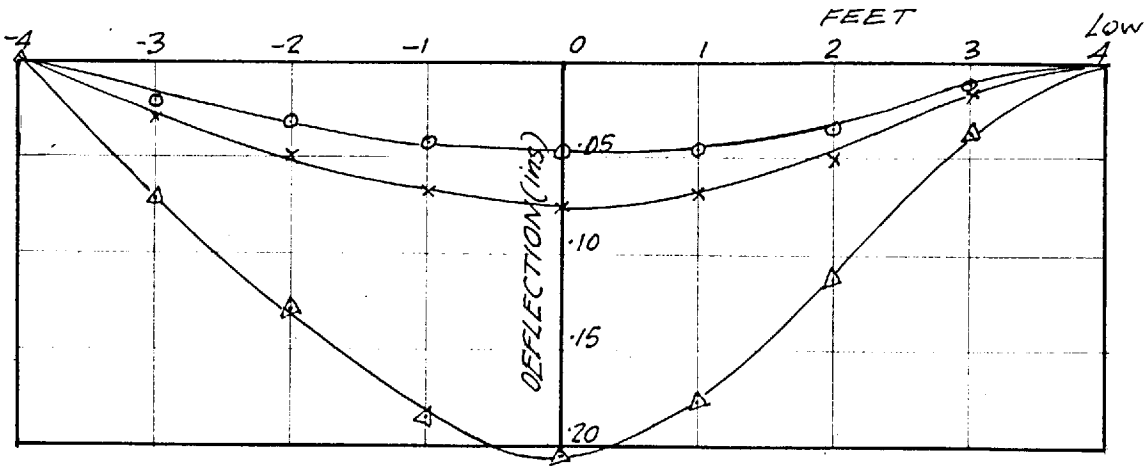
TEST NO.10. CRACKS ON BOTTOM SURFACE.

FIG. 6.47.

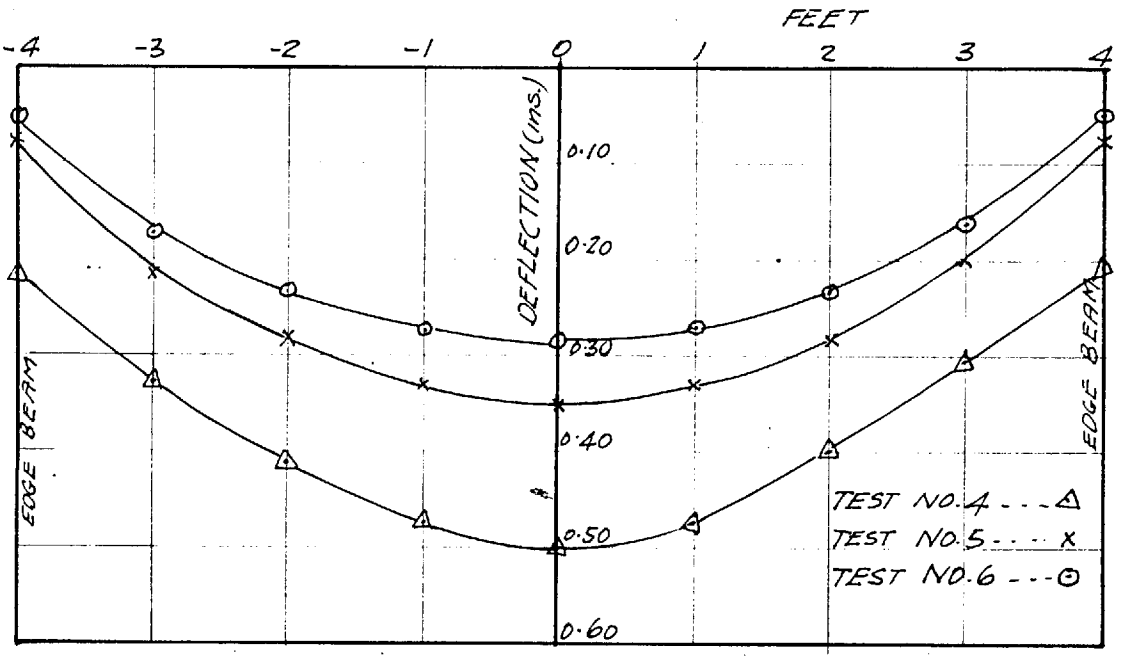


TESTS 4, 5 & 6. - TYPICAL LOAD vs. DEFLECTION CURVES

FIG. 6. 48.



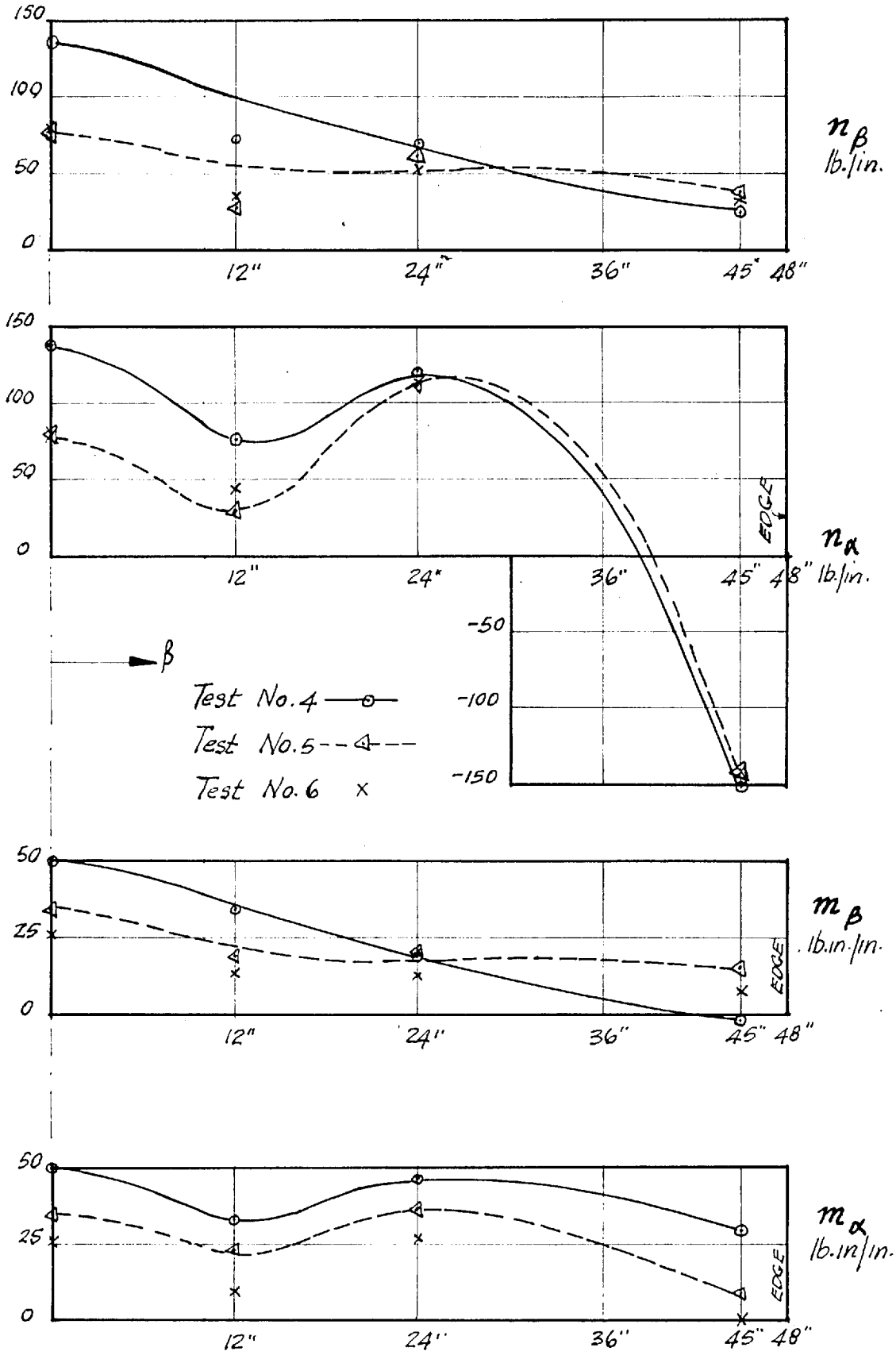
DEFLECTION AT EDGE, $\beta = 4'-0"$



DEFLECTION ALONG $\alpha = 0$

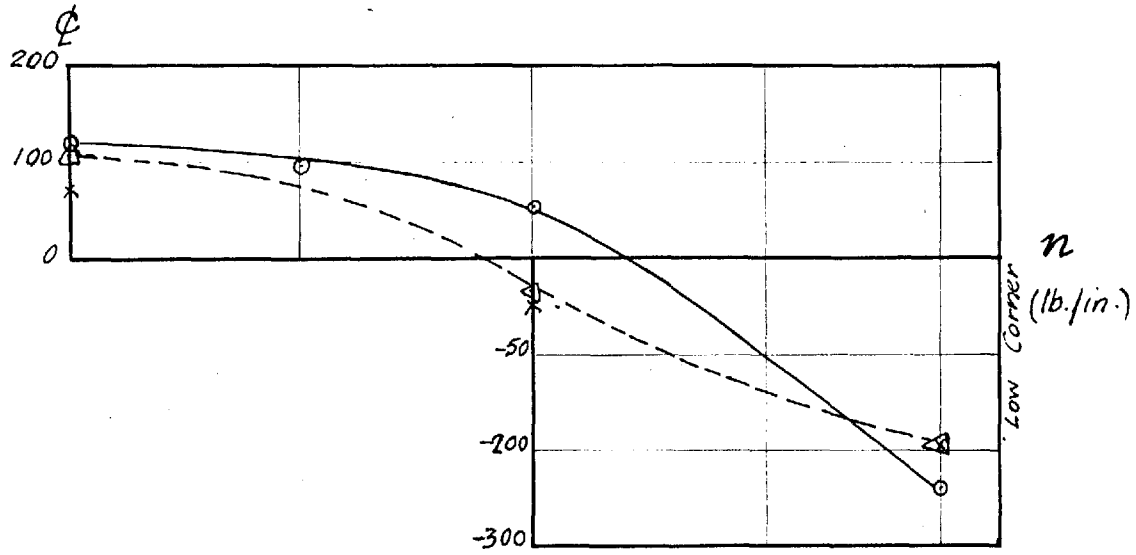
TESTS NOS. 4, 5, 6.

FIG. 6. 49.

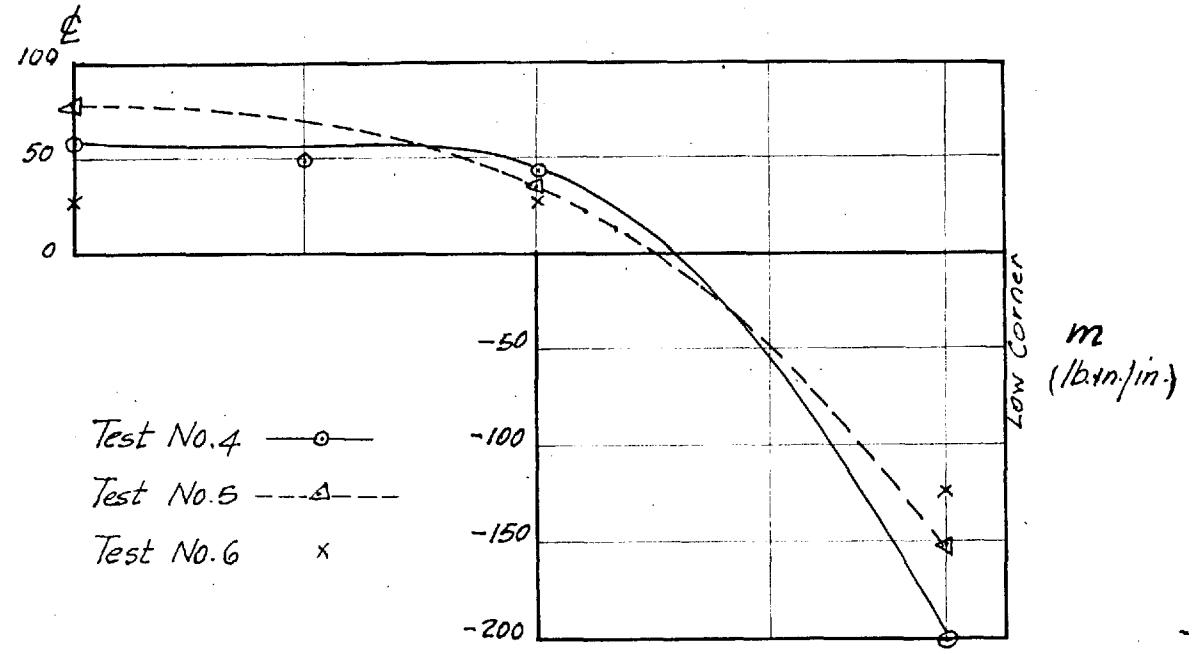


TESTS NOS. 4,5,6. ACTIONS ALONG $\alpha = 0$

FIG. 6.50.



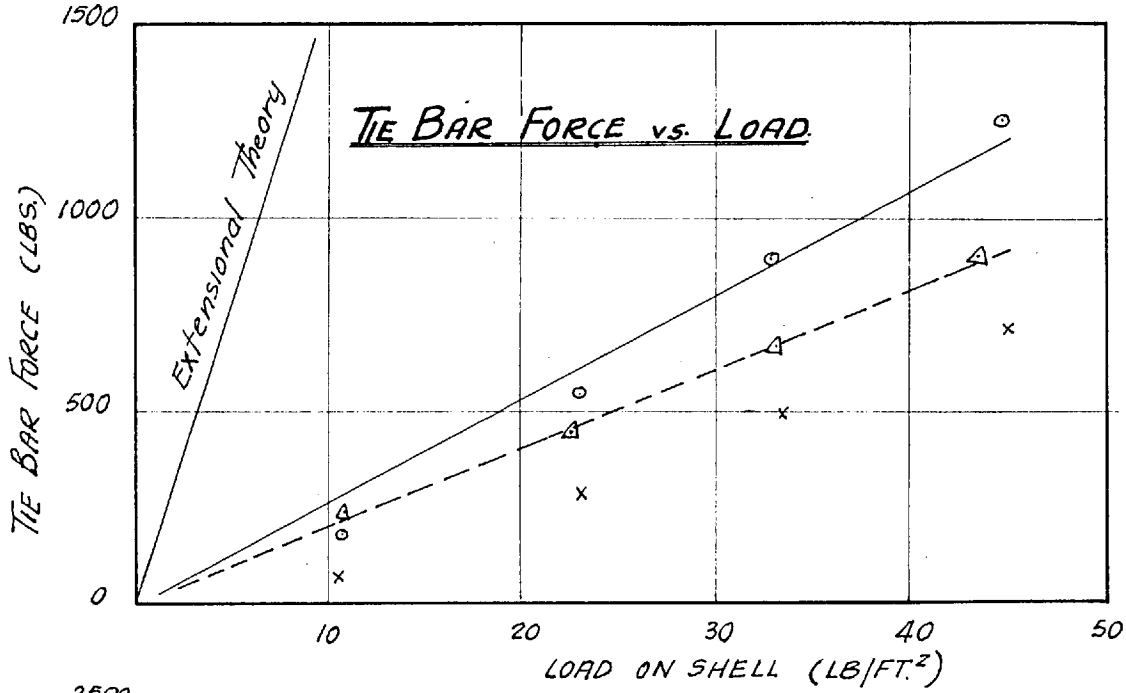
FORCE ALONG ARCH ℄

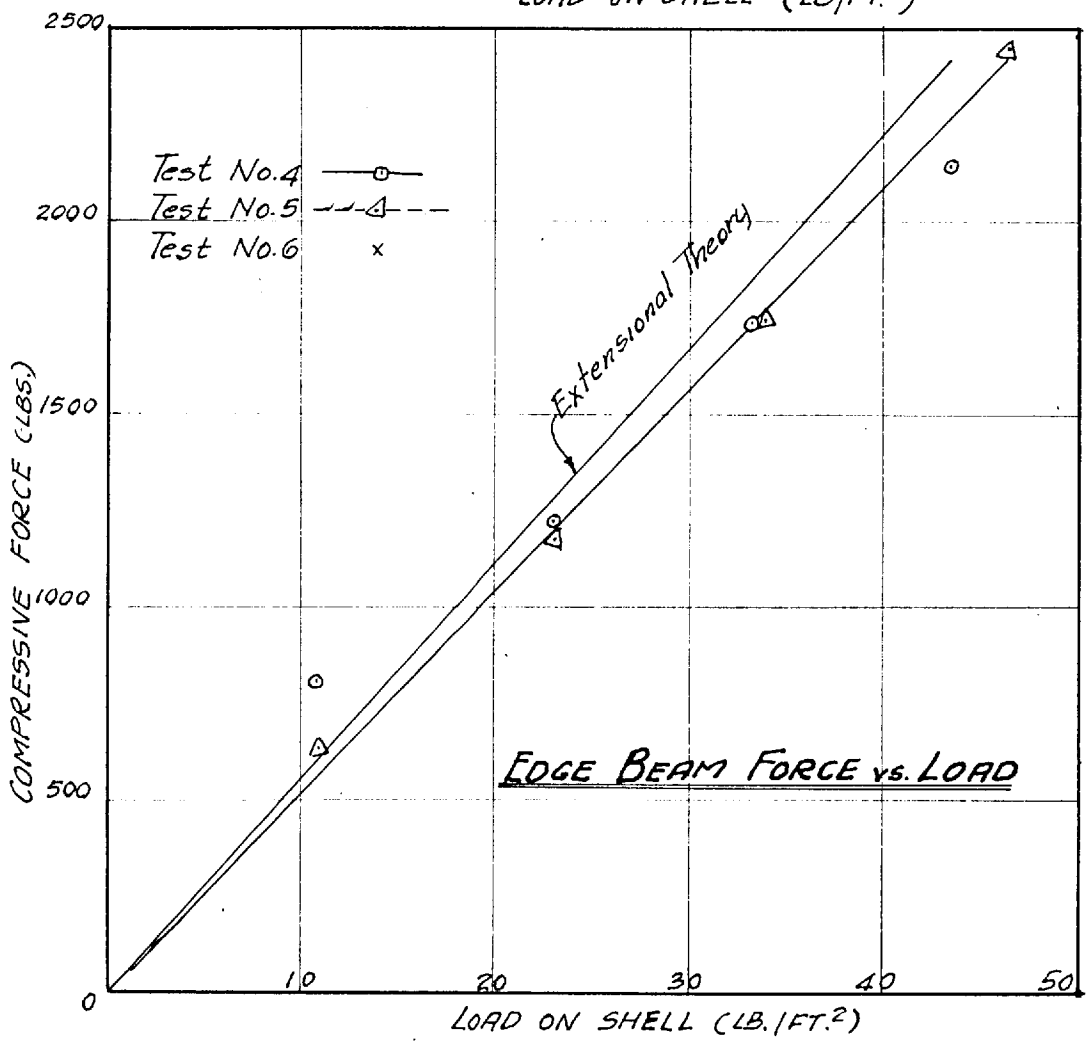


MOMENT ALONG ARCH ℄

TESTS NOS. 4, 5, 6.

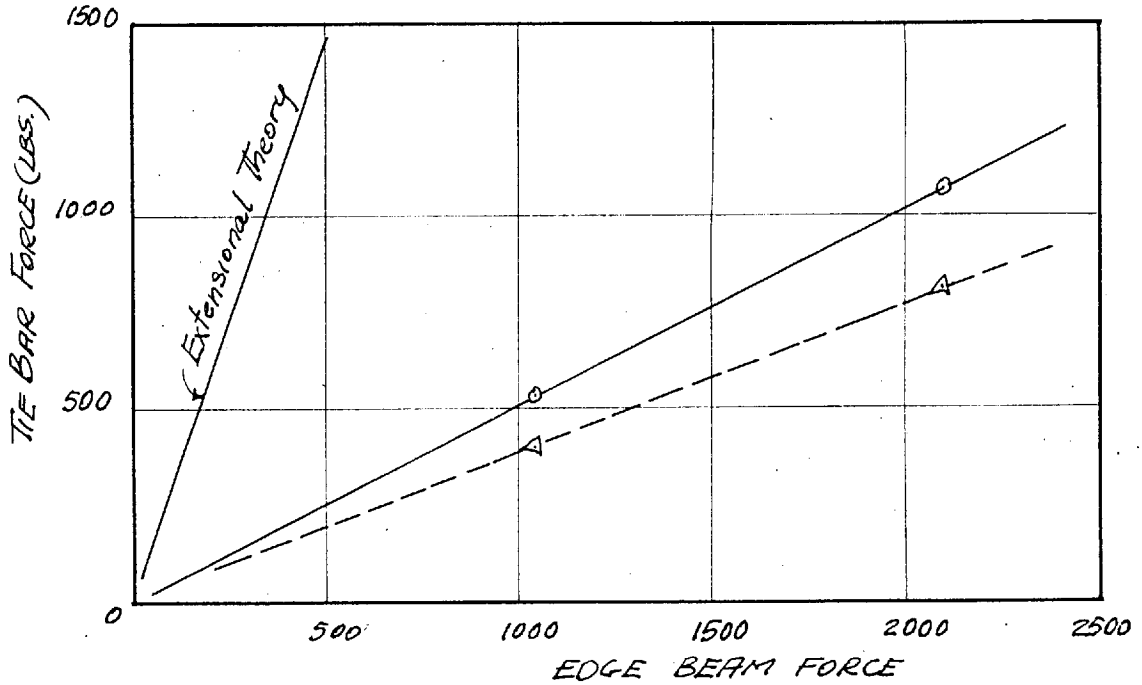
FIG. 6.51.



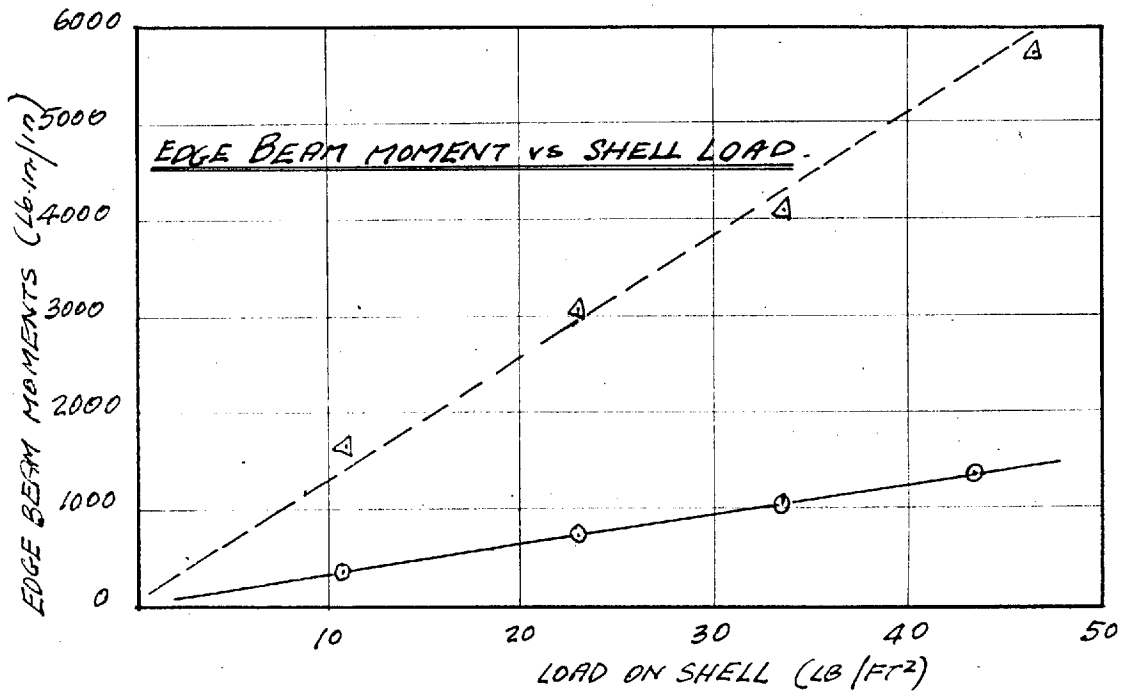


TESTS NOS. 4, 5, 6.

FIG. 6.52.

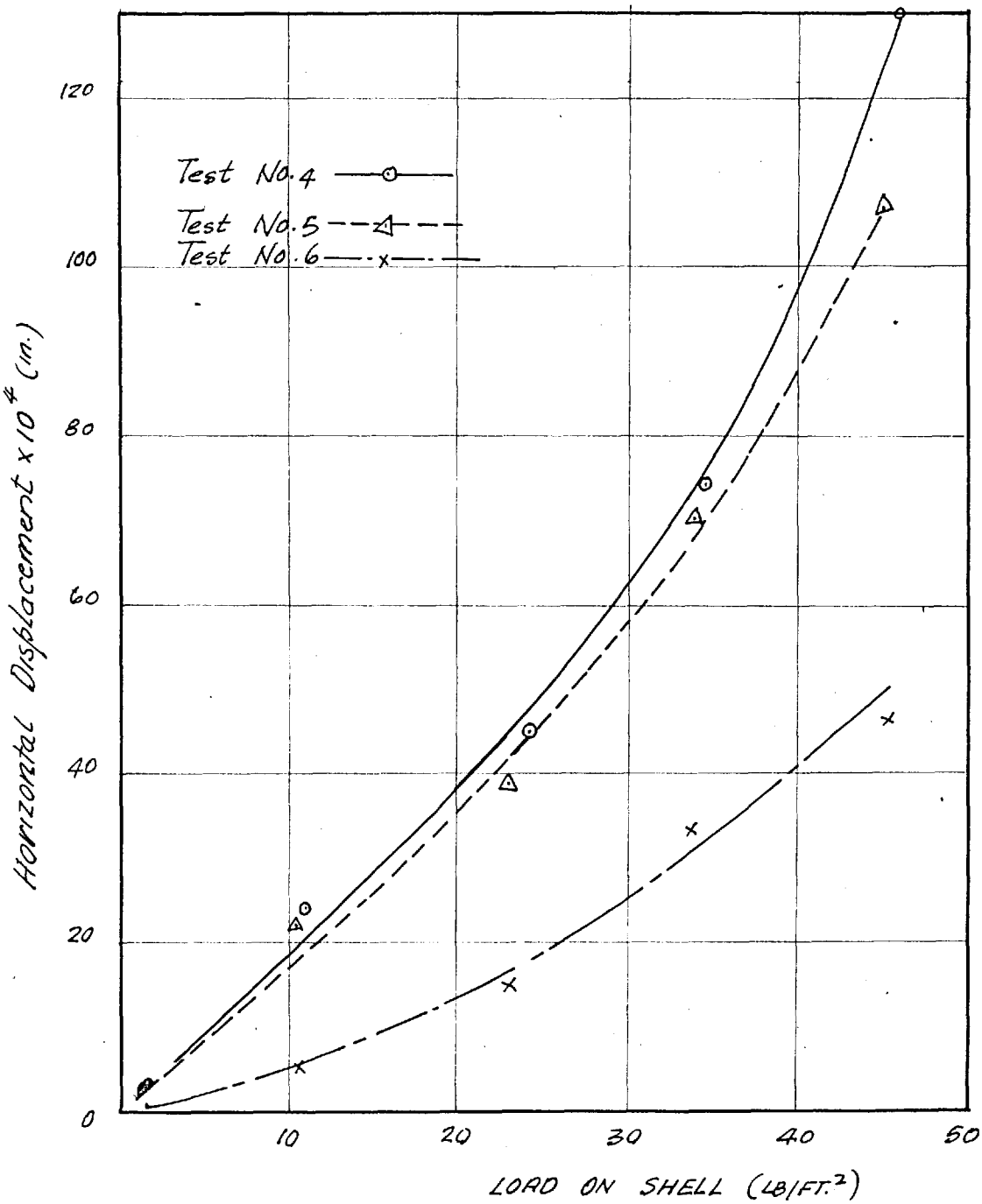


Test No 4 .. ⊙
Test No. 5 . ◁



TESTS NOS. 4 & 5.

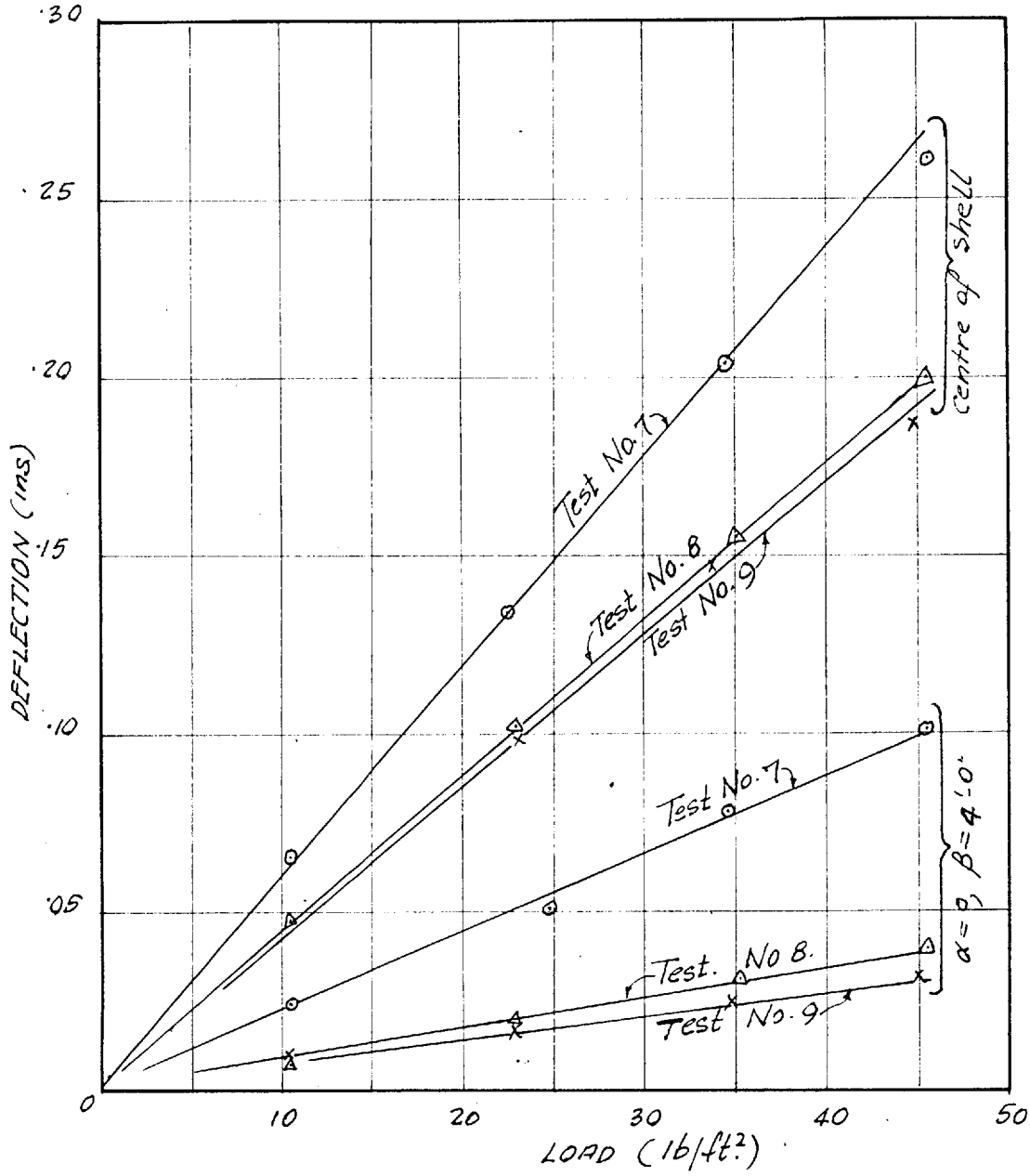
FIG. 6.53.



HORIZONTAL DISPLACEMENT AT MIDSPAN BEAM NO. 2

TESTS NOS. 4, 5, 6.

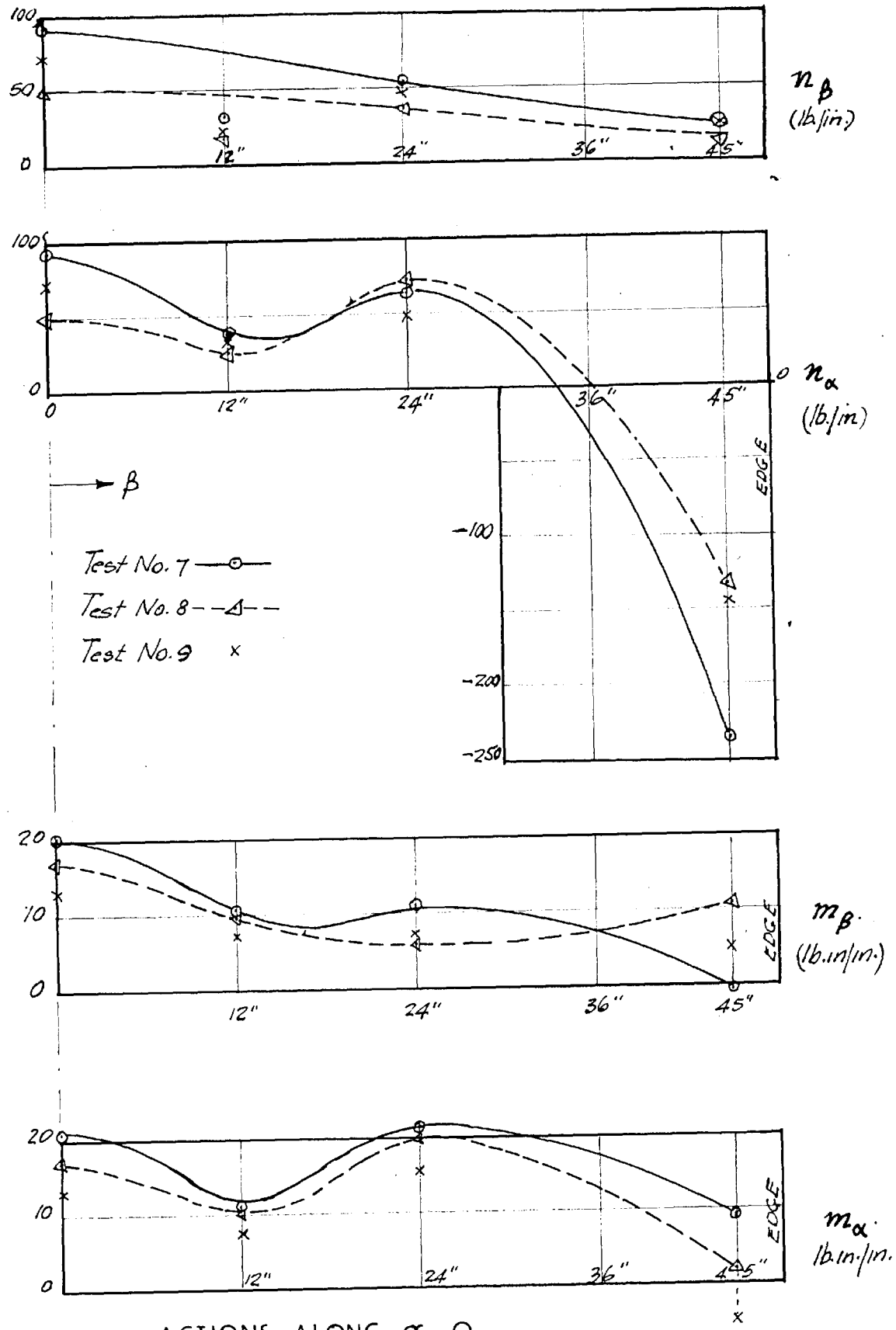
FIG. 6.54.



TYPICAL LOAD - DEFLECTION CURVES

TESTS NOS. 7, 8, 9.

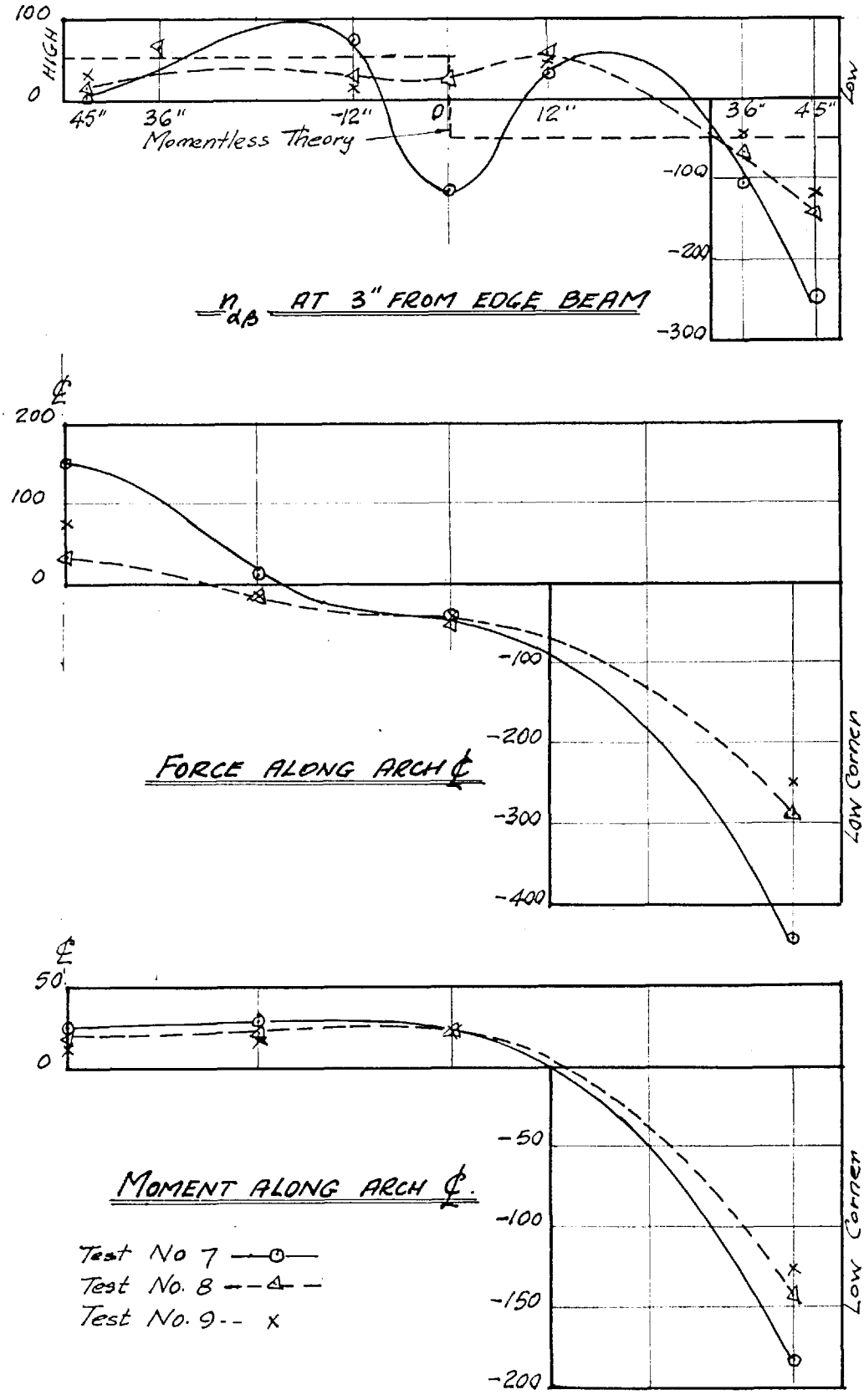
FIG. 6.55.



ACTIONS ALONG $\alpha = 0$

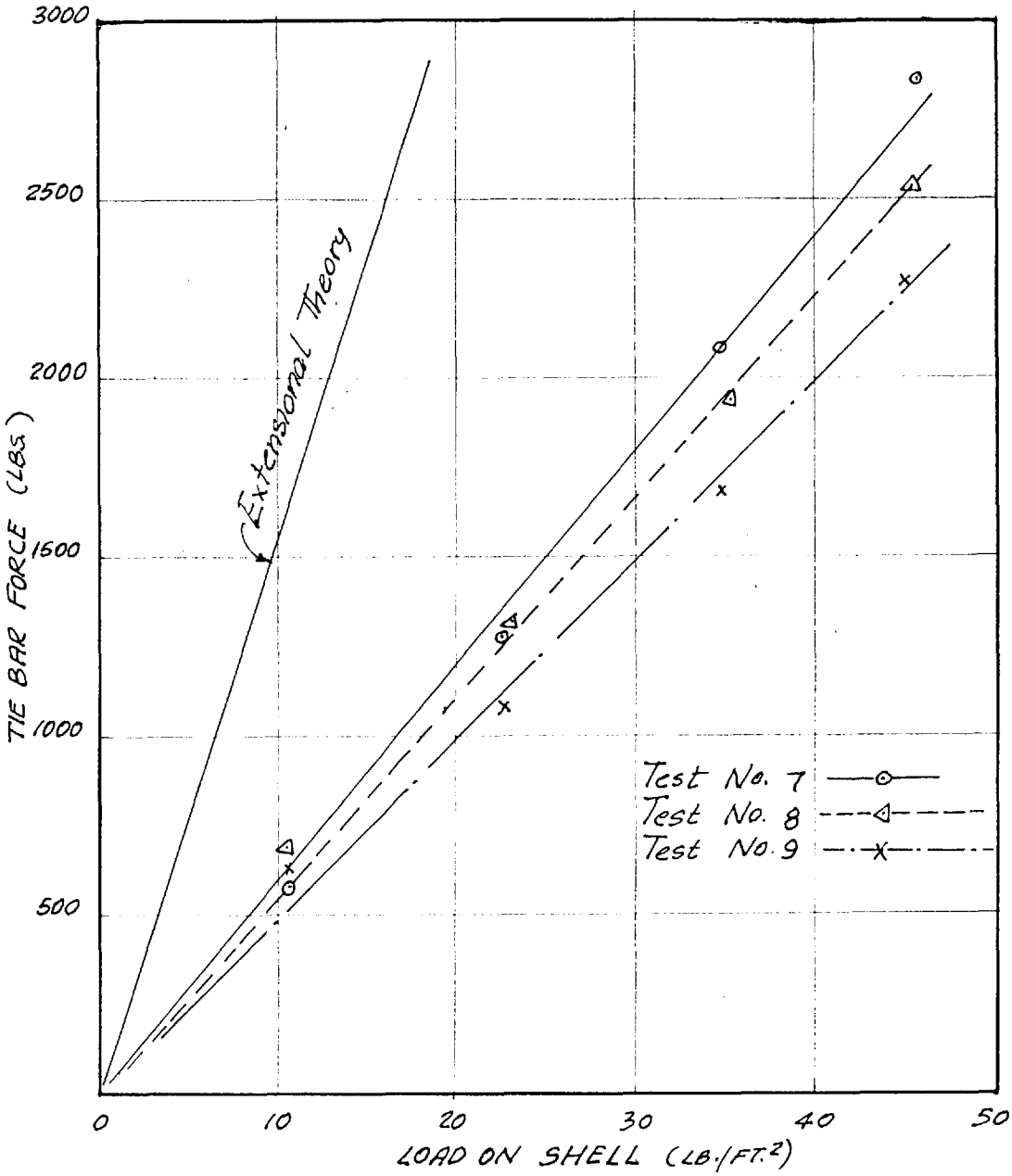
TESTS NOS. 7, 8, 9.

FIG. 6.56.



TESTS NOS. 7, 8, 9.

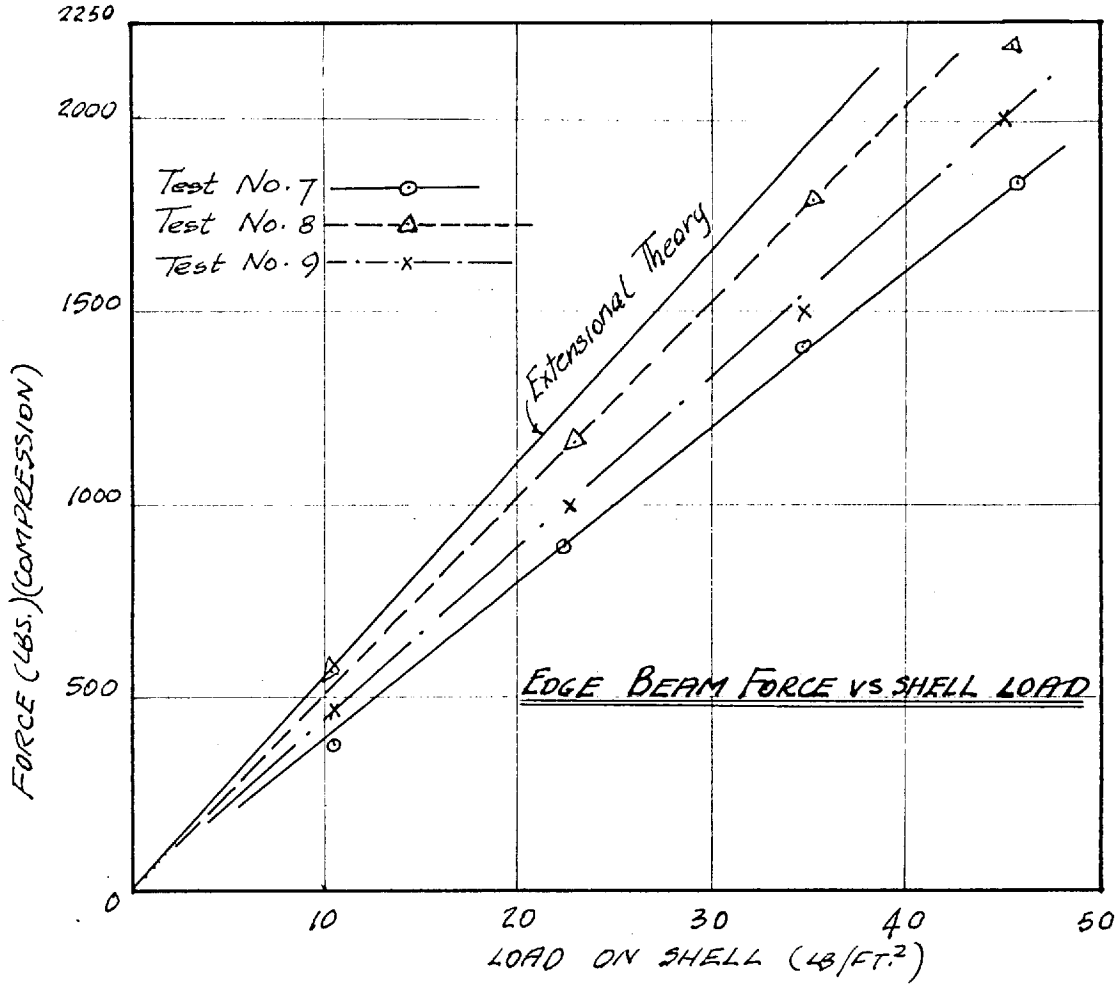
FIG. 6. 57.

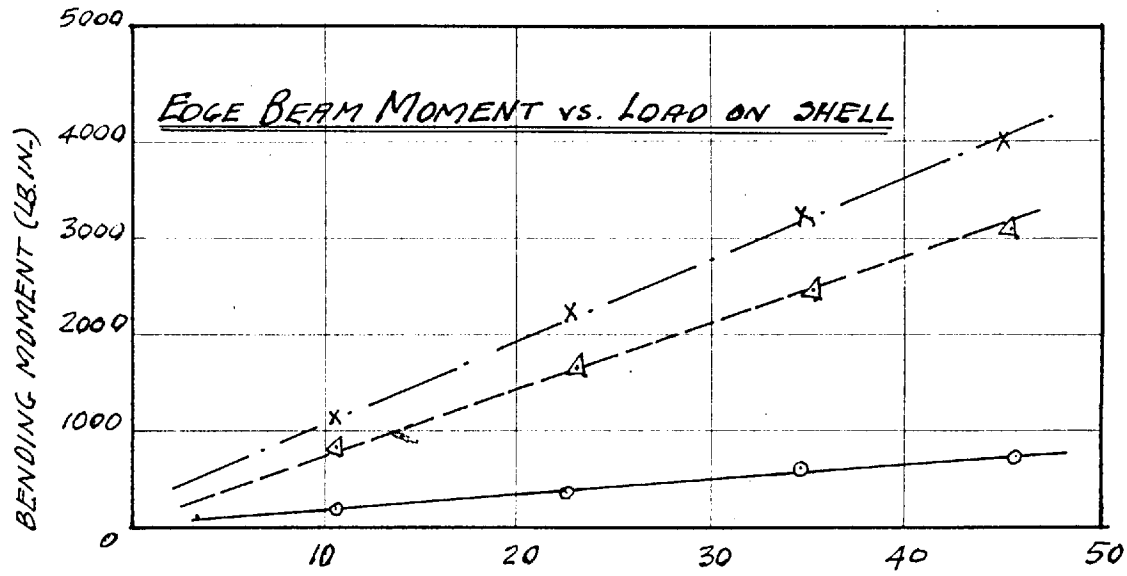


TIE BAR FORCE vs LOAD

TESTS NOS. 7, 8, 9.

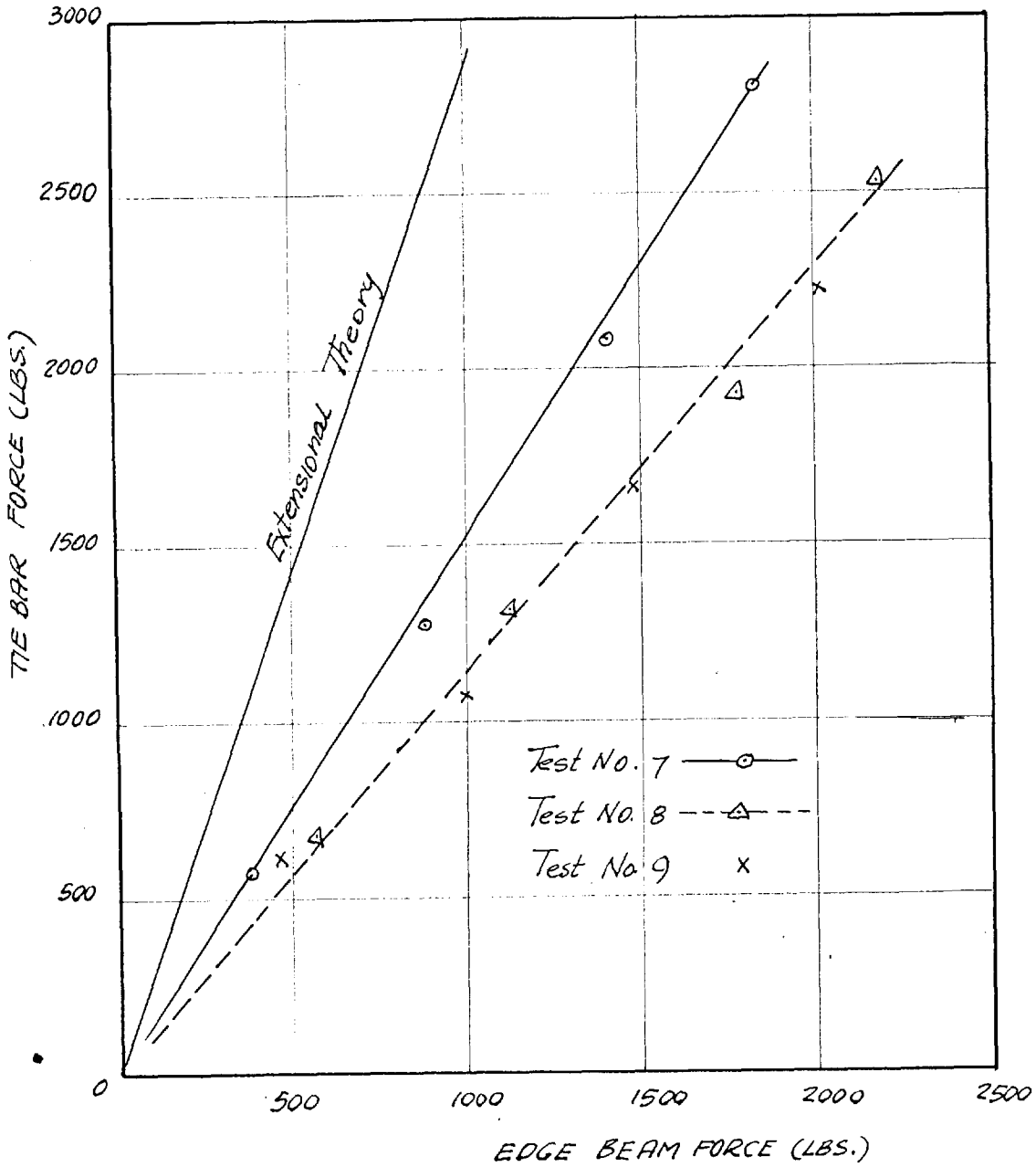
FIG. 6. 58.





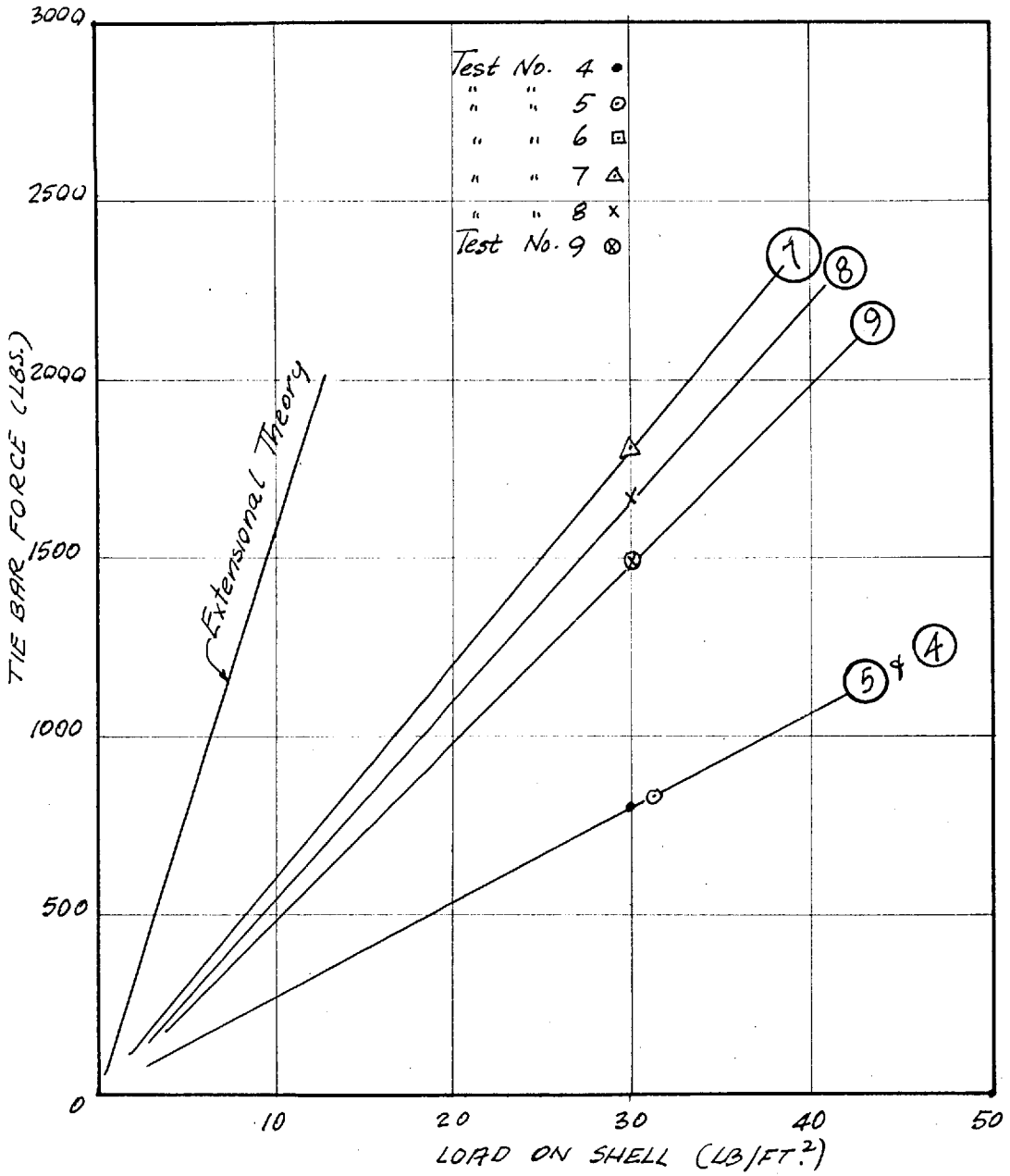
TESTS NOS. 7, 8, 9.

FIG. 6-59.



TESTS NOS. 7, 8, 9.

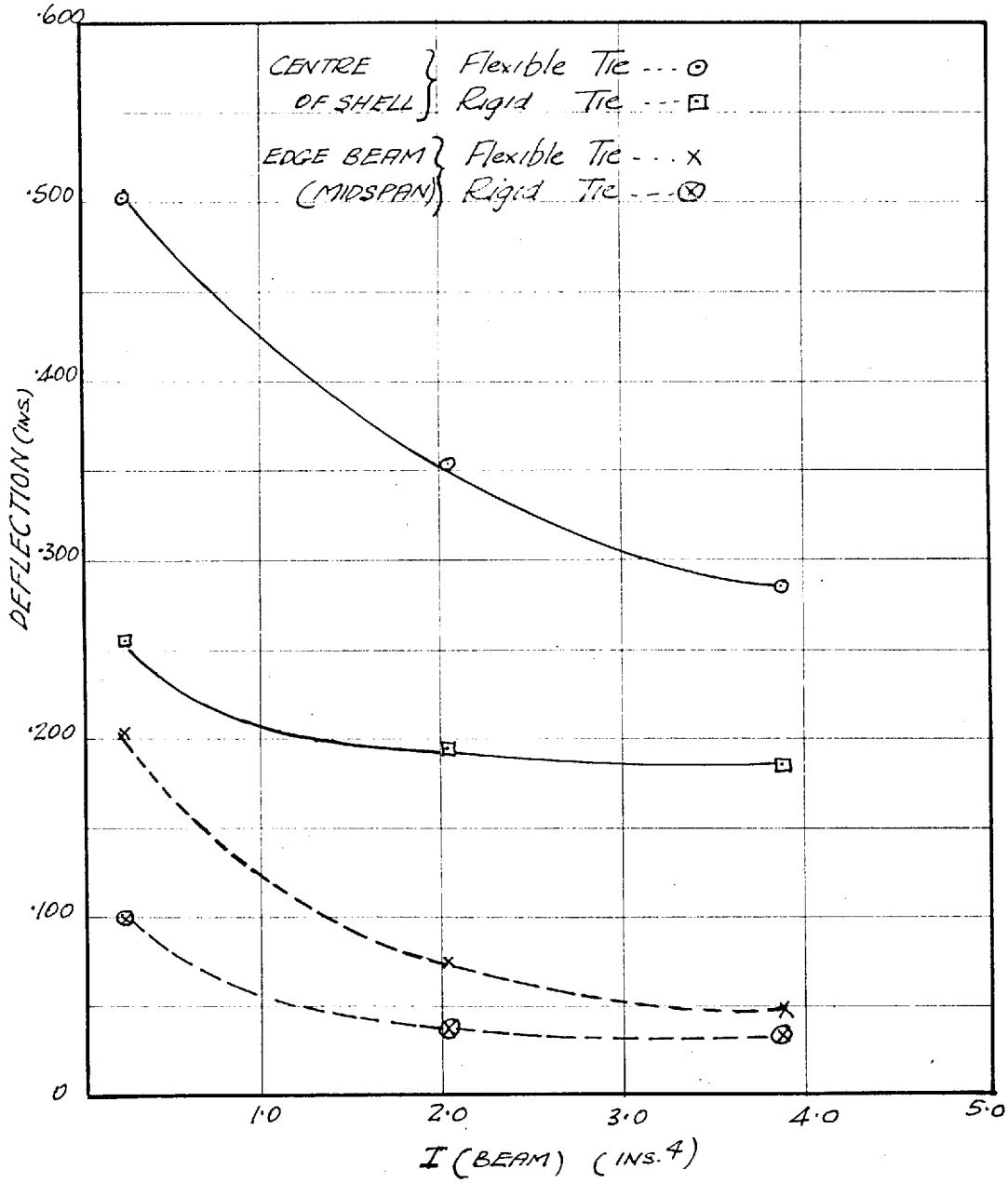
FIG. 6.60.



VARIATION OF TIE BAR FORCE

TESTS NOS. 4 - 9.

FIG. 6. 61.

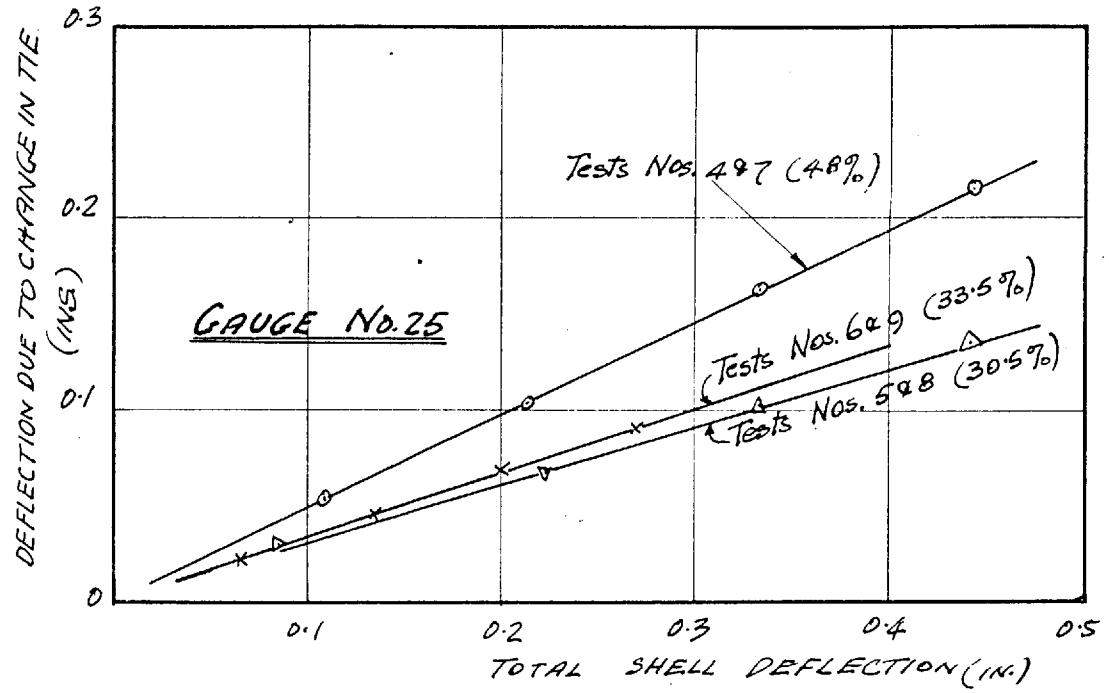


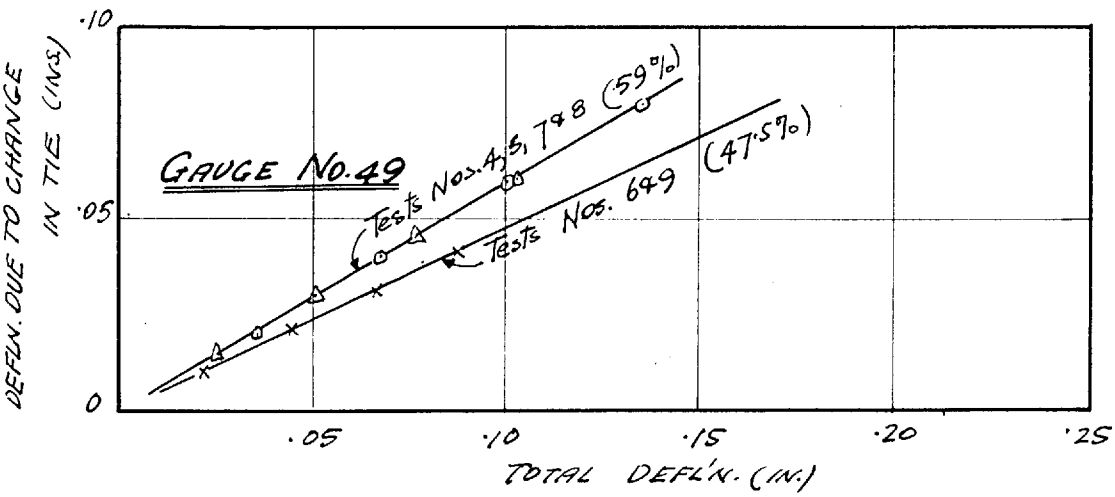
DEFLECTION VS. EDGE BEAM STIFFNESS.

TESTS NOS. 4 - 9.

FIG. 6.62.

EFFECT OF TIE BAR CHANGE ON DEFLECTION





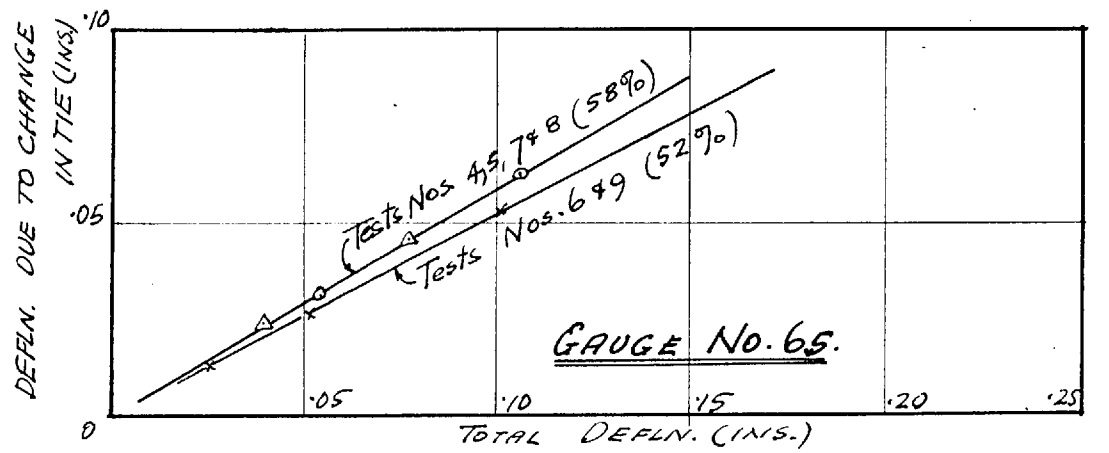
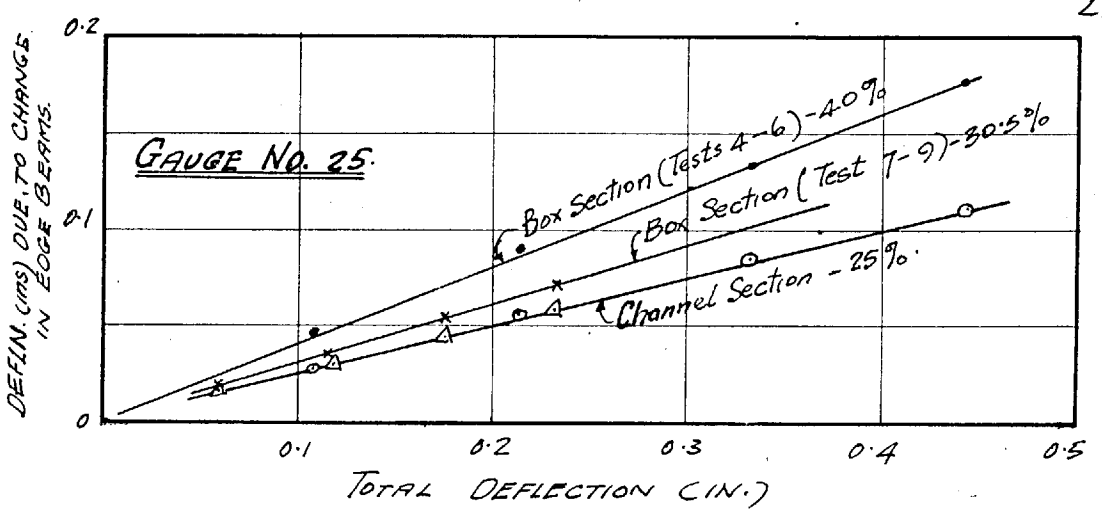
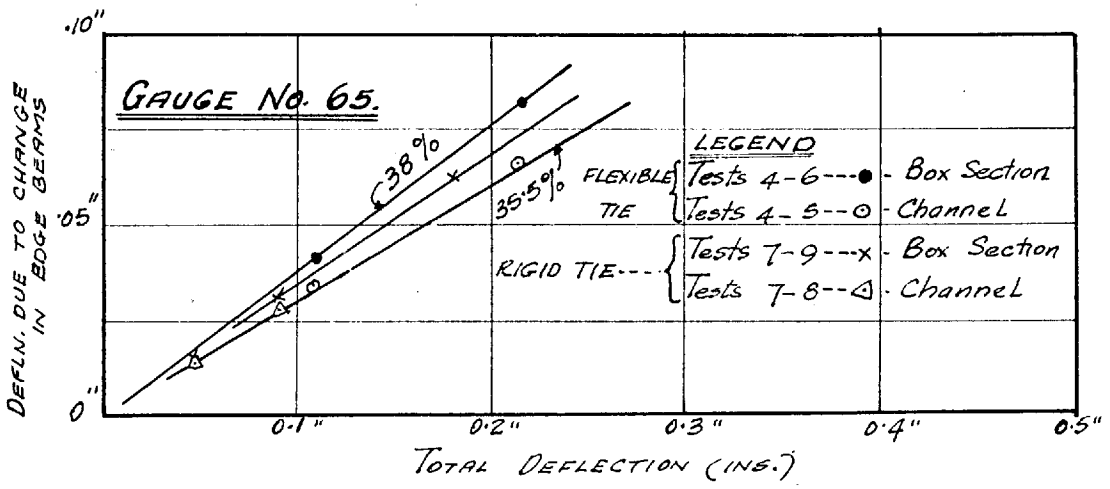
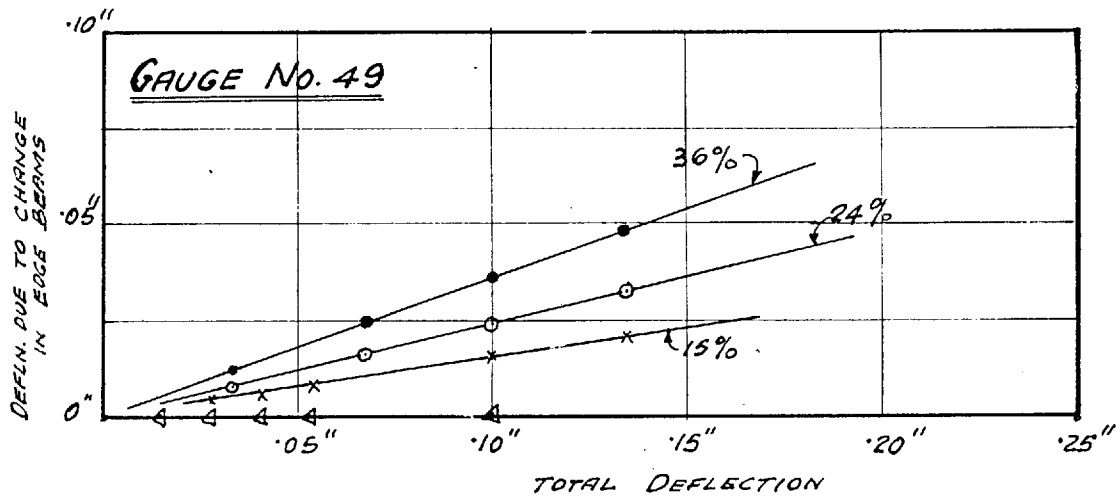


FIG. 6.63.

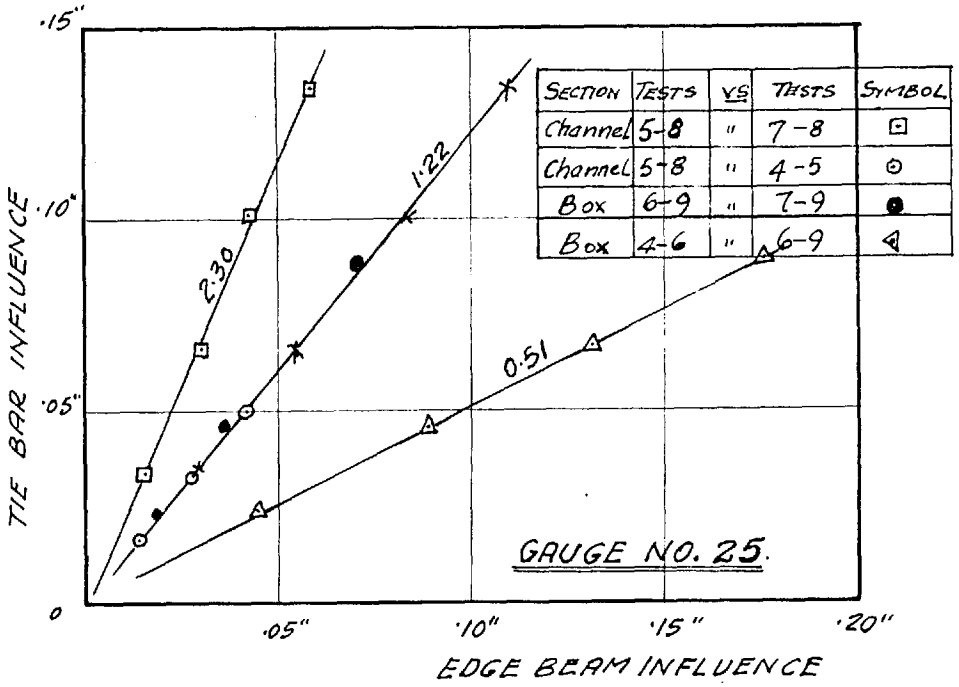


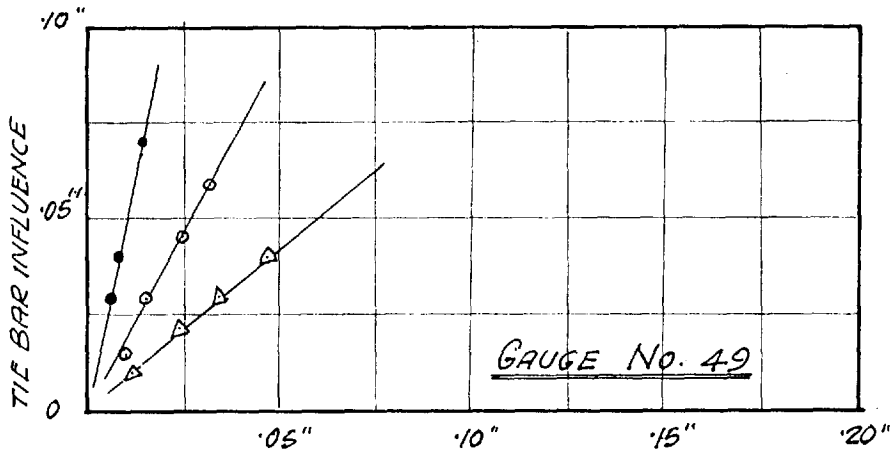


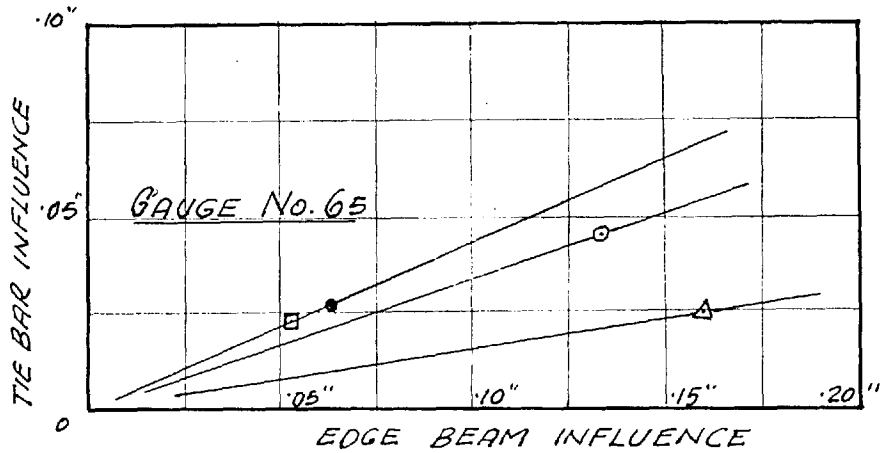


EFFECT OF CHANGE OF EDGE BEAM ON DEFLECTION

FIG. 6.64.

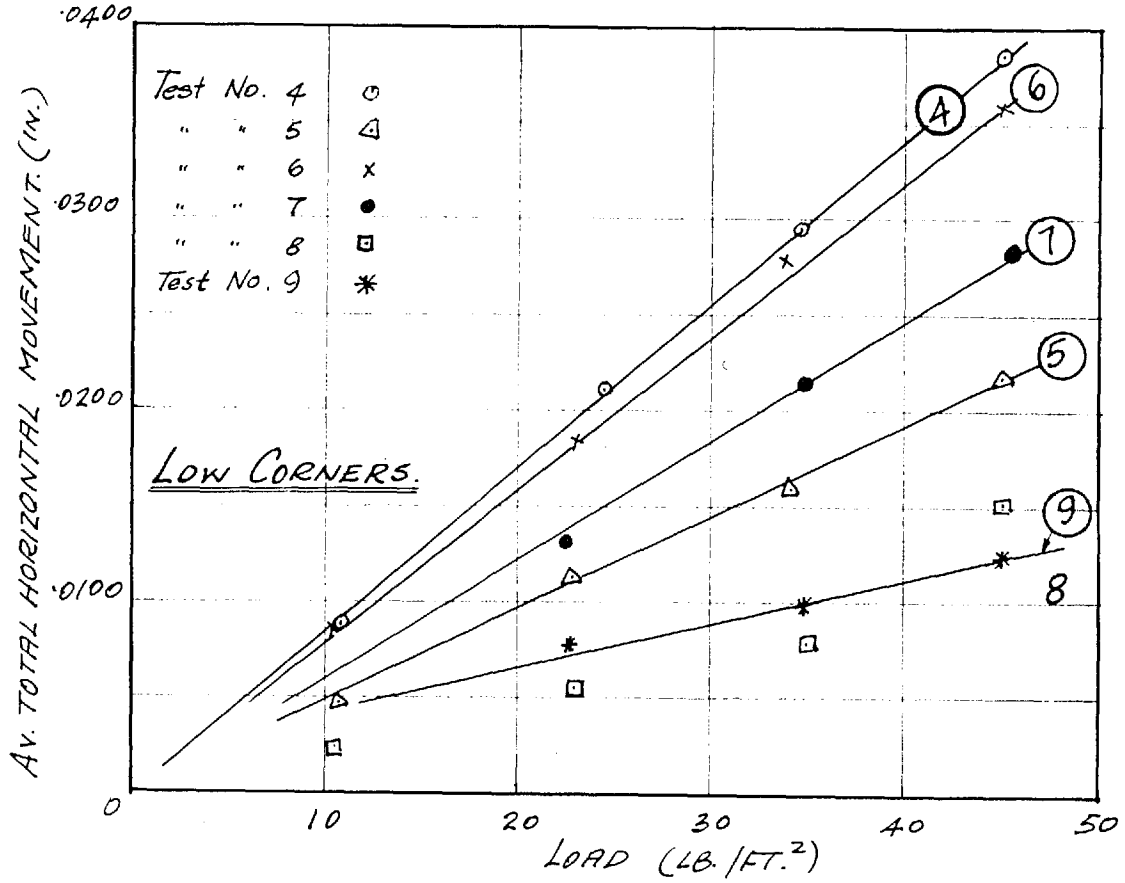


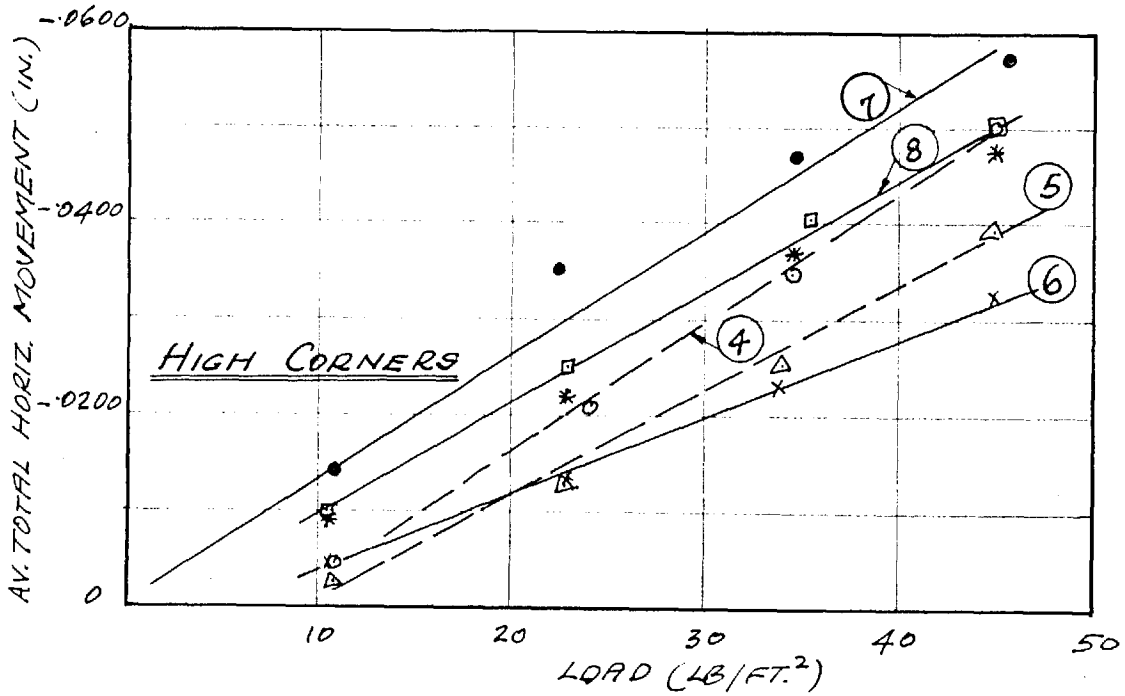




COMPARISON OF TIE BAR AND EDGE BEAM INFLUENCE

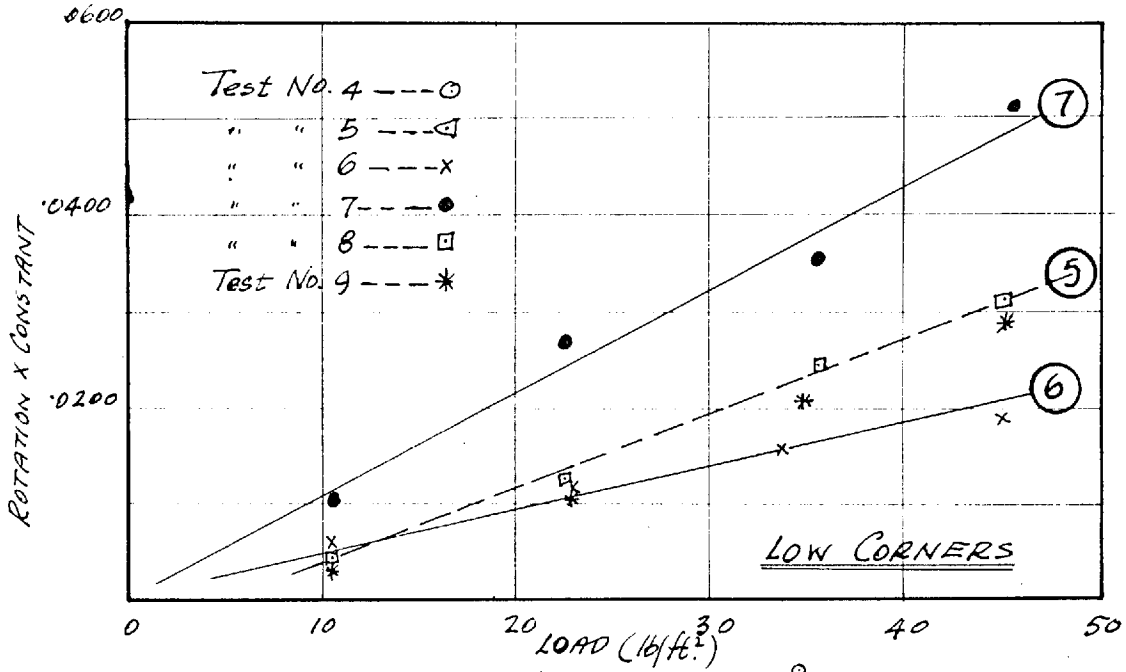
FIG. 6-65.

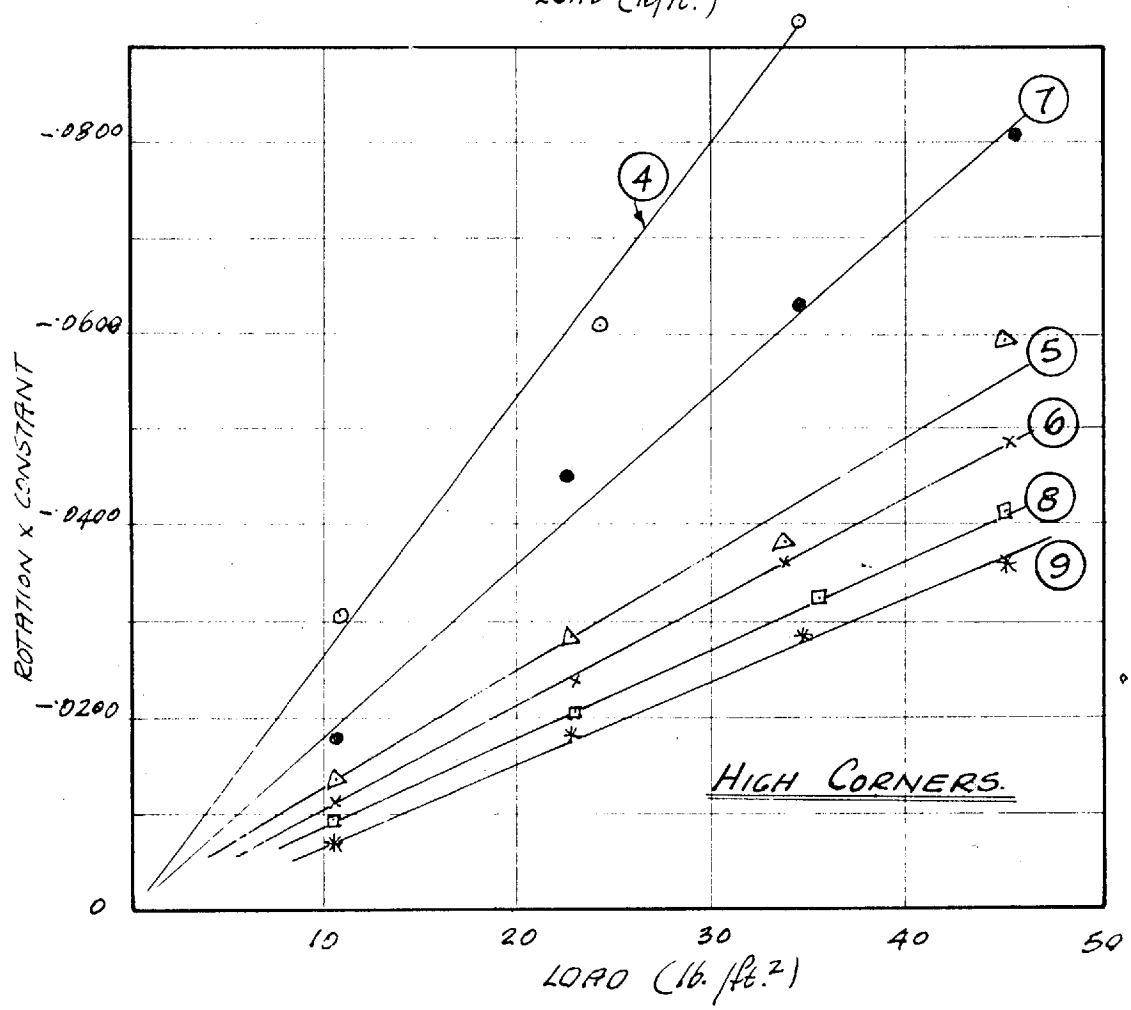




TESTS NOS. 4 9 HORIZ. CORNER MOVEMENTS.

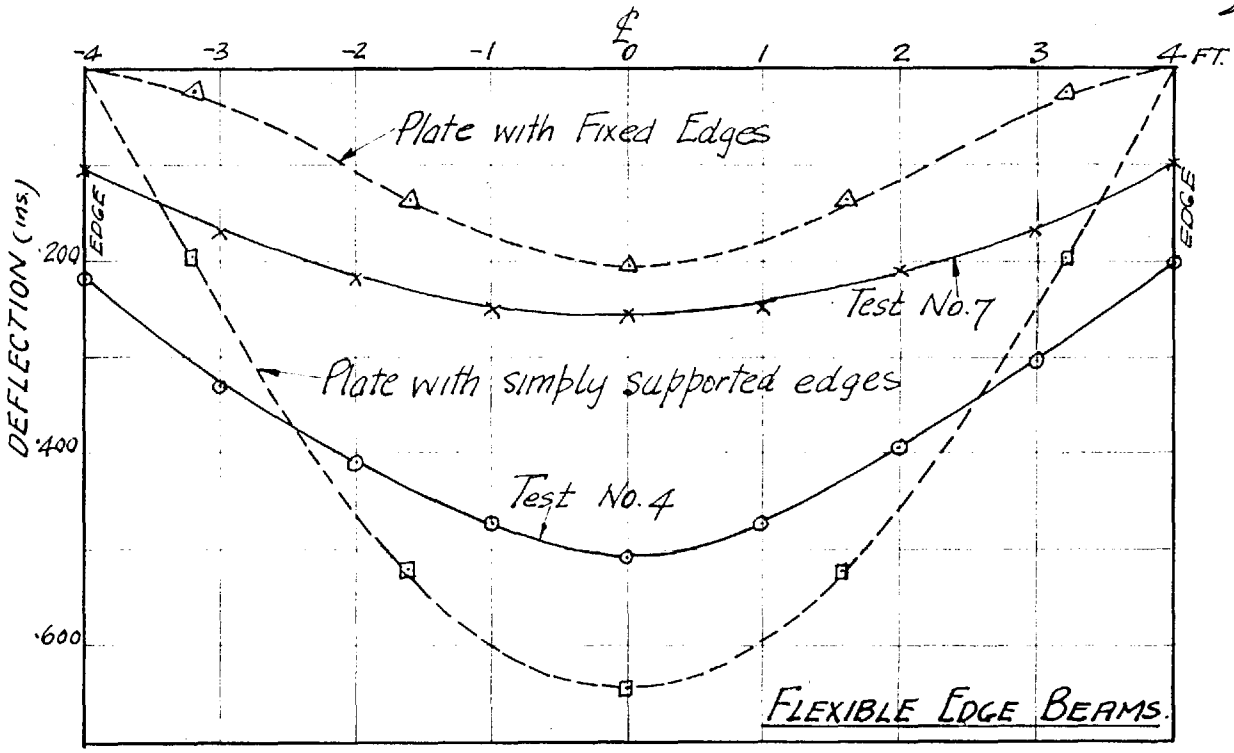
FIG. 6.66.





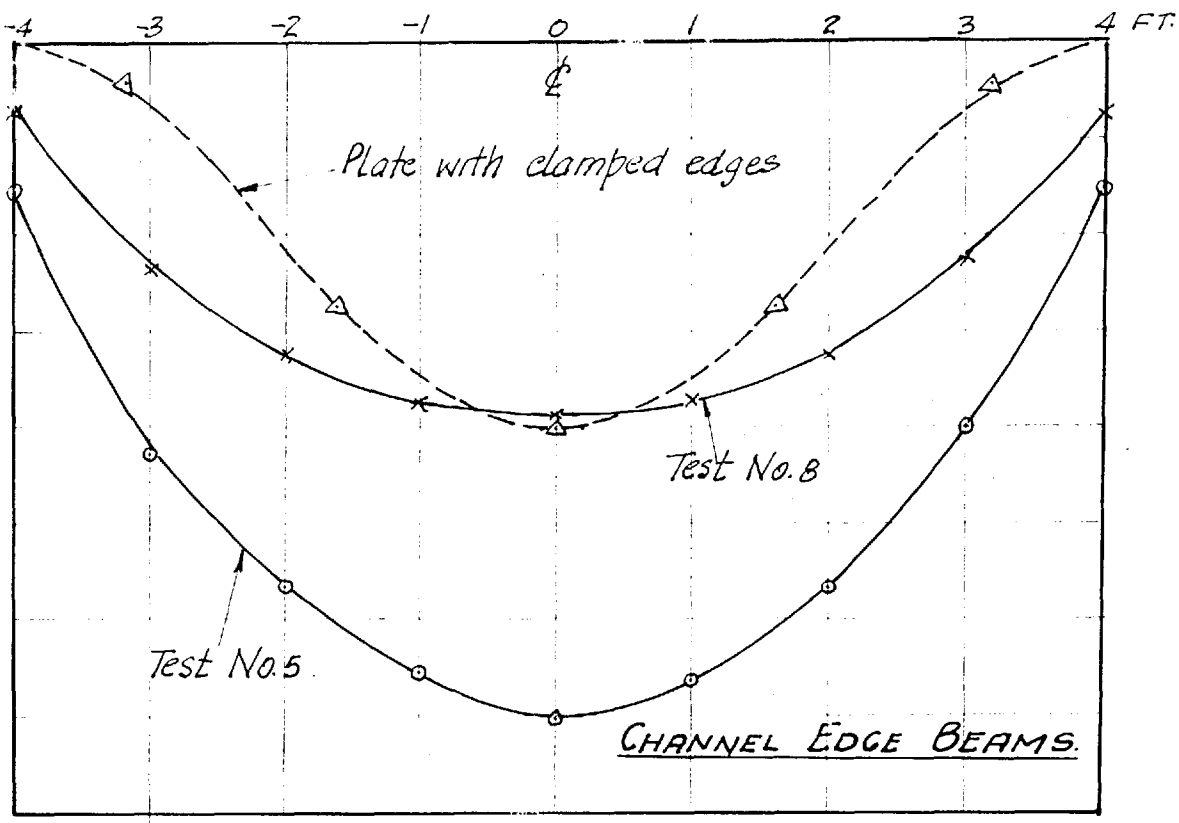
TESTS NOS. 4 - 9 CORNER ROTATIONS

FIG. 6.67.



PROFILES ALONG $\alpha = 0$

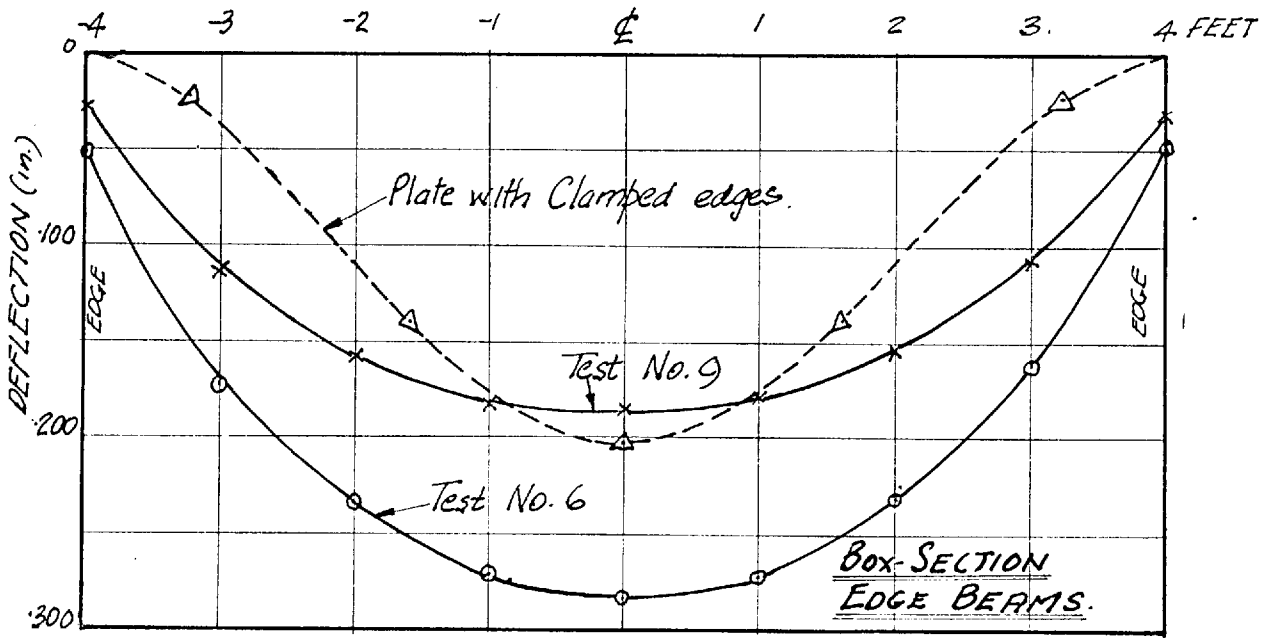
FIG. 6.68.



PROFILES ALONG $\alpha = 0$

FIG. 6.69.

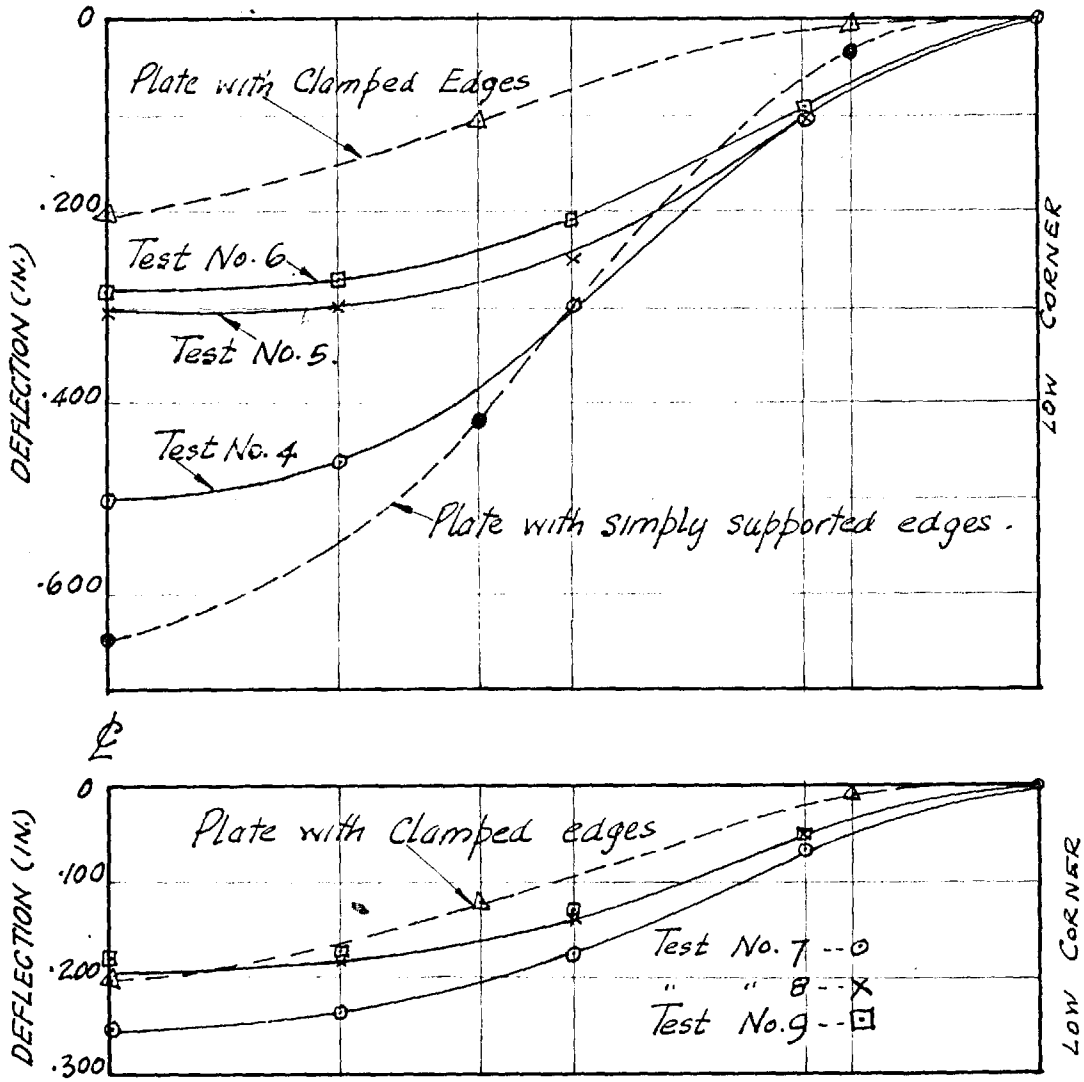
COMPARISON OF PLATE SOLUTIONS WITH EXP. RESULTS.



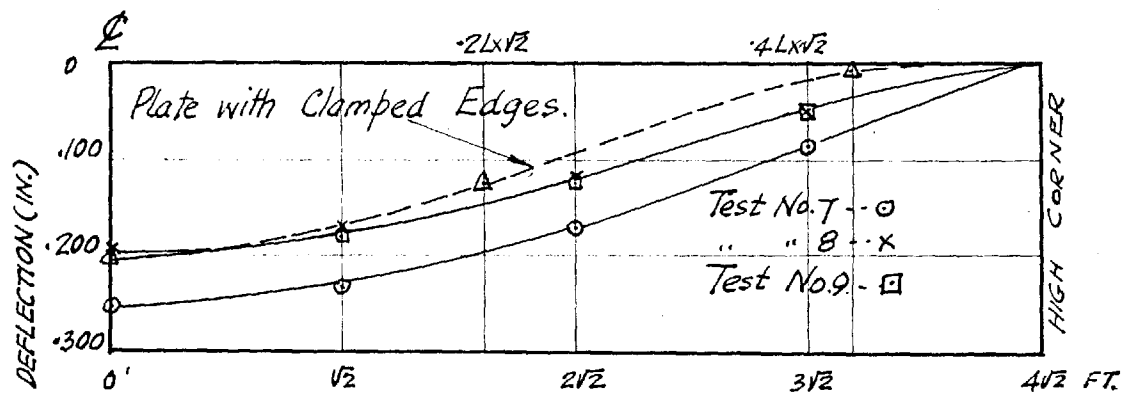
DEFLECTION ALONG $\alpha = 0$

COMPARISON OF PLATE SOLUTIONS WITH EXP. RESULTS.

FIG. 6.70.



DEFLECTIONS ALONG ARCH ℄.



DEFLECTIONS ALONG CATENARY ℄.

COMPARISON OF PLATE SOLUTIONS WITH EXP. RESULTS.

FIG. 6·71.

CHAPTER 7

7.1 DISCUSSION OF TEST RESULTS AND OBSERVATIONS

7.1.1 EDGE LOADING - TESTS Nos. 1 and 2

The results for tests with edge loading are given in Figs.(6.1) to (6.8) inclusive. It is seen from Fig (6.8) that a disturbance in the form of an edge deflection (u_γ) dies out reasonably rapidly with distance from the disturbed edge. Further, such disturbances have very little effect on deflections at the other edges. This fact is clearly revealed in the displacement contours in Figs.(6.2) and (6.5) the forms of which suggest that bending moments were confined to the vicinity of the disturbed edge region. The effect of edge moment on deflections appeared to be negligible (Fig.(6.8), however, in the Test No.2, the importance of avoiding cracking of the shell made it imperative that only relatively small moments should be applied at the edge. The strains produced in the shell for an edge shear and moment of 26.4 lb/ft and 39.3 lb.in./ft. respectively were very small.

The edge beam obviously played an important part in the ability of the shell to withstand such edge loadings. However, in view of the very small flexural rigidity of the edge beam used in the test, it may be inferred that such shells exhibit considerable rigidity as far as these types of edge loadings are concerned.

Typical deflection profiles plotted for different loads, (Figs.(6.3) and (6.6)), together with load-deflection curves shown in Fig.(6.7) for gauges nos.28 and 65, reveal the linear behaviour of the structure under the applied edge loads.

7.1.2 HALF LOADING - TEST No.3

Figs (6.9) to (6.14) relate to this type of loading for which linear behaviour is revealed in Figs (6.9) and (6.10). The structure has accommodated this type of unsymmetrical loading up to 29.5 lb/ft^2 ($65\frac{1}{2}$% of the maximum uniform loading in subsequent tests) without any serious effects.

7.1.3 UNIFORM LOADING

In order to compare the results effectively, Tests Nos.4 - 9 are discussed collectively. The results are incorporated in Figs (6.15) - (6.44) and (6.48) - (6.71).

7.1.3a ACTIONS

In view of the erratic behaviour of many of the strain gauges attached to the concrete surface, particularly when small strains were being measured, any comments on results based on strain readings can only be general. It is possible to observe general trends especially in cases where large strains occurred, eg. at centre of the shell and in the vicinity of the low corners.

In practice, for the type of structure tested, it is customary to provide edge beams having small torsional rigidity, and to restrict the movements at the low corners as much as possible. These conditions were most nearly met in Test No.7, in which the rigid tie was used in conjunction with flexible steel edge beams. Thus, as shown in Chapter 5, the direct forces at the edges of the shell should in this case be zero; especially at points far removed from the edges. Therefore, if the extensional theory is applicable, it could be anticipated that the direct forces along any generator would vanish, while the bending moments throughout the shell should be negligible. However, Figs (6.50) and (6.56) show that this was not the case in the tests. Along the generator $\alpha=0$, for example, n_β has a relatively small value near the edge; its value tends to increase towards the centre of the shell.

In the other tests in which the more rigid edge beams were used, the extensional theory appears to be more nearly satisfied, so far as direct forces were concerned. Fig (6.50) shows that in Tests 5 and 6 the value of the direct stress-resultant n_β along $\alpha=0$ does not change appreciably along the generator.

The tangential action $n_{\alpha\beta}$ is by no means constant along a generator (Fig (6.56)); rather, its value tends to oscillate about zero with rapid increase in its magnitude towards the low corners of the shell. There appears to be better agreement with the extensional

theory in the quadrant of the shell near the high corners. This was particularly so in Tests Nos. 8 and 9, involving the rigid tie together with the channel sections and with the box-section edge beams.

The actions in general, tend to be reduced in the middle regions when the edges of the shell were stiffened. A very interesting point emerges from Figs (6.56) and (6.57); that is, with the rigid tie there is a marked reduction in the magnitude of the actions when the flexible edge beams were stiffened with the channel sections. On the other hand, when the box-sections were added to the flexible edge beams, the actions were almost identical to those obtained for the case of channel sections. This would seem to indicate that with a rigid tie no useful purpose is served by also using a very rigid edge beam. With the flexible tie however, this effect is not quite as marked, due, no doubt, to the more important role of the edge beam stiffness under these conditions. Incidently, this point is also brought out from a study of the vertical deflections in the next section.

Again, in Figs (6.50) and (6.56), it is seen that the effect of the more rigid beam is for the moments to increase in the edge regions while decreasing towards the middle of the shell. It was not possible to observe strains in the shell beyond a point 3" away from the edge beam, however, the increase in moments near the edges may be explained if the connection between the shell and edge beam

is regarded as approaching a hinged one. With the more rigid edge beam, the deflections at the edges of the shell are reduced; this reduction may be achieved by applying an upward shear at the edge, which would tend to increase the positive bending moment in the edge region. This means, however, that the torsional rigidity of the beams is negligible, which was probably the case in the test, since the ability of the bolt to transfer torsional stresses across the gap in the edge beam was questionable. The bolts in the steel flats were not necessarily perpendicular to the latter, therefore, it was found necessary in some instances to make the holes in the additional edge beams larger than would otherwise be required in order to accommodate the bolts. The nuts used to secure the edge beam in position on the bolt, were tightened only nominally, otherwise high direct forces might have been transferred to the shell edges.

In all cases, actions tended to concentrate about the low corners of the shell (Figs (6.51) and (6.57)). Along the line joining the two low corners, the actions were considerably reduced in the middle region when the more rigid edge beams were attached. This effect of damping was more marked in the stress resultant n, particularly when the rigid tie was used. Again, however, the reduction in actions along the low diagonal was negligible when the channels were replaced by the box beams.

7.1.3b DISPLACEMENTS

Vertical deflections were observed in all tests while horizontal displacements at the midpoints of two edge beams were noted in Tests 4, 5 and 6. Corner movements were recorded by dial gauges appropriately placed. Figs (6.15) - (6.44) include the deflections for the different tests. Typical deflection profiles for each stage of loading as well as vertical deflection contours have been plotted for each test as aids to the study of shell behaviour with regard to linearity and symmetry.

As strain readings of gauges on the concrete surface were in many cases unreliable, the deflections constitute a more reliable basis of comparison of such effects as those due to edge beam stiffness and tie bar stiffness. By combination of the results from the different tests, it is possible to separate out certain of these effects. However, deflections are not necessarily a good guide as to the magnitude of bending moments in the shell although they may give a reasonable indication of general distribution of moments.

It is obvious from the results that the use of the more rigid edge beams resulted in a more rigid structure with consequent reduction in displacements. This can be seen in Figs (6.48) and (6.55) for Tests 4, 5 and 6 and Tests 7,8,9 respectively, in which

are compared deflections at the centre of the shell and at midspan of the edge beam. These diagrams also reveal that the deflections are not necessarily directly proportional to edge beam stiffness. In particular, the deflections for the tests involving channel sections and those involving box sections show very little difference despite the fact that the box was twice as stiff as the channel in bending, while the torsional rigidity of the former was several times that of the latter. It has already been pointed out that the shell actions also displayed this characteristic. This would seem to indicate that flexural rigidity of edge beam is more important than torsional rigidity. This, however, is not necessarily the case in practice. By thickening the edge region of the shell and eliminating the gap in the edge beam, the torsional stiffness of the latter would assume greater importance.

7.1.3c CORNER MOVEMENTS

(i) Horizontal Movements: These are shown in Fig (6.66) in which is plotted load vs. total corner movement along the diagonals, at low and high corners. It is true that these do not necessarily represent the movements at the level of the tie bar. Nevertheless, they do provide some indication of the horizontal stiffness of the corners. It can be seen that in all cases involving uniform loading, the low corners moved outwards while the high corners moved inwards; also, except in Test No.6, (flexible tie with box sections) the movement at the high

corners was about twice as much as that at the low corners. There is very little difference between the movements obtained with the channel sections or with the box sections, which again suggests some upper limit to the desirable rigidity of the edge beams. The considerable influence of the tie in restricting corner movements is brought out by a comparison of Tests 4 and 6 with Tests 5 and 8 and with Tests 7 and 9. The displacement profiles along the edge beams for different stages of loading, Figs (6.15),(6.20),(6.25),(6.30),(6.35), and (6.40), indicate a high degree of fixity at the low corners.

(ii) Corner Rotations: These are indicated in Fig (6.67) from which the rotations for Tests Nos. 4 and 5 have been omitted because of the erratic nature of certain deflection gauge readings. The curves represent averages of corner rotations. The above remarks in connection with horizontal moments also apply here, with Test No.6 providing no exception to the general trend.

7.1.3d SEPARATION OF EDGE BEAM AND TIE BAR INFLUENCES

An attempt has been made to separate the edge beam effects from those of the tie bar. This is done in Figs (6.62) to (6.65) inclusive. For example, by substituting the deflections for Test No.8 (channel sections with rigid ties) from those for Test No.5 (channels with flexible tie), the deflections due to the change in the tie bar are obtained. Similarly for Tests Nos.6 and 9, and also for Tests Nos.4 and 7.

It must be borne in mind that the effect of edge beam stiffness in the first series of tests (4,5, 6) was not necessarily the same in the second series (7,8,9). This point is evident in Fig (6.64).

The influences of tie bars and of edge beams have been studied at three representative points; namely, at the centre of the shell (gauge no.25), at midspan of an edge beam (no.65) and at a point in the vicinity of a low corner (no.49).

Figs (6.63) and (6.64) give respectively the proportion of the total deflection due to changes of tie bar and of edge beam, while Fig (6.65) can be used to assess the relative importance of the tie bar and edge beams. The effect of tie bar change (59% - 47½%) is of equal importance near the low corners as at midspan of the edge beam (Gauge No.65) where the effect varies from 58% with the flexible beam to 52% with the box sections. Thus the effect of tie bar change was practically constant when considering the low corners and the edge beams. At the centre of the shell however, the effect of changing the tie bar varied from 48% with the flexible edge beam to 30.5% with the more rigid channel and box-section beams. Fig (6.65) therefore brings out the fact that the less rigid tie, by allowing greater movements at the corner, also caused larger deflections in the central portion of the shell. Fig (6.64) shows that the importance of edge beam stiffness was lowered with the more rigid tie, the effect of edge

beam change on vertical deflections being approximately the same at all points on the shell.

The effect of edge beam stiffness on deflections at the centre of the shell and at midspan of edge beams is shown in Fig (6.62). The great importance of tie bar stiffness on shell behaviour is again clear. A study of Fig (6.62) in conjunction with the moment diagrams in Figs (6.50) and (6.56) reveals that with a rigid tie, a relatively flexible edge beam is not detrimental, and from the point of view of economy, may even be more desirable than the more rigid edge beam which leads to only small reductions in moments and deflections.

Since strain gauges on the edge beams and tie bars fared much better than those on the concrete surface, it is possible to make more definite remarks as far as edge beam moments and forces are concerned. Figs (6.53) and (6.59) show that the moment at midspan of the edge beam increases with edge beam stiffness though the variation is not linear. Thus in Fig (6.59), the midspan moment with the box sections (Test No.9) is not much greater than when the less rigid channel section is used (Test No8). Unfortunately, it was not possible to include the results for Test No.6 in Fig No.(6.53) since the strain readings in this test exhibited large zero errors, apparently due to a disturbance in the zero setting of the strain reading equipment. These diagrams also indicate that the effect of

increase in tie bar stiffness was to reduce the bending moments in the edge beams by about one-half. This reduction in moments was also accompanied by a large reduction in the magnitude of m_α near the edge beam (Figs (6.50) and (6.56)).

Since strain gauges were attached to the edge beams only at midspan, it is not possible to make any pronouncement as to the distribution of moments and forces along the edge beams. However, the extensional theory has been applied to determine the direct forces in the beams, assuming that such forces vary linearly from zero at the high corners to a maximum at the low corners, and the results have been plotted in Figs (6.52) and (6.59). It is remarkable that in both cases the above assumptions give a fair indication of edge beam force at midspan. This was especially so when the channel sections were attached to the edges. With the flexible tie, these assumptions gave the edge beam force almost exactly (Fig (6.52)).

7.1.3c TIE BAR FORCE

The behaviour of the tie bar is shown in Figs (6.52),(6.58), and (6.61). This force was reasonably constant for each series of tests, though higher in the second series (Tests 7,8,9) than in the first (Tests 4,5,6) in which a flexible tie was used. In neither case was a good agreement obtained with the value of tie bar force predicted by the extensional theory. This discrepancy could be due to the fact

that the tie bar was not allowed to take up the total movement at the corner because the clamped bases of the shell provided some restraint. In this respect it would have been more desirable if the shell corners were designed to permit free movement horizontally in the direction of the tie bar.

7.1.4 TEST TO FAILURE

The shell failed in bending in the immediate vicinity of the low corners. At each low corner, a large crack formed on the top surface running at right angles to the diagonal and meeting the edge beams at a point about $3\frac{1}{2}$" from the corner (Figs (6.46) and (6.47)). This was accompanied by severe crushing of the mortar along the same line on the bottom surface, resulting in the reinforcement being exposed. The pattern of failure at the low corners is also shown in Plates (9 - 12). The cracking pattern in these regions is similar to that of the corresponding flat plate with edge beams supported at the four corners. The direction of these cracks indicate the existence of high twisting moments in these regions.

There was a complete absence of cracks along the catenary diagonal. The cracks here were at right angles to this diagonal and particularly near the high corners, cut right through the shell - an evidence of high tensile forces along the diagonal in these regions.

A large crack formed near to edge No.1 in the bottom surface running from the low corner in a direction parallel to the edge. Crushing on the top surface also occurred along this line. This was probably due to uneven distribution of load. This crack occurred after those in the low corners had formed and after several of the jacks in the other regions of the shell were observed to be fully extended and were no longer contributing to the loading.

The spacing of cracks along the straight line generators exactly coincided with the reinforcement. Some of these cracks were barely visible prior to the test, but those near the centre of the shell opened up considerably during the test.

7.2 GENERAL REMARKS

7.2.1 LINEARITY AND SYMMETRY IN TESTS

In all the Tests 1 - 9 inclusive, the results indicate linear behaviour of the structure, except in regard to the horizontal displacements at midspan of edge beams (Fig (6.54)). Some slight degree of non-linearity is also displayed in the horizontal corner movements (Figs (6.66)), but this could have been due to errors involved in using dial gauges to measure such small movements. All tests were repeated at least twice, and in each case the deflection curve obtained for a particular test repeated itself almost exactly.

The symmetrical behaviour of the structure has been amply revealed in all the tests.

7.2.2 LOADING SYSTEM

Although the loading system functioned smoothly, there were certain disadvantages inherent in the method of loading. One great disadvantage is that the lower surface of the shell was rendered inaccessible by the suspension wires of the loading system, except in the regions near the edges of the shell. It was therefore not possible to trace the development of cracks except in a relatively small area. In the test to failure this constituted a serious defect in the loading system. This disadvantage was aggravated by the nature of the framework supporting the deflection gauges. This made the upper surface of the shell almost inaccessible. The versatility and dependability of the loading system were demonstrated in the tests, and these factors offset the above disadvantages to a great extent. The method of loading the shell by an air bag together with the dial gauge assembly adopted by Scrivener[22] renders one surface of the shell accessible throughout testing; but the other surface is entirely inaccessible. Futher, the behaviour of the air bag is very dependent on atmospheric conditions - a fact which could lead to uncertainty in accurate estimation of loads.

7.2.3 STRAIN GAUGES

The behaviour of many of the strain gauges fixed to the concrete surface left much to be desired despite the many elaborate precautions taken to control drifting in the gauges. It is unlikely that this was attributable to deterioration of bond between gauge and concrete or to the possibility of cracking of the shell. The latter can be ruled out since this would be reflected in deflections; further, the behaviour of the slabs tested in order to determine characterisics of the shell section showed that after minor initial cracking the load-deflection relationship was linear and repeated itself during several cycles with load increasing. The possibility of breakdown of bond between gauge and concrete was not overlooked. Prior to commencement of the first series of tests, checks carried out on several of the gauges indicated that the bond was still quite satisfactory. The use of mechanical strain gauges was precluded owing to the small magnitude in the strains to be measured, and the low headroom in the laboratory making it difficult to obtain readings at points away from the shell edge. Further, the large number of points at which strains were to be measured would make the use of mechanical gauges a most time-absorbing effort.

Strain readings were generally acceptable in the case of gauges attached to steel and in most of the gauges recording large strains. The unreliable behaviour of the Savage and Parsons equipment used

in the earlier tests have already been described in Section 4.8.

The difficulties described above in the use of electrical strain gauges on a concrete shell were also encountered by Scrivener[22]. This would lead one to consider seriously the point put forward by him; namely, that before testing such a large-scale shell structure in concrete, it may be advisable to test smaller models made from material more elastic than concrete such as steel or perspex. However, the difficulty of forming a hyperbolic paraboloid shell surface from such materials must not be under-estimated.

7.3 COMPARISON OF THEORETICAL AND EXPERIMENTAL RESULTS

7.3.1 EXTENSIONAL THEORY

In no case did the extensional theory predict, even reasonably, the behaviour of the shell except in the tie bar force in Tests Nos.4 and 5. The actions, in some cases, were small at the edges but they all tended to increase towards the middle region of the shell. The force in the tie bar was much less than that predicted by this theory. Deflections in experiment were too large to be explained by this theory.

7.3.2 PARTICULAR SOLUTION

The experimental results were on the whole much larger than those given by the particular solution in section 3.3. Further, the

distribution of actions and displacements in most cases shows no similarity to that specified by the particular solution.

7.3.3 APPROXIMATE SOLUTIONS

The approximate solutions discussed in Chapter 3 assume the existence of the typical edge effect problem in considering the complementary solution. This phenomenon of rapid damping away from the edge was not evident in any of the tests involving uniform loading; moments, in particular, increased away from the edges. There is evidence of rapid damping in the actions occurring at the shell corners both in a direction along the generators as well as along the low diagonal (Figs (6.51) and (6.57)).

The magnitude of tie bar force predicted by Loof's method is conservative; however, the effect of clamping of the shell bases during test would be to reduce the tie bar force. Though the method gives reasonable estimation of edge beam forces, the experimental value of edge beam moments is underestimated. If Loof's method of analysis were acceptable, one would expect reasonable agreement in Tests Nos.7 and 8 with rigid ties and rigid edge beams; however, this is not borne out by the results of these experiments.

An attempt has already been made in Section 7.1.3a to explain qualitatively the behaviour of the m_β in Figs (6.50) and (6.56). An approximate analysis has been carried out in Appendix 2 in which it is assumed that the change in edge shear associated with the change

in edge beams may be deduced from the method given by Bleich and Salvadori (Section 3.5a), the edge of the shell being regarded as hinged. The load on the edge beam at midspan is obtained by considering the shear necessary to produce the change in deflection observed for the different edge beams. This loading is applied to the edge beam in a sinusoidal manner and the midspan deflection compared with the actual results of the experiment. It is shown that for this approach to be correct for the shell tested, a very rigid edge beam would be necessary. This approximate method has been extended to take into account the effect of fixity at the low end of the edge beam and of moments at the shell edge.

7.3.4 PLATE SOLUTIONS

In Figs (6.68) to (6.71), the deflections obtained in experiment are compared with those predicted by regarding the shell as a flat plate with edges fixed or simply supported. This comparison was prompted by the magnitude of deflections observed experimentally especially in the middle region of the shell.

From Fig (6.68), it is seen that with the rigid tie and flexible beam, the deflection at the centre of the shell is predicted to within 30% accuracy by a plate solution involving fixed edges. When the rigid tie is replaced by the flexible one this comparison is not good and shell deflections would then be more reasonably predicted

by assuming simple supports at the edges of the plate. This condition would give zero deflection at the edges which is not the case in experiment because flexible edge beams were used.

Fig (6.69) deals with the comparison with the plate solution when the shell edges are comprised of the combination of flat steel beams and channel sections. The agreement in the deflections at midspan is quite good when the plate is assumed to have clamped edges. The discrepancy at the edges in Fig (6.68) is then reduced by the use of a more rigid edge beam.

The case of box-sections is shown in Fig (6.70). With the rigid tie, there is very good agreement between the experimental results and the plate solution for fixed edges. The discrepancy at the edge is further reduced and it would appear that the introduction of an edge fixing moment in the shell would eliminate the discrepancy in the diagrams.

The comparisons between theoretical and experimental deflections across the diagonals are made in Fig (6.71). The comparisons in the case of the flexible tie bar are not good; however, in the tests in which the rigid bar was used (Tests 7,8,9), the plate solution for fixed edges gives a very good approximation to the deflections along both diagonals of the shell. The comparison of movements however,

does not yield such good agreement. In the case of a plate with clamped edges, there should exist a relatively high negative bending moment at the edge (-147.7 lb.in./in.), becoming positive (66.53 lb.in./in. at the centre. Figs (6.50) and (6.56) show that this magnitude and distribution of moment is not fulfilled in experiment. In the case of the simply supported plate, the theoretical moments far exceed the experimental ones.

The analysis for the flat plate supported on elastic edges gives results that are much too conservative when compared with those obtained experimentally for the shell.

CHAPTER 8

8.1 CONCLUSIONS

(1) The hyperbolic paraboloid shell tested displayed considerable rigidity when subjected to edge loading in the form of vertical shear and moment. This was the case despite the fact that a very flexible edge beam was used in the tests involving edge loading. In practice, a beam with large flexural stiffness about its horizontal axis would be used for such a shell, and it would therefore be permissible to hang moderate loads at the edges of the shell. The loaded edge affects the other edges only to a very small extent, therefore it would appear that there is some support for the method whereby in studying the effect of disturbances from an edge, it is assumed that the effect of adjacent edges may be neglected.

(2) The shell also exhibited high rigidity to half loading. It has been deduced from a comparison of readings obtained for this case of loading and for total uniform loading, that this type of shell is quite capable of accommodating unsymmetrical loads due to wind, snow etc. up to the value of the uniformly distributed load for which the shell is designed. This is relevant in practice, since such shells besides being used as roofs, have also been used in foundations where the distribution of soil reaction is unpredictable.

(3) The tie bar exerts a very important influence on the behaviour of such shells. The more rigid tie by limiting corner movements, also produces a much more favourable stress distribution throughout the shell. Its effect in reducing actions in the important low corners of the shell is significant. There is not much to be gained by using a very rigid edge beam in conjunction with a rigid tie.

(4) In the tests carried out, the flexural stiffness of the edge beam about its horizontal axis was of much greater importance than its torsional stiffness. As this may have been due to the defects in the junction between the flexible edge beam and the detachable edge beam, no attempt has been made to translate this to practice.

(5) There is a tendency for actions to be concentrated in the low corners of the shell, while actions at the high corners are, in most cases, negligible. The possibility of using a rigid tie to reduce the stress concentration in the low corners has already been pointed out.

(6) The extensional theory fails in all respects to predict the behaviour of the shell, though it gives a reasonable indication of the forces in the edge beam (midspan) if it is assumed that the force varies from zero at the high corner to a maximum at the low corner.

(7) The particular solution of the bending theory is not acceptable as a complete solution of the problem. The range of variation of edge beams used in the tests covers most of the boundary conditions specified for this particular solution to be regarded as a complete solution. The only such boundary condition not approximately covered is that in resect of $n_{\alpha\beta}$. It could be that this boundary condition has a great effect on the solution.

(8) All the approximate solutions dealt with failed to predict shell behaviour. In particular, the typical edge effect phenomenon did not exist.

(9) The deflections in the middle region of the shell are reasonably predicted by regarding the structure as a flat plate with clamped edges. This could be of practical significance, since codes of practice usually specify maximum allowable deflections. However, this point needs further experimental investigation.

8.2 SUGGESTIONS FOR FURTHER RESEARCH

The tests have shown that the shell tended to behave like a flat plate. The low rise/span ratio was deliberately chosen so that the bending effects would be accentuated; therefore, it would be interesting to investigate the extent to which similarity with plate behaviour is evident when several parameters of the problem are varied,

particularly the rise/span ratio. The effect of variation of edge beam and tie bar stiffness could also be simultaneously studied for different values of this ratio. Such a series of test could also be useful in determining whether the typical edge effect phenomenon exists for such shells.

It would be instructive to observe experimentally the extent to which the particular solution of the bending theory is satisfied by testing a shell constructed in such a manner that the $n_{\alpha\beta}$ action at the edges can be released.

It is probable that by restricting corner rotations, the stress distribution in the shell would be affected to some degree - certainly, the deflections would be reduced. Tests designed to determine the exact effects of corner rotations would therefore contribute to the study of behaviour of hyperbolic paraboloid shells.

In concrete shells it is necessary to limit the strains to low ranges in order to avoid cracking. It may be advisable, therefore, to test much smaller shells from a more elastic material, embracing at the same time, variation of the different parameters. The results of such a test would then provide a reliable basis of comparison when the larger concrete shell is tested. Of course, with small models, inaccuracies in shell construction could have a large effect on shell behaviour, in particular, shell thickness would have to be critically controlled.

APPENDIX I

NUMERICAL CALCULATIONS BASED ON LOOF'S METHOD

The following calculations refer to the approximate method given in Section 3.5b.

The calculations are made for a uniform loading of 45 lb/sq.ft. (.3125 lb/sq.in.).

$k = 3.038 \times 10^{-3}$ in.$^{-1}$

$$n_{\alpha\beta} = -\frac{q}{2k} = -\frac{.3125}{2 \times 3.038 \times 10^{-3}} = -51.43 \text{ lb/in.}$$

Actual length of shell edge $= \sqrt{(96)^2 + (14)^2} = 97.02$ ins.

Total force transmitted to edge = 97.02 x 51.43 = 4989.7 lbs.

Horizontal component of this force = 96 x 51.43 = 4937.28 lbs.

Tie bar force = $4937.28\sqrt{2}$ = 6981.3 lbs.

The force in the beam is assumed to vary from zero at the high corner to a maximum at the low corner.

Vertical component of force = 14 x 51.43 = 720 lbs.

Vertical reaction at two low corners = 2 x 720 x 2 = 2880 lbs.

Total load on shell = 45 x 8 x 8 = 2880 lbs.

Vertical equilibrium is checked.

The parameter $p = \frac{kl^2}{t} = \frac{3.038 \times 10^{-3} \times 96^2}{0.75} = 37.33$

The value of p is within the limit for which the approximate formulae for shear and moments have been derived by Loof.

In the experiment, the loading was vertical. This loading is to be

corrected by the factor $\left(\frac{96}{97.02}\right)^2$ = .9791 at the edge beams.

Hence effective loading at edge G'_γ = .9791 x .3125 = .3050 lb/sq.in.

For rigid boundaries and no moment whatsoever along the edge beam the magnification factor A = 1 (see eqn. 3.73), hence the following from Section 3.1b:

CLAMPED EDGES

$$m_{edge} = -.511\, G'^{2}_{\gamma}\, \ell^{-4/3} = .511 \times 30.5\, 10^{-2} \times (97.02)^2 \times (37.33)^{-4/3}$$

$$= 11.76 \text{ lb.in./in.}$$

The moment first becomes zero at distance = $.40 \ell^{-1/3} \times \ell$

$$= .40 \times 97.02 \times (37.33)^{-1/3}$$

$$= 11.6 \text{ ins.}$$

Maximum +ve moment = $.167\, G'_\gamma \ell^2 \ell^{-4/3}$ = 3.846 lb.in./in.

This occurs at distance = $0.85 \ell^{-1/3} \ell$ = 24.7 ins.

Normal edge shear (q) = $1.732\, G'_\gamma \ell^{-1} \ell = \frac{1.732 \times 30.5 \times 10^{-2} \times 97.02}{37.33}$

$$= 1.373 \text{ lb/in.}$$

Vertical edge shear r = q x $\frac{97.02}{96}$ = 1.0106r = 1.388 lb/in

Total vertical edge shear = r x 96 x 4 = 533 lbs.

Portion of load carried by edge shear (slab action) = $\frac{533}{2880}$ = .1851

This proportion of the load carried by edge shear has been derived with A = 1, hence generally:-

Portion of load carried by slab action = .1851 A .....(A1)

Portion of load carried by membrane action = (1 - .1851 A)...(A2)

HINGED EDGES

In this case:-

Normal edge shear $q = .577\ G_\gamma l p^{-1} = .4574$ lbs/in.

Vertical edge shear $r = 1.0106\ q = .4622$ lbs/in.

$= .0617$ of total load

∴ Generally:

Portion of load carried by slab action = $.0617A$.....(A3)

Portion of load carried by membrane action = $(1 - .0617A)$...(A4)

Max. +ve B.M. occurs at $0.55 p^{-1/3} l = 15.92$ ins.

Value of max. +ve B.M. = $.149\ G_\gamma l^2 p^{-4/3} = 3.429$ lb.in./in.

In the above formulae, l = length of edge of shell.

The following cases have been investigated:-

CASE 1

Edges fully restrained and supported by edge beams comprised of box section and flexible in-situ beam.

All beams are assumed supported along their lengths. (i.e. no normal deflection at edge.)

No movement is allowed at low corners.

CASE 1A

As in Case 1 but edges hinged.

CASE 2

(a) Fully restrained edges.

(b) Edge beams comprised of "in-situ" flexible beam with channel sections attached.

(c) All beams supported along their lengths.

(d) No movement allowed at low corners.

CASE 2A

As in Case 2, but edges hinged.

CASE 3A

(a) Fully restrained edges.

(b) Box sections attached to "in-situ" flexible beams.

(c) Edge beams supported at their ends.

(d) No movement allowed at low corners.

CASE 3B

As in Case 3A, but edges hinged.

CASE 4A

(a) Fully restrained edges.

(b) Channel sections attached.

(c), (d) As in Case 3A

CASE 4B

As in Case 4A but edges hinged.

CASE 5A

(a) Fully restrained edges

(b) Box sections attached.

(c) Edge beams supported at their ends.

(d) Movement allowed at low corner, equivalent to that observed in corresponding experiment.

CASE 5B

As in Case 5A, but edges hinged.

CASE 6A

(a) Fully restrained edges.

(b) Channel sections attached.

(c) Edge beams supported at their ends.

(d) Movement at low corner, equivalent to that observed in experiment.

CASE 6B

As in Case 6A, but edges hinged.

CASE 7A

(a) Fully restrained edges.

(b) Flexible edge beams only.

(c) Edge beams supported at their ends.

(d) No corner movement allowed.

CASE 7B

As in Case 7A, but edges hinged.

CASE 8A

(a) Edges fully restrained.

(b) Flexible "in-situ" edge beams only.

(c) Edge beams supported at ends only.

(d) Movement allowed at low corner as observed in experiment.

CASE 8B

As in Case 8A, but edges hinged.

In view of the low torsional stiffness of the flexible edge beam, it is doubtful whether condition (a) in Cases 7A and 8A would be met.

CASE 1

Since no movement is permitted at the low corner, then movement u at the midspan of the beam is given by,

$$u = \frac{1}{S_b E_b}\int_0^{\ell} \frac{N_x}{\ell}\,dx \;-\; \frac{1}{S_b E_b}\int_0^{\ell/2} \frac{N_x}{\ell}\,dx$$

where N = Total axial force on beam

$= n_{\alpha\beta} \times \ell$

S_b = Area of edge beam

E_b = Young's Modulus of beam

$$\therefore\ u = \frac{1}{S_b E_b \ell}\left[\frac{Nx^2}{2}\right]_0^{\ell} - \frac{1}{S_b E_b \ell}\left[\frac{Nx^2}{2}\right]_0^{\ell/2}$$

giving $u = \frac{3N\ell}{8 S_b E_b}$

Edge beam area:-

$2\frac{1}{4}$" x $\frac{1}{4}$" tk. plate	= 0.5625 sq.in.
2/ 3"x $1\frac{1}{2}$" M.S. Channels at 4.60 lb/ft	= 2.70 sq.in.
Total Area S_b	= 3.2625 sq.in.

$$\therefore\ u = \frac{3}{8}\,\frac{N \times 97.02}{3.2625 \times 30 \times 10^6} = 3.7172 \times 10^{-7} N$$

Since the load is carried by a combination of slab and membrane action, then from (A2),

$$N = (1 - .1851A) \times \left\{ \begin{array}{l} \text{total load in edge beam assuming} \\ \text{membrane action only.} \end{array} \right\}$$

$$\therefore N = (1 - .1851A) \times 4989.7 \text{ lbs.}$$

$$\therefore u = 3.7172 \times 10^{-7} \times 4.9897 \times 10^{3}(1 - .1851A)$$

$$= 1.8548 \times 10^{-3}(1 - .1851A)$$

$u_\gamma = 0$ along edges (supported edge beam)

From symmetry, in expression (3.73),

$$u_{\alpha 1} = -u_{\alpha 2} = u$$

$$u_{\beta 3} = -u_{\beta 4} = u$$

$$\therefore A = 1 + \frac{1}{u_\gamma^o}\left[\frac{2u}{2ka} + \frac{2u}{2kb}\right]$$

$$\therefore A \simeq 1 + \frac{2u}{k\ell u_\gamma^e} \quad \text{for square shell}$$

But $u_\gamma^o = .0047$ ins. (from Section 3.5a)

$$\therefore A = 1 + \frac{2(1 - .1851A) \times 1.8548 \times 10^{-3}}{3.038 \times 10^{-3} \times 96 \times .0047}$$

$$A = 1 + 2.7063(1 - .1851A)$$

from which $A = 2.4694$

$\therefore$ Portion of load carried by slab action $= .1851A = .4571$

Portion of load carried by membrane action $= (1 - .1851A) = .5429$

Hence all moments etc. as derived for the case of rigid boundaries (A = 1), in which no longitudinal extension of edge is possible, are now to be multiplied by the factor A = 2.4694.

$$\therefore N = .5429 \times 4989.7 = 2708.9 \text{ lbs.}$$

$$\text{Edge moment} = - A \times .511\, G_Y l^2 \beta^{-4/3}$$

$$= - 2.4694 \times 11.76 = - 29.04 \text{ lb.in./in.}$$

Referring to Fig (3.6):-

At 11.6 ins. from edge (point A), moment = zero

At 24.7 ins. from edge (point B), $m_{max.} = .167\, G_Y l^2 \beta^{-4/3} \times A$

$$= .167/.511 \times 11.76$$

$$= 10.06 \text{ lb.in./in.}$$

The moment again becomes zero at 45.8 ins. from edge.

CASE 1A

In this case the edges are considered hinged.

Proceeding as in Case 1:-

$$A = 1 + 2.7063(1 - .0617A)$$

which gives $\underline{A = 3.1759}$

Max. +ve moment occurring at 15.92 ins. from edge (point D) = 3.429A

$$= 10.89 \text{ lb.in./in}$$

These values have been plotted in Fig (3.6) and this diagram will be used as a basis for the other cases.

Portion of load carried by membrane action = (1 - .0617A)

= .8041

N = .8041 x 4989.7 = 4012.2 lbs.

CASE 2

This is similar to Case 1 but channel sections are used instead of box sections.

Area of edge beam = (.5625 + 1.35) = 1.9125 sq.in.

$$u = \frac{3}{8}\frac{Nl}{S_b E_b} = \frac{3.2625}{1.9125} \times 3.7172 \times 10^{-7} N$$

$$\therefore u = 3.1641 \times 10^{-3}(1 - .1851A)$$

$$\therefore A = 1 + (1.7059 \times 2.7063)(1 - .1851A)$$

which gives:

$$A = 3.0285$$

$\therefore$ Portion of load carried by slab action = .1851A = .5606

" " " " " membrane " = (1 - .1851A) = .4394

$\therefore$ N = 0.4394 x 4989.7 = 2192.5 lbs.

The magnitude of the moments are derived by multiplying those in Case 1 by the factor = $\frac{3.0285}{2.4694}$ = 1.2264

CASE 2A

Problem similar to Case 2 but edges hinged.

$A = 1 + 5.6167(1 - .0617A)$

giving $A = 4.9360$

Moments are increased over Case 1A in the ratio of $\frac{4.9136}{3.1759} = 1.5742$

Portion of load carried by membrane action = $(1 - .0617A) = .6968$

$N = .6968 \times 4989.7 = 3476.8$ lbs.

N.B. In the four cases investigated above, it is seen that with the edge beam supported along its length, the moments in the shell are increased when the cross-sectional area of the edge beam is decreased. Hence, under such conditions it is advantageous, in practice, to use as large an edge beam section as possible, thus approaching the condition of rigid boundaries assumed in theory.

CASE 3A

In this case the edge beams are taken as unsupported along their lengths. The high corners of the shell are supported by rocker columns, while the low corners are fixed.

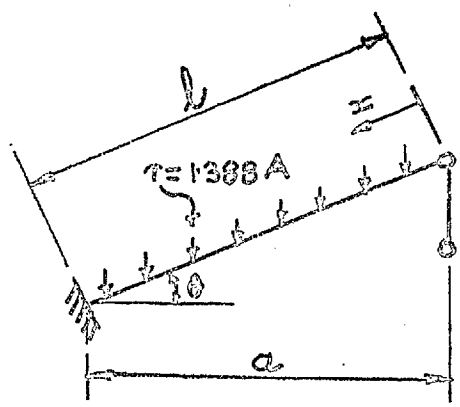
In the case of restrained edges and perfectly rigid boundaries ($A = 1$), then the vertical loading along the edge beam is given by,

$r = 1.388$ lb/in.

In the general case therefore,

$r = 1.388A$ lb/in.

The edge beam can therefore be analysed as a uniformly loaded propped cantilever ≡ a standard case.



Thus:-

Reaction at P = $5/8\ r\ell$

" " Q = $3/8\ r\ell$

Resolving r at right angles to the edge beam axis and taking moments at Q:-

$$M_Q = -1/8\ r\frac{a}{\ell}\ell^2 = -1/8\ ra\ell$$

$$= -1/8 \times 1.388A \times 96 \times 97.02$$

$$\therefore \underline{M_Q = -1615.97A}$$

The Max. +ve B.M. occurring at a distance $3/8\ell$ from P is:

$$M_{max.} = +\ 9/128\ ra\ell$$

$$\therefore M_{max.} = 9/128 \times 1.388 \times 97.02 \times 96\ A = 908.9805A$$

The deflection at any point is:

$$u_y = \frac{w\ell^3}{48E_bI_b}(m - 3m^3 + 2m^4)$$

where $m = x/\ell$, $W = r\ell\cos\theta = ra$

At midspan ($x/\ell = 1/2 = m$);

$$u_\gamma = \frac{ra\ell^3}{48E_bI_b}(1/2 - 3/8 + 1/8) = \frac{ra\ell^3}{192E_bI_b}$$

i.e. $u_\gamma = \frac{1.388Aa\ell^3}{192E_bI_b}$

For the flexible edge beam with box section attached:-

$$E_bI_b = 11.6319 \times 10^7 \text{ lb.sq.in.}$$

$\therefore$ At midspan: $u_\gamma = \frac{1.388 \times 96 \times (97.02)^3}{192 \times 11.6319 \times 10^7} A = .0055A$

From Case 1: $\frac{1}{u^o_\gamma}\left[\frac{u_{\alpha 1} - u_{\alpha 3}}{2kb} + \frac{u_{\beta 2} - u_{\beta 4}}{2ka}\right] = \frac{2u_c}{kau^o_\gamma}$

From (A3),

$$A = 1 + 2.7063(1 - .1851A) - \frac{.0055A}{.0047}$$

which gives $\underline{A = 1.4128}$

$\therefore$ Portion of load carried by slab action = $.1851A = .2615$

" " " " " membrane " = $(1 - .1851A) = .7385$

$\therefore$ N = $.7385 \times 4989.7 = 3684.9$ lbs.

Check on equilibrium:

Due to N, $R_p = \frac{14}{97.02} \times 3684.9$ = 531.7 lbs.

Due to R, $R_p = \frac{5}{8} \times 1.4128 \times 1.388 \times 97.02$ = 118.9 lbs.

Total vertical reaction at low corner = $2(531.7 + 118.9)$ = 1301.2 lbs.

Due to N, $R_Q = 0$

Due to R, $R_Q = 3/8\ r\ell = 71.3$ lbs.

∴ Total vertical reaction at high corner = (2 x 71.3) = 142.6

∴ Total vertical reaction at 4 corners = 2(1301.2 + 142.6) = 2887.6 lbs.

This reaction should be 2880 lbs., hence the check can be regarded as satisfactory.

Deflection at midspan of beam = .0055A = .0055 x 1.4128 = .0078 lbs.

$M_{max.}$ = 908.9805A = 1284.2 lb.in.

Edge moment in shell = -11.76A = - 16.61 lb.in./in.

At point A (Fig (3.6)), Moment = 0

At point B, max. +ve B.M. = $\frac{.167}{.511}$ x 16.61 = (.3268 x 16.61) = 5.43 lb.in./in.

CASE 3B

Conditions similar to Case 3A, but edges hinged.

∴ Portion of load carried by membrane action = (1 - .0617A)

∴ $A = 1 + 2.7063(1 - .0617A) - \frac{.0055A}{.0047}$

giving $\underline{A = 1.6189}$

Portion of load carried by slab action = .0617A = .0999

" " " " " membrane " = .9001

∴ N = 4989.7A = 4491.2 lbs.

∴ In Fig (3.6):

Moment at edge of shell = 0

At point D, moment = 3.429A = 5.55 lb.in./in.

Deflection at midspan of edge beam = .0055A = .0089 ins.

B.M. near midspan of edge beam = 9/128 x .4622Al_a = 302.70A = 490 lb.in.

CASE 4A

Conditions as in Case 3A but channel sections fixed to flexible edge beams instead of box sections.

$$E_b I_b = 6.1719 \times 10^7 \text{ lb.sq.in.}$$

Following the computations for Case 3A, the following have been derived:

$A = 1.0038$

$N = 4989.7(1 - .1851A) = 4989.7 \times .8142 = 4062.6$ lbs.

At edge of shell, moment = $-11.76A = -11.80$ lb.in./in.

At point B (Fig (3.6)) moment = $.3268 \times 11.80 = 3.80$ lb.in./in.

B.M. near midspan of edge beam = $908.9805A = 912.43$ lb.in.

Deflection at midspan of edge beam = .0103 in.

CASE 4B

Conditions as in Case 3B, but channels instead of box section attached to flexible edge beams.

In this case, $A = 1.1036$

Portion of load carried by membrane action = $(1 - .0617A) = .9319$

$\therefore N = 4989.7 \times .9319 = 4649.9$ lbs.

Max. +ve B.M. occurs at D (Fig (3.6)) = $3.429A = 3.78$ lb.in./in.

Deflection at midspan of edge beam = .0114 in.

Max. +ve B.M. in beam near midspan = 334.1 lb.in.

CASE 5A

In this case the edges are taken as fully restrained with box sections attached to the flexible "in-situ" edge beams. These are regarded as supported by rocker columns at the high corners.

The shear deformations of the edge structure and of the shell are first considered separately, and the actual bending moments in the shell derived by eliminating the discrepancy.

The total deformation is therefore divided as follows:-

(a) Deformation of edge structure due to the extension of the tie bar. The edge structure is regarded as being completely stiff, the low corners supported on spherical hinges and the high corners on rocker columns.

(b) Deformation due to deflection of the edge structure resulting from the vertical edge shear. Here again, the high corners are taken as supported in rocker columns; but no movement is allowed at the low corners.

(c) Deformation due to compression of the edge beam, with no movement allowed at the low corner.

It should be noted, however, that in (a) above, any relative movement of the opposite edges in the α or β directions introduce an additional gap to be closed. Hence, the extensional rigidity of

the shell in these directions ought to be taken into account. The edge structure has been assumed detached from the shell, but, since this is actually not the case, the presence of the shell will certainly affect the deformation of the edge structure as deduced from conditions (a) thus complicating the problem. Loof overcomes this difficulty by considering the midspan of opposite edges connected by inextensible cables - a reasonable assumption in view of the considerable stiffness of the shell in its plane. For the shell under consideration, the condition of "inextensible cables" is exactly fulfilled since extension of tie bar under the specified conditions results simply in a rotation of the vertical plane of the edge structure without any alteration in the distance between the midpoints of opposite edges. It is concluded, therefore, that so far as bending moments are concerned, the three types of deformation (a),(b),(c) are compatible, and therefore the magnification factor A defined in (3.73) may be applied. The calculations for this case follow:-

(a) Extension of tie

Let d be outward movement of low corners. Then as shown in Ref.(16) the total contribution to $u_{\alpha 1}$ and $u_{\beta 1}$ in the expression for A is:

$$\frac{1}{u_Y^0}\left[\frac{\sqrt{2}}{2} \times \frac{d}{ka}\right]$$

Note:

The contribution of tie bar extension to the term u_γ in the expression for A (3.73) is small compared with its contribution to $u_{\alpha 1}$ and $u_{\beta 1}$. This can be shown to be $\frac{1}{u_\gamma^\circ}\left[\frac{\sqrt{2}}{32}\,dka\right]$ which is small in comparison to the preceding expression.

(b) Deflection of Edge Beam

The vertical edge shear as in previous cases is

$$r = 1.388A \text{ lb/in.}$$

The deflection at midspan has been derived in Case 3A.

The contribution due to this deflection in the expression for A is $\frac{.0055A}{u_\gamma^\circ}$

Near midspan, B.M. = 908.9805A.

(c) Compression of Edge Beam

From Case 1 , $u = \frac{3}{8}\frac{N\ell}{S_b E_b} = 3.7172 \times 10^{-7} N$

where N = (1 - .1851A)(Total load in Edge Beam assuming membrane action only)

$\therefore u = 1.8548 \times 10^{-3}(1 - .1851A)$

Since the movements at opposite edges have opposite signs, and also in view of the symmetry of the edge structure, the contribution to $u_{\alpha 1}$ and $u_{\beta 1}$ in the expression for A is:

$$\frac{1}{u_\gamma^\circ}\left[\frac{4u}{2ka}\right] = \frac{1}{u_\gamma^\circ}\left[\frac{2u}{ka}\right] = \frac{1}{u_\gamma^\circ}\left[\frac{3.7096 \times 10^{-3}}{ka}(1 - .1851A)\right]$$

From (a),(b),(c) above,

$$A = 1 + \frac{1}{u^{\circ}_{\gamma}} \left[\frac{\sqrt{2}}{2} \frac{d}{ka} + \frac{3.7096 \times 10^{-3}}{ka} (1 - .1851A) - .0055A \right]$$

from which:

$$\underline{A = 203.8057d + 1.4099}$$

From Experiment No.9:-

Average strain in tie bars at a loading of .3125 lb/sq.in. = 45×10^{-6}

$\therefore$ Observed extension of tie = $96\sqrt{2} \times 45 \times 10^{-6}$ = .0061 in.

$\therefore$ A = (203.8057 x .0061) + 1.4099 = 2.6531

Portion of load carried by slab action = .1851A = .4911

" " " " " membrane " = (1 - .1851A) = .5089

$\therefore$ N = .5089 x 4989.7 = 2539 lbs.

Deflection at midspan of beam = .0055A = .0146 in.

B.M. near midspan of beam = 908.9805A = 2411.61 lb.in.

So far, no account has been taken of the eccentricity of the tie bar and of the shell and edge beam. In the experiment, the latter is zero.

If eccentricity of tie = e_t, and x is distance from the high corner measured along the edge beam,

Then $M_x = - \frac{N_x e_t}{a}$

At midspan $M = - \frac{N\ell}{2a} e_t$

With e_t = 1.75 in.

$$M = -\frac{N \times 97.02 \times 1.75}{2 \times 96} = -.8843N = -2245 \text{ lb.}$$

∴ Net Moment at midspan of edge beam = (2411.61 - 2245) = 166.6 lb.in.

At edge of shell, moment = - 11.76A = - 31.20 lb.in./in.

At point B (Fig (3.6)), m = .3268 x 31.20 = 10.19 lb.in./in.

CASE 5B

Conditions as in Case 5A but shell hinged at edges.

(a) Extension of tie:-

$$\text{Effect on } A = \frac{1}{u_\gamma^0}\left[\frac{\sqrt{2}}{2}\frac{d}{ka}\right]$$

(b) Deflection of edge beam:-

In this case, $r = .4622A$

∴ Effect of midspan deflection on A is as in Case 3B

$$= \frac{.0055A}{u_\gamma^0}$$

(c) Compression of Edge Beam:-

$$u = \frac{3}{8}\frac{Nl}{E_b S_b}$$

$$= 1.8548 \times 10^{-3}(1 - .0617A)$$

$$\therefore A = 1 + \frac{1}{u_\gamma^0}\left[\frac{\sqrt{2}}{2}\frac{d}{ka} + \frac{3.7096 \times 10^{-3}}{ka}(1 - .0617A) - .0055A\right]$$

giving $A = 234.7835d + 1.6241$

With d = .0063 in., $A = 3.0563$

∴ Portion of load carried by slab action = .0617A = .1886

" " " " " membrane " = (1 - .0617A) = .8114

∴ N = 4989.7 x .8114 = 4049 lbs.

Deflection at midspan of edge beam = .0055A = .0168 ins.

B.M. near midspan of edge beam = 302.70A = 925.1 lb.in.

Correcting this for eccentricity of tie gives:-

Net B.M. at midspan of edge beam = (.8843N - 925.1) = - 2612.7 lb.in.

Max. +ve B.M. at D (Fig (3.6)) = 3.492A = 10.48 lb.in./in.

Note:

The eccentricity of the tie causes a great reduction in the moment at midspan of the edge beam; in the above case the sign of the moment is reversed.

CASE 6A

Conditions as in Case 5A but channel sections used instead of box sections.

$$u = \frac{3}{8}\frac{N\ell}{E_b S_b}$$

from which, $u = 3.1641 \times 10^{-3}(1 - .1851A)$

$$\therefore A = 1 + \frac{1}{u\theta\gamma}\left[\frac{\sqrt{2}}{2}\frac{d}{ka} + 2 \times 3.1641 \times 10^{-3}(1 - .1851A) - .0103A\right]$$

which gives.. $\underline{A = 1.4019 + 131.9890d}$

In Experiment No. 8:-

Average strain in tie = 51.0×10^{-6}

$\therefore$ Extension of tie = $96\sqrt{2} \times 51.0 \times 10^{-6} = .0067$ ins.

$\therefore$ A = $1.4019 \div (131.9890 \times .0067) = \underline{2.2862}$

$\therefore$ Portion of load carried by slab action = $.1851A = .4232$

" " " " " membrane " = $(1 - .1851A) = .5768$

$\therefore$ N = $.5768 \times 4989.7 = 2578.1$ lbs.

Midspan deflection of edge beam = $.0103A = .0235$ ins.

B.M. near midspan of edge beam = $908.9805A = 2078$ lb.in.

B.M. due to eccentricity of tie = $-.8843N = -2545$ lb.in.

$\therefore$ Net B.M. near midspan beam = -46.7 lb.in.

At edge of shell, m = $-11.76A = -26.89$ lb.in./in.

At B (Fig (3.6)), m = $.3268 \times 26.89 = 8.79$ lb.in./in.

CASE 6B

Conditions as in Case 6A but edges of shell hinged.

In this case,

$$u = 3.1641 \times 10^{-3}(1 - .0617A)$$

$$\therefore A = 1 + \frac{1}{u\frac{\theta}{\gamma}}\left[\frac{\sqrt{2}}{2}\frac{d}{ka} \div 2 \times 3.1641 \times 10^{-3}(1 - .0617A) = .0103A\right]$$

from which: $\underline{A = 1.6412 + 154.5142d}$

with d = .0067 in., $\underline{A = 2.6754}$

$\therefore$ Portion of load carried by membrane action = $(1 - .0617A) = .8349$

$\therefore$ N = $4989.7 \times .8349 = 4166$ lbs.

Deflection at midspan of beam = .0103A = .0276 ins.

B.M. near midspan of beam = 302.70A = 810.1 lb.in.

B.M. due to eccentricity of tie = -.8843N = - 3684.0 lb.in.

∴ Net B.M. near midspan = - 2873.9 lb.in.

Moment at edge of shell = 0

At point D (Fig (3.6)), m = 3.429A = 9.18 lb.in./in.

The calculations for Cases 7A to 8B, involving the flexible "in-situ" edge beam alone, are similar to the corresponding foregoing cases. However, in this case:-

$$S_b = 0.5625 \text{ sq.in.}$$

$$I_b = 0.2373 \text{ sq.in.}$$

The results of the calculations for Cases 7A to 8B have been included in Table (3).

APPENDIX II

FURTHER CHECKS ON APPROXIMATE METHODS

In Section 7.1.3a, it is pointed out that the change in the bending moment (m_β) near the edges of the shell due to the stiffening of the flexible edge beam, could be explained by assuming that the vertical reaction at the shell edge was increased. (See Figs 6.50 and 6.57). By examining the deflection at midspan of the edges it is possible to deduce from Section 3.5a what this edge reaction should be, and hence, also, the distribution of the moment across the shell and deformation of the edge beams. In this section, this is done by regarding the shell with the flexible edge beam as a particular solution and then determining the value of the edge shear required to correct the discrepancy in midspan deflection when the flexible edge beams are stiffened.

Let δ_m and $w_{max.}$, respectively, be the experimental and theoretical discrepancy between midspan deflections obtained when the flexible edge beams are used alone, and when they are stiffened.

Q = Vertical edge shear

It is shown in Section 3.5a that in order to correct an edge deflection of .0047 in., an edge shear of 1.57 lb./in. is necessary.

∴ Edge shear required to correct a discrepancy of 1 in. is:-

$$Q_1 = \frac{1.57}{.0047} = 334.04 \text{ lb./in.}$$

The loading Q may then be applied to the edge beam to determine the theoretical midspan deflection. This loading will be taken as distributed along the beam in a sinusoidal manner with the beam regarded as simply supported at its ends; or the loading may be taken as uniformly distributed along the beam with the latter acting as a propped cantilever fixed at the low corner of the shell. The edge beam profiles in Tests 4 - 9 suggest that the latter assumption is the more reasonable one.

CASE 1 Sinusoidal Distribution of Loading

The equation of the beam is:-

$$E_b I_b \frac{d^4 w}{dx^4} = Q \sin\frac{\pi x}{\ell}$$

Let the deflection curve be given by:-

$$w = D \sin\frac{\pi x}{\ell}$$

$$\text{Then } \frac{\pi^4}{\ell^4} D \sin\frac{\pi x}{\ell} = \frac{Q}{E I_b b} \sin\frac{\pi x}{\ell}$$

$$\text{Thus:- } w = \frac{Q}{E_b I_b} \frac{\ell^4}{\pi^4} \sin\frac{\pi x}{\ell} \qquad \text{.....(A4.)}$$

At $x = \frac{\ell}{2}$:-

$$w_{max.} = \frac{Q}{E_b I_b} \frac{\ell^4}{\pi^4} = \frac{334.04\ \delta m}{E_b I_b} \left(\frac{96}{\pi}\right)^4$$

$$\text{i.e. } w_{max.} = 29.1264 \times 10^7 \frac{\delta m}{E_b I_b} \quad \ldots\ldots\ldots\ldots\ldots\ldots\ldots\ldots\ldots\ldots (A5)$$

It follows, therefore, that for agreement between experimental and theoretical deflection,

$$w_{max.} = \delta m$$

$$\text{i.e. } E_b I_b = 29.1264 \times 10^7 \text{ lb.sq.in.}$$

This is a section almost three times as stiff as the combined flexible and box section edge beams; i.e., an almost completely stiff edge beam.

If the loading were taken as uniformly distributed, the value of $E_b I_b$ would be even greater than that derived above.

CASE 2 Beam regarded as a propped cantilever with uniform loading

In this case:-

$$w_{max.} = \frac{Q\ell^4}{185 E_b I_b} = \frac{334.04\ \delta m \times (96)^4}{185\ E_b I_b}$$

$$= 15.33 \times 10^7 \frac{\delta m}{E_b I_b}$$

For $w_{max.} = \delta m$:-

$$E_b I_b = 15.33 \times 10^7 \text{ lb.sq.in.}$$

The maximum value of $E_b I_b$ used in the experiments was 11.6319×10^7, hence, in this case, experimental and theoretical deflection of edge beam would agree reasonably.

CHECK ON MOMENTS NEAR SHELL EDGE

On the basis of the above approximate analysis, a check will be carried out to see whether the change in bending moments in the edge regions of the shell compares with the changes in m_β reflected in Figs (6.50) and (6.56). The edges of the shell are taken as hinged.

From Section 3.5a :-

$$m_\beta = 15.73\ C\ F_2\ (\lambda\beta)$$

where C = Factor by which the figures in Table I (for hinged edges) are to be multiplied.

$$\text{i.e. } C = \frac{Q}{1.57} = .6369\ Q$$

m_β should first become zero at $\lambda\beta = \pi$, i.e. $\beta = 31.35$ ins., so that, theoretically, this is the point where the moment diagram for flexible edges should cross the diagram for stiffened edges. In Figs (6.50) and (6.56), this point occurs at approximately 20 ins. and 12 ins. respectively, from the edge of the shell. The greatest discrepancy in moments should occur at 7.84 ins. from the edge and should be $5.07 \times .6369Q = 3.229Q$.

The following table summarises the values of the moments and edge reactions derived by the above approximate considerations:-

	Observed Deflns. (ins.)	Diff. (δm) (ins)	Q = 334.048m (lb/in)	$M_{max.}$ (lb.in./in.)
Flexible Tie				
Test No.4	.205	0	0	-
Test No.5	.076	.129	43.1	139.1
Test No.6	.049	.156	52.1	167.3
Rigid Tie				
Test No.7	.100	0	0	0
Test No.8	.039	.061	20.4	65.8
Test No.9	.031	.069	23.1	74.5

In Figs (6.50) and (6.56), the actual values of m_β in the edge regions are much lower than those in the above table.

BIBLIOGRAPHY

1.) Flugge, W. and Geyling, F.T.

"A General Theory of Deformations of Membrane Shells"
(Memoirs of the International Association of Bridge and Structural Engineering, Vol.17, 1957. pp.23-46)

2) Parme, A.L.

"Hyperbolic Paraboloids and other Shells of Double Curvature"
(Journal of the Structural Division. Proc. of the American Society of Civil Engineers. Sept.1956. pp.1057-1-32)

3) Vlasov, V.Z.

"The Basic Differential Equations in the General Theory of Elastic Shells"
(Prikladnaia Matematika i Mekhanika, Vol.8, 1944 also National Advisory Committee for Aeronautics (U.S.A.) Tech. Memo No.1241)

4) Vlazov, V.Z.

"Cylindrical Shells and New Ways of developing Thin-walled Spatial Systems in Structural Mechanics."
(Procs. of Symposium on Concrete Shell Roof Construction, Oslo, 1957. pp.121-146.)

5) Munro, J.

"The Linear Analysis of Thin Shallow Shells"
(Journal of the Institution of Civil Engineers, July, 1961. Vol.19. pp.291-305)

6) Ambartsumyan, S.A.

"On the Calculation of Shallow Shells"

(Prikladnaia Matematika i Mekhanika, Vol.11, 1957. pp.527-532; also National Advisory Committee for Aeronautics, Tech. Memo No.1425)

7) Fluggo, W. and Conrad, D.A.

"A Note on the Calculation of Shallow Shells"

(Journal of Applied Mechanics, Dec. 1959. pp.683-86)

8) Bouma, A.L.

"Some Applications of the Bending Theory regarding Doubly Curved Shells"

(Procs. on the Theory of Thin Elastic Shells. Delft, Aug.1959, pp.202-234)

9) Apeland, K. and Popov, E.P.

"Analysis of Bending Stresses in Translational Shells"

(Procs. of the Colloquium on Simplified Calculation Methods, Brussels, Sept.1961, North Holland Publishing Co., pp.9-43)

10) Apeland, K.

"Stress Analysis of Translational Shells"

(Procs. of the American Society of Civil Engineers, Engineering Mechanics Division, Feb.1961, pp.111-139)

11) Das Gupta, N.C.

"Using Finite Difference Equations to find the Stresses in Hyper Shells"

(Civil Engineering and Public Works Review, Vol.56, No.655, Feb.1961, pp.199-201)

12) Gerard, F.A.

"The Analysis of Hyperbolic Paraboloid Shell Roofs"

(Transactions of the Engineering Institute of Canada. Vol.No.3, pp.32-42. 1959)

13) Reissner, E.

"On some aspects of the Theory of Thin Elastic Shells"

(Journal of the Boston Society of Civil Engineers, Vol. No.42 April 1955, No.2, pp.100-133)

14) Bleich, H.H. and Salvadori, M.G.

"Bending Moments on Shell Boundaries"

(Journal of the Structural Division, American Society of Civil Engineers. Oct.1959)

15) Vreedenburgh, C.J.

"The Hyperbolic Paraboloid Shell and its Mechanical Properties"

(Philips Technical Review No.1, Vol.20, 1958/59)

16) Loof, H.W.

"Eenvoudige formules voor de buigings-storingen in hyperschalen, die volgens beschrijvenden zijn begrensd"

(Rapport 8-61-3-hw-1 Stevin Laboratory, Delft, March 1961)

17) Novozhilov, V.V.

"The Theory of Thin Shells"

(P. Nordhoff Ltd, Groningen, The Netherlands)

18) Leicester, R. and Massey, P.C.

"Model Analysis of a Concrete Shell Roof"

(Architectural Science Review, Nov. 1960)

19) Proceedings of the Symposium on Shell Research.

(Delft, August 1961)

a) Flint, A.R.

"Some Model Tests in Shell Structures as an aid to Design" (pp.291-301)

b) Rowe, R.E.

"Tests on Four Types of Hyperbolic Shells" (pp.16-34)

c) Lauletta, E.

"Statics of Hyperbolic Paraboloidical Shells studied by means of models" (pp.47-57)

d) Munro, J and Ahuja, B.M.

"An Investigation of the Strain Distribution in Reinforced Concrete Shallow, Thin Shells of Negative Gaussian Curvature" (pp.57-78)

20) Jones, L.L.

"Tests on a One-tenth Scale Model of a Hyperbolic Paraboloid Shell Roof"

(Magazine of Concrete Research, March 1961)

21) Ahuja, B.M.

"Stress Distribution in Shells of Negative Gaussian Curvature"

(Ph.D.Thesis, London University. Oct. 1961)

22) Scrivener, J.C.

"An Investigation of Concrete Hyperbolic Paraboloid Shells"

(Ph.D.Thesis, London University. Oct. 1962)

23) Wood, R.H.

"Plastic and Elastic Design of Slab and Plates"

(Pub. Thames and Hudson, London. 1961)

24) Wood, R.H.

"Studies in Composite Construction"

Part II, The Interaction of Floors and Beams in Multistorey Buildings. (National Building Studies - Research Paper No.22, Dep't. of Scientific and Industrial Research, H.M.S.O., London.

25) Hetenyi, M.

"Beams on Elastic Foundation"

(Ann Arbor, The University of Michigan Press)

26) Den Hartog, J.P.

"Advanced Strength of Materials"

(McGraw Hill Book Co. Inc., 1952)

27) Timoshenko, S.P.

"Theory of Plates and Shells"

(McGraw Hill Publishing Co.)

28) Munro, J.

"An Analytical and Experimental Investigation of the Stress Distribution of Reinforced Concrete Shell Roofs with particular reference to Longitudinal Continuity." (Ph.D. Thesis, London University, August 1963)

29) Tottenham, H.

"The Analysis of Hyperbolic Paraboloid Shells." (Research Report E/RR/5, Timber Development Assn. July 1958)